2011

STABLE CARBON AND OXYGEN ISOTOPIC STUDY OF IMPACT-INDUCED HYDROTHERMAL CALCITE AT THE HAUGHTON IMPACT STRUCTURE, DEVON ISLAND, NUNAVUT, CANADA

Simon Auclair

STABLE CARBON AND OXYGEN ISOTOPIC STUDY OF IMPACT-INDUCED HYDROTHERMAL CALCITE AT THE HAUGHTON IMPACT STRUCTURE, DEVON ISLAND, NUNAVUT, CANADA

(Spine title: Impact-Hydrothermal Calcite Isotope Geochemistry)

(Thesis format: Monograph)

by

Simon Auclair

Graduate Program in Earth Science

A thesis submitted in partial fulfillment
of the requirements for the degree of
Master of Science

The School of Graduate and Postdoctoral Studies
The University of Western Ontario
London, Ontario, Canada

Abstract

From over 60 terrestrial impact craters with evidence of impact-induced hydrothermal alteration, only a dozen have been examined for stable isotopic compositions of hydrothermal carbonates. A variety of impact-induced carbonate precipitates have been identified at the Haughton impact structure (23 km, 39 Ma) on Devon Island, Canadian Arctic. The hydrothermal carbonates are found in three distinct settings: (1) as fracture fillings in shocked lithologies of the inner crater; (3) as vug fillings within impact melt breccias, and (3) as interstice fillings in pipe structures of the crater rim. X-Ray Powder Diffraction, X-Ray Fluorescence and carbon and oxygen stable isotope analyses were performed on rock and calcite mineralisation samples. Values of $\delta^{13}C_{calcite}$ range from -14 to -2‰, indicating an inorganic carbon source. Values of $\delta^{18}O_{calcite}$ range from +8 to +18 ‰, corresponding to a $\delta^{18}O_{fluid}$ of -7 to +2‰, most likely an enriched polar meteoric source at temperatures of mineralisation >130°C.

Keywords: Astrobiology, calcite, Canadian Arctic Archipelago, carbon and oxygen stable isotopes, Devon Island, , dolomite, fluid inclusion, hydrothermal mineral, hydrothermal system, impact crater, XRD, isotopic analysis, Mars, mineralogy, water-rock interaction

Acknowledgements

This work would not have been possible without the help of many contributors, starting with my supervisors Dr. Gordon Osinski and Dr. Neil Banerjee. A scientific project like this one requires a lot of work in the field and in the laboratory. I would like to thank the team in charge of the Haughton Mars Project Research Station on Devon Island, Nunavut, Canada, who made possible this study on planetary impacts. I also want to thank the scientists and technicians working in the Laboratory for Stable Isotope Science at the University of Western Ontario, in particular Kim Law and Li Huang for their enormous dedication. Additional contributors to this work to whom I express my recognition are Dr. Roberta Flemming, Dr. Elizabeth Webb, Dr. Fred Longstaffe, Matt Izawa, Joanne Potter, Grace Yau, Duane Petts, Laura Thomson, Mike Craig, Alaura Singleton, Natasha Bumstead, Nathan Bridge, Nicky Barry, Raymond Ho, Erena Kawamoto, Mike Laliberty, Marie-Claude Gilbert and Deana Schwarz. Finally, this project would not have been possible without financial support from the William S. Fyfe Award, the Canadian Space Agency CARN Grant and the Northern Scientific Training Project Research Grant.

Table of Contents

Certificate of Examination ii
Abstract iii
Aknowledgements iv
List of Figures ix
List of Tables xii
List of Appendices xiii
List of Abbreviations, Symbols, Nomenclature xiv

1 Introduction 1
1.1 Purpose of the Study 1
1.2 Study Area 4
1.2.1 Regional Geology 4
1.2.2 Geology of the Haughton Impact Structure 5
1.2.3 Impact-Induced Hydrothermal Activity 8

2 Literature Review 15
2.1 Impact Cratering Processes 15
2.1.1 The Three Stages of Impact Cratering 15
2.1.2 Impact Cratering in the Solar System 16
2.1.3 Impact Craters on Earth 18
2.2 Hydrothermal Processes 19
2.2.1 Planetary Distribution of H_2O 19
2.2.2 Geological Environments Hosting Hydrothermal Activity 19
2.3 Hydrothermal Systems in Impact Craters 20
2.3.1 Transient Nature of Impact-Induced Hydrothermal Activity 20
2.3.2 Terrestrial Occurrences of Hydrothermal Activity in Impact Craters 20
2.3.3 Evidence for Impact-Induced Hydrothermal Activity on Mars 27
2.4 Impact-Generated Hydrothermal Systems as Habitats for Life 28
2.4.1 Favourable Conditions to Life 28
2.4.2 Evidence for Life in Hydrothermal Systems of Impact Craters 31
2.4.3 Implications for Astrobiology 32
2.5 Principles of Stable Isotope Science 33
2.5.1.1 Introduction to Isotopic Fractionation 33
2.5.1.1.1 Carbon Isotope Ratios 34

2.5.1.1.2 Oxygen Isotope Ratios....35
2.5.1.2 Isotopic Compositions of Natural Carbonates....35
2.5.1.2.1 Seawater and Freshwater Carbonates....35
2.5.1.2.2 Hydrothermal Carbonates....36
2.5.1.2.2.1 Study of Impact-Hydrothermal Carbonates....39

3 Methods and Experimental Approach....41
3.1 Samples....41
3.2 X-Ray Fluorescence Spectroscopy....41
3.3 X-Ray Diffraction Spectroscopy....42
3.4 Stable Isotope Analysis....43
3.4.1 Oxygen and Carbon Isotope Analysis of Calcite Samples....43
3.4.2 Oxygen and Carbon Isotope Analysis of Mixed Carbonate Samples....45
3.4.2.1 Problem of Mixed Samples....45
3.4.2.2 Selection of Internal Laboratory Standards for Dolomite....47
3.4.2.3 Conventional and MultiPrep Extraction Techniques....51
3.4.2.4 Development of an Experimental Approach....58

4 Sample Description, Mineralogy and Geochemistry....65
4.1 Characterisation of Reference Carbonate Material....65
4.1.1 Sample Locations....67
4.1.2 Field Observations....69
4.1.3 X-Ray Diffraction and X-Ray Fluorescence....70
4.1.3.1 Allen Bay Formation....73
4.1.3.2 Irene Bay Formation....74
4.1.3.3 Thumb Mountain Formation....75
4.1.3.4 Bay Fiord Formation....76
4.1.3.5 Eleanor River Formation....77
4.1.3.6 Blanley Bay, Cape Clay and Cass Fiord Formations....77
4.1.3.7 Thumb Mountain and Eleanor River Formation from the Crater Region....78
4.2 Characterisation of Syn- and Post-Impact Lithologies....81
4.2.1 Impact Melt Breccias....81
4.2.2 Haughton Formation....82
4.3 Characterisation of Impact-Induced Hydrothermal Calcite....85
4.3.1 Sample Locations....85
4.3.2 Field Observations....87
4.3.3 X-Ray Diffraction Data....91

4.3.3.1 Intra-Melt Breccia Hydrothermal Vugs....92
4.3.3.2 Intra-Melt Breccia Hydrothermal Vugs at Haughton River Locality....93
4.3.3.3 Hydrothermal Veins....96
4.3.3.4 Hydrothermal Pipe Structures....97

5 Carbon and Oxygen Stable Isotope Geochemistry....100
5.1 Introduction....100
5.1.1 Rationale for Stable Isotope Geochemistry....102
5.1.2 X-Ray Diffraction Geochemistry Link to Stable Isotopes....105
5.2 Results from Stable Isotope Analysis....106
5.2.1 Non-Hydrothermal Carbonates Results....107
5.2.1.1 Unshocked Lithologies....107
5.2.1.2 Shocked Lithologies....108
5.2.1.3 Impact Melt Breccias....111
5.2.2 Hydrothermal Carbonates Results....112
5.2.2.1 Vug Fillings within Impact-Melt Breccias....113
5.2.2.2 Marcasite-Rich Vug Fillings within Impact Melt Breccias....114
5.2.2.3 Vein Fillings within Shocked Target Rocks....119
5.2.2.4 Cavity fillings within Hydrothermal Pipe Structures....121
5.2.3 Predicted hydrothermal Fluid Composition....121
5.3 Discussion....123
5.3.1 Overview of Available Data and Rationale....123
5.3.1.1 Significance of Results and Distinction from Previous Studies....125
5.3.2 Interpretation of Results for Non-Hydrothermal Carbonates....127
5.3.3 Interpretation of Results for Hydrothermal Carbonates....131
5.3.3.1 Calcite Vug Fillings within Impact Melt Breccias....138
5.3.3.1.1 Evidence from Oxygen-Isotope Data....139
5.3.3.1.2 Evidence from Carbon Isotopic Compositions....142
5.3.3.2 Vein and Pipe Structure Calcite Fillings....145
5.3.3.2.1 Evidence from Oxygen-Isotope Data....146
5.3.3.2.2 Evidence from Carbon-Isotope Data....148
5.3.4 Characterisation of Fluid....151
5.3.5 Oxygen Isotopic Composition of the Hydrothermal Fluid....153
5.3.4.2 Mechanisms of ^{18}O-enrichment....162
5.3.4.2.1 Water-Rock Interactions....163
5.3.4.2.2 Vaporisation of Fluid....169

5.3.5 Model of Hydrothermal Activity at Haughton.....178

6 Conclusions and Recommendations.....188

6.3 Pre-, Syn- and Post-Impact Lithologies.....188

6.4 Impact-Induced Hydrothermal Deposits.....189

6.5 Hydrothermal Fluids.....191

6.6 Implications for Astrobiology and Planetary Exploration.....193

6.7 Recommendations for Future Work.....193

7 References.....195

8 Appendices.....216

Appendix 1 X-Ray Diffraction Data.....216

Appendix 2 Stable Isotope Data.....221

VITA.....224

List of Figures

Figure 1.1 Regional geology of Devon Island and location of the Haughton impact structure (Osinski et al., 2005c).....6

Figure 1.2 Geological map of the Haugthon impact structure (Osinski, 2005c).....7

Figure 1.3 Stratigraphy at Haughton showing the extent of bedrock excavation caused by the impact (Mod. from Thorsteinsson et al., 1987).....9

Figure 1.4 The three stages of hydrothermal activity at the Haughton impact structure and associated temperatures (Osinski et al. 2005a).....12

Figure 1.5 Cross-section of the Haughton impact structure and general hydrothermal settings (Osinki et al., 2005a).....13

Figure 2.1 The formation stages of an impact crater (the contact and compression stage is ommitted) (Osinski et al., 2005d).....17

Figure 2.2 General stages of hydrothermal fluid circulation within an impact structure (Naumov, 2005).....24

Figure 2.3 Distribution of terrestrial impact craters with evidence of post-impact hydrothermal alteration as full circles (Naumov, 2005).....25

Figure 2.4 $^{13}C/^{12}C$ ratios of important carbon compounds (δ-variations in ‰ relative to VPDB) (Versh et al. 2006).....37

Figure 2.5 $^{18}O/^{16}O$ ratios of important oxygen compounds (δ-variations in ‰ relative to SMOW) (Hoefs 1973).....38

Figure 3.1 Electric hand-held rotary drill and sampling tools used for sampling calcite vein and vug fillings for XRD and stable isotope analysis.....49

Figure 3.2 The two natural dolomite samples selected as internal laboratory standards for stable isotope analysis.....50

Figure 3.3 Results of carbon and oxygen stable isotope analysis of dolomites by conventional off-line technique at 50°C for 18 hours.....55

Figure 3.4 Results of carbon stable isotope analysis of dolomites by MultiPrep technique at 90°C for 10 minutes, 4 and 5 hours.....56

Figure 3.5 Results of oxygen stable isotope analysis of dolomites by MultiPrep technique at 90°C for 10 minutes, 4 and 5 hours.....57

Figure 3.6 Comparison or results between $\delta^{13}C$ average values for all dolomites standards from conventional and MultiPrep techniques.....59

Figure 3.7 Comparison of results between $\delta^{18}O$ average values for all dolomites standards from conventional and MultiPrep techniques.....60

Figure 4.1 Location of reference samples analysed in this study (Map Source) 68

Figure 4.2 Location of lake sediment and impact melt breccia samples selected for this study (Map Source) 80

Figure 4.3 Ternary diagram showing CaO, MgO and SiO_2 contents of selected rock samples from Haughton.....84

Figure 4.4 Location of hydrothermal calcite samples selected for stable isotope geochemistry in this study (Mod.from Osinski et al., 2001) 88

Figure 4.5 Field images of hydrothermal calcite-marcasite vug mineralisation at the Haughton River Valley locality.....89

Figure 4.6 Simplified geological map and location of sampling transects at the Haughton River Valley locality.....90

Figure 4.7 Representative occurrences of intra-melt breccia hydrothermal vug fillings at the Haughton impact structure.....94

Figure 4.8 Intra-melt breccia calcite vug fillings with marcasite at the Haughton impact structure, and evidence for hydro-fracturation.....98

Figure 4.9 Representative occurrences of hydrothermal calcite vein fillings within target rocks at the Haughton impact structure.....99

Figure 5.1 Stable isotopic compositions of reference target limestones at the Haughton impact structure.....109

Figure 5.2 Variations of $\delta^{18}O$-values of marine and freshwater limestones through geological time (Keith et al., 1964) 110

Figure 5.3 Compiled carbon and oxygen isotopic compositions of impact-hydrothermal carbonates (Mod. from Versh et al., 2006) 114

Figure 5.4 Carbon and oxygen isotopic compositions of terrestrial carbonates formed in hydrothermal environments (Mod. From Rollinson, 1995) 118

Figure 5.5 Carbon and oxygen isotopic compositions of the various hydrothermal calcite deposits at the Haughton impact structure.....120

Figure 5.6 Stable isotopic compositions of rock samples from the longitudinal transect at the Haughton River Valley vug locality.....132

Figure 5.7 Distribution map of carbon and oxygen isotopic compositions of vein and pipe structure calcite at Haughton (After Osinski et al., 2005c) 134

Figure 5.8 Calculated $\delta^{18}O$-values of the hydrothermal fluid, based on $\delta^{18}O$-values of calcites using equations by O'Neil et al. (1969) and Zheng (1999).....158

Figure 5.9 Average $\delta^{18}O$-values of three hydrothermal calcites, average fluid-inclusion temperatures of homogenisation and fluid $\delta^{18}O$-values.....159

Figure 5.10 Contour map of average annual $\delta^{18}O$-values of meteoric precipitation at stations in the global network of the IAEA.....161

Figure 5.11 $\delta^{18}O$-values of residual water vs. fraction of H_2O vaporised in an isothermal Rayleigh fractionation model (After Sturchio et al., 1990).....168

Figure 5.12 Comparative textural observations between in-situ hydrothermally-generated breccias (Uysal, 2009) and a breccia block at Haughton..... 172

Figure 5.13 Inferred equilibration of initial carbonate country rocks with initial water at Haughton, as a function of increasing water-rock ratio (W/R) 175

Figure 5.14 Distribution of the four main types of impact-hydrothermal calcite deposits at Haughton (Mod. from Osinski, 2001; 2005).....186

List of Tables

Table 3.1 Results of carbon and oxygen stable isotope analysis of dolomites by conventional off-line technique at 50°C for 18 hours.....54

Table 3.2 Results of carbon and oxygen stable isotope analysis of dolomites by MultiPrep technique at 90°C for 10 minutes, 4 and 5 hours.....55

Table 3.3 Compilation of average $\delta^{13}C$- and $\delta^{18}O$-values for all dolomites standards from conventional off-line and MultiPrep techniques.....59

Table 3.4 Techniques used for carbon and oxygen isotope analysis of carbonates in the Laboratory for Stable Isotope Science (Li, 2008).....63

Table 4.1 Relative mineral composition based on XRD data juxtaposed to stratigraphy (Mod. From Thorsteinsson et al., 1987).....71

Table 4.2 X-Ray Fluorescence data for target and post-impact lithologies at Haughton (Data partly from Osinski et al., 2005) 72

Table 4.3 Representative mineralogy of the four major hydrothermal settings at Haughton, based on X-Ray Diffraction analysis. 95

Table 5.1 Compiled carbon and oxygen isotopic composition of carbonates from impact structures worldwide, including Haughton.....104

Table 5.2 Stable isotopic compositions of representative hydrothermal calcite samples from the Haughton impact structure.....116

Table 5.3 Range of predicted oxygen isotope composition of the hydrothermal fluid at Haughton using equations by O'Neil et al. (1969) and Zheng (1999).....157

Table 5.4 Summary of the main styles of hydrothermal mineralisation at the Haughton impact structure (Modified from Osinski et al., 2001).....181

Table 5.5 Average stable isotopic compositions of calcite deposits from the four hydrothermal settings, and temperatures of hydrothermal fluid.....181

List of Appendices

Appendix 1 X-Ray Diffraction Data.....216

Appendix 2 Stable Carbon and Oxygen Isotope Data.....221

List of Abbreviations, Symbols, Nomenclature

DOLO368	An international dolomite standard
EDS	Electron Dispersive Spectrometry
Fm	Formation
HZ	Habitable Zone
IMB	Impact Melt Breccias
LiDAR	Light Detection and Ranging
LHB	Late Heavy Bombardment
LN_2	Liquid Nitrogen
LSIS	Laboratory for Stable Isotope Science
MER	Mars Exploration Rover (Spirit and Opportunity)
NAD 83	North America Datum 1983 - Geographic coordinates (Easting, Northing)
NBS-18,-19	International calcite standards
OMEGA	Observatoire pour la Minéralogie, l'Eau, les Glaces et l'Activité
PDB	Pee Dee Belemnite International Carbonate Standard
REE	Rare-Earth Element
SMOW	Standard Mean Ocean Water
Th	Temperature of homogenisation of a fluid inclusion
V-PDB	Vienna-Pee Dee Belemnite
V-SMOW	Vienna-Standard Mean Ocean Water
W / R_O	Water-rock ratio, expressed as the atom percent of oxygen
WS-1	An international calcite standard
XRD	X-Ray Powder Diffraction
XRF	X-Ray Fluorescence
%NaCl eq.	Percentage of salt ions in solution, expressed as NaCl percent equivalent
‰	Part per thousand – Permil

$\delta^{18}O$-value	Oxygen isotopic composition, in permil (‰) relative to the V-SMOW standard, calculated from $[(^{18}O/^{16}O_{sample} - {}^{18}O/^{16}O_{standard}) -1] \times 1000$
$\delta^{13}C$-value	Carbon isotopic composition, in permil (‰) relative to the V-PDB standard, calculated from $[(^{13}C/^{12}C_{sample} - {}^{13}C/^{12}C_{standard}) -1] \times 1000$
σ	Standard deviation
2θ	Summed angle of x-ray diffraction beam
°C	Degree Celsius
g	Gram
mg	Milligram
Ga	Billion years
K	Kelvin (1Kelvin = 273 °C)
kV	Kilovolt
mA	Milliamperes – Milliamps
Ma	Million years
n	Number or samples
Vol%	Mean composition in volume percent
Wt%	Mean composition in weight percent
$BaSO_4$	Barium sulfate - Barite
$CaCO_3$	Calcium carbonate - Calcite
CaF_2	Fluorite
CO_2	Carbon dioxide
$H_2{}^{16}O$	Light water
H_2O	Water
H_3PO_4	Phosphoric acid
Mn	Manganese
Na	Sodium
SiO_2	Silicon oxide – Quartz
$SrSO_4$	Strontium sulfate – Celestine

Chapter 1. Introduction

1.1 Purpose of the Study

The primary purpose of this study is to evaluate the mineralogy and stable isotope geochemistry of hydrothermally-formed calcite found in various settings within the Haughton impact structure, Arctic Canada. In parallel, it was deemed important to examine the geochemistry of pre-impact carbonate rocks, as well as impact-generated lithologies, in which hydrothermal calcite deposits occur. These mineralogical and geochemical studies helped to characterise these host-rocks and hydrothermal carbonates, which was also important for selecting appropriate samples for stable isotopes analysis. More specifically, the focus of this study is on the carbon and oxygen stable isotopic composition of impact-induced hydrothermal calcite. The overarching goal is to provide indications about the timing and evolution of the transient hydrothermal system that developed at the Haughton impact structure. Geochemical data from carbonate deposits reveal crucial information about the conditions of carbonate deposition (e.g., temperature interval) and the hydrothermal fluid source (Hoefs, 1973). It is important to note that stable isotope geochemistry has been carried at several impact craters mainly for dating purposes, using radiogenic isotopes (Ames et al., 1998). However, the study of impact craters by stable isotope geochemistry is not common practice. In reality, less than a dozen terrestrial impact craters have been investigated using stable isotope geochemistry (Versh et al., 2005). Stable isotope studies have been carried out at impact craters in northern Europe, particularly at the Siljan and Lockne impact structures (Komor et al., 1990; Sturkell et al., 1998). For several craters, however, scientific studies and exploratory drilling were undertaken but hydrothermal deposits were not directly

targeted. From an economic geology perspective, the potential for impact craters as a source of commodities is increasingly interesting. Naumov (2005) presents a list of more than 60 terrestrial impact craters that are known to host hydrothermal alteration. Moreover, approximately 25% of all 176 known impact craters on Earth have natural resources and 50% of craters in hydrocarbon-rich sedimentary basins produce oil (Grieve et al., 1994).

Ultimately, this study has implications for astrobiology, or the search of life in the Universe. Minerals deposited in hydrothermal environments, such as carbonates, are excellent exploration targets in the search for extant life since they are known to keep fossil records (Schulze-Makuch et al., 2007). Moreover, carbonates on Earth can be directly precipitated by living organisms which, in this case, depict unique geochemical signatures indicative of biogenic activity. The Phoenix spacecraft has recently shown, with the help of a robotic arm and a meteorological station, notably with the Canadian-engineered LiDAR, that there is a hydrological cycle on Mars (Whiteway et al., 2009). In fact, H_2O is present in the atmosphere, on the surface and in the subsurface of Mars at various latitudes (Smith et al., 2009). This supports the hypothesis that impact-related hydrothermal activity might have been a common geological process on this planetary body, since the surface of Mars is covered by impact craters at all latitudes. Surprisingly, carbonates are practically not visible on Mars. This is in part explicable by the fact that a weak carbon-based cycle is predominant on Earth, inducing carbonate precipitating, whereas a sulfur-based cycle is strongly controlling the precipitation of sulfate minerals on Mars (Bibring et al., 2006). However, evidence for the existence of Martian carbonates has been proposed based on the recovery of a Martian meteorite on Earth (Eiler et al.,

targeted. From an economic geology perspective, the potential for impact craters as a source of commodities is increasingly interesting. Naumov (2005) presents a list of more than 60 terrestrial impact craters that are known to host hydrothermal alteration. Moreover, approximately 25% of all 176 known impact craters on Earth have natural resources and 50% of craters in hydrocarbon-rich sedimentary basins produce oil (Grieve et al., 1994).

Ultimately, this study has implications for astrobiology, or the search of life in the Universe. Minerals deposited in hydrothermal environments, such as carbonates, are excellent exploration targets in the search for extant life since they are known to keep fossil records (Schulze-Makuch et al., 2007). Moreover, carbonates on Earth can be directly precipitated by living organisms which, in this case, depict unique geochemical signatures indicative of biogenic activity. The Phoenix spacecraft has recently shown, with the help of a robotic arm and a meteorological station, notably with the Canadian-engineered LiDAR, that there is a hydrological cycle on Mars (Whiteway et al., 2009). In fact, H_2O is present in the atmosphere, on the surface and in the subsurface of Mars at various latitudes (Smith et al., 2009). This supports the hypothesis that impact-related hydrothermal activity might have been a common geological process on this planetary body, since the surface of Mars is covered by impact craters at all latitudes. Surprisingly, carbonates are practically not visible on Mars. This is in part explicable by the fact that a weak carbon-based cycle is predominant on Earth, inducing carbonate precipitating, whereas a sulfur-based cycle is strongly controlling the precipitation of sulfate minerals on Mars (Bibring et al., 2006). However, evidence for the existence of Martian carbonates has been proposed based on the recovery of a Martian meteorite on Earth (Eiler et al.,

2002) and remote sensing data (Bibring et al., 2006). Hypotheses to explain the apparent absence of carbonate deposits on Mars are that the absorption bands of carbonates are weak and geological processes, such as impact shock metamorphism, would make them hardly detectable (Cloutis et al., 2009). Despite the unique and recognisable geochemical signature of carbonates, other mineral phases on the surface of Mars might inhibit their easy detection. The current challenge for remote sensing and surface surveys is to identify the optimal constraints to identify carbonates within various morphological and geological features of the Martian surface. New evidence for the presence of carbonate traces in the Martian soil has recently been proposed (Boynton, 2009). The oxygen isotopic composition of carbonates found within Martian meteorites has been documented (i.e., Eiler et al., 2002), but an unequivocal impact-hydrothermal origin based on isotopic compositions has yet to be observed. The apparently weak nature of hydrothermal carbonate alteration at the Haughton impact structure highlights the fact that putative hydrothermal carbonates on Mars might be very difficult to identify. Finally, stable isotope geochemistry of carbonate minerals can be considered a useful tool for assessing hydrothermal conditions within an impact crater or any H_2O-bearing planetary body, and might provide clues to the potential of finding living organisms. In other words, the possibility of high-temperature microbial activity during the development of the impact-induced hydrothermal system can be assessed.

In short, in terms of stable isotope studies at the Haughton impact structure, only Martinez et al. (1994) have published stable isotope results on shocked and unshocked target rocks and impact-generated breccias. A regional study by Land et al. (1975) suggests a fluid interaction model for the genesis of the Allen Bay Formation dolomite

target rocks based on O, Mn and Sr isotopes data, without mention of the Haughton impact structure. Thus, the work of Martinez et al. (1994) is unique with regards to the Haughton impact structure, but only provides carbon and oxygen isotopic compositions of major rock types and none on impact-hydrothermal deposits. In consequence, stable isotope data on hydrothermal minerals at Haughton has been absent from the scientific literature, therefore, the present study aims at providing new data on hydrothermal deposits at Haughton. Additionally, the possibility of finding evidence of high-temperature microbial inhabitants in the hydrothermal system was also considered.

1.2 Study Area

1.2.1 Regional Geology

The Haughton impact event occurred in the north-western part of Devon Island, Nunavut, Canada (Figure 1.1). The well-exposed sedimentary sequence on Devon Island shows a general northern strike and a slight 3–5° dip to the west, so that the different lithologies outcrop in bands more or less oriented north-south (Thorsteinsson et al., 1987). The main rocks of the platform found in the region are shelf-type carbonates and evaporites deposited during the lower Ordovician to upper Silurian period (500–345 million years) (Figure 1.1); they unconformably overlie >1.7 billion years old Precambrian Canadian Shield (Thorsteinsson et al., 1987). Precambrian crystalline basement rocks consist of gneisses, micaceous slates and calc-silicates, and are found in the eastern part of the island, where most of it is covered by an ice field (Bischoff and Ostertag, 1986). Continuous vertical sections of the Paleozoic sedimentary sequence are found mainly on the sea cliffs surrounding the whole island, and in glacial valleys.

1.2.2 Geology of the Haughton impact Structure

The 23km-diameter Haughton impact structure, situated at 75°22'N and 89°40'W in the Canadian Arctic Archipelago, is the northernmost impact structure in a polar desert. Periglacial processes are common on Devon Island; however, the morphology and geology of the crater are very well-preserved since it has undergone minimal weathering due to the dry polar environment (Figure 1.2) (Osinski et al., 2005c). Haughton was formed approximately 39 million years ago when an asteroid or comet travelling at hypervelocity hit the Earth (Sherlock et al., 2005). Griener et al. (1963) first identified the Haughton structure as a piercement dome, a common geological feature in the Queen Elizabeth Islands. The impact crater hypothesis was only proposed about ten years later, but the first workers to finally recognise it as an impact structure were Robertson and Mason (1975) who found definite evidence of shock metamorphism indicated by the presence of shatter cones. Later, Robertson and Grieve (1978) published a more detailed report of the Haughton impact structure and associated lithologies.

The Haughton impact structure is a complex crater divided in six structural or tectonic domains or sectors namely the central, northern, eastern, southern, south-western and north-western sectors (Osinski and Spray, 2005). Moreover, it possesses an outward-collapsed central peak and an inward-collapsed rim (Osinski et al., 2005d). A significantly unique structural setting is found within each domain defined by Osinski et al. (2005d), which were not recognised by Bischoff et al. (1988).

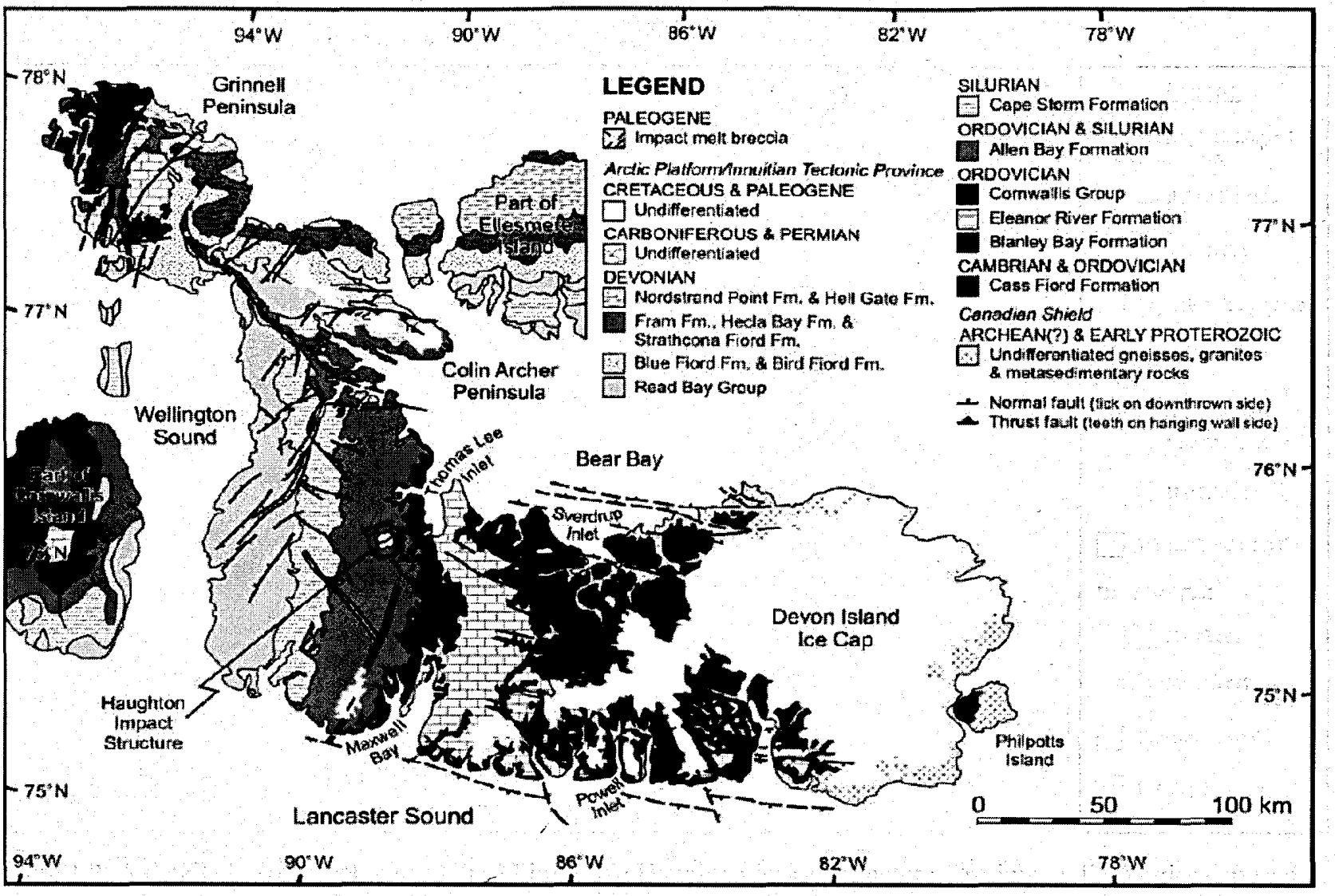

Figure 1.1. Geological map of Devon Island, with current extent of ice field. The Haughton impact structure is located in the northwest portion of the island, in a belt of Allen Bay Formation. (After Okulitch, 1991). Abbreviation: Fm. = Formation.

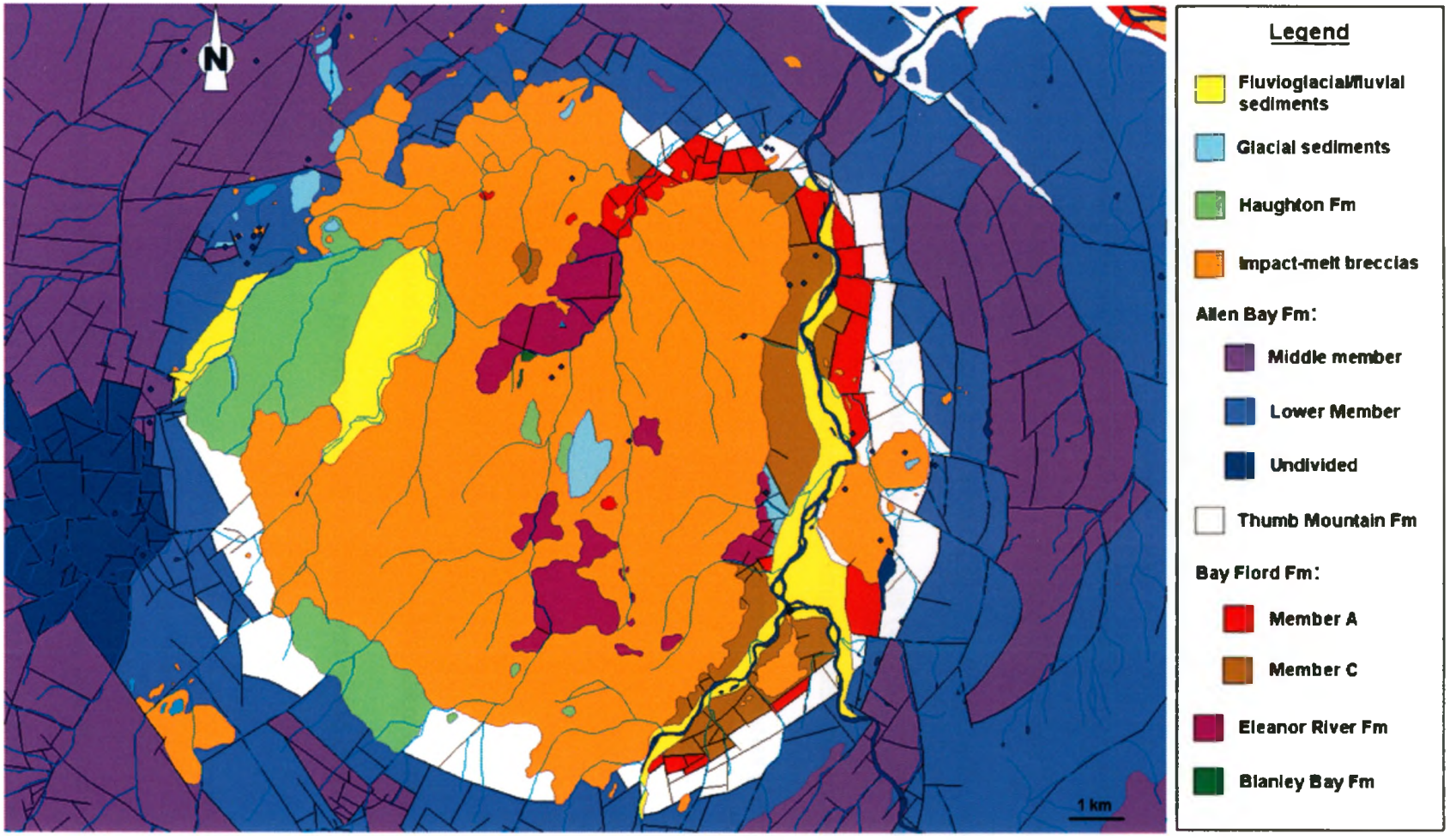

Figure 1.2. A detailed geological map of the 23 km-wide Haughton impact structure. Pre-impact lithologies exposed in the central uplift are older than those in the periphery. Post- and syn-impact lithologies are also shown: impact melt breccias (orange unit) cover a large area of the inner crater, while lacustrine sediments (pale green unit) are less extensive and restricted to western half of the crater region. Note the dissymmetry between the western and eastern halves with respect to the types of lithologies exposed. (From Osinski, 2005).

The undeformed faulted sedimentary rock sequence has a thickness of ~1880 metres at the Haughton impact site (Osinski et al., 2005c), but the total structural uplift is believed to be approximately 1750 metres (Robertson et al., 1978). The surrounding plateau consists of the Allen Bay Formation, except in the easternmost part of the crater rim region, where stratigraphically lower rocks such as the Thumb Mountain and Irene Bay Formations outcrop (Frisch et al., 1978). The oldest rocks exposed in the crater, as part of the central uplift, are the Lower Ordovician Eleanor River Formation (Figure 1.2). Stratigraphically lower rocks, such as the Cape Clay and Cass Fiord Formations, only outcrop east of the crater. Lithic clasts from crystalline basement rocks underlying the sequence were incorporated in the impact melt breccias (Robertson and Grieve, 1978) (Figure 1.3). Most of the inner crater is overlain by impact melt breccias containing target rock clasts of various compositions, ranging from dolomite to gneiss (Metzler et al., 1988; Osinski et al., 2005b). These allochthonous impact breccias were only recognised later as being emplaced as a melt, and include sulfate and carbonate melts (Osinski et al., 2001; 2003). They form a continuous cover over the central basin and inner ring (Robertson et al., 1985). The melt sheet occurs more sporadically in isolated patches around the faulted annulus, indicating it was once more extensive. Post-impact lake sediments overly all other units and have only been preserved in the eastern part of the crater (Osinski et al., 2005e) (Figure 1.3).

1.2.3 Impact-Induced Hydrothermal Activity

Hydrothermal activity refers to geological processes associated with the circulation of heated fluids in the Earth's crust (Taylor, 1977). At Haughton, three heat sources have likely contributed to the development of a hydrothermal system in the target rocks.

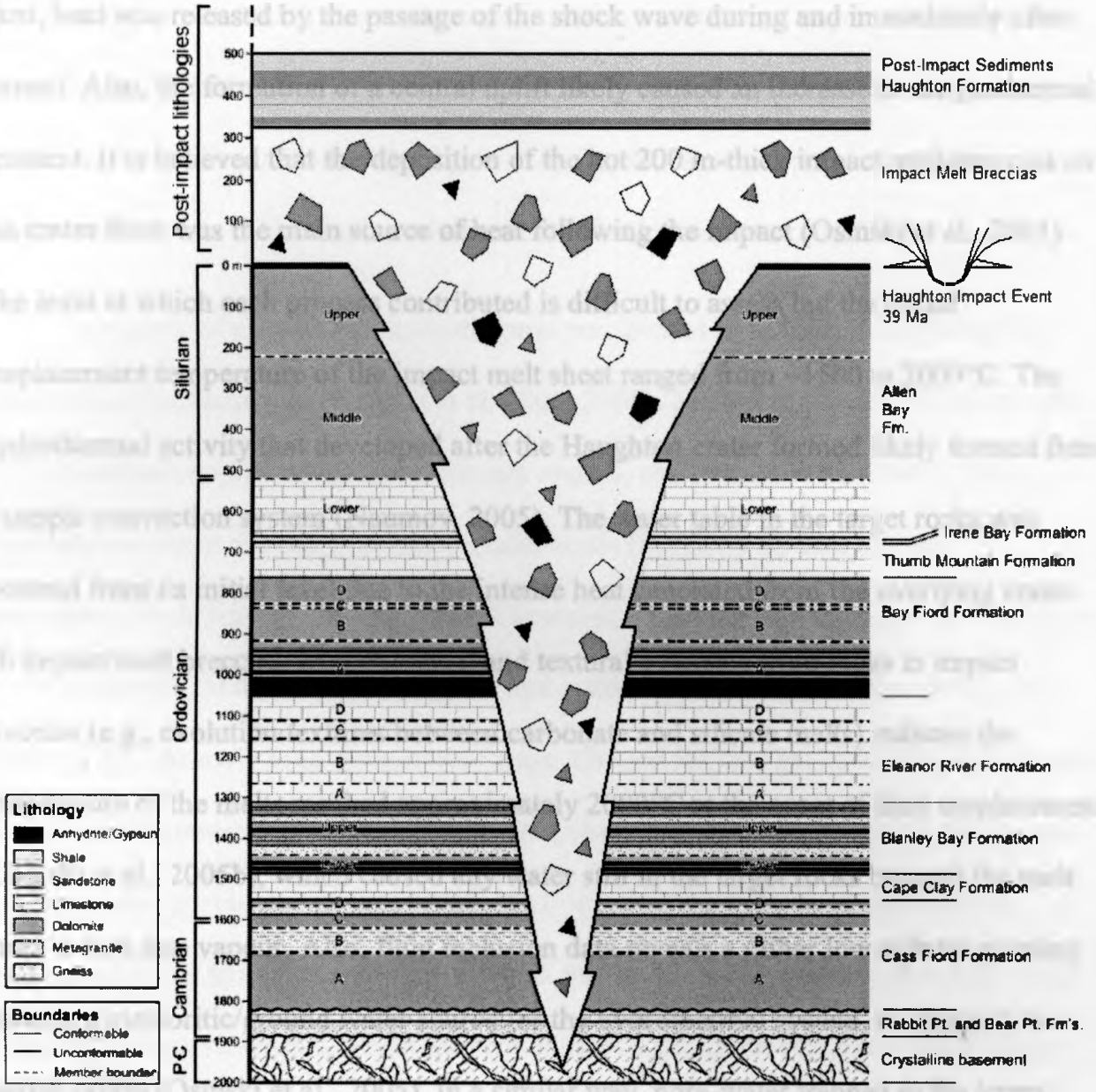

Figure 1.3. Stratigraphy at the Haughton impact crater site showing the extent of bedrock excavation caused by the impact. Approximately 1800 metres of sedimentary rocks were affected by the impact, and fragments were brought to the surface and incorporated as lithic clasts in the impact melt breccias layer covering the inner crater. Surface erosion of the impact melt breccias and surrounding country rocks, coupled with the development of a crater lake, are responsible for the deposition of intra-crater lacustrine sediments. Locally, glaciogenic deposits overlay this sequence. (Modified from Thorsteinsson et al., 1987).

First, heat was released by the passage of the shock wave during and immediately after impact. Also, the formation of a central uplift likely caused an increase in the geothermal gradient. It is believed that the deposition of the hot 200 m-thick impact melt-breccias on the crater floor was the main source of heat following the impact (Osinski et al., 2001). The level at which each process contributed is difficult to assess but the initial emplacement temperature of the impact melt sheet ranged from ~1500 to 2000°C. The hydrothermal activity that developed after the Haughton crater formed likely formed from a simple convection system (Naumov, 2005). The water table in the target rocks was lowered from its initial level due to the intense heat generated from the overlying crater-fill impact melt breccias. Mineralogical and textural evidence from melts in impact breccias (e.g., exolution textures between carbonate and silicate melts) indicate the temperature of the melts reached approximately 2000°C at the onset of their emplacement (Osinski et al., 2005b), which caused any water still in the target rocks beneath the melt sheet to turn into vapour. Also, fluid inclusion data reveals a rather low salinity pointing towards a meteoritic/ground water source for the hydrothermal system, as opposed to a marine origin (Osinski et al., 2005). In a similar way, pore-water trapped in the target sedimentary rocks sequence could not have been a significant contributor to the post-impact hydrothermal fluids. The 200-metres (or more) thick impact melt breccias would have provided enough latent heat to sustain a system of water-circulation cells from deep beneath the central uplift and up towards the outer rim, where the cooler water would have percolated back down towards the center of the crater, forming a continuous recharge possibly for an extended period of time. Three main stages are recognised at the Haughton crater based on mineral assemblages, presented here in chronological order following the impact (Osinski et al., 2001, 2005): the early stage dominated by water

vapour with T~340–200°C, the main stage in which a mixture of vapour and liquid were present with T~200° – 100°C, and finally the late hydrothermal stage characterised by liquid fluids with T~100° – 60°C) (Figure 1.4). These stages are consistent with progressive cooling of the fluids and decreasing fluid flow (Naumov, 2005).

A variety of post-impact hydrothermal precipitates have been identified at the Haughton impact structure (Osinski et al, 2001; 2005). For a complete overview specific to the Haughton impact crater hydrothermal system, see Osinski et al. (2001, 2005). These authors have defined four main spatial zones that show distinct mineral paragenesis, including: 1) the impact melt breccias, 2) the heavily faulted outer margin of the central uplift, 3) the crater rim region, and lastly, 4) the interior of the central uplift (Figure 1.5). The early high-temperature stage allowed for the first hydrothermal mineral, quartz, to precipitate mainly into vugs of the melt-breccias. The impact melt sheet acted as a cap, likely preventing vapour and fluids from escaping in large amounts. This constrained fluids to migrate laterally towards the rim and, consequently, resulted in the formation of pipe structures, which are only found on the crater rim. As a result, quartz also precipitated in these zones during the early stage, along with minor sulphides such as pyrite and chalcopyrite. During the main stage, barite, celestite and fluorite were deposited at the same time as calcite into the impact breccias. The drop in pH of the fluids, as well as the remaining water vapour, induced the precipitation of marcasite, both in the melt sheet and in the pipe structures: a likely source of sulfur for marcasite precipitation is the sulfate-bearing sedimentary rocks. During the late hydrothermal stage, quartz was predominant in the impact breccias and the interior of the central uplift, and

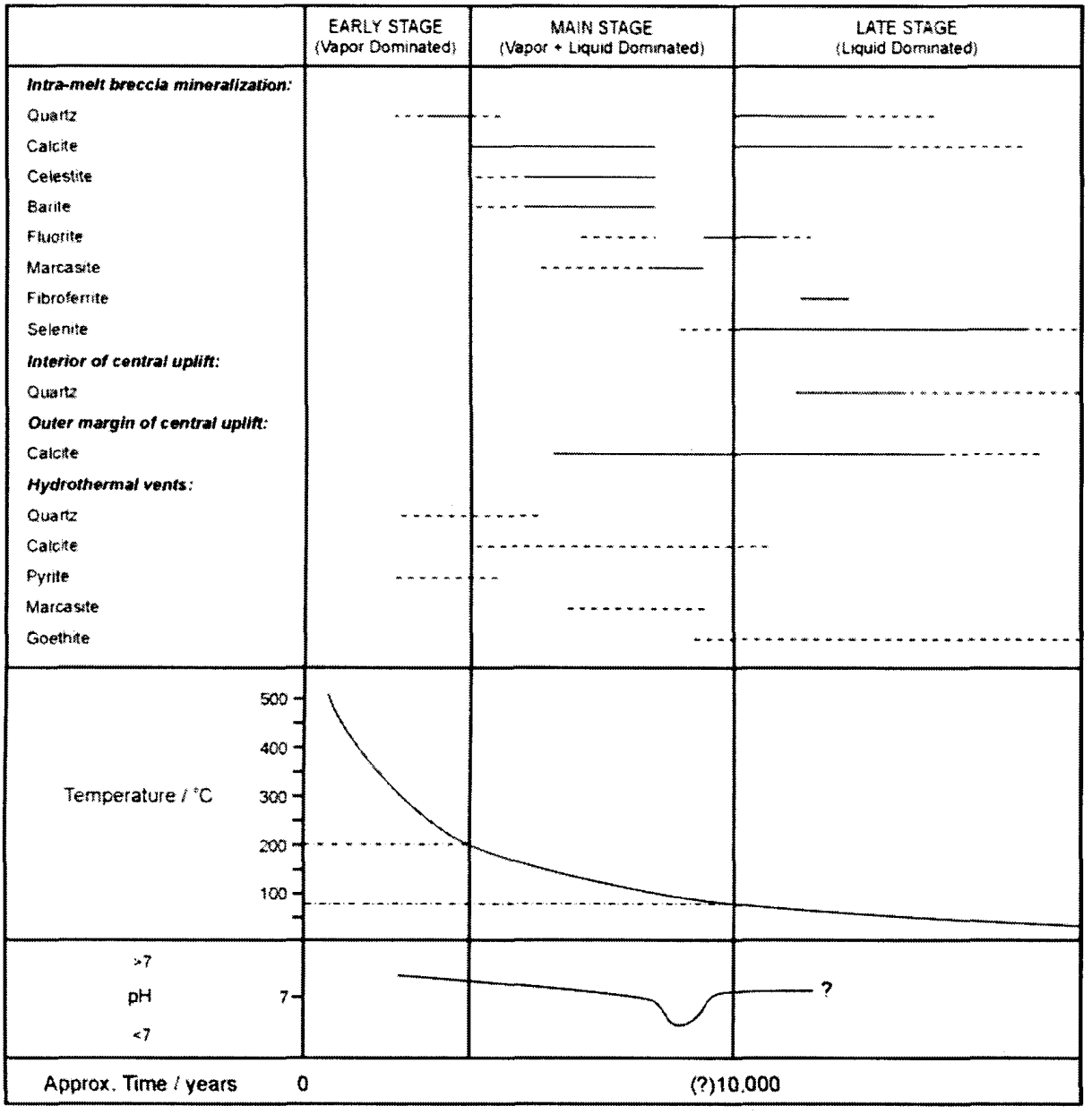

Figure 1.4. The paragenetic evolution of hydrothermal mineralisation within the Haughton impact structure. The spatial distribution of minerals is shown on the vertical axis by the four types of deposits. The temporal distribution of minerals within each deposit is shown by the three stages of hydrothermal activity on the horizontal axis. Dashed lines indicate sporadic occurrence of a mineral. Also shown on the vertical axis are the temperature intervals for each hydrothermal stage. The mineral on which this study focuses, i.e. calcite, seems to have been deposited during the main stage of hydrothermal activity, but also in a second episode during the late stage, associated with an increase in pH. The formation of calcite seems to have occurred at temperatures between ~200°C down to <60°C. See text for complete description of each depositional setting of calcite. (From Osinski et al., 2005a).

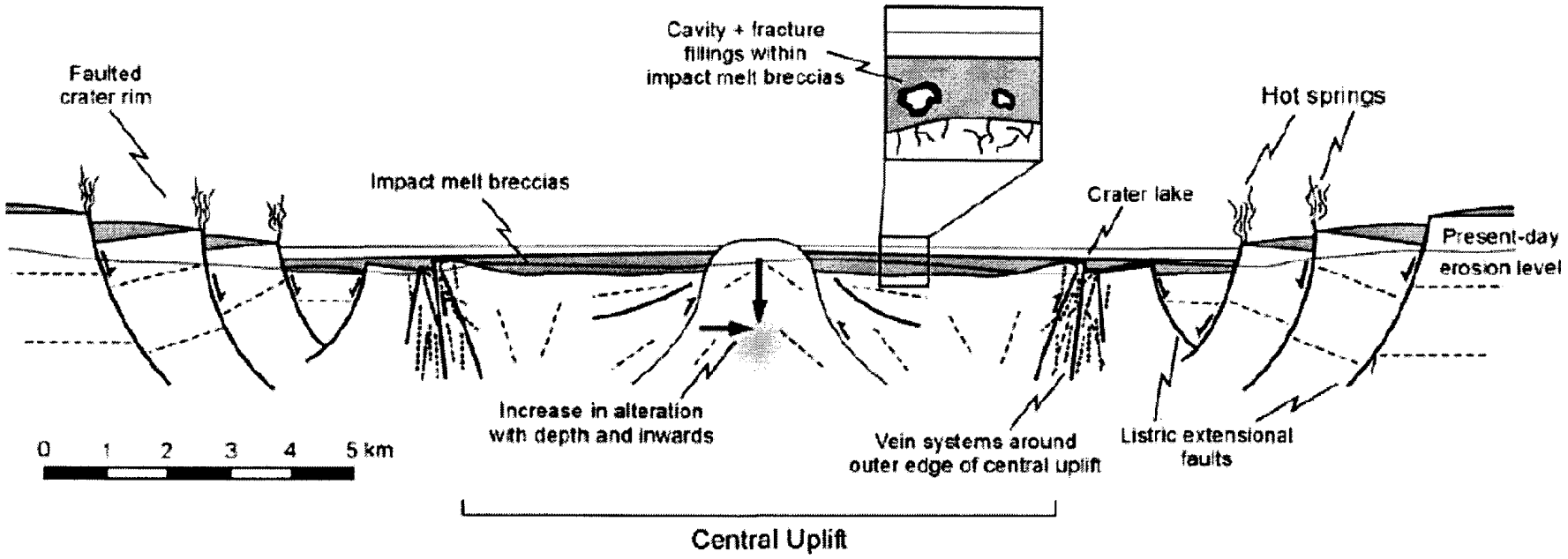

Figure 1.5. A schematic cross-section through the center of the Haughton impact structure. The hydrothermal system is generated by the heating of ground water mainly induced by cooling impact melt breccias. The fluids are mobilised through fractures and permeable target rocks, and secondary mineral fillings are produced. A crater lake forms in the crater depression, as evidenced by lacustrine sediments. (From Osinski et al., 2005a).

fibroferrite (an iron oxy-hydroxide) and selenite were deposited in the melt-breccias. Goethite is associated with the late stage of hydrothermal activity (and normal weathering) within the pipe structures (Osinski et al., 2001). Osinski et al. (2005a) show how thousands of years of slow cooling of the melt blanket induced a single hydrothermal system that led to the deposition of this series of alteration minerals into the impact sheet, the central uplift and structures around the rim. Hydrothermal calcite was precipitated from high temperature fluids (< 200–340°C) during the main stage as vug-infill in the impact melt breccias and hydrothermal pipe structures around the crater periphery (Osinski et al., 2001). It was later deposited in fractures of the central uplift and possibly outer crater rim, down to lower temperatures below the boiling point of water.

The Haughton crater is in the size range to be considered a complex impact structure and, because of its asymmetry, in both target lithologies and structures, it has yet to be proven that the hydrothermal fluids were similar or different in all portions of the crater interior and rim. Other impact craters with similar dimensions, target lithologies and hydrothermal alteration to the Haughton crater include the Ries and the Siljan craters. Although the Chicxulub structure is much larger than Haughton, it also occured in a sequence of carbonates and evaporitic-type of rocks, and was also affected by post-impact hydrothermal activity (Zürcher et al., 2004).

Chapter 2. Literature Review

2.1 Impact Cratering Processes

Impact cratering is an irreversible geological process occurring on all planetary bodies of our solar system with a solid surface. The hypervelocity impact of an asteroid or comet on a body could metamorphose, melt and vaporise both the impactor and the target, as well as cause a permanent impact crater on the target's surface (French, 1968; French and Short, 1968). This is evidenced by telescope and spacecraft observations of the rocky planets, moons and asteroids (Taylor, 1992). However, direct field observations and scientific measurements made at a terrestrial impact structure could provide much data on impact cratering processes. Studying terrestrial craters is useful since it gives access to the third-dimension, in other words, to the subsurface. Many processes of impact cratering were first understood on terrestrial craters (i.e., modification stage, central uplift) and concepts were then applied to craters on other planetary bodies where subsurface access is impossible (French, 1998). Potentially, knowledge on hydrothermal processes seen within impact craters on Earth could be extrapolated to Mars and to the Jovian moons.

2.1.1 The Stages of Impact Cratering

Independently of the size of the impactor, an impact event is defined by three simplified stages, each encompassing unique characteristics. The three stages of an impact event are known as contact and compression, excavation, and modification (Gault et al., 1968; Melosh, 1989). In Figure 2.1, the contact and compression stage is omitted on purpose since it represents the flash-instant when the object arriving at hyper-velocity of several kilometres per seconds encounters the planetary surface. The second step is the

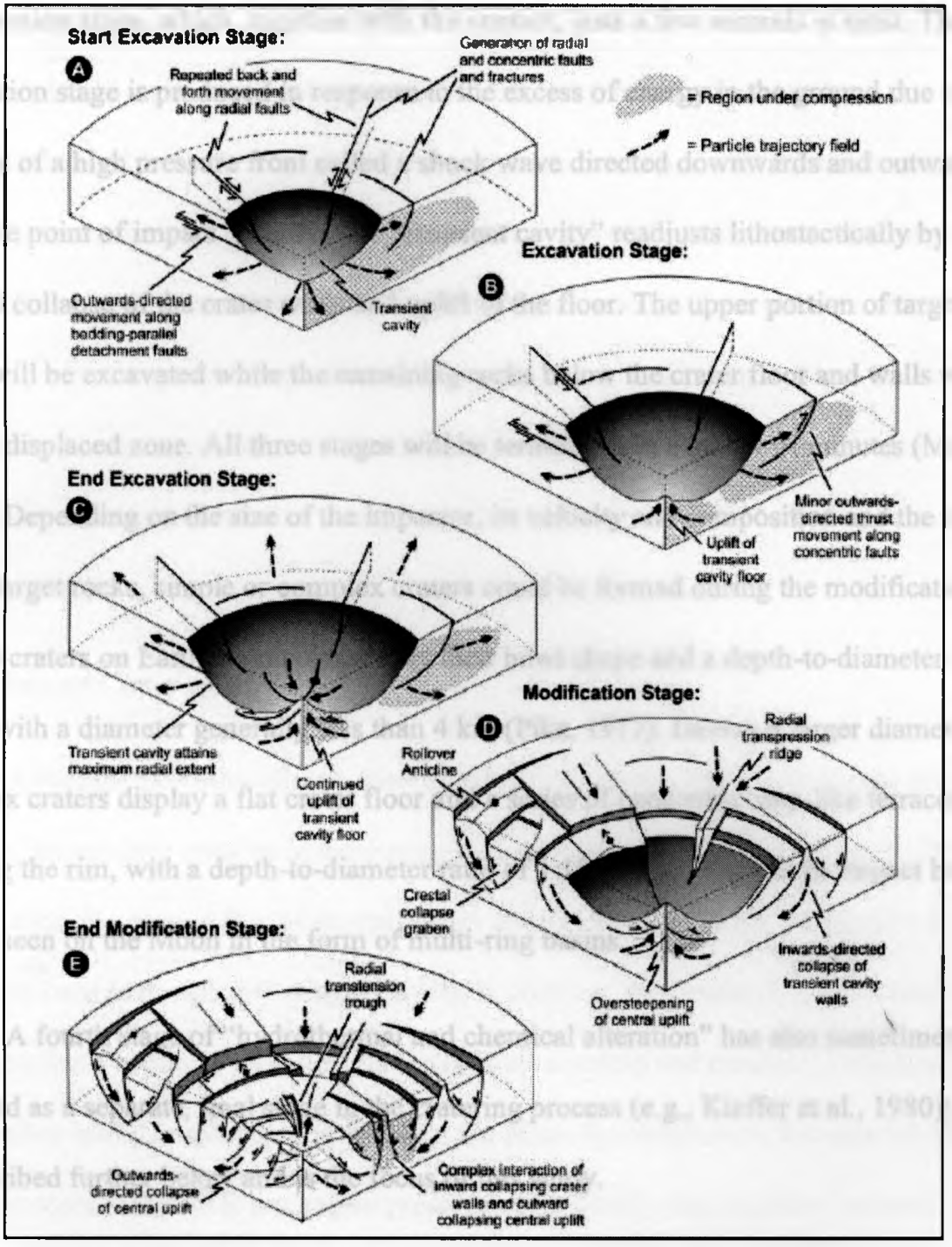

Figure 2.1. Schematic diagrams of the evolution of an impact crater. The first stage, i.e. contact and compression stage, is not shown. Shock waves propagate in the target rocks in specific ways that produce an excavation flow, leading to the formation of a transient cavity. After that, the transient crater attains a maximum depth and width. However, this crater undergoes a series of deformations (inwards and upwards) since it is not structurally stable. Radial and concentric faults accommodate structural movements during the modification stage. Eventually, the crater floor and central uplift readjust to a new configuration by gravity-related processes. Crater walls collapse inwards and, in the case they are unstable, blocks from the central uplift show an outward-directed movement. (From Osinski et al., 2005d).

compression stage, which, together with the contact, lasts a few seconds at most. The excavation stage is produced in response to the excess of energy in the ground due to the passage of a high pressure front called a shock wave directed downwards and outwards from the point of impact. Finally, this "transient cavity" readjusts lithostactically by a general collapse of the crater walls and uplift of the floor. The upper portion of target rocks will be excavated while the remaining rocks below the crater floor and walls will form a displaced zone. All three stages will be terminated in a matter of minutes (Melosh, 1989). Depending on the size of the impactor, its velocity and composition and the nature of the target rocks, simple or complex craters could be formed during the modification. Simple craters on Earth are recognised by their bowl shape and a depth-to-diameter ratio of 1:5 with a diameter generally less than 4 km (Pike, 1977). Having a larger diameter, complex craters display a flat crater floor and a series of concentric step-like terraces forming the rim, with a depth-to-diameter ratio of 1:10 to 1:20. Very large impact basins can be seen on the Moon in the form of multi-ring basins.

A fourth stage of "hydrothermal and chemical alteration" has also sometimes been included as a separate, final stage in the cratering process (e.g., Kieffer et al., 1980); this is described further below and is the focus of this study.

2.1.2 Impact Cratering in the Solar System

The bulk of asteroid and cometary impact events occurred at the onset of our Solar System 4.55 billion years ago when planets formed (Wilhelms et al., 1987). A final period of intense bombardment, known as the Late Heavy Bombardment (LHB), is believed to

have occurred from 4.0 to 3.8 Ga. The resulting craters on the surface of the Moon and the inner planets were preserved. The possible cause of this cataclysm is the destabilisation of the main asteroid belt by gas giants resonance effects, which caused asteroids to acquire new planet-crossing orbits throughout the solar system (Gomes et al., 2005). The modification of the planets and moons as we know them today is, therefore, due to repetitive impacts that prevailed during the young solar system. Since the Late Heavy Bombardment, a constant rate of impacts is generally proposed with larger impacts being less probable than smaller ones, partly due to the size distribution of impactors (Taylor, 1992).

2.1.3 Impact Cratering on Earth

Although the observational, theoretical and laboratory data available are always growing, uncertainty remains in estimating the rate of impacts on Earth (French, 1990). For instance, the current flux of interplanetary debris in the 10-30 m size range to Earth is especially hard to decipher (Prantzos, 2007). In addition, the record of impact cratering events on Earth is poorly preserved due to crustal recycling and erosion, or masked by sedimentary burial or tectonic deformation. On Mars, by comparison, the general stability of the crust since the LHB has helped preserve substantially more craters – several thousand – although erosion and superimposed larger impacts with ejecta blankets have erased some of them.

There are currently over 176 confirmed impact craters on Earth, ranging in diameter from as little as a few tens of metres to about 300 km (Grieve, 1991; Grieve et

al., 1996; Earth Impact Database, 2010). This represents a small fraction of all impact structures on Earth but the number increases constantly as new discoveries are made.

2.2 Hydrothermal Processes

2.2.1 Planetary Distribution of H_2O

Planetary bodies with a solid surface have the potential to host or trap liquid water or water ice, depending on the nature, composition and temperature of its atmosphere. More than 70% of the Earth's surface is covered by oceans and has an active hydrological cycle. Water is believed to have flowed on the surface of Mars billions of years ago as observed by the Mars Exploration Rovers (Squyres et al., 2004), and orbital spectroscopy (Bibring et al., 2004). The recent discovery of water ice in the first tens of centimetres of Martian regolith by the Phoenix Lander shows that widespread subsurface water could exist on this planet (Smith et al., 2009). It had already been acknowledged that today's surface water on Mars had to be frozen and not liquid, as in the polar caps, as atmospheric temperatures and most importantly pressures are too low to support liquid water at the surface. However, it is uncertain as to how water originated and evolved in different regions and time periods in Mars' history, as well as how much water is liquid and could be trapped underground during impact events (Lunine et al., 2003).

2.2.2 Geological Environments Hosting Hydrothermal Activity

The main environment that comes to mind when searching for hydrothermal activity is the ocean floor, usually at spreading centers, where various structures such as white and black smokers tower many metres high as chimneys releasing their fluids (Früh-Green, 2003). The laws of thermodynamics have direct consequences where high-

temperature fluids, rich in metals, sulfur and sometimes methane, mix with low-temperature undersaturated seawater to deposit sulphides later used by microbial communities and sea life (Staudigel et al., 2006). Overall, throughout Earth history, the upper portion of the oceanic crust in general but especially subduction zones, accreted terranes (i.e., ophiolites) and rifts have been host of major hydrothermal activity (Kelley et al., 2002). Pirajno et al. (2005) made an excellent review of hydrothermal processes and systems on Earth, and their implications for Martian analogues. A diverse range of geological settings exists for small and large hydrothermal systems to form on Earth, where usually magmatic intrusions provide a heat source for convective water cells to circulate and migrate continuously in the rocky surroundings. Dewatering of heated and buried sediments or rocks could induce migration of waters towards cooler terrains where a hydrothermal system and eventually mineral deposits would form (Lindgren, 1933). Understanding that higher porosity and permeability is required in order to generate significant fluid flow, it is also equally important to assess directions of fluid flow and amounts of ions in solution in a hydrothermal system (Jamtveit and Yardley, 1997).

2.3 Hydrothermal Systems in Impact Craters

2.3.1 Transient Nature of Impact-Induced Hydrothermal Activity

The essential condition for the formation of hydrothermal systems in impact craters is that water should be present in sufficient amounts in target lithologies (Naumov, 2005). An impact into a dry landmass (i.e., water table is absent) could also trigger post-impact hydrothermal activity if it contains enough volatiles and hydrous minerals that could be decomposed upon impact to release water (Reimold et al., 2005). Once the water requirement is met, hydrothermal processes could begin beneath and in the vicinity of the

impact structure as long as thermal energy keeps this water in circulation. The heat principally originates from the kinetic energy of the impactor transferred to the target rocks by the passage of the shock wave, generating shock heating *per se* and frictional melting and heating (Melosh, 1989). Moreover, heat from friction during fault movement will be accumulated in the central region of the crater during the modification stage as the structural uplift is forming (French, 1988) (Figure 2.1). In recent decades, the recognition of impact melt rocks in several terrestrial impact craters led to the conclusion that most craters would have had this additional type of in situ heat source to induce prolonged hydrothermal convection of subsurface water (Dressler and Reimold, 2001). Most of the heat will therefore be concentrated towards and beneath the center of impact craters, generally causing more pronounced and diverse types of hydrothermal alterations in the centre rather than on the outer edges (e.g., Osinski et al., 2005a). Temperature gradients must exist within different zones of permeable rocks, even impact melt rocks, for water to be entrained into a regenerative circulation system. An important factor in facilitating fluid circulation is the possible increase in permeability due to shock-fracturing and volatilisation of lower-temperature phases. In large craters, this zone could extend to several kilometres deep (Naumov, 2005). Since the central uplift has generally greater permeability and more heat per unit volume than the rim, it is believed that fluids should flow up and then laterally, away from the central region, at shallow depth. These cooling fluids would then migrate deeper in the rim region and recharge the central uplift back again in the form of a circulation cell, as described by Naumov (2005) (Figure 2.2).

Although shock-induced hydrothermal processes could be very active, they tend to last only for a certain amount of time (debatable, but possibly thousands to a million

years) before they vanish, hence their transient nature. There is no exception to this rule, as indicated by models and geological data (Melosh, 1989). However, the duration of the convective process is directly related to the magnitude of the impact event: the larger an impact is, the longer the system is expected to remain active. With time, heat dissipation results in a decrease in temperature contrast between the colder and warmer parts of the circulation cells, and the system becomes less effective in displacing fluids into the brecciated rocks. Subsequently, the circulation cells will stop and fluid pathways will be sealed. The duration of an impact-generated hydrothermal system is variable; yet, extended periods of many thousands of years are thought to be common (Abramov et al., 2004; Jõeleht et al., 2005). Million-year-long hydrothermal regimes are hypothesised for the largest structures on Earth such as the Sudbury impact structure (Ames, 1998; Molnar et al., 1999), which could have been subject to one to two millions years of hydrothermal activity. In the long term, hydrothermal activity can cause noticeable alteration patterns within the host-rocks of sufficiently large impact craters because these structures can sustain hydrothermal activity for a longer period.

2.3.2 Terrestrial Occurrences of Hydrothermal Activity in Impact Craters

Because thermal energy dissipates and it cannot be replenished, the hydrothermal system cools down over time. In all cases, field observations support this concept as the typical hydrothermal mineral paragenesis of terrestrial impact craters is always retrograde (i.e., from higher- to lower-temperature forming secondary minerals over time) (Naumov, 2005). Whereas the development of a hydrothermal system depends on the kinetic energy of the impactor as well as the presence of water in the target rocks, the nature of hydrothermal minerals is strictly dependent on target composition and the setting (i.e.,

continental versus marine). Secondary mineral paragenetic sequences are, therefore, diversified both in composition and intensity, based on target lithologies and water availability, respectively.

From the ~176 craters found on Earth to date, more than 60 are believed to have been subject to impact-induced hydrothermal activity (Figure 2.3) (Naumov, 2002). A crater must have a minimum diameter of about 2 kilometres but there is no upper size limit. Craters formed in shelf or intra-continental shallow basins are usually those showing the more extensive post-impact hydrothermal alterations (Newsom et al., 1986; Osinski, 2005) and Manson impact structures (Boer et al., 1996). The magnitude of the alteration is much less on a dry landmass, such as for the Popigai impact crater, although the degree of water saturation of the target rocks and the size of the circulation cells play an important role (Naumov, 2005). Impacts occurring in marine environments are also host to alteration processes that are similar to other settings although the water source could be complex to identify, such as for the shallow-marine impact origin of the Wetumpka structure in Alabama, USA (King et al., 2002), and the Siljan crater, Sweden, which is the largest impact crater in Europe (Hode et al., 2003). At the Siljan impact crater, drilling and surface geology indicate that hydrothermal fluids affected the entire 52-km diameter structure to a depth greater than 1 km (Komor et al. 1988). The marine location of the Chicxulub impact event is thought to have contributed to large-scale hydrothermal alteration from percolating waters mainly into the impact-breccia horizons (Zürcher et al., 2004). Impacts that have occurred in sedimentary sequences overlying crystalline basement are common, and examples of known craters displaying secondary mineral assemblages are again the Siljan crater, but also the Lockne (Sturkell et al., 1998)

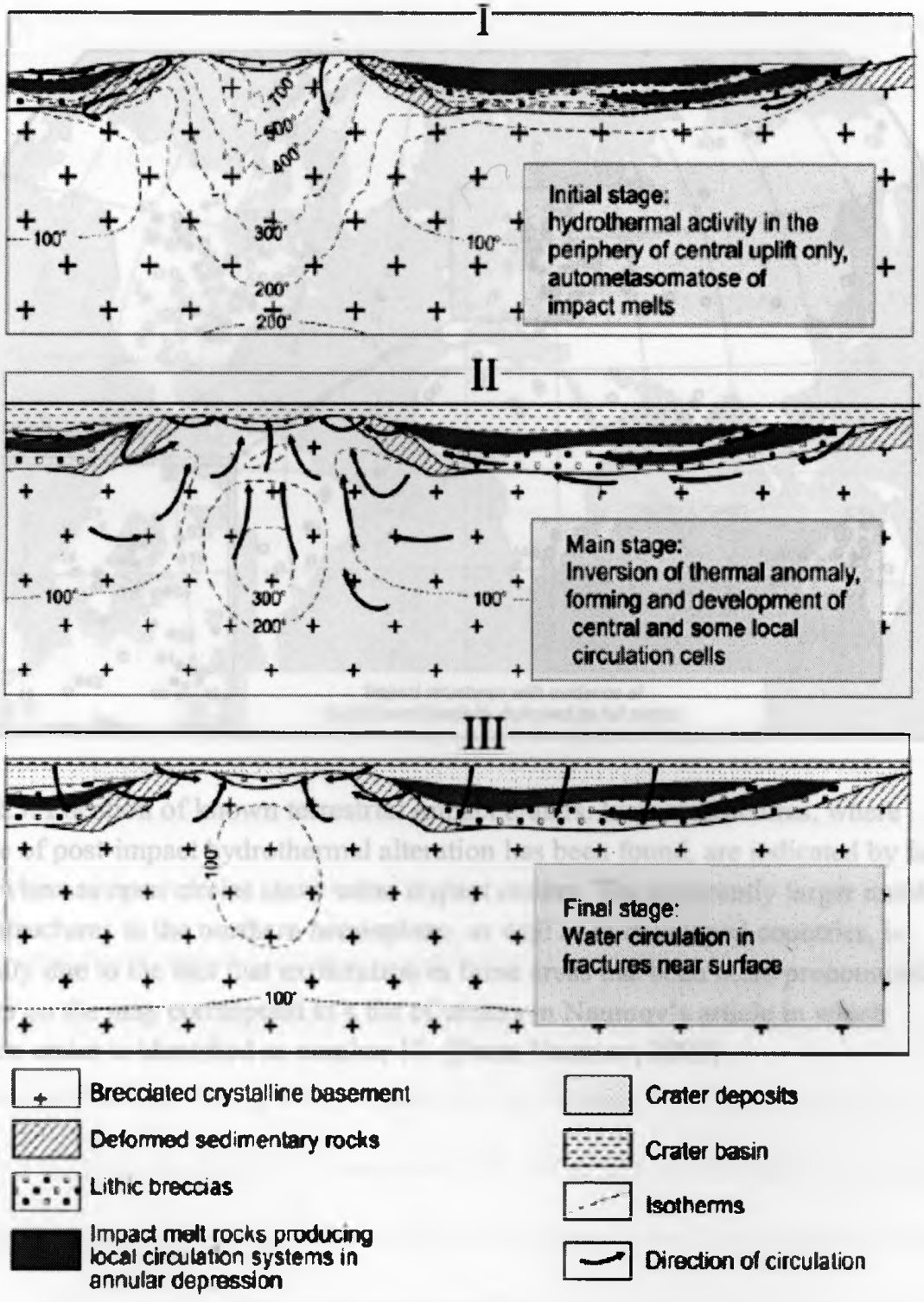

Figure 2.2. Generally accepted stages of hydrothermal fluid circulation within an impact structure. The hydrothermal system in this case is hosted by a complex impact structure partially covered by impact melts, thus comparable to the Haughton impact structure. The three stages illustrate the regressive nature of thermal gradients within fluid circulation cells. (From Naumov, 2005).

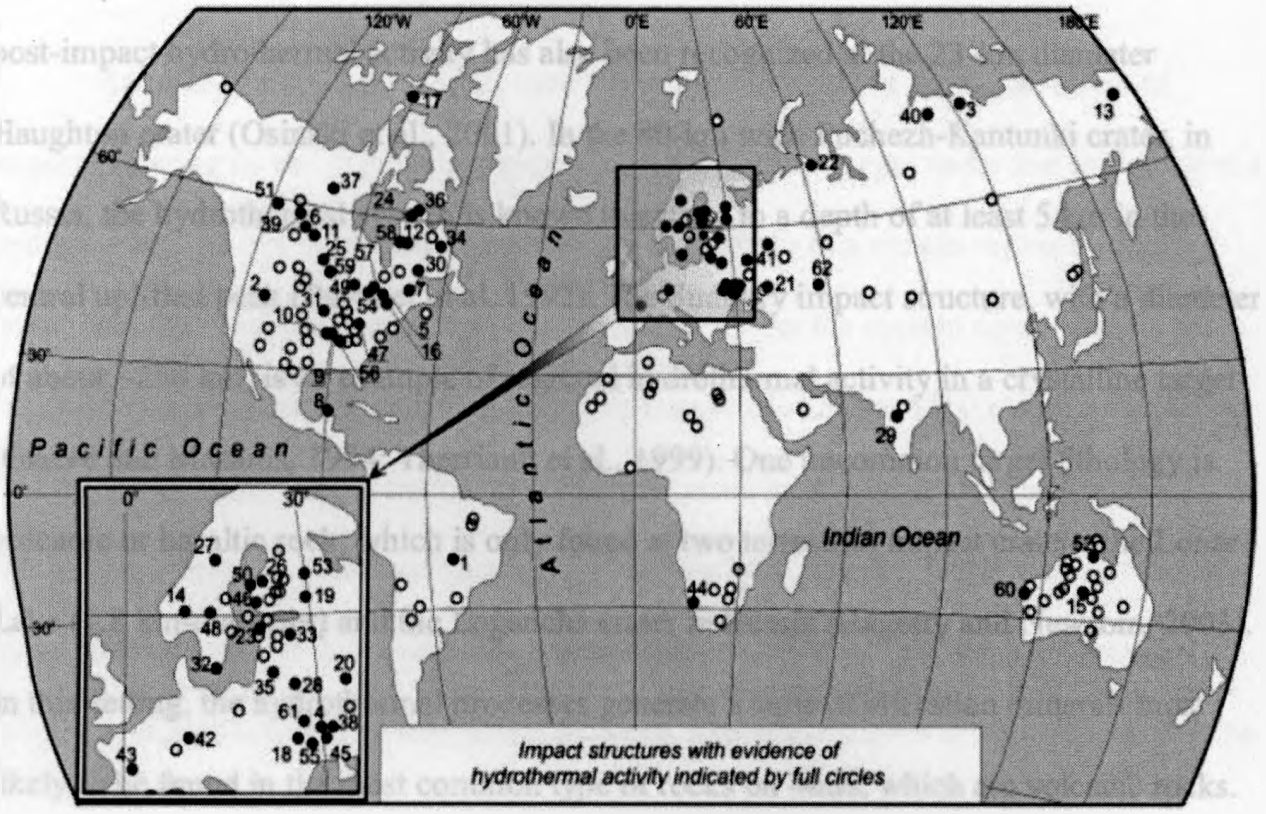

Figure 2.3. Location of known terrestrial impact craters. Impact structures, where evidence of post-impact hydrothermal alteration has been found, are indicated by full circles, whereas open circles show other impact craters. The apparently larger number of impact structures in the northern hemisphere, as well as in developed countries, is principally due to the fact that exploration in these areas has been more pronounced. Numbers on the map correspond to a list of craters in Naumov's article in which Haughton crater is identified as number 17. (From Naumov, 2005).

and the Kärdla impact structures (Versh et al., 2003). As discussed throughout this study, post-impact hydrothermal activity has also been recognized at the 23-km diameter Haughton crater (Osinski et al., 2001). In the 80-km wide Puchezh-Kantunki crater, in Russia, the hydrothermal system is known to extend to a depth of at least 5 km in the central uplifted peak (Pevzner et al. 1992). The Sudbury impact structure, with a diameter of about ~250 km, is an example of regional hydrothermal activity in a crystalline target (Grieve and Masaitis, 1994; Therriault et al., 1999). One uncommon target lithology is volcanic or basaltic rock, which is only found at two terrestrial impact craters, the Lonar Lake (1.8 km-diameter) and the Logancha crater in Russia (Hagerty and Newsom, 2003). In this setting, the hydrothermal processes generate a suite of alteration minerals most likely to be found in the most common type of rocks on Mars, which are volcanic rocks.

In general, impact craters in different settings exhibit similar mineral assemblages dominated by clays, zeolites, calcite and pyrite, with the possibility of other silicates, like quartz. The temperatures of formation are also similar, generally ranging from 300 °C to less than 50 °C. The presence or absence of sedimentary and/or crystalline rocks will influence the final mineralogy of the hydrothermal alteration. For example, clays will not be formed in carbonate targets. It is however difficult at first to distinguish the origin of their formation, as to whether they were formed by other types of hydrothermal system. (Naumov, 2005) Usually, shock-metamorphic effects are unequivocal evidence that an impact has occurred, which could later be altered by hydrothermal fluid circulation (French and Short, 1968).

2.3.3 Evidence for Impact-Induced Hydrothermal Activity on Mars

Rathbun and Squyres (2002) used computer modeling to verify the effect of impact cratering on the distribution patterns of water in the target rocks and showed that a hydrothermal system is created, but it evolves differently in a simple versus a complex crater, and the timescales are not well constrained. Under the current conditions on Mars (atmospheric pressure of 0.006 bars and temperature of -125° to 25°C), they show that a hydrothermal system could be formed. As many as ~40,000 impact craters have been formed on Mars throughout its history, representing considerable sources of heat for hydrothermal systems to be induced (Thorsos et al., 2001). Besides impact structures, large volcanic provinces are also found on Mars, although edifices are not supposed to be active anymore. The widespread surface features indicative of flowing water early in Mars history (and possibly still today) and the recent discovery of water ice in the northern pole regolith by the Phoenix lander (Smith et al., 2009) strengthen the hypothesis for hydrothermal activity on Mars. Brakenridge et al. (1985) discuss the possibility of hot springs on Mars but do not specifically target impact craters. Squyres (1989) defends the case for water on Mars years before succeeding in sending the two Mars Exploration Rovers that continue to explore the surface (Squyres et al., 2004). They found sedimentary deposits, notably in impact craters, rich in minerals such as jarosite that would have had to be formed by subsurface water. More recently, Bibring et al. (2006) interpreted OMEGA (Observatoire pour la Minéralogie, l'Eau, les Glaces et l'Activité) data from the Mars Express spacecraft and showed the presence of hydrous mineral phases such as phyllosilicates in a cratered region cut by flow channels, which is strong evidence for water on Mars.

The different types of environments where hydrothermal activity might be expected on Mars have been compiled in Schulze-Makuch et al. (2007), who highlight the potential for large impact craters as hosts of hydrothermal systems. The preponderance of impact craters in the southern highlands of Mars implies more impact-induced hydrothermal systems can be found in these terrains, for example in the Hellas Basin, the largest impact crater on Mars. Furthermore, Martian meteorites recovered on Earth are a direct piece of evidence for hydrothermal activity of the Martian crust since they show hydrothermal minerals (Bridges, 2001). If the subsurface is widely saturated in water as it is believed to be, then the potential for finding fossil hydrothermal systems on Mars is high, especially in regions excavated by impacts and associated ejecta deposits (Schulze-Makuch et al., 2007).

2.4 Impact-Generated Hydrothermal Systems as Habitats for Life

2.4.1 Favourable Conditions to Life

During its accretion, Earth accumulated elements and compounds essential for life, such as oxygen, hydrogen, carbon and nitrogen. In order to have a general idea about where to find more hospitable areas in the universe, the concept of the Habitable Zone (HZ), which encompasses the older idea of Circumstellar Habitable Zone of Huang (1959) and the more recent concept of Galactic Habitable Zone introduced by Gonzalez (2001), is put forward. Any form of life-as-we-know-it requires the presence of H_2O, in liquid state, to exist. Because the presence of water is considered essential for life, zones within our Solar System and in the whole galaxy having the right conditions for liquid water are targets for astrobiology (Schulze-Makuch, 2004). To maintain this water, temperature will have to be in a specific range (0-100°C at 1kilobar of atmospheric

pressure). Life on other celestial bodies is a possibility, even if it is too cold for water to be in a liquid state (Irwin and Schulze-Makuch, 2001). It is believed that other solvents or mixtures of solvents with water, such as methane found on Europa, one of Jupiter's moons, or Titan, one of Saturn's moons, would act in a similar way as water alone, but the fact that it is less efficient causes debate (Schulze-Makuch, 2004; Javaux, 2006).

In the past few decades, the discovery of living communities in once-thought inhospitable habitats has obliged scientists to redefine the range of environmental conditions acceptable for life. Although rare in nature, some organisms can not only survive but also proliferate in extremely harsh terrestrial environments (i.e., extreme in temperature, salinity, pH, water, oxygen, radiation, or many of these at a time). For instance, microorganisms have been found living in deep oceanic volcanic vents under high pressure and temperatures of up to 123°C (Kelley et al., 2002), permafrost, sea-ice and glaciers (Price, 2007), with temperatures of growth below 0 °C, and even at a depth of 2.7 km underground (Kounaves, 2007).

The thermophilic or "heat-loving" micro-organisms are characterised as microbes that could survive in high temperatures of up to well above the boiling point of water (Schulze-Makuch, 2004). These microorganisms are particularly interesting for the search for the origins of life as they occupy the most primitive branches of the tree of life (Wiegel et al., 1998). This implies that they might have existed already on the early Earth, when conditions prevailing at that time were probably considerably warmer, such as in hydrothermal hot springs or deep-sea vents. In addition, microbes that use chemosynthesis as a way to get their energy do not have to rely on solar energy, which proves beneficial to colonise sub-surface environments. The exact origin of life has not

yet been established and the debate is still open (Wiegel et al., 1998). However, it is important to remember is that life was already thriving in extreme conditions not long after the Earth formed, and has survived to this date. The survivability and potential for adaptation of such thermophiles throughout geological time make them great candidates for first colonising a freshly formed impact crater, as long as a sustained source of fluid is present (i.e., hydrothermal water).

Several studies have shown that life is possible in either extremely hot or cold environments (Kelley et al., 2002; Priscu et al., 2005; Furnes et al., 2007). A hot origin of life is often based on the fact that the lowest branches of the tree of life, in other words the most primitive life forms, are more occupied by hyperthermophilic (heat-loving) than psychrophilic (cold-loving) organisms, suggesting that life appeared in hot environments (Setter, 2006; Bada et al., 2002). Alfonso et al. (2005) describe a recent example of the implications of biological chemosynthesis processes in hydrothermal deposits. Their work on carbon, oxygen and sulfur isotopes from gasohydrothermal vent mineralisation in Mexico tends to strengthen the case for biogenic precipitation as the main process involved (Alfonso et al., 2005). This is the first documented case into a shallow submarine hydrothermal environment, thus the correlation to Haughton crater is easier to do than with deep-sea vents.

It is argued that life could have arisen before the Late Heavy Bombardment period but then meteoritic impacts sterilized Earth from previously developed organisms (Lineweaver, 2004; Javaux, 2006). This would imply that Earth became inhospitable, in addition to ozone build-up in the atmosphere almost two billion years later,therefore,

fragile organisms would have been exposed to continuous solar radiation that would have been lethal. If indeed life had emerged before the Late Heavy Bombardment, the fossil record would have vanished (Javaux, 2006). Certainly, transient conditions during and following impact events are believed to be favourable for life (Osinski et al., 2005c; Cockell et al., 2006).

2.4.2 Evidence for Life in Hydrothermal Systems of Impact Craters

Hode et al. (2003) evoke that the most likely niche for life in the complex and mineralised Siljan impact structure, the largest in Europe, would have been the hydrothermal system around the rim of the crater. After progressive heat dissipation of the system, the central uplift would have become a potential habitat. Then, thermophilic micro-organisms could have migrated inwards as the temperatures cooled below 150°C. The Siljan crater, as for Haughton crater, is of high interest because of the similar ranges of fluid temperatures and host rocks, as well as the preponderance of hydrothermal activity around the crater rim region (Osinski et al., 2005a).

Recognition of life in impact-hydrothermal systems could be done by looking for evidence of fossil biofabrics within hydrothermal mineral assemblages (Hofmann, 2000). For instance, microbes could generate anomalous micro-textures within minerals or at their surfaces, leaving behind (Hode et al., 2008). Although such biological activity is thought to last for millions of years in some cases (Furnes et al., 2007), the proof is often not equivocal, mainly because the small size of these bio-traces (orders of magnitudes lower than mineral grain size) makes them very difficult to analyse.

2.4.3 Implications for Astrobiology

The implications of hydrothermal systems in impact craters regarding the origins of life are significant. Microbial colonisation of the early Earth, Mars and satellites of the Solar System could well have been common in the past when the rate of impact cratering was much higher. Therefore, it is reasonable to suspect that impact craters are a possible niche for life to develop, mainly because of the transient hydrothermal conditions prevailing for many thousand years. The possible discovery of fossils in the hydrothermal alterations at Haughton crater is a driver for the present thesis, and future work on hydrothermal alteration at Haughton.

The question as to whether or not hydrothermal systems generated by impact craters could harbour life has astrobiological implications. No study has yet demonstrated that micro-organisms were responsible for mineral precipitation or micro-textures, and/or isotopic fractionation within a hydrothermal system formed after the impact of an asteroid or comet on a planetary surface. Thus, this study focuses on chemical and isotopic compositions of mineral assemblages found specifically in the hydrothermal veins and vugs within the Haughton impact structure, Canada, as well as pipe structures on its outer rim, to bring insight into the nature of the hydrothermal fluids. Perhaps microbial communities have colonised the system at an early stage. Several constraints on the origins and properties of the fluids, using fluid inclusions, have already been discussed in Osinski et al. (2005a). However, the isotopic analysis of the hydrothermal carbonate phases should provide even more insights on the evolution of the hydrothermal system, especially on the temperature history of the fluids.

Sulfur-metabolising micro-organisms are probably the most interesting group of thermophilic organisms to search for as they survive under a wide range of temperatures and have the highest growth temperatures of all extremophiles (Wiegel and et al., 1998). Consequently, they could have had a very good potential for an early and sustained colonisation of the Haughton crater hydrothermal system. Certainly, observation of all mineral phases of a thin section is the key, as some organisms could prefer quite unexpected settings such as aphanitic glass (Furnes et al., 2007).

2.5 Principles of Stable Isotope Science

2.5.1 Introduction to Isotopic Fractionation

Stable isotopes are a powerful tool in identifying the compositional source of atoms in minerals. The carbon and oxygen isotopic ratios of minerals might be relevant for understanding what mixture of fluids involved in the hydrothermal deposits, and under which conditions the minerals formed.

The carbon and oxygen isotopic compositions are usually reported in δ-notation relative to VSMOW (Vienna Standard Mean Ocean Water; Coplen, 1996) for oxygen and VPDB (Vienna Pee Dee Belemnite) for carbon. The δ-notation is defined by McKinney et al. (1950) as

Eq. 2.1

$$\delta = \left(\frac{R_x - R_{std}}{R_{std}}\right) \times 1000$$

where R represents the ratio of the heavy isotope over the light isotope of an element (e.g., $^{18}O/^{16}O$ or $^{13}C/^{12}C$) for a sample x and a standard std, reported in permil (‰).

The carbon and oxygen isotopic compositions of carbonates are determined based on a standard procedure which is the reaction with 100% phosphoric acid to liberate CO_2, which is later analysed in a mass spectrometer for isotopic ratios (Hoefs, 1973). The reaction is expressed as follows

Eq. 2.2

$$3\ CaCO_3 + 2\ H_3(PO_4) \rightleftharpoons 3CO_2 + 3\ H_2O + Ca_3(PO_4)_2$$

Fractionation processes, which are responsible for preferential partitioning of stable isotopes in two substances or phases, are numerous. In general, isotope exchange reactions under equilibrium conditions and kinetic effects (incomplete or unidirectional reactions) are the most common processes. The temperature at which these processes occur normally plays a role in the degree of fractionation observed (Hoefs, 2004).

2.5.1.1 Carbon Isotope Ratios

Carbon has two stable isotopes, ^{12}C and ^{13}C, occurring in nature at 98.89% and 1.11% respectively, which are subject to fractionation by inorganic and organic reactions (Nier, 1950). The difference between the $^{13}C/^{12}C$ ratio of a specimen and that of a standard is called $\delta^{13}C$, expressed in parts per thousand on the internationally recognised VPDB scale (‰, VPDB) (Hoefs, 1973). There is a wide variation in $\delta^{13}C$-values of more than 100‰ in natural compounds, as low as -80‰ for light methane, and extra-terrestrial matter shows a wide range of values that could be significantly different from terrestrial compounds (Figure 2.4). The two main reservoirs on Earth are sedimentary carbonates and organic matter. In general, carbonates are enriched in ^{13}C because of carbon exchange with the atmosphere, while organic material is depleted in ^{13}C due to photosynthesis.

2.5.1.2 Oxygen Isotope Ratios

Oxygen is the most common element on Earth, and because it is stable over a wide range of temperature, oxygen isotope studies are very useful for solid, liquid or gaseous phases or a combination of these phases. Oxygen has three stable isotopes, ^{16}O, ^{17}O and ^{18}O, in abundances of 99.763%, 0.0375% and 0.1995% respectively, which are also subject to fractionation by inorganic and organic reactions (Garlick, 1969). In general, from solid to gaseous phases, compounds tend to get depleted in the heavy isotope ^{18}O by different mechanisms such as evaporation-condensation and kinetic effects. As for carbon isotopes, the difference between the $^{18}O/^{16}O$ ratio of a specimen and that of a standard is called $\delta^{18}O$, expressed in parts per thousand on the VSMOW scale (‰, VSMOW) (Hoefs, 1973). In nature, a wide range of $\delta^{18}O$-values of about 100‰ is observed (Figure 2.5). The ^{17}O isotope is not taken into consideration here, but a three-isotope study could reveal additional information, notably to differentiate between terrestrial and extra-terrestrial oxygen compounds.

2.5.2 Isotopic Compositions of Natural Carbonates

2.5.2.1 Seawater and Freshwater Carbonates

Carbonates that are precipitated at the Earth's surface under normal low-temperature conditions vary in carbon and oxygen isotopic compositions (Figures 2.4 and 2.5). Several types of sedimentary deposits and biogenic carbonates show various $\delta^{13}C$-values. The $\delta^{13}C$-values observed are usually close to or above 0‰ (VPDB), although some data exist in the literature for heavy carbonates with $\delta^{13}C$-values above +20‰

(VPDB). The $\delta^{18}O$-values for natural carbonates normally cluster around +30‰ (VSMOW) but could vary (Hoefs, 2004). These values are discussed further in Chapter 5.

2.5.2.2 Hydrothermal Carbonates

Hydrothermal carbonates are normally depleted both in heavy carbon and oxygen isotopes relative to low-temperature carbonates (Versh et al., 2005). The carbon and oxygen isotope compositions of carbonates can be used to estimate the isotopic composition of the source fluid or mixture of fluids. The $\delta^{13}C$- and $\delta^{18}O$-values of carbonates precipitated in isotopic equilibrium with a fluid depend on many variables: 1) the isotopic composition of the fluid, 2) the temperature of formation and, 3) the proportions of carbon species such as CO_2, H_2CO_3, HCO_3- and CO_3^{2-} dissolved in the fluid. The presence or absence of species is directly related to pH and temperature. In most hydrothermal fluids with temperatures >100 °C, however, CO_2 and H_2CO_3 are the predominant species. The solubility of carbonates increases with decreasing temperature, as experimental studies have shown (Hoefs, 2004). Therefore, cooling of a hydrothermal fluid cannot be solely responsible for the precipitation of carbonate minerals in a closed system. The hydrothermal system must be open and processes such as CO_2 degassing, fluid-rock interaction or mixing of fluids will cause the precipitation of carbonate minerals (Hoefs, 2004).These processes result in correlation trends between $\delta^{18}O$ and $\delta^{13}C$ as often observed in nature and in the laboratory. Zheng et al. (1992) discuss the main contributing factors for covariation of $\delta^{18}O$- and $\delta^{13}C$-values in hydrothermal calcites illustrated in two-dimensional space diagrams. Isotopic investigations are particularly useful for discriminating between the different mixing processes.

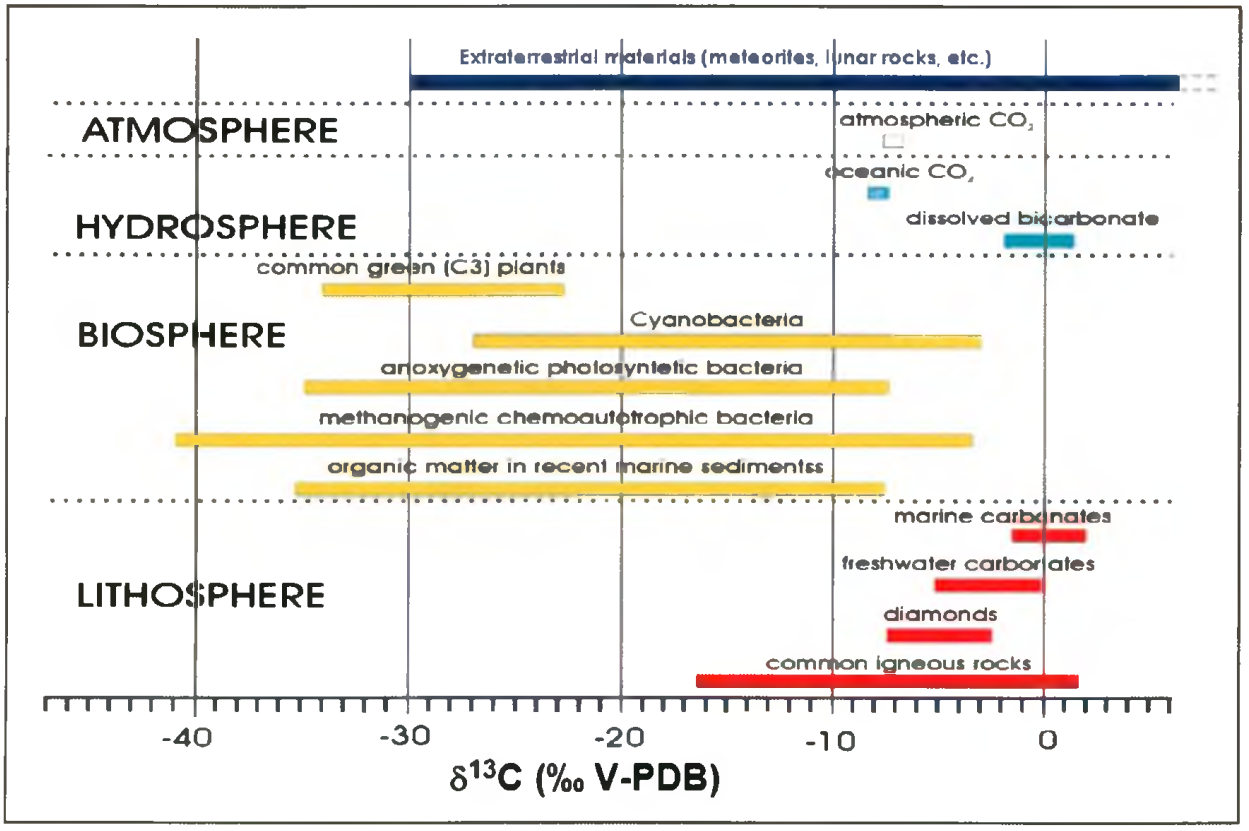

Figure 2.4. $^{13}C/^{12}C$ ratios of important carbon-bearing compounds. Carbon isotopic compositions, noted as $\delta^{13}C$-values expressed in ‰ relative to VPDB, are shown for commonly occurring compounds on Earth in the lithosphere, biosphere, hydrosphere and the atmosphere, as well as for extra-terrestrial materials. Atmospheric and oceanic carbon dioxides have narrow ranges of $\delta^{13}C$-values between -7 and -8‰. In general, carbonate minerals and rocks have $\delta^{13}C$-values between -20 and +5‰; the biosphere generates more depleted ^{13}C-compounds down to approximately -40‰. (From Versh et al., 2006).

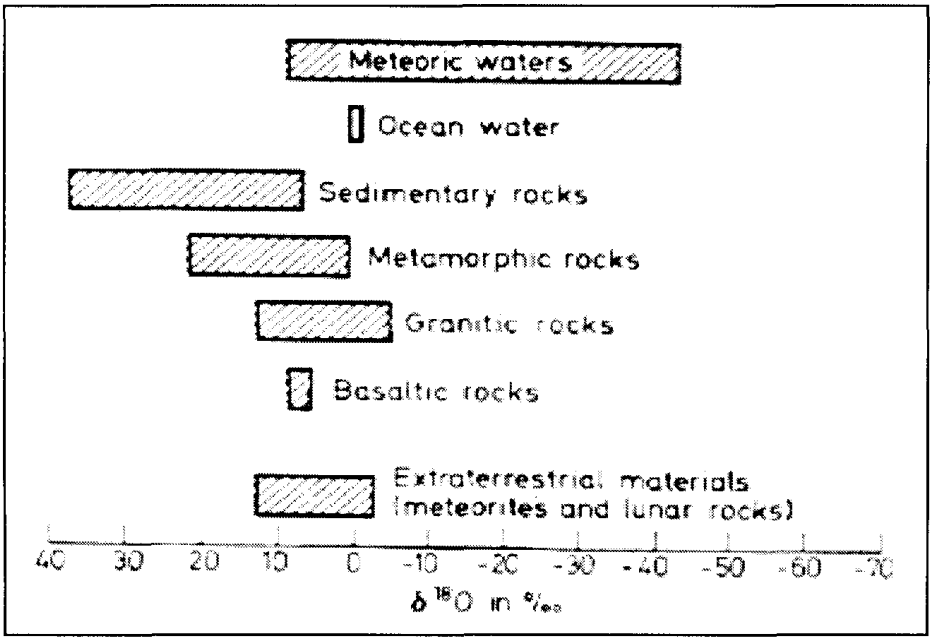

Figure 2.5. $^{18}O/^{16}O$ ratios of important oxygen-bearing compounds. Oxygen isotopic compositions, noted as $\delta^{18}O$-values expressed in ‰ relative to V-SMOW, are shown for terrestrial waters and rocks, as well as extra-terrestrial materials. Sedimentary rocks usually display higher ^{18}O- values compared to granitic and metamorphic rocks. Ocean water has a value close to 0‰. Meteoric waters display a wide range of values [-48 to +10‰] since they are derived from oceanic water that has undergone ^{18}O-enrichment or depletion through natural fractionation processes. (From Hoefs, 1973).

The fit of isotope data sets to one of the three simplified models proposed: 1) two-fluid mixing, 2) evolution of a single fluid, or 3) wall-rock interaction, can be utilised to place limits on the origin of fluids, mineralising temperature, and the mechanism of hydrothermal mineralisation (Zheng et al., 1993). There are significant temperature-dependent fractionation effects during deposition of hydrothermal calcite. It is possible to calculate fluid temperatures at the time of mineral precipitation, considering there was equilibration, by using the difference in $\delta^{18}O$-values of mineral pairs, possibly calcite-quartz, with $\Delta^{18}O$ calc-qz = $\delta^{18}O$calc - $\delta^{18}O$qz $\approx 10^3 \ln \alpha$ (Zheng et al., 1992). Thus, it should be feasible to identify when and where in the crater the range of temperatures were favourable to thermophilic microbial communities possible inhabiting the hydrothermal system before it inevitably cooled down. Significant isotopic fractionation can obviously result from the assimilation or the fixation of carbon by different organisms (Hayes, 2001); therefore, special attention should be given when strongly depleted isotopic signatures indicate a biogenic origin.

2.5.2.3 Study of Impact-Hydrothermal Carbonates

To study carbonates that occur in an impact crater, a combined study of carbon and oxygen stable isotopes can be used to determine the context of their genesis, since distinct compositions characterise the main natural isotopic reservoirs. However, such reservoirs are numerous both for carbon and oxygen with ranges in composition that may overlap, thus complicating the interpretation of the origin of carbonates. Nevertheless, our stable isotope study offers data that can be used to help deciphering the conditions under which carbonates were deposited over time beneath the crater floor, and possibly on the surface as hot spring deposits. Since the study of post-impact minerals had not been done

before at the Haughton structure using stable isotope geochemistry, our data are essential in understanding the long-term effects of the Haughton impact event on the surrounding terrain. They also complement other data acquired at different impact craters worldwide where impact-generated hydrothermal alteration has been observed.

Chapter 3. Methods and Experimental Approach

3.1 Samples

The geological material upon which this study was first based is the field sample collection from G. R. Osinski at the University of Western Ontario. This collection comprises, for the most part, hand-size rock samples gathered over 10 field expeditions from 1999 to 2008. Some unshocked samples originate from outside the crater, but most were collected within the various settings of the Haughton impact structure, and display characteristic features consistent with shock and hydrothermal alteration. Field sampling was performed in July 2008 by the author to add to the collection of hydrothermal samples and also to collect more unshocked reference material. More than a hundred samples were brought back from this expedition. Approximately a hundred and fifty samples were directly analysed for this study, split equally between the 2008 field season and the G. R. Osinski collection. Appendix 1 provides the geographic coordinates, short description and relevant data. In addition, Appendix 2 shows stable isotopic data for some samples. At least one hand sample image of each sample was taken for reference. Polished thin sections of hydrothermal samples were also made for study under a polarising transmitted light microscope.

3.2 X-Ray Fluorescence Spectroscopy

X-Ray Fluorescence (XRF) analyses were carried out on 21 samples from the collection of G.R. Osinski on a PHILIPS PW2440 4kW automated XRF spectrometer system by Geochemical Laboratories, McGill University, Montréal, Canada. This system uses a rhodium 60kV end window X-ray tube, five X-ray detectors, four primary beam

filters, eight analysing crystals, two fixed channels for simultaneous measurement of Na and F, and PW2540 168 sample x-y autochanger. The major elements were analysed using 32mm-diameter fused beads prepared from a 1:5 sample: lithium tetraborate mixture. Minor element analyses were performed on 40mm diameter pressed pellets prepared from a mixture of 10g sample powder with 2g Hoechst Wax C Micropowder. These data were used as a first approximation to evaluate the mineral content prior to XRD analysis, especially for dolomite standards as described in later sections.

3.3 X-Ray Diffractometry

A sub-sample of each rock sample (~10 g) was collected using a small chisel and tweezers, or a small hand drill with a millimetre-size carbide drill bit (Figure 3.1), depending on the heterogeneity of the sample. Very small and delicate samples generally required the use of the electric hand drill; the detailed purpose of using this technique is explained in the following paragraph. Samples were then ground into a very fine powder (~50 μm) with a hand mortar and pestle for approximately twenty minutes to ensure uniform grain-size. Randomly oriented powdered samples were prepared on aluminum backpack mounts and were analysed for ~8 minutes ($2\theta = 2 - 82°$) using a Rigaku high brilliance rotating anode diffractometer with Co K-α radiation, with operating conditions of 160 kV and 45 mA. The minerals were then identified by comparing and matching the resulting X-ray diffraction profiles to pre-existing profiles in a pre-existing database. The results are compiled in Appendix 1.

3.4 Stable Isotope Analysis

3.4.1 Oxygen and Carbon Isotope Analysis of Calcite Samples

The main sampling strategy for stable isotope analysis was to select pure calcite that was fresh, with no or extremely little Fe-oxide alteration, no secondary recrystallisation, and if possible not friable. Appropriate hydrothermal vug-fillings averaging ~10cm in diameter were sampled on the margin, which is assumed to be the earliest crystallisation phase, and often at one or more occasions towards the centre point (i.e., the latest crystallisation phase) (i.e., Uysal et al., 2009). The thickness of hydrothermal vein samples in this study varies from ~1mm to ~1cm.

The main concern while sampling was the close spatial proximity between hydrothermal calcite deposits and carbonates from the target rocks in which they occur. Carbonates from the impact melt breccias, as well as those from shocked and unshocked target rocks, needed to be identified before hydrothermal calcites could be analysed. Thus, care was taken to sample precisely and solely the hydrothermal calcite to prevent contamination from host-rock carbonates. For the majority of hand specimens, the characterisation and identification of hydrothermal calcite is straightforward: the hydrothermal calcite is in sharp contact with minerals from the host-rock, and an isolated sample can be taken.

The use of a hand-drill with a millimetre-sized carbide bit proved to be an efficient method to accurately sample the hydrothermal calcite, and not the wall-rock (Figure 3.1). For the most part, hydrothermal calcite vugs are already detached from the impact melt breccia matrix; therefore, the only requirement is to sample separately each hydrothermal

calcite layer (when present), which is also done using the hand-drill. The bit is cleaned with acetone and distilled water after each sample has been taken, and samples are put in individual sealable vials. In some instances, carbonates from the host-rock were also sampled using either the chisel or, if the sample was delicate or in close proximity to hydrothermal calcite, the electric hand-drill. Indeed, it was important to differentiate between impact melt and hydrothermal calcites within them. Although some studies do not make the distinction between carbonates of the matrix host-rock (i.e., Zurchers et al., 2005) versus post-impact hydrothermal precipitates, the origin matters when stable isotopic compositions have to be interpreted. In this study, it was necessary to differentiate the host-rock from the hydrothermal calcites as to gain separate insights on the rock-bearing and hydrothermal carbonates, respectively. In this study, the distinction between host-rock and hydrothermal calcite has been made and isotopic compositions reflect that of the hydrothermal phases *per se.* In one case, however, for samples from the Haughton River valley vug deposits, it was difficult to interpret the stable isotopic data; results might represent a mixture of calcite from the impact melt breccias groundmass overprinted by pervasive hydrothermal calcite. This is only the case when isolating the hydrothermal calcite from the host-rock was not totally possible. Additional XRF analysis would certainly be useful to better characterise hydrothermal minerals. At this point, XRD and XRF data reported in up-coming sections have allowed the selection of pure samples, most preferably pure hydrothermal calcite, for stable isotopes analysis.

Once sampling was done, powdered samples of pure calcite were brought to the Laboratory for Stable Isotope Science (LSIS), approximately 0.1 mg for each sample was accurately weighed on a micro-balance, and placed in reaction vials. Then, samples were

dried in a furnace at 70 °C overnight. Duplicates were made every 5 samples and standards were evenly distributed into the series, representing about 10% of the total number of samples. A septum-lined cap was screwed on the dry sample vials, which were then loaded on a MultiPrep autosampler. Orthophosphoric acid (H_3PO_4) was delivered automatically and introduced in the sample vials, by means of a needle connected to a tube, which reacted at 90 °C for 10 minutes. The complete analysis time for a sample is 35 minutes before the next sample is started. The reaction produced CO_2 gas from which the oxygen and carbon isotope ratios were measured using a dual-inlet VG Optima mass spectrometer. The $\delta^{18}O$- and $\delta^{13}C$-values were determined by calibrating after the method of Coplen (1996), and calibration was made against international standards NBS-18 and NBS-19. Internal calcite standards, WS-1 and Suprapur, were also run to measure precision and accuracy of the analysis. Data from standards indicate the reproducibility of $\delta^{13}C$- and $\delta^{18}O$-values was generally better than ±0.2‰ and ±0.5‰, respectively.

3.4.2 Oxygen and Carbon Isotope Analysis of Mixed Carbonate Samples

3.4.2.1 Problem of Naturally-Occurring Mixed Samples

Calibration of instruments in the LSIS for analysis of dolomite samples is normally performed with various calcite standards (i.e., NBS-18, NBS-19, etc.) and a single dolomite standard (DOLO368). A methodology that would involve multiple dolomite standards to analyse carbon and oxygen isotope ratios of dolomite samples is ideal; however, DOLO368 is the only standard currently available in the LSIS. For this reason, internal laboratory standardsintroduced from the Earth Sciences Dana collection were identified and put to the test via different techniques. Eventually, these dolomites could serve as reliable standards in the laboratory for analysing pure dolomite and

dolomite-rich samples. There are characteristic differences in the isotopic fractionation factors associated with phosphoric acid liberation of CO_2 from calcite versus dolomite and this has to be considered when isotopic compositions of different carbonates are compared (Hoefs, 1973). This is especially critical for this study since some samples are natural mixtures of dolomite and calcite and these two carbonate phases are difficult to physically separate for stable isotope analysis. Many studies in the past have not decided to ignore the literature on the ratios of different carbonate minerals in mixed samples for stable isotope analysis, and considered even less the best analytical method to be used. Being faced with samples containing dolomite and calcite is challenging since the right method should be used to minimise contamination issues and consequently false isotopic compositions. Once it is feasible to calibrate dolomite-bearing samples to have meaningful isotopic composition values, both calcite and dolomite from a single sample could be analysed independently. Thus, mixed carbonate samples could be analysed and their $\delta^{13}C$- and $\delta^{18}O$-values interpreted correctly.

Many stable isotope studies have over-simplified methodology and data interpretation procedures by assuming that a multiple carbonate sample (i.e., mixture of different carbonate minerals) can be analysed as a monomineralic sample, and that the $\delta^{13}C$- and $\delta^{18}O$-values are not significantly affected (e.g., Stoffers et al., 1994). Depending on the nature of the carbonates present in a mixed sample, the implementation of a methodology where separate analyses are made for each carbonate phase can have a significant influence on the resulting $\delta^{13}C$- and $\delta^{18}O$-values of a sample. Different carbonates see their carbon and oxygen isotopes fractionate differently under exactly the same conditions of extraction, plus different fractionation factors have to be used for

different carbonates. As a result, the determination of the carbon and oxygen isotope ratios from the extracted gas (i.e., CO_2) derived from the reacted sample is most certainly not representative of the sum of all carbonate constituents, since equilibrium has not been reached. This will alter or create uncertainty on the exact nature of the isotopic composition of the studied sample, and comparison with other samples will be difficult to make. It is a fact that certain samples containing a carbonate mixture are more sensitive than others, depending on the nature of each carbonate phase and, for instance, if the carbonates have similar reaction times before attaining equilibrium. Certainly, mixtures of dolomite and calcite are a good example of potentially large discrepancies that could arise between measured δ-values and ideal values. The study by Al-Aasm et al. (1990) on multiple-carbonate sample extraction techniques is an appropriate example of laboratory research applied to the development of ideal extraction techniques.

3.4.2.2 Selection of Internal Laboratory Standards for Dolomite

Potential dolomite crystals to be tested as dolomite standards were identified in the Dana Mineral Collection at the University of Western Ontario with the assistance of Dr. Roberta Flemming. Various carbonate minerals from worldwide locations are found in this collection. Altogether, a series of seven dolomite crystals were selected as potential candidates on the basis of their homogeneous apparence, euhedral crystal habit, and sample size sufficient to act as a standard. The dolomite crystal samples selected include: #423 from Guanajuato, Mexico; #1323 from Guelph, Ont., Canada; #2039 from Queenston, Ont., Canada; #2182 from Innsbruck, Austria; #3331 from Jelšara, Slovakia; #3617 from Pine Point, N.W.T., Canada; and a dolomite from Lockport, Niagara County, N.Y., USA.

One prerequisite for consideration of the candidate dolomite crystals as an internal standard is to confirm that they are indeed pure dolomite. X-ray diffraction (XRD) analysis was used in order to determine the purity of dolomite crystals and, therefore, to conclude whether or not a candidate was appropriate. A sub-sample of each crystal (~10 g) was collected using a small chisel and tweezers, and then ground into a fine powder (~50 μm) with a hand mortar and pestle for about an hour to ensure uniform grain-size. The candidate #438 was discarded at this point because of the sub-sample size being too small. Randomly oriented powders of the six remaining candidate standards were analysed for ~8 minutes ($2\theta = 82°$) using a Rigaku high brilliance rotating anode diffractometer with Co K-α radiation set at 160 kV and 45 mA. From X-ray diffraction profiles, mineral phases were identified. From the six candidates analysed, two were confirmed as pure dolomite: #3331 and #3617 (Figure 3.2). Remaining candidates were rejected based on various criteria: #2039 and Lockport dolomites contained minor calcite, whereas #1323 contained lots of calcite, and #2182 was composed of quartz and gypsum, as suspected. Once candidates #3331 and #3617 were identified as pure dolomite, it was necessary to evaluate their carbon and oxygen isotopic compositions and compare these with DOLO368. Since only three dolomites were plausible candidates, including DOLO368, it would be desirable if their relative isotopic compositions were spread over a wide range so that the range of the isotopic values from these newly selected internal standards would encompass the range of naturally occurring isotopic values of future unknown samples. If the range of values is large enough, which it was in our case, a calibration curve could also be constructed to correct unknown sample analyses in a similar way to the normally used calcite fractionation calibration curve which is a plot of known standard values from which values for unknown samples are corrected.

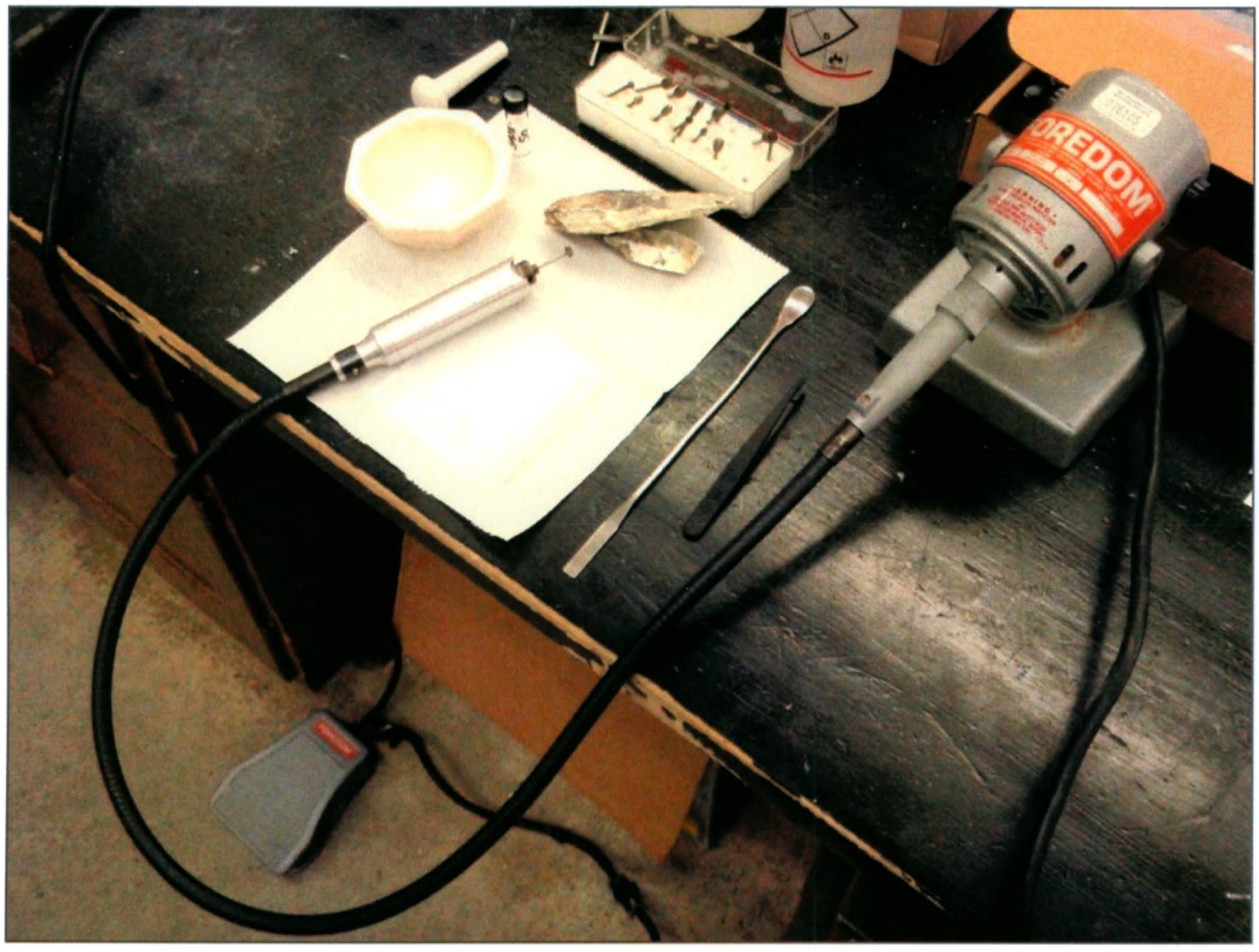

Figure 3.1. Sampling equipment used in this study for producing powdered mineral samples. The electric rotary drill is activated by a pedal, and various carbide bit sizes are available for sampling finer calcite vein and vug fillings. Sampling tools, such as tweezers and chisels, are also used for coarser calcite mineralisation. A mortar and pestle are necessary for grinding crystals prior to geochemical analysis.

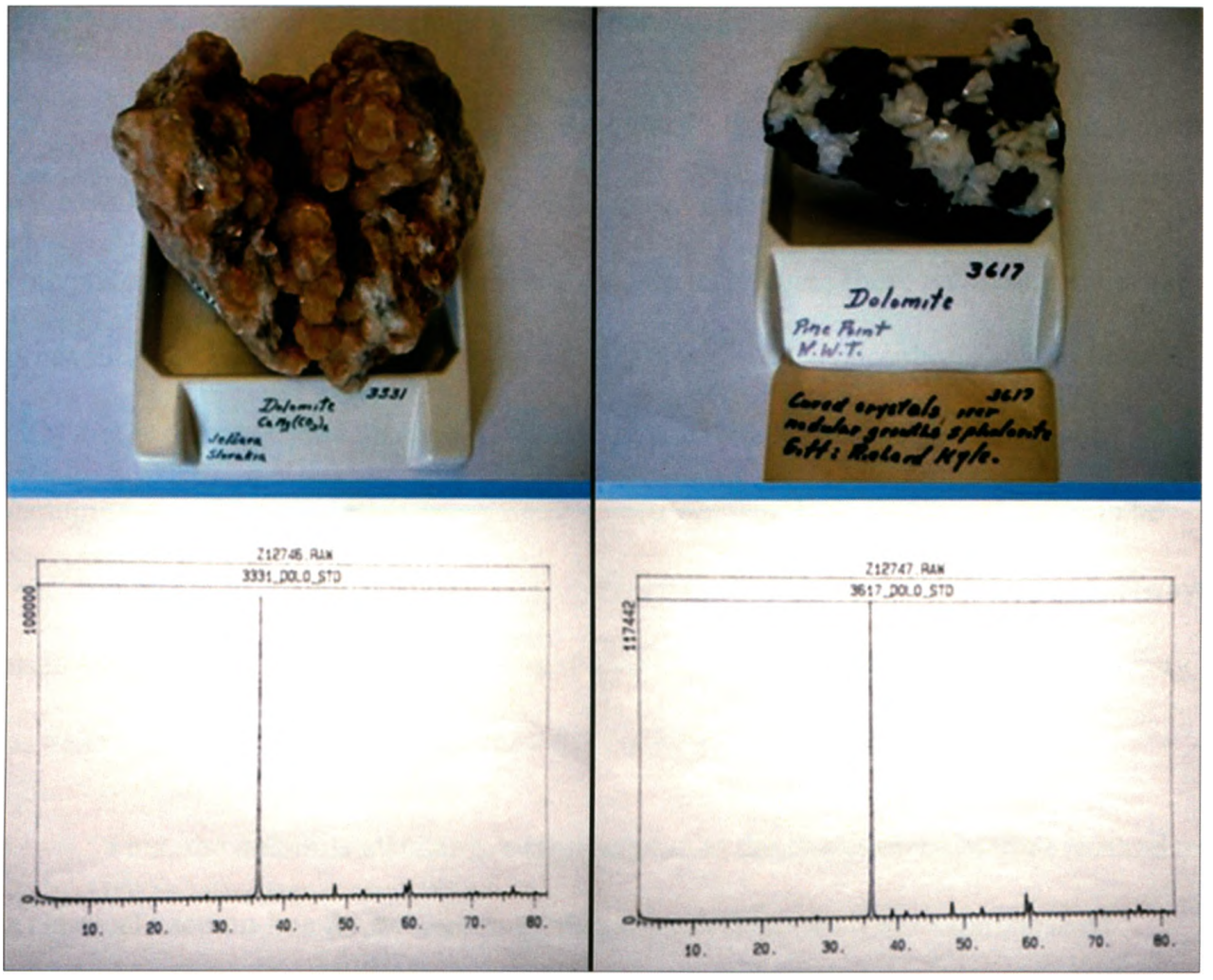

Figure 3.2 Natural dolomite mineralisation samples selected as internal laboratory standards for stable isotope analysis. Samples were powdered and analysed by XRD. The selection was first based on the sufficient quantity of crystal being available. More importantly, these two dolomites were the purest in composition as shown by their respective XRD profiles: the main diffraction peak of dolomite is at 36, as opposed to calcite which has a main peak at 34. The monomineralic nature of dolomites was essential for a meaningful characterisation of their carbon and oxygen isotopic compositions.

3.4.2.3 Conventional and MultiPrep Extraction Techniques

The $\delta^{13}C$- and $\delta^{18}O$-values of the candidate internal laboratory dolomite standards were evaluated using two independent techniques that have long been accepted: the conventional off-line technique and the MultiPrep technique. These are based on normal procedures for carbonates which involve reaction with 100% phosphoric acid to liberate CO_2 that is then analysed on a mass spectrometer to determine carbon and oxygen isotopic ratios. These isotopic ratios for dolomite standard DOLO368 are known to be +6.7 ± 0.5‰ (VPDB) and +30.7 ± 0.2‰ (VSMOW), respectively. DOLO368 was always used as a standard, along with the series of calcite standards, and analysed the same way as #3331 and #3617 for both techniques to verify the precision of the analyses.

First, the dolomite standards were analysed by the conventional offline method on a classical vacuum line for extraction of CO_2 from carbonates. The technique used followed the conventional methods of McCrae (1950) as well as that of Rosebaum et al. (1986) and has proven effective for $\delta^{13}C$ and $\delta^{18}O$ analysis of carbonate minerals. Duplicate powdered dolomites #3331, #3617, DOLO368 and calcite WS-1 were weighted (~5mg), put in reaction vessels and dried for two days in an oven at 70 °C. Then, 5ml of 103% orthophosphoric acid was pipetted in the side arm of the reaction vessel, separated from the dolomite sample itself. Vessels were capped and evacuated under vacuum for 2 hours. To remove all air bubbles and traces of water, if any, samples were heated using a heat gun. Prior to this stage, a large water bath was set at 50 °C. Since dolomite does not react significantly at room temperature, reaction times are shortened with increasing temperatures. The water bath could not easily maintain temperatures higher than 50 °C, so this temperature was chosen. Once samples were evacuated, vessels were carefully

immersed in the water bath and left there for 20 minutes to equilibrate to 50 °C. Then, the vessels were tipped to allow the reaction of dolomite with acid to begin and were left in the bath overnight (~15 hours). The samples were then put on the extraction line. Once more, a heat gun was used so that no CO_2 would be trapped in the acid residue. The carbon dioxide liberated from the carbonate mineral powder was extracted on the carbonate line. First, a liquid nitrogen (LN_2) and ethanol slurry traps water vapour at -80 °C and the remaining CO_2 is condensed and trapped in a sample vial using pure LN_2. Non-condensable phases are evacuated from the line during the process. Yields were measured on a separate line to make sure the reaction had gone to completion. Carbon and oxygen isotopic ratios were then measured using a dual-inlet DeltaPlus XL mass spectrometer (Table 3.1 and Figure 3.3).

The δ-values of DOLO368 are reproducible, $\delta^{13}C = +6.4 \pm 0.2‰$ and $\delta^{18}O = +30.6 \pm 0.2‰$, and compare well with its accepted values of $\delta^{13}C = +6.7‰$ and $\delta^{18}O = +30.7‰$. Similarly, dolomite #3331 analyses showed $\delta^{13}C = -1.6 \pm 0.1‰$ and $\delta^{18}O = +16.2 \pm 0.2‰$. The second vessel containing #3617 did not yield any valuable gas, thus only one analysis could be made which gave $\delta^{13}C = +0.7‰$ and $\delta^{18}O = +20.8‰$. Reproducibility was also verified by the WS-1 standards which was very close to theoretical values of $\delta^{13}C = +0.8‰$ and $\delta^{18}O = +26.2‰$. Most importantly, these results were especially valuable since the isotopic values of DOLO368, #3331 and #3617 were not clustered. The $\delta^{13}C$-values showed a total range of ~8‰ (from -1.6 to +6.4‰) and $\delta^{18}O$-values had a total range of ~15‰ from (+16.1 to +30.6‰), which may be sufficient for correction of naturally occurring samples and could potentially be used to form a calibration curve.

The second technique used to evaluate the isotopic composition of dolomites was the MultiPrep technique. Compared to conventional extraction, this is less time consuming and required less technical skill due to automation, but with very reliable results. The procedure for loading and reacting these carbonates is the same as for the natural samples from Haughton described in section 3.5.1. The reaction produced CO_2 gas from which stable isotope ratios were measured with a mass spectrometer, and the $\delta^{18}O$- and $\delta^{13}C$-values were determined by following the method of Coplen (1996). Twelve analyses were made, each time making sure that standards were within range of accepted values for carbon and oxygen isotopic ratios (Table 3.2, Figures 3.4 and 3.5).

The DOLO368 sample has averaged values of $\delta^{13}C = +6.1$ and $\delta^{18}O = +30.7‰$, which compares to its accepted values of $\delta^{13}C = +6.7‰$ and $\delta^{18}O = +30.8‰$. Dolomite #3331 had $\delta^{13}C = -1.6‰$ and $\delta^{18}O = +15.9‰$, whereas dolomite #3617 gave $\delta^{13}C$- and $\delta^{18}O$-values of +0.8‰ and +20.8‰, respectively. In general, a shorter reaction time generated similar δ-values as for longer reaction times, possibly because of the very high temperature of reaction in all cases. It appears that the averaged $\delta^{13}C$-values for DOLO368 are relatively lower than the accepted value of +6.7‰. However, by considering only the values for longer reaction times, results are closer to the accepted value. Moreover, the samples that yielded $\delta^{18}O$-values closer to the accepted value similarly show $\delta^{13}C$-values closer to the accepted value. As in this case, it is by considering the entire isotopic signature of a sample that results could be better interpreted.

Table 3.1. Table of results from carbon ($\delta^{13}C$) and oxygen ($\delta^{18}O$) stable isotope analyses of 3 dolomite standards (DOLO368, 3331 and 3617) by conventional off-line extraction technique. Reaction time of 18 hours, at a constant temperature of 50 °C. Each line shows data for a different sample. Standard deviation is indicated by σ. Values without a sign are assumed positive (+).

Sample ID	$\delta^{13}C$ VPDB [‰]	σ	$\delta^{18}O$ VSMOW [‰]	σ
Dolo368	6.48	0.15	30.84	0.21
"	6.46		30.29	
"	6.50		30.78	
"	6.50		30.66	
"	6.48		30.77	
"	6.10		30.39	
"	6.33		30.60	
3331	-1.64	0.03	16.03	0.17
"	-1.60		16.27	
3617	0.65	-	20.8	-

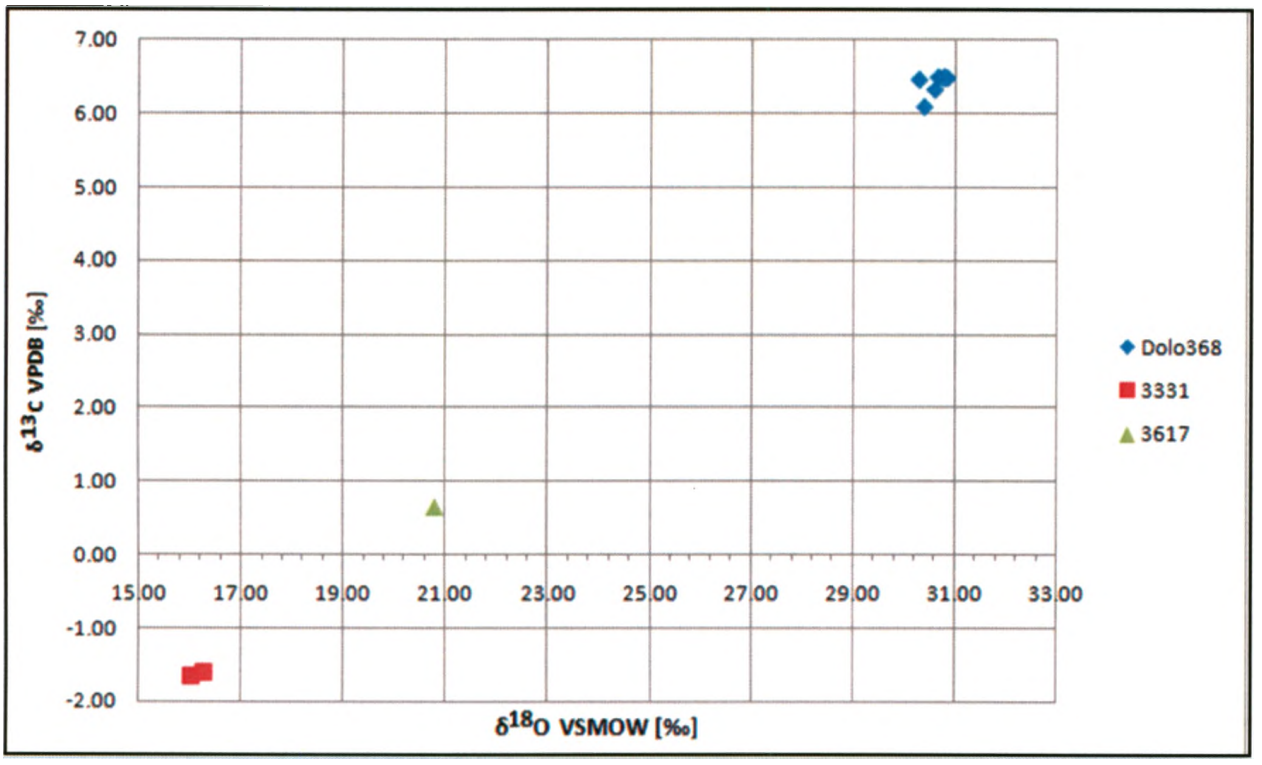

Figure 3.3. Results from carbon and oxygen stable isotope analyses of dolomite standards (DOLO368, 3331 and 3617) by conventional off-line extraction technique (as shown in Table 3.1). Reaction time of 18 hours, at a constant temperature of 50°C. Data reproducibility can be evaluated by the proximity of sample points for a given dolomite.

Table 3.2. Table of results from carbon and oxygen stable isotope analyses of dolomite standards (DOLO368, 3331 and 3617) by MultiPrep extraction technique. Reaction times of 10 minutes, 4 hours and 5 hours, at a constant temperature of 90°C. Standard deviation indicated by σ. Values without a sign are assumed positive (+).

Sample ID / Rx Time		Dolo368				3331				3617			
	Mins	δ13C	σ	δ18O	σ	δ13C	σ	δ18O	σ	δ13C	σ	δ18O	σ
10 minutes	10	5.63	0.57	30.48	0.40	-1.73	0.01	15.74	0.04	0.68	0.01	20.72	0.01
"	10	6.43		31.04		-1.74		15.80		0.69		20.74	
4 hours	240	-	-	-	-	-1.53	-	16.06	-	0.74	-	20.99	-
5 hours	300	6.02	0.26	30.16	0.64	-1.32	-	15.79	-	1.07	-	20.85	-
"	300	6.39		31.07		-		-		-		-	

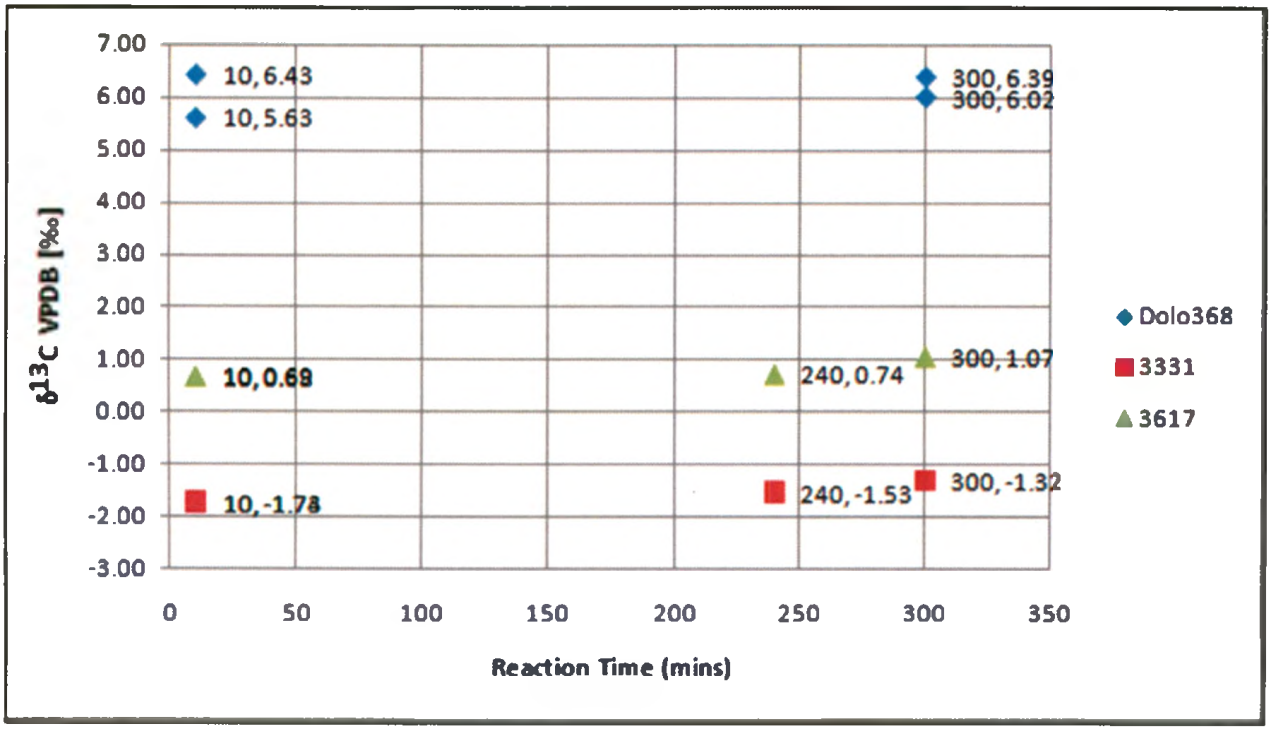

Figure 3.4. Results from carbon ($\delta^{13}C$) stable isotope analyses of 3 dolomite standards (DOLO368, 3331 and 3617) by MultiPrep extraction technique (as shown in Table 3.2). Reaction times of 10 minutes, 4 hours and 5 hours, at a constant temperature of 90°C. Data reproducibility can be evaluated by the proximity of the different sample points for a given dolomite (Dolo368, 3331 or 3617) at a given reaction time. As the reaction time increases (horizontal axis), shifts in $\delta^{13}C$-values can be evaluated (vertical axis). Here, DOLO368 show relatively constant $\delta^{13}C$-values, but 3331 and 3617 show a small increase in their $\delta^{13}C$-values with time.

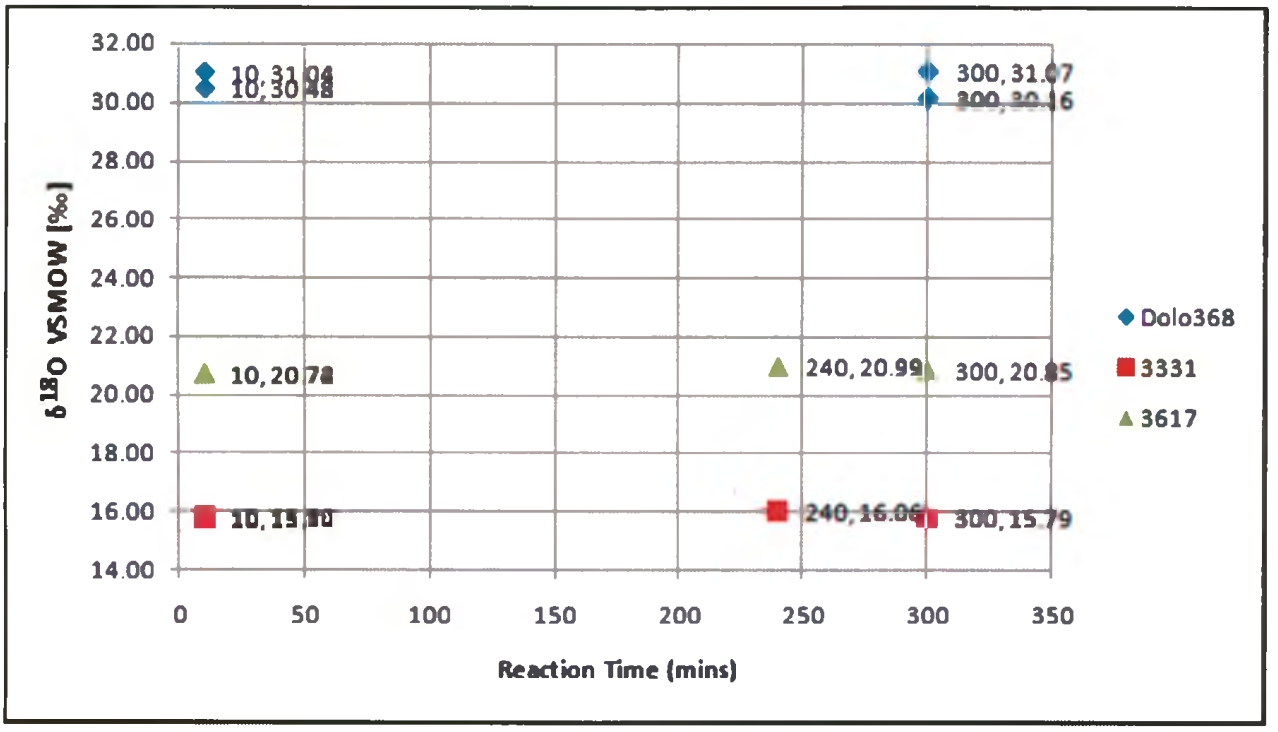

Figure 3.5. Results from oxygen ($\delta^{18}O$) stable isotope analyses of 3 dolomites (DOLO368, 3331 and 3617) by MultiPrep extraction technique (as shown in Table 3.2). Reaction times of 10 minutes, 4 hours and 5 hours, at a constant temperature of 90°C. Data reproducibility can be evaluated by the proximity of the different sample points of a given dolomite (DOLO368, 3331 or 3617) at a given reaction time. As the reaction time increases (horizontal axis), shifts in $\delta^{13}C$-values can be evaluated (vertical axis). Here, relatively constant $\delta^{18}O$-values for all three dolomites are observed over time.

The present data strongly suggest that values collected by both conventional and MultiPrep techniques are similar, within range of expected values and reproducibility (Table 3.3). The carbon- and oxygen-isotope values of DOLO368 along with natural samples #3331 and #3617 are not clustered and could potentially be used as internal standards if additional analyses were performed to confirm they are isotopically homogeneous. However, this is beyond the scope of the present study. The $\delta^{13}C$-values show a total range of ~8‰ (from -1.6 to +6.4‰) and $\delta^{18}O$-values have a total range of ~15‰ (from +16.2 to +30.6‰), which may be sufficient for correction of naturally occurring samples and potentially could be used to form a calibration curve (Figures 3.6 and 3.7). Moreover, the differences in measured isotopic ratios between two acknowledged techniques used for carbonate materials are relatively small and allow us to be confident in the accuracy of the data collected.

In order to have a more representative set of values for all samples studied on the MultiPrep, it would be useful to conduct additional analyses to increase the current dataset, especially for dolomite sample #3617, which has fewer data points in comparison to #3331 and DOLO368.

3.4.2.4 Development of an Experimental Approach

A third alternative technique considered as a tangible option for stable isotope analysis of carbon and oxygen ratios in natural samples of mixed carbonates is the GasBench technique. The GasBench technique is very similar to the MultiPrep technique with respect to automation. On the GasBench, samples are normally flushed with helium

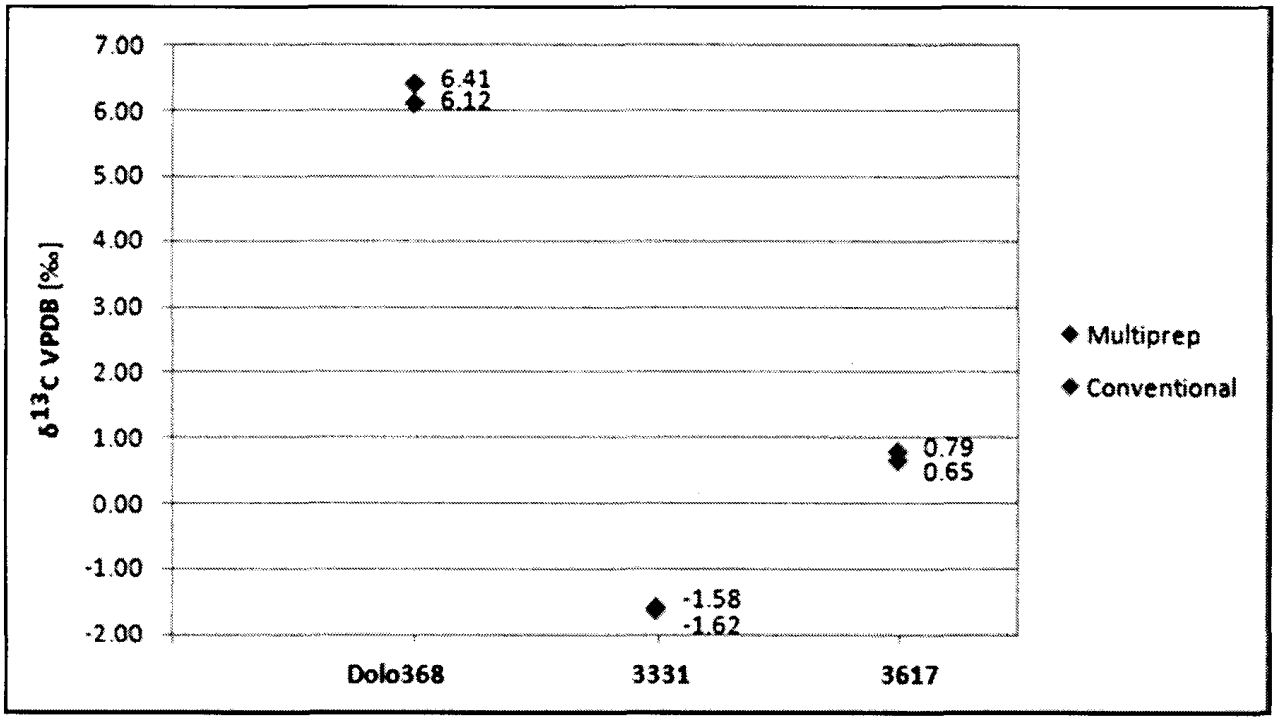

Figure 3.6. Comparison of results between conventional and MultiPrep extraction techniques based on the average $\delta^{13}C$-values (disregarding reaction times and temperatures) observed for all three dolomite standards (as shown in Table 3.3). Data reproducibility can be evaluated by the proximity of the different sample points for a given dolomite (DOLO368, 3331 or 3617). See text for discussion on $\delta^{13}C$-values.

Table 3.3. Compilation and comparison of average $\delta^{13}C$- and $\delta^{18}O$-values for all three dolomite standards standards (disregarding reaction times and temperatures) from conventional off-line and MultiPrep techniques. See text for discussion on values.

	Averaged δ13C VPDB [‰]		Difference in	Averaged δ18O VSMOW [‰]		Difference in
Sample ID	Multiprep	Conventional	δ13C VPDB [‰]	Multiprep	Conventional	δ13C VPDB [‰]
Dolo368	6.12	6.41	0.29	30.69	30.62	0.07
3331	-1.58	-1.62	0.04	15.85	16.15	0.30
3617	0.79	0.65	0.14	20.83	20.80	0.02

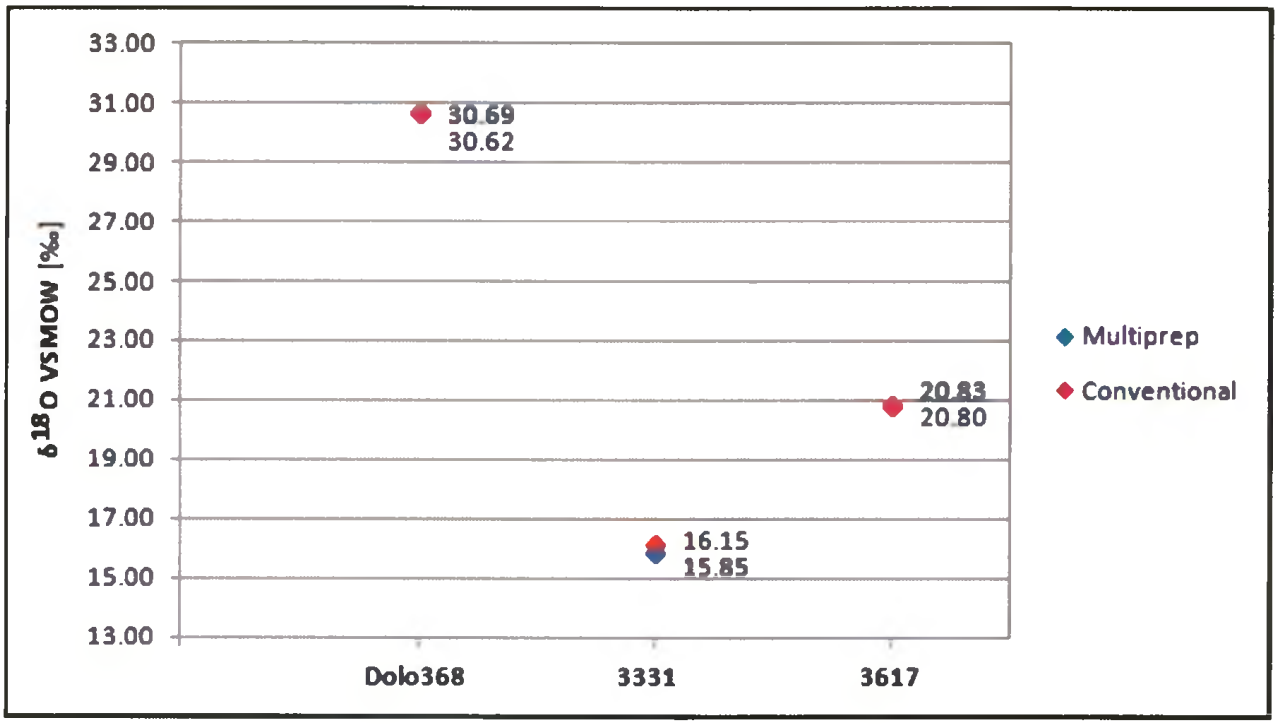

Figure 3.7. Comparison of results between conventional and MultiPrep extraction techniques based on the average $\delta^{18}O$-values (disregarding reaction times and temperatures) for all three dolomites standards (as shown in Table 3.3). Data reproducibility can be evaluated by the proximity of the different sample points for a given dolomite (DOLO368, 3331 or 3617). See text for discussion on $\delta^{18}O$-values.

and reacted at a temperature of 50 °C for CO_2 to be diverted directly into the mass spectrometer. This technique is indeed helpful in the case of dolomite because a higher temperature (up to 80 °C for GasBench) lowers significantly the time needed for the reaction to reach completion. A large number of samples, as for the MultiPrep, could be reacted overnight. The use of the MultiPrep and Gasbench techniques are relevant in terms of automation, and could be used as an alternative for laboratories that do not have the facilities to perfrom conventional extraction techniques.

As mentioned in the introduction, the dolomite standards methodology could be applied to the study of carbon and oxygen isotope composition of naturally occurring carbonate samples that are heterogeneous in terms of mineral content. In rocks containing a mixture of carbonates, two chemical methods are generally used. One removes all of the more soluble calcite with weak-acid (such as acetic acid) leaching (e.g., Glover, 1961; Humphrey, 1988; Swart and Melim, 2000) and the other makes use of differential phosphoric acid extraction time (e.g. Epstein et al., 1964; Walters et al., 1972; Al-Aasm et al., 1990; Ray and Ramesh, 1998). The latter is being utilised in our case with a combination of two techniques such as the MultiPrep and the GasBench (Table 3.5). A proposed technique to be used for mixtures would be to have a first sample analysed on the MultiPrep for 1 hour at 25°C to get the calcite CO_2 component, and then a second identical sample would be reacted at 25°C for x hours, evacuated to eliminate the calcite CO_2 component, and finally analysed at 50°C on the GasBench overnight for dolomite CO_2 component. Together, the values would represent the whole carbonate content of a single sample. The advantage would be that it constitutes a uniform experimental procedure. The accuracy of the method is somewhat lower than a one-step process used

for pure samples; however, it minimises the risk of contamination and the time required for sample analysis.

It was seen that the information provided by XRD allows identifying the presence or absence of calcite in any sample (standard as well as natural sample) and gives its approximate proportion relative to dolomite. If a given sample were to have a pure carbonate composition, either dolomite or calcite, the sample would be treated independently from mixtures; it would simply have to be analysed by a single-step process on the MultiPrep along with its respective standards (i.e., DOLO368, #3331 and #3617 for pure dolomite; or NBS-18, NBS-19, WS-1 and Suprapur for calcite) under appropriate reaction times and temperatures. If, however, a given sample were composed of a mixture of calcite and dolomite, it would be analysed using the methodology described above. In order to confirm that the technique is viable, preliminary tests have to be performed. Samples have to be weighed and put in vials with dolomite and calcite standards of known isotopic values mixed together in known proportions, with various calcite to dolomite ratios such as 1:4, 2:3, 1:1, 3:2 and 4:1, respectively. This would ensure that CO_2 extracted from the first component (i.e., calcite), and the second component (i.e., dolomite), generate the expected values of their respective standard values and independently from the proportions they were mixed in.

As a final note, the reaction rate between dolomite and phosphoric acid is sensitive to grain size but also to stoichiometry of dolomite, as experimentally demonstrated by Yui and Gong (2003). Acceptable results for stable isotopic compositions could be achieved by strictly confining the sample grain size and,

Table 3.4. Characteristics of conventional, GasBench and MultiPrep extraction techniques used for carbon and oxygen isotope analysis of powdered carbonates. All three techniques are commonly used in the Laboratory for Stable Isotopes Science at the University of Western Ontario. Analysing mixtures of carbonates (discussed here are mainly calcite-dolomite mixtures) is a long process that could be improved by using a combination of these techniques, either in parallel or in series, with appropriate standards. (Li, 2008).

	Conventional	GasBench	Multiprep
Online	no	yes	yes
Reaction media	vacuum	helium	vacuum
Water trap	cryogenic	Nafion tubing	electrical
LN_2	yes	no	yes
Labour (min/sample)	60	10	1
Sample (mmol carbonate)	50	3	0.8
Reaction temperature (°C)	25	50	90
Calibration	fractionation factor	internal standards	internal standards
Accuracy, stdev	0.2	0.2	0.2
Total time for 60 calcite samples	10 days	30 hours	30 hours
Dolomite and whole rock option	yes	yes	yes
Bone sample option	yes	?	?
Skil level	vacuum line and CO2 analysis	Isodat software	Optima software
Maintenance	vacuum line	needles, linearity	acid line, needles, vacuum, linearity
Technical level	intermediate	intermediate	high

according to predetermined dolomite chemical composition (e.g., XRD), by minimising reaction time between the sample and the acid. However, it is crucial to ensure that the yield for CO_2 gas from the calcite component is sufficient (>55% of expected yield). As one might expect, a consequence of a sufficiently long reaction time would be that differential leaching of dolomite in the acid is quite probable and may induce additional errors. Such an effect on analytical results must be taken into consideration before making meaningful interpretation on isotopic data of coexisting calcite and dolomite (Yui and Gong, 2003).

Chapter 4. Sample Description, Mineralogy and Geochemistry

4.1 Characterisation of Reference Carbonate Material

Mineral deposits from hydrothermal systems within impact craters are strongly dependant on the composition of host lithologies (e.g., Naumov, 2002; Ames et al., 2006). The type of target will directly influence the mineralogy of hydrothermal alteration: in crystalline rocks, clays and zeolites are the predominant alteration minerals observed, whereas clays are not formed in carbonate targets. It is, therefore, imperative to fully characterise the target rocks at Haughton in order to better explain the effects of hydrothermal alteration resulting from the impact. This is especially relevant at Haughton as target lithologies and secondary hydrothermal deposits studied here are both carbonates.

The bulk of the mineralisation at Haughton in terms of volume is comprised of calcite and selenite (gypsum), with significantly lesser amounts of marcasite, quartz and goethite, and rare barite, celestite, fibroferrite, fluorite and pyrite occurrences (Osinski et al., 2001, 2005). This alteration assemblage is very different from the alteration products generally reported at most impact structures (clays, zeolites and K-felspar) described by Naumov (2002). The correlation that exists between the type of target lithology and the mineralogy of impact-induced alteration assemblage is clearly witnessed at Haughton: as a matter of fact, no typical silicate minerals such as zeolite or feldspar were produced from hydrothermal activity. A majority of terrestrial impact events have occurred on a strictly crystalline or metamorphic basement, as these rocks are widespread and represent most of the oldest rocks on Earth. Nonetheless, a large number of craters were formed in

sedimentary host lithologies, or a in a mixed crystalline and sedimentary basement (Gurov et al., 1988). The post-impact crater-fill melt layers produced in sedimentary targets like at Haughton are also different than those developed in crystalline targets. Impact events occurring in carbonate and sulfate-bearing sequences produce devolatisation (releasing CO_2) and the formation of carbonate and sulfate melts, as opposed to silicate melts in crystalline basement rocks, and at different generation temperatures (Osinski et al., 2005b). Thus, the post-impact interaction between impact melt rocks and hydrothermal fluids will also be dissimilar in carbonate- and sulfate-rich target rocks, as observed at Haughton. This is in several aspects similar to present-day geothermal activity in geologically active parts of the Earth's crust, where alteration assemblages and mineralisation are different in crystalline versus sedimentary host rocks (Ellis et al., 1977). Not surprisingly, impact craters in sedimentary lithologies, including carbonate rocks, are under-represented in the literature. The study of sedimentary-hosted impact-hydrothermal deposits has been a neglected topic, although it is definitely a key element in the understanding of impact cratering processes in this type of target. Consequently, the present study on the dominant type of hydrothermal mineralisation at Haughton – calcite – expands our knowledge not only on the syn- and post-impact processes affecting sedimentary layers at Haughton, but also at other similar impact structures elsewhere on Earth and other planetary bodies.

As a foundation stone to the stable isotopes analysis, pre-impact and crater-fill lithologies – hereafter called reference samples –were characterised by means of X-Ray Powder Diffraction (XRD) and X-Ray Fluorescence (XRF). Similarly, these analytical procedures were applied to samples of hydrothermal origin. Altogether, the data

complements previous field descriptions of the rocks found on Devon Island (i.e., Thorsteinsson et al., 1987) and provides new insights on the distribution and formation of hydrothermal carbonates from a mineralogical perspective.

4.1.1 Sample Locations

The locations of reference samples analysed by means of XRD are shown in Figure 4.1. The vast majority of samples were selected from the collection made during previous years of mapping carried out by Dr. G.R. Osinski. Unshocked reference material was collected by helicopter from the eastern plateau far beyond the crater area since the older formations of the target sequence only crop out in the east. Three cliff-sections east of the crater were chosen for helicopter sampling sites as they contain a majority of the rock formations under study. These sections are those covered in Thorsteinsson et al. (1987) as Sections #28 (466350E, 8383100N), #31 (439375E, 8364300N) and #32 (439875E, 8381300N), the geographic coordinates throughout this study being reported in the NAD 83 datum. Altogether, the selection of samples covers every main rock formation present within and in the vicinity of the Haughton impact structure. Unfortunately, due to the small number of helicopter traverses that could be done in 2008, none of the Eleanor River Formation samples were collected outside of the crater zone. Nevertheless, at least one sample from each of the other formations was found outside the crater area and is described herein as unshocked reference carbonate material. Since it was not always possible to collect more than one carbonate sample from each lithology at different sites, we ensured that the most representative samples of these formations were chosen for analysis.

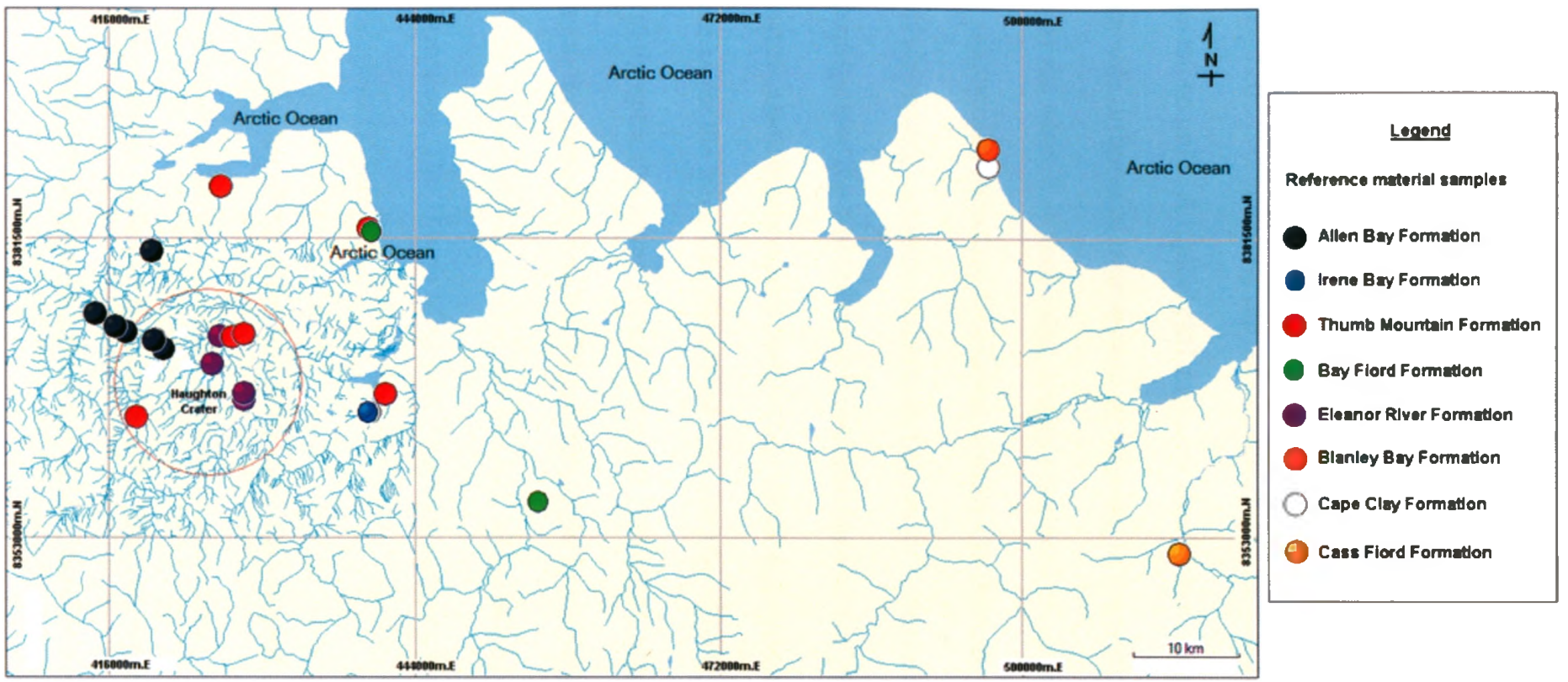

Figure 4.1. Simplified map with hydrography (blue) of the distribution of reference material samples investigated in this study. Sample selection was based on sample availability and on the requirement of a single-carbonate composition for isotopic analysis. Most rock formations are represented in this study by samples located outside the crater region, at a distance of up to 80 km, where shock-metamorphism effects are less important or absent. (From MapSource, 2006).

4.1.2 Field Observations

As previously mentioned, a large proportion of the unshocked target lithologies were sampled by helicopter at eastern sections outside the zone of influence of the impact event. The stratigraphy exposed at these natural geological cross-sections is formed by virtually flat-lying beds (3-5° westerly dip) of variable thicknesses and consists mainly of dolomite and limestone units. A typical cliff exposure clearly shows superimposed lithological units with differential resistance to weathering. In the sections visited, the Lower Member of the Allen Bay Formation, mainly composed of massive and uniform limestone beds, overlies the Irene Bay Formation, a relatively thin unit (<10 metres on Devon Island) of alternating recessive and resistant dolomitic limestone beds. The contact is difficult to identify since it is unconformable, but also because the basal units of the Allen Bay Formation also contain macro-fossils (i.e., corals and stromatoporoids) and interbeds of shale as for the Irene Bay Formation. The steep location did not allow access to units of the stratigraphically lower Thumb Mountain Formation; however, it seems that the contact between the Irene Bay and the Thumb Mountain formations was cropping out directly beneath the last sample collected at this transect, which helped in correlating the different rock formations. The Thumb Mountain Formation samples studied here come from different locations (Figure 4.1).

The Middle Member of the Allen Bay Formation was sampled in the north-western region, where shock processes where minimal to nonexistent, as evidenced by the absence of impact-produced faults and fractures and the relatively large distance from the central uplift. A majority of the dolomites from the Middle Member were collected in a radial transect from the crater center and sampling was made at regular intervals (Figure

4.1). The medium brown, thickly bedded to massive dolomite units of the Middle Member of the Allen Bay Formation differ from the thinner Lower Member, the latter being predominantly composed of limestone (Thorsteinsson et al., 1987).

The Bay Fiord Formation is composed, for most of its extent, of limestone and dolomite, which is argillaceous or silty, and of evaporitic rocks. This formation is recognisable by its greenish colour, its overall recessive nature as well as the presence of characteristic beds of crystalline, often brownish, anhydrite and gypsum that stand out in outcrops. The basal contact is sharp and separates the carbonate rocks of the underlying Eleanor River Formation from the lowermost evaporites of the Bay Fiord Formation (Thorsteinsson et al., 1987). The Eleanor River Formation is the lowermost carbonate unit which outcrops significantly as uplifted blocks within the central parts of the crater, overlain or in contact with impact melt breccias. Lastly, rare exposures of the underlying Blanley Bay Formation are found in the central uplift of Haughton.

4.1.3 X-Ray Diffraction and X-Ray Fluorescence

XRD analysis was used to characterise the mineralogy of samples selected for this study while XRF provided geochemical data. The analytical results for non-hydrothermal reference material discussed in this section are compiled in Table 4.1 and Table 4.2 for XRD and XRF data, respectively. Data is available for all of the main pre-impact sedimentary target rocks) at Haughton. Fifty unshocked reference samples were characterised by XRD analysis, and five unshocked samples underwent XRF analysis. In Table 4.2, the XRD results are given as semi-quantitative mineral compositions, which is the case since no Rietveld cell refinement of the XRD profiles were made to

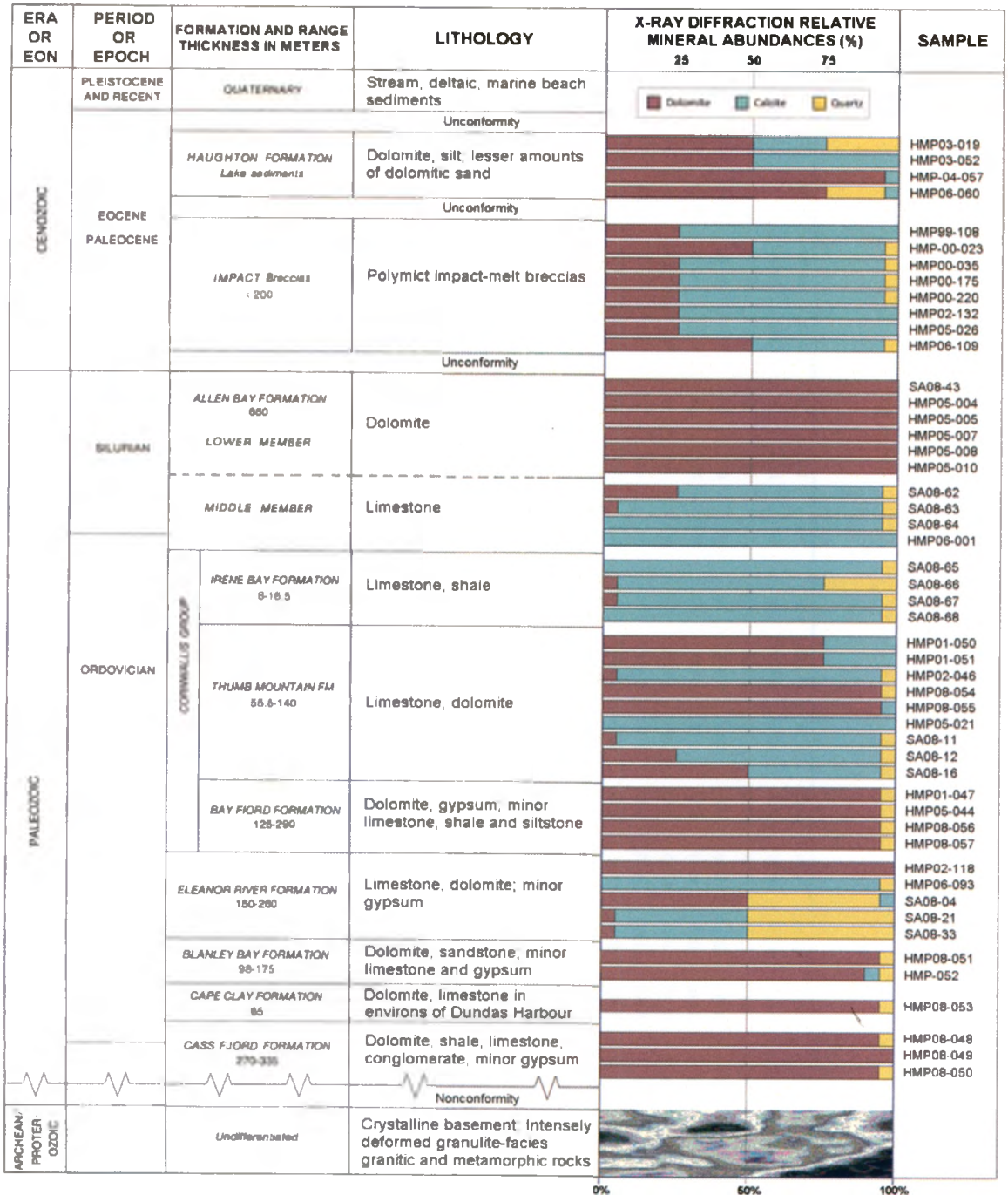

Table 4.1. Semi-quantitative mineral compositions of rocks investigated in the current study based on X-Ray Diffraction (XRD) data. The dolomite, calcite and quartz (silica) relative compositions are noted as relative increments of 25%, and <10% is shown by a square. The data is juxtaposed to the stratigraphy of Devon Island as from the Geological Survey of Canada (GSC), and syn- and post-impact lithologies found at Haughton are included from Osinski et al. (2005c). Basement rocks of Precambrian age (not studied here) are nonconformably overlain by a sequence of Paleozoic sedimentary rocks, in turn overlain by Cenozoic impact melt breccias and crater-fill lake sediments of the Haughton impact event. The XRD data presented tend to verify and is concordant with geological descriptions from the GSC. (First four columns from Thorsteinsson et al., 1987).

Table 4.2. X-Ray Fluorescence data for reference materials from the Haughton impact structure. (Acquired from G. R. Osinski).

Sample ID	Sample Description / Location	SiO2 wt%	TiO2 wt%	Al2O3 wt%	Fe2O3 wt%	MnO wt%	MgO wt%	CaO wt%	Na2O wt%	K2O wt%	P2O5 wt%	BaO ppm	Co ppm	Cr2O3 ppm	Ni ppm	LOI wt%	Total	CO2 wt%	SO3 wt%	N wt%
05-005	Middle Memb. Allen Bay Fm.	0.77	0.009	0.17	0.04	<d/l	20.13	30.68	0.19	0.01	0.013	<d/l	<d/l	34	<d/l	47.82	99.83	47.31		<d/l
05-007	Middle Memb. Allen Bay Fm.	0.47	0.010	0.22	0.07	<d/l	21.14	30.92	0.20	0.01	0.012	<d/l	<d/l	<d/l	<d/l	46.84	99.89	47.55		<d/l
05-008	Middle Memb. Allen Bay Fm.	0.31	0.010	0.08	0.05	0.003	21.52	31.36	<d/l	<d/l	0.006	<d/l	<d/l	<d/l	6	46.58	99.91	49.94		<d/l
02-118	Eleanor River Fm.	0.64	0.017	0.22	0.18	0.012	20.39	30.84	<d/l	0.04	0.009	<d/l	<d/l	19	5	47.73	100.07	47.98		<0.01
05-021	Ballistic ejecta, Thumb Mountain Fm	1.03	0.014	0.28	0.11	0.005	0.60	46.83	0.17	0.03	0.014	<d/l	<d/l	29	<d/l	48.76	99.84	44.68	<d/l	<0.01
99-108	Breccia dike	0.34	0.012	0.12	0.06	0.024	1.51	52.80	0.01	<d/l	0.012	<d/l	<d/l	<d/l	7	44.92	99.81	44.67		<0.01
00-023	Impact melt breccia	21.78	0.216	4.28	1.73	0.033	10.29	27.26	0.11	0.97	0.051	299	<d/l	40	16	33.23	99.99	28.59		0.02
00-035	Impact melt breccia	22.96	0.244	4.87	1.91	0.034	9.56	26.42	0.11	1.05	0.058	248	<d/l	46	21	32.86	100.11	27.32		0.02
00-175	Impact melt breccia	11.77	0.081	1.86	0.71	0.014	9.37	37.36	0.05	0.41	0.027	376	<d/l	28	13	38.36	100.05	33.75		<0.01
00-220	Impact melt breccia	18.53	0.140	3.17	1.19	0.024	11.12	30.99	0.08	0.66	0.037	247	<d/l	29	12	33.81	99.78	26.91		<0.01
05-026	Impact melt breccia	12.25	0.084	1.86	0.78	0.016	10.88	35.78	0.02	0.47	0.029	778	<d/l	20	13	37.85	100.10	43.80	0.42	<0.01
06-109	Impact melt breccia	17.53	0.136	3.33	1.12	0.024	10.77	30.60	0.10	0.47	0.043	213	<d/l	30	13	36.41	99.96			
04-003	Sandstone clast from IMB	73.43	0.026	0.21	0.24	0.007	0.47	13.64	0.03	0.07	0.019	275	<d/l	36	8	11.72	99.89			
04-001	Sandstone clast from IMB	95.26	0.027	0.07	0.39	0.005	0.18	1.46	0.04	0.09	0.013	<d/l	<d/l	82	12	2.28	99.62			
05-024	Carbonate clast from IMB	2.18	0.026	0.39	0.15	0.008	3.60	50.52	0.04	0.03	0.010	<d/l	<d/l	15	11	43.10	100.06	45.15	0.10	
05-025	Carbonate clast from IMB	2.06	0.025	0.38	0.15	0.008	3.80	50.12	0.02	0.04	0.009	<d/l	<d/l	18	8	43.19	99.80		0.11	
03-019	Haughton Formation	6.32	0.060	0.88	0.47	0.010	18.26	30.11	0.24	0.12	0.017	<d/l	<d/l	98	26	43.63	100.12	34.79	0.67	<0.01
03-052	Haughton Fm., limestone layer	7.33	0.109	2.28	1.00	0.083	10.15	36.25	0.24	0.43	0.340	36	<d/l	83	31	41.64	99.87	37.69	1.14	<0.01
04-057	Haughton Fm.	5.71	0.056	0.91	0.40	0.010	17.36	31.82	0.03	0.25	0.025	49	<d/l	16	8	43.58	100.16	44.77	0.22	<0.01
06-060	Haughton Fm.	27.38	0.115	1.50	0.57	0.010	12.24	24.06	0.09	0.38	0.024	50	10	28	9	33.49	99.87			
03-053	Haughton Fm., nodule	6.45	0.099	1.87	1.41	0.074	10.15	36.54	0.08	0.33	12.179	152	<d/l	24	16	30.68	99.85	27.00	1.51	<0.01

quantitatively measure the fraction of each mineral component. As such, the XRD profiles were interpreted semi-quantitatively based on relative peak heights and width of the different mineral species detected for each sample analysed. In Table 4.2, the dolomite, calcite and quartz (silica) relative compositions are noted as relative increments of 25%, and <10% is simply represented as a square. Additional samples were analysed by XRF for this study and belong to the syn- and post- impact crater fill lithologies (section 4.2). The following paragraphs provide geological and geochemical observations for the aforementioned target formations in descending stratigraphic order, from the uppermost Allen Bay down to the Cass Fiord Formation.

4.1.3.1 Allen Bay Formation

The Allen Bay Formation has direct implications for understanding the Haughton impact structure since this was the main body of rock cropping out at the site of impact. The name Allen Bay Formation was first introduced by Thorsteinsson and Fortier (1954). It was ascribed to a rock unit composed chiefly of dolomitic beds, found in the southern part of Cornwallis Island, directly west of Devon Island. The formation is exposed on Devon Island as a northerly-trending belt of generally resistant and topographically prominent outcrops, with an approximate thickness of 660 metres. It comprises three members, two of which were mentioned previously: the Upper and Middle Members are composed of dolomite for the most part, whereas the Lower Member comprises mostly limestone which resembles the uppermost lithology of the Thumb Mountain Formation (Thorsteinsson et al., 1987).

Only the Middle and Lower Members of the Allen Bay Formation have been studied here as the Upper Member was absent around the Haughton impact structure at the time of impact (Osinski et al., 2005c). In this study, a total of six samples from the Middle Member of the Allen Bay Formation were analysed by XRD. Massive dolomite is known to be the predominant lithology in the Middle Member, but it is difficult to assess in hand specimen as to whether a proportion of calcite cement or limestone interbeds might be present. The results from XRD analyses show that all samples are entirely composed of dolomite (Table 4.1). Three of these samples were also analysed by XRF (Table 4.2). This data indicates clearly dolomite as the main component, with ~21wt% MgO and ~31wt% CaO, which matches the theoretical oxide-content of dolomite. Minor SiO_2 (~0.5 wt%) is also noted in all three samples and is likely detrital quartz. Regarding the Lower Member of the Allen Bay Formation, four samples were analysed by XRD. The uniform succession of limestone described by Thorsteinsson et al. (1987) is, as anticipated, verified by XRD. In addition to calcite, there are also variable but minor amounts of dolomite and quartz in the samples studied. Although quartz is not mentioned by Thorsteinsson et al. (1987), fossil remains such as sponge spicules are abundant in both the Lower and Middle Members, which might be siliceous in composition. The possibility of sedimentary quartz, detrital or cement, is a possibility although it is not mentioned in the literature.

4.1.3.2 Irene Bay Formation

Kerr (1967, 1968) described the Irene Bay Formation in the central part of Ellesmere Island. Its distribution is practically the same as that of the underlying Thumb Mountain Formation. As stated earlier, the Irene Bay Formation is relatively thin, rarely

exceeding 40 metres thickness in any outcrop of the entire Arctic Archipelago, which implies that a significantly smaller volume of rock compared to other formations was affected by the Haughton impact event. An additional characteristic to note is the large fossil content, particularly as fossil debris. It is in this formation that the diversity and abundance of the Arctic Ordovician fauna attained its peak (Thorsteinsson et al., 1987).

In terms of geological units, this recessive rock formation is made up of limestone and shale. Although there are two different lithofacies described in the literature, no distinction is made in this study simply because the whole formation is relatively thin and would not affect the regional scale interpretation. Based on the XRD analytical results shown in Table 4.1, the calcareous shale and limestone interbeds are indeed composed of calcite, but also show variable amounts of minor dolomite and quartz (<10%).

4.1.3.3 Thumb Mountain Formation

The topographically prominent Thumb Mountain Formation, named by Kerr (1967), appears similar to other massive Ordovician formations. This thick succession of carbonate rocks is known to be composed mainly of limestone with a smaller proportion of dolomite, and rich in megafossils (Thorsteinsson et al., 1987). This formation is split into two geological members in some parts of the Arctic Platform, with a dolomitic lower member and a heterogeneous upper section indicative of shallower water deposition (Kerr 1967). Here, the Thumb Mountain Formation is discussed as a single entity, since the separate members were not obvious nor distinguished during sampling.

Seven rock specimens were collected from the Thumb Mountain Formation, from which many of them have not been altered by post-impact hydrothermal activity. In fact,

this formation has been sampled at several unperturbed localities covering a large area (see Figure 4.1). XRD analyses show that there is a continuous range in composition, from specimens exclusively composed of calcite, to others predominantly made of dolomite. Examples of calcareous dolomite (i.e., sample HMP01-050), dolomitic limestone (i.e., sample SA-08-16) and limestone (i.e., sample HMP05-021) can be discerned. Overall, there are similar proportions of calcite-rich and dolomite-rich samples. Additional samples are considered hydrothermally altered and are briefly mentioned in a later paragraph.

4.1.3.4 Bay Fiord Formation

A more distinguishable geological unit is the Bay Fiord Formation, which underlies the Thumb Mountain Formation. A regional study on Ellesmere Island supports a thickening of the formation (up to 290 metres) and increasing amounts of shale and silt to the west, with evaporites constrained to a central belt (Kerr, 1968). The main lithologies are grouped in four informal members, composed of carbonate and evaporitic beds that coexist in extremely variable amounts on the regional scale. Thinly bedded dolomite is seen interlaminated with gypsum, and thickly bedded dolomite is often fossiliferous and burrowed. Rocks from the base of the formation, dominated by evaporites, crop out in the central uplift of the Haughton impact structure while the stratigraphically higher rocks, mainly carbonates, are exposed towards the eastern rim of the crater (Kerr, 1968).

The four samples from the Bay Fiord Formation selected for XRD analysis were gathered at different sites, distant from one another, in order to cover the whole unit as

much as possible. Dolomite is the major component and is the sole carbonate phase present, with quartz content less than a few percent (Table 4.1). Silicified stromatolites noticed by Thorsteinsson et al. (1987), and thinly bedded siltstone, might be the cause of the presence of quartz. Carbonate-bearing rocks were prioritised for XRD, which meant evaporites were not considered, which explains why the data show no anhydrite or gypsum in the samples analysed. Thorsteinsson et al. (1987) reveal that an X-Ray Diffraction analysis done on a dolomite specimen from the uppermost unit of the formation collected in the east contained three percent chlorite. However, they note that western rocks such as those from the Haughton region only show negligible amounts. The XRD patterns of of this study do not show chlorite as a component of the samples, however, the higher sensivity of their analysis could explain the presence of chlorite.

4.1.3.5 Eleanor River Formation

As for many other rock formations in the Canadian Arctic Archipelago, the Eleanor River Formation was established by Thorsteinsson (1958). With a similar thickness to the Bay Fiord Formation (~150-250 metres), this unit is divided in four sub-units all largely composed of limestone, with subordinate amounts of dolomite. Rocks exhibit textures ranging from massive to thinly bedded, and labyrinthine dolomite mottling within limestone is a characteristic feature. Also, sparse megafossils are found throughout the formation. The presence of chert nodules is a characteristic feature of this formation. The samples that were collected from this formation are not pristine and suspected of being altered by post-impact hydrothermal processes; therefore, they will not be used as a reference. Nonetheless, they are briefly discussed further in this section.

4.1.3.6 Blanley Bay, Cape Clay and Cass Fiord Formations

Unshocked reference material from the Blanley Bay, Cape Clay and Cass Fiord Formations (e.g., samples HMP08-48 to 53) were collected outside of the Haughton impact structure. The Blanley Bay Formation is present in the central uplift of the impact structure and the other formations are likely to be present in the subsurface in the central uplift. All three formations were sampled within undisturbed horizontally-lying strata located several tens of kilometres away from Haughton (Figure 4.1). The main lithologies found within the Blanley Bay Formation are dolomite and sandstone. As presented herein (see Table 4.1), samples from the Blanley Bay Formation studied by XRD show dolomite as the main component with very minor quartz and traces of calcite. In the same way, rocks of the Cape Clay and Cass Fiord Formations are almost entirely dolomitic in composition with rare amounts of quartz. These observations by XRD analysis agree well with those of Thorsteinsson et al. (1987) who report dolomite as a major rock-type for these formations. On Devon Island, the striking Cass Fiord Formation is almost entirely composed of dolomite. As well, the Cape Clay Formation is described by Thorsteinsson et al. (1987) as a "more or less pure carbonate unit". It is worth noting that the same authors measured up to nine percent montmorillonite and one percent illite by XRD in one lower Blanley Bay Formation dolomite sample; however, no such argillaceous minerals were detected in our series of samples.

4.1.3.7 Thumb Mountain and Eleanor River Formations from the Crater Region

Additional samples of the Thumb Mountain Formation, and all of the samples collected from the Eleanor River Formation are thought to be altered and, therefore, are

not considered reference samples *per se*. However, the data for these samples have not been completely put aside and are also considered useful to some extent for this study.

The three possibly altered Thumb Mountain Formation samples belong to the outer margin of the central uplift, a zone where hydrothermal activity was more pronounced. A noticeable difference between these samples from the crater area compared to reference unshocked samples is that the former contain quartz (<10%), which might indicate late-stage hydrothermal cementation by silica-rich fluids. XRF analysis done on one of these potentially altered samples (e.g., sample HMP05-021) reveals that CaO is the major oxide present, consistent with a uniform limestone. Again, since this sample was taken from an ejecta block within the crater that could have travelled from its original location, hydrothermal alteration might have altered the host rock.

All samples of the Eleanor River Formation were collected in the periphery of the central uplift, but since they are the only samples studied (with no sample from outside the crater) they could still provide geochemical information on the nature of this formation. XRD data show that dolomite, calcite and quartz are the rock-forming mineral phases. In the uplifted blocks of the crater central region, pervasive calcite and quartz alteration, along with calcite veining, generally occurs (Osinski et al., 2005a). Thus, the presence of quartz (up to ~40-50 vol%) in a majority of samples is believed to represent hydrothermally altered rocks by impact-generated fluids. Samples HMP06-093 and SA08-33, originating from the eastern outer edge of the central uplift, could be described as limestones; however, sample SA08-33 shows minor quartz content. From XRD data, sample SA08-21 found in the very center of the impact structure could be described as a

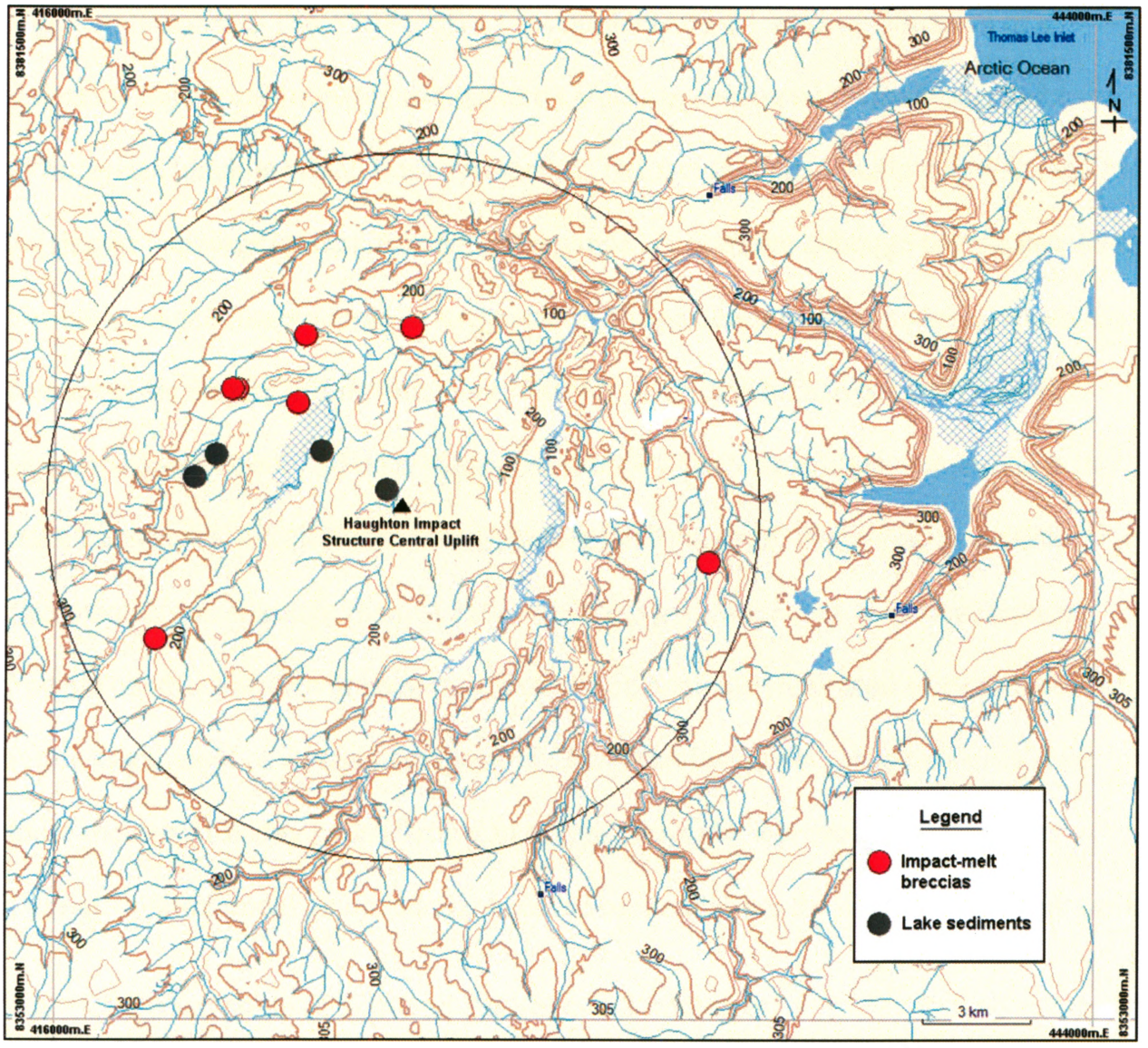

Figure 4.2. Topographic map showing impact melt breccia (red circles) and lacustrine sediment (grey circles) sample localities for this study. These syn- and post-impact rock units were deposited in the interior of the crater region, thus no sample site is located beyond the crater rim region. The great circle outlines the outer crater rim of the Haughton impact structure. The Haughton River Valley appears in the eastern part of the impact structure with a north-south orientation. (From Map Source, 2006).

silicified limestone. The XRD profile for sample SA08-04 is more indicative of a dolomitic limestone, probably cemented by silica, as evidenced by the brecciated nature of the ejecta block in which it was preserved. The fact that this sample was collected from an ejecta block implies that its exact provenance is uncertain, although the Eleanor River Formation is the likely source as suggested by the presence of chert nodules, which is a characteristic feature of this formation. There is XRF data for sample HMP02-118 yielding approximately 20 wt% MgO and ~31 wt% CaO, showing that dolomite is the main constituent, which is also recognised by XRD analysis. From this, an overall statement is that although these samples are not representative of unaltered Eleanor Formation, it is possible to gain insight on the carbonate composition of these rocks for future assessment of isotopic composition. Morever, the quartz cement suspected for these rocks is probably hydrothermal in origin. However, this study will no longer evaluate hydrothermal quartz simply because carbonates are the main focus of this work.

4.2 Characterisation of Syn- and Post-Impact Lithologies

Syn-impact impact melt breccias and post-impact lacustrine sediments (Haughton Formation) are located exclusively in the interior of the Haughton impact structure (Robertson and Grieve, 1978) (Figure 4.2). These geological units overly the Paleozoic target rocks discussed in previous sections. In brief, XRD analyses were carried out on 27 samples and XRF analyses on 16 samples from those two lithologies (Table 4.2).

4.2.1 Impact Melt Breccias

The rocks described as impact melt breccias occur as a nearly continuous unit and crop out within the central area of the crater, but also as discrete patches on the crater rim

region (Redeker et al., 1988; Osinski et al., 2005b). Coherent bedrock described in the previous section is overlain by impact-generated mega-breccias, which in turn are overlain by monomict breccias and polymict impact melt breccias (Osinski et al., 2005b). It is worth mentioning that carbonates found within impact melt breccias have to be taken into consideration when trying to understand impact-induced hydrothermal deposits. As indicated by microscopic observations made by Osinski and Spray (2001), and later supported by Osinski et al. (2005b), impact melt breccias contain abundant calcite (<10 to >50 vol%) as a groundmass-forming phase which crystallised from a primary impact melt phase. These breccias also contain various amounts of clasts from target lithologies that are for the most part carbonate-rich, with calcite and dolomite being the major phases.

In this study, bulk samples of impact melt breccias, as well as clasts within these breccias have been studied by XRD and XRF analysis. According to XRD data shown in Appendix 1, calcite is always predominant or equal to dolomite in impact breccias. In addition, most of the bulk samples also exhibit quartz, generally a few percent and up to ~20 vol%. From the dozen of target rock clasts analysed by XRD, ten are calcite-rich carbonates with dolomite contents much less than 50 vol%. The two remaining clasts are compositionally different, that is of quartz and quartz/calcite compositions: they represent shocked sandstone. Moreover, the dolomite is completely absent from those clasts. In addition to the XRD data, XRF analyses show similar compositional variations of whole rock breccias and clast samples. Figure 4.3 illustrates XRF data for impact melt breccias and lithic clasts, along with some data points from sedimentary target rocks for reference. Whole rock breccias samples have various CaO, MgO and SiO_2 contents, and clasts with a lower MgO/CaO+MgO ratio seem to show a higher SiO_2 content. Also, as expected,

sandstone clasts display mainly SiO_2, whereas carbonate clasts are mainly CaO-rich indicative of limestone.

4.2.2 Haughton Formation

Crater-fill lake sediments of the Haughton Formation (Hickey et al., 1988) are relatively younger than the impact event (Miocene), and post-date the impact melt breccia units described above (Osinski et al., 2005e). The series of relatively unconsolidated dolomitic silts and muds, with subordinate fine-grained dolomitic sands (Hickey et al., 1988), crop out in the western and central portions of the crater. It is believed that most of it has been eroded and that impact-induced hydrothermal activity at Haughton had ceased before their deposition, as no sign of alteration could be found (Osinski and Lee, 2005).

The mineralogy of five samples was characterised by XRD and XRF analyses. Both techniques render dolomite as the main phase, followed by quartz (<15 %) or calcite (<20 %), depending on the sample. The most dolomite-rich (i.e., sample HMP04-057) and calcite-rich (i.e., sample HMP03-052) sedimentary layers could be identified by both XRD and XRF analyses. This is in agreement with the fact that their composition should represent the bulk of surrounding target rock types (Osinski and Lee, 2005). The high dolomite-content as observed in most samples represents the high concentration of dolomite in the area of deposition (e.g., Allen Bay Formation) from which sedimentary mineral grains originate. Also, a nodule from the Haughton Formation (sample HMP03-063) is shown to be dolomite-rich with a few percent calcite and no iron present, indicative of a lime nodule as opposed to a pyrite concretion.

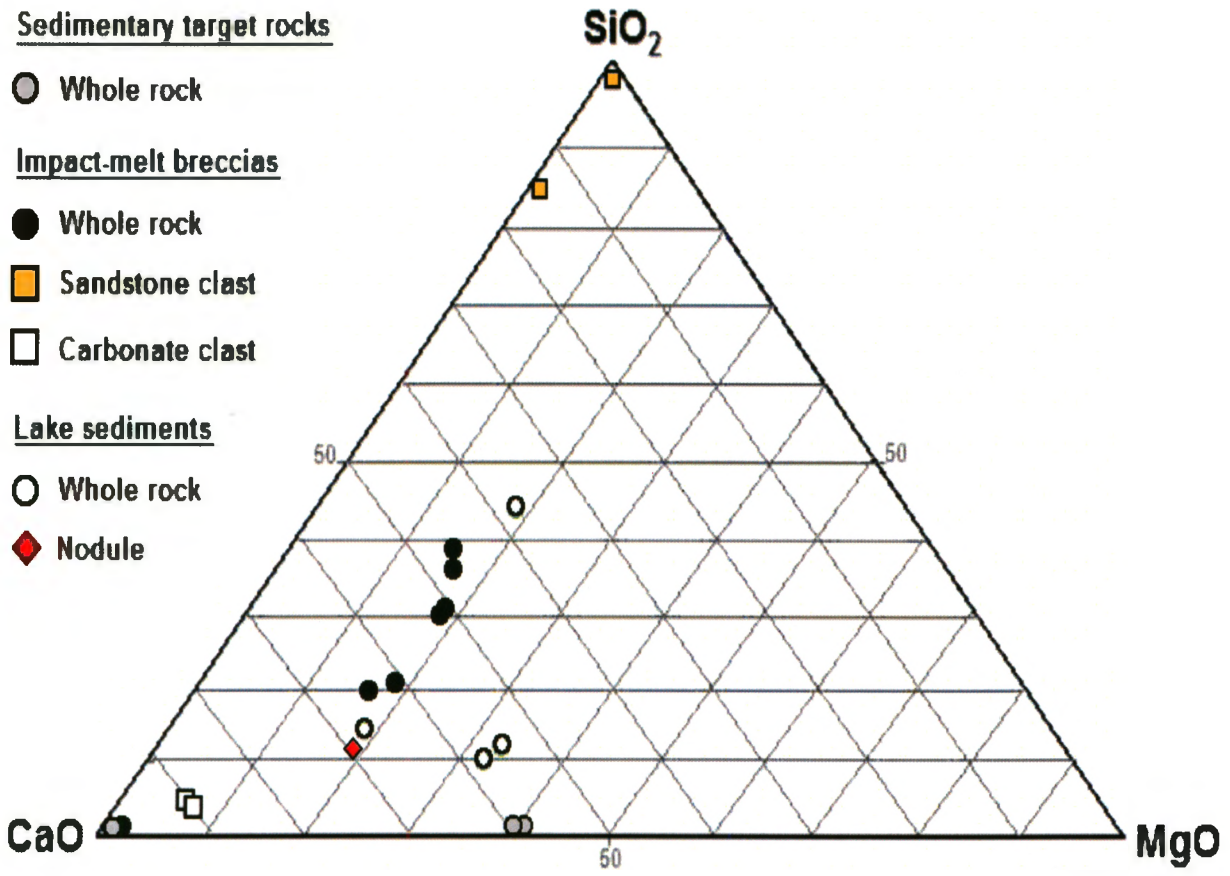

Figure 4.3. CaO-MgO-SiO_2 ternary diagram illustrating the composition of the different lithologies at Haughton, for which XRF data is available. The plotting parameters were calculated by summing the three main oxides (CaO, SiO_2 and MgO) and recalculating each as a percentage of the sum. Since these oxides generally make the bulk of the rocks at Haughton, the differences in composition of target versus impact-generated rocks can be evaluated. The composition of target rocks is represented both by whole-rock (grey circles) and lithic clast within the impact melt breccias (yellow and white boxes). As such, sandstone clasts (yellow boxes) within impact breccias plot at the SiO_2 apex; however, carbonate clasts (white boxes) are closer to the CaO apex (calcite-rich) or half-way between the CaO and MgO apex (dolomite-rich). The compositions in oxides of whole-rock impact breccias (black circles), diagenetic carbonate nodule (red diamond) and lake sediments (white circles) are similar, and represents the bulk of the target sequence at Haughton from which these lithologies were derived after the impact event.

4.3 Characterisation of Impact-Induced Hydrothermal Calcite

The Haughton structure has been studied by means of geophysical surveys (Pohl et al., 1988; Scott et al., 1988; Osinski et al., 2005d), as well as aerial and satellite imagery (Tornabene et al., 2005). Nonetheless, the full extent of the Haughton impact structure was revealed by geological field mapping (Osinski et al., 2005c). Similarly, impact-induced hydrothermal deposits were also recognised *in situ* during traverses (Osinski et al., 2001, 2005a). The crater-wide distribution of these deposits, and more specifically of calcite, is found in various settings in which hydrothermal fluids have deposited solid minerals in interstices of the rocks. In this section, the geological context and X-Ray Diffraction results for impact-generated hydrothermal calcite samples are presented. These samples are the main focus of the study in the following chapter on carbon and oxygen stable isotope geochemistry.

4.3.1 Sample Locations

Sampling of the four major styles of impact-induced hydrothermal calcite deposits (e.g., marcasite-free and marcasite-rich vug fillings within impact melt breccias, fracture and pipe structure fillings within target rocks) occurred over most of the crater region but more extensively in the eastern portion. This is due partly to the higher exposure of rocks in the Haughton River valley. Outcrops of impact melt breccias dominate the interior of the impact-structure; therefore, sampling of separate intra-breccia vugs was relatively simple. For a complete listing of geographic coordinates for hydrothermal samples analysed in this study, refer to Appendix 1. The distribution of the most important subset of samples collected for this study is shown in Figure 4.4. These samples represent those

that have been analysed by XRD as well as for stable isotopic composition (see Chapter 5). Following XRD analysis, these samples were selected for stable isotope analysis since they exhibited a pure calcite composition. They are also distributed over the whole crater region, which might be helpful to identify spatial heterogeneities in isotopic compositions. As for calcite vug and fracture fillings, hydrothermal pipe structures have been sampled throughout the crater rim. However, only two samples from a hydrothermal pipe structure located on the eastern rim were analysed for their isotopic composition (Figure 4.4). The remaining samples are heterogeneous in composition.

The main occurrences of intra-breccia vug calcite-marcasite mineralisation are found at the Haughton River valley locality, in the south-east part of the impact structure (Figure 4.5). Detailed sampling was performed every 5 metres over a 100-metre long north-south transect across the outcrop and the collapsed zone (Figure 4.6). At each sampling site, two samples were collected at different height to investigate any vertical heterogeneity in isotopic composition at a same site. Generally, a first sample was collected at waist-level and a second sample taken from higher on the outcrop. In addition to this horizontal transect, two vertical cross-sections (Sections 1 and 2) of approximately 2.5 metres in height were made ~10 metres apart. Section 1 was situated across the main mineralised zone in the centre of the collapsed zone, and Section 2 was placed on its northern edge. Systematic sampling was made on the various carbonate lithologies and hydrothermal mineralisation in order to see if there were any lateral and vertical variations in stable isotope compositions within the outcrop.

4.3.2 Field Observations

Impact-generated structural features within the Haughton crater have played a major role in the deposition of hydrothermal calcite after temperatures started to decrease. An intense zone of listric and radial faults surrounds and affects the outer rim (Osinski et al., 2005d), thus allowing efficient focussing of hot volatiles and fluids coming from the interior of the crater. The hydrothermal pipe structures that developed in proximity to these faults strongly support this concept (Osinski et al., 2001, 2005d). In addition, such evidence of localised alteration is absent in other parts of the crater, either within the impact melt sheet or the central uplift, which also supports the correlation between fractures and enhanced fluid flow.

As mentioned previously, a large proportion of the target lithologies exposed within the eastern part of the inner crater and rim regions are affected by intense fracturing and veining, whereas the western portion is less altered (Figure 4.4). Furthermore, the presence of hydrothermal calcite is generally confined to the exterior of the central uplift and to the crater rim region, as seen on Figure 4.4. Rocks from the interior of the central uplift (i.e., blocks from the Eleanor River Formation) do not exhibit fracture-filling calcite but rather show pervasive quartz alteration. A different fracture-filling mineral that was not investigated here is gypsum. It is common to see late-stage hydrothermal gypsum veins cross-cutting the matrix and clasts of impact melt breccias, as well as uplifted target

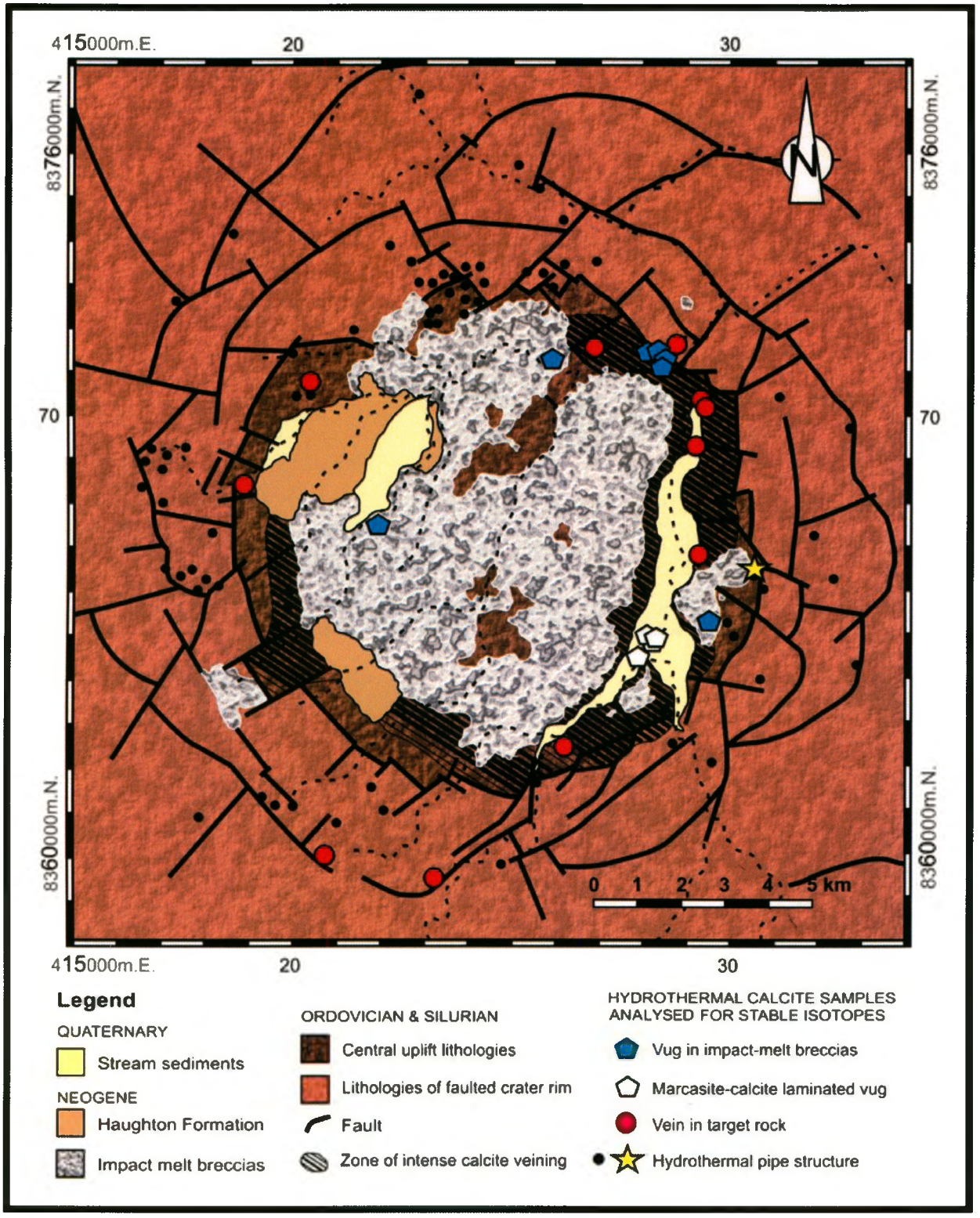

Figure 4.4. Simplified geological map of the Haughton impact structure, showing hydrothermal calcite sample localities selected for stable isotope geochemistry in this study. Intra-breccia monomineralic vugs (blue pentagons) and veins within target rocks (red circles) were sampled at several localities across the crater, whereas calcite-marcasite vugs (white pentagons) and pipe structures (yellow stars) are from localities in the south-east region. Black dots on the crater rim are hydrothermal pipe structures identified prior to this study. (Modified from Osinski et al., 2001).

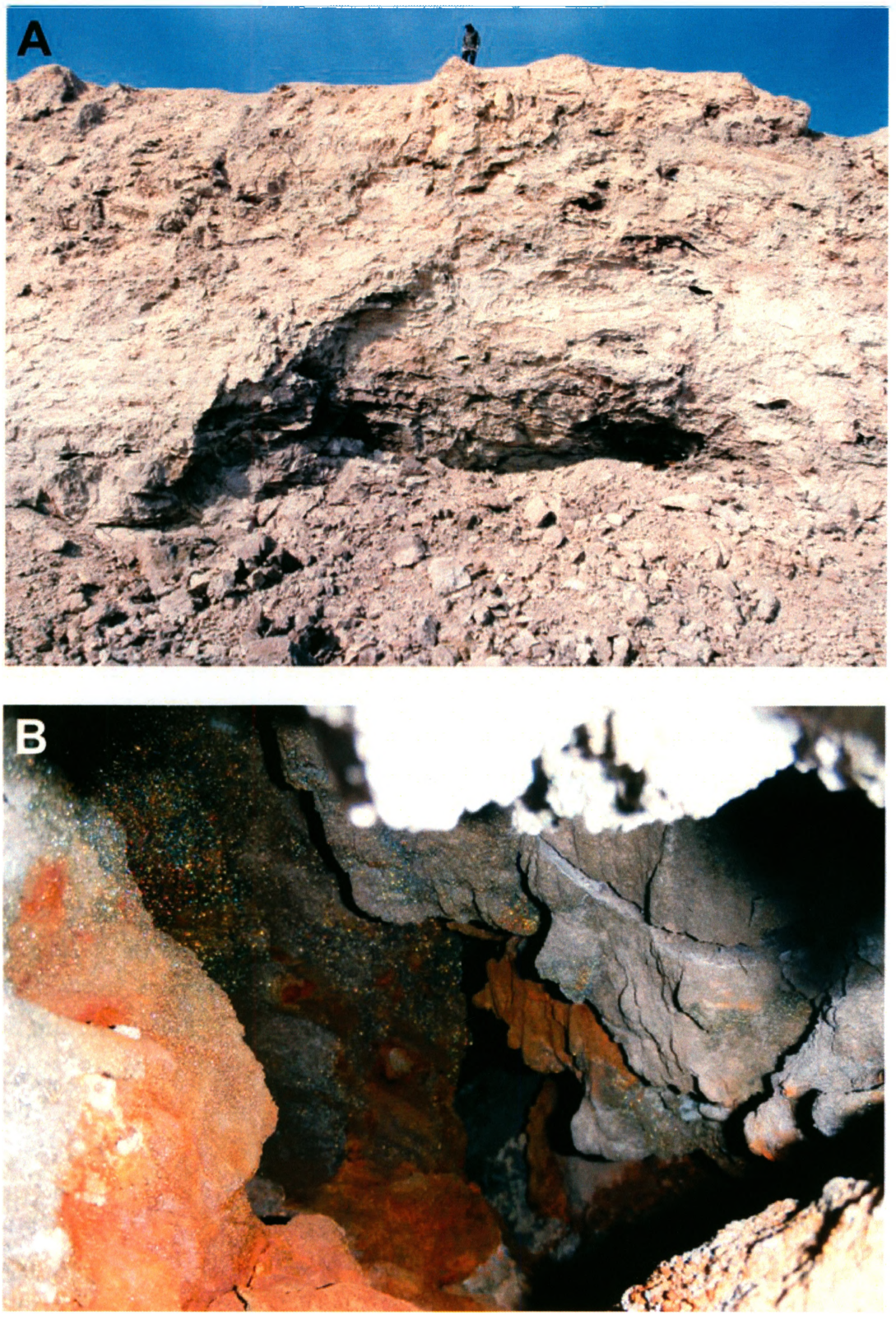

Figure 4.5. Field images of hydrothermal calcite-marcasite vug mineralisation at the Haughton River Valley locality. A: Overview of the study area, where the partial collapse of impact melt breccias exposes relatively unaltered mineralisation. Note the geologist for scale; B: View inside the vug, with extensive rusty-green marcasite lining overlying grey calcite. The width of the visible cavity is approximately 1 meter.

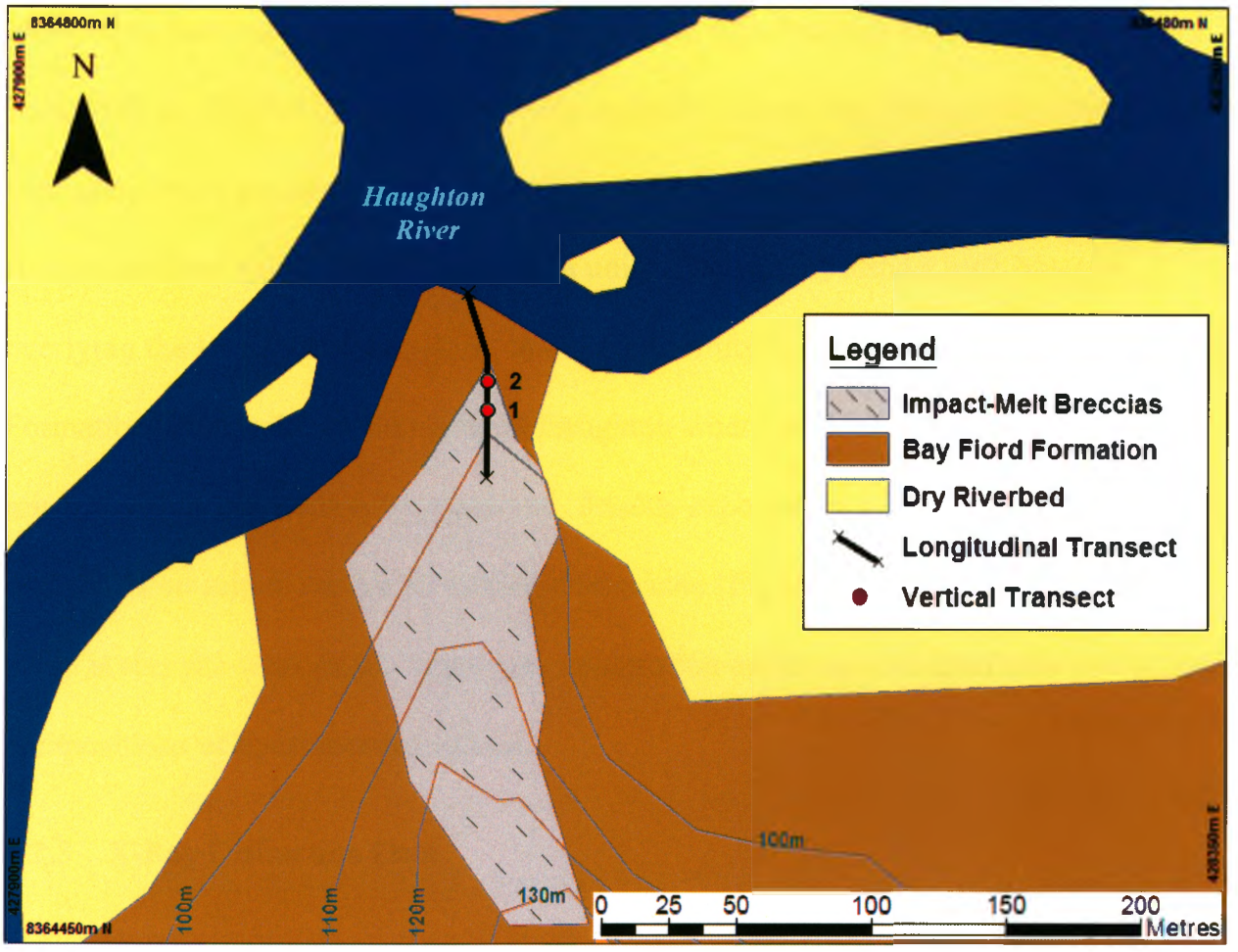

Figure 4.6. Simplified geological map of the Haughton River valley at the site of intra-melt breccia mineralisation. The locations of the longitudinal (black line) and vertical (red circles) sampling transects are shown. The longitudinal transect was prolonged lower in the geological sequence into target rocks belonging to the Bay Fiord Formation (brown unit), but mineralisation is concentrated in impact melt breccias (grey unit).

lithologies. Rare calcite vein filling within impact melt breccias have been reported by Osinski et al. (2005a) but, here, we solely consider calcite vug fillings. Moreover, gypsum vein samples do not usually contain calcite so they are excluded from this study. The Haughton River valley locality exhibits a unique outcrop of impact melt breccias overlying the Bay Fiord Formation, in close proximity to exposures of the Eleanor River Formation. This is the only locality at Haughton where such undisturbed hydrothermal mineralisation is known to be preserved. Freshly exposed intra-breccia voids host layered hydrothermal calcite coated by radiating marcasite (Figure 4.5B). The cross-sections made at this site were meant to provide information on the spatial distribution of isotopic compositions of hydrothermal calcite.

4.3.3 X-Ray Diffraction Data

The X-Ray Diffraction (XRD) data for hydrothermal samples can be found in a table in Appendix 1. Most of the samples contain calcite as they were identified as calcite-bearing prior to XRD analysis; however, other minerals than calcite could be present in a single sample. Moreover, their origin is not always hydrothermal as contamination from the host-rock might occur. Thus, XRD data proved to be helpful in discriminating unsuitable samples for stable isotopes analysis. Most of the samples of pure calcite composition were then analysed for stable isotopic composition (see Chapter 5), provided that host-rock contamination was avoided. The XRD data available herein will allow future stable isotopes work to be done on the remaining pure calcite samples.

4.3.3.1 Intra-Melt Breccia Hydrothermal Vugs

Hydrothermal calcite occurs as very-fine grained to coarse-grained, clear, translucent or milky. Discrete calcite vug-fillings from the impact melt breccias are often monomineralic and fine-grained; however, some vugs have a medium- to coarse-grained core. Vugs are either totally filled by calcite or show calcite crystals of several millimetres in length projecting in cavities. In contrast, some vugs have a different mineral composition in the outer rim compared to the core portion. For instance, a vug might have been filled by quartz at first and later by calcite. The various types of calcite vug filling occurrences are shown in Figure 4.7.

Sixteen distinct intra-melt breccia hydrothermal vugs, averaging 10 cm in diameter, were selected for XRD analysis. From those, twelve are carbonate vug fillings and four are quartz vug fillings (± calcite). A subset of the results is shown in Table 4.3. Carbonate vugs are either uniformly pure, or nearly pure calcite with trace amount of dolomite or quartz. The only exception (e.g., sample SA08-58C) is a dolomite-rich vug with lesser amounts of calcite and minor quartz content. The dolomite fraction is interpreted as being derived from the impact melt breccias, on which calcite crystals have grown, and incorporated in the powdered sample. Thus, some of the calcite vugs that present a very small fraction of dolomite are believed to be contaminated by dolomitic wall-rock. A larger number of vugs, seven in total, were analysed twice because of textural or compositional variations in their inner and outer portions (i.e., sample SA08-18). Most commonly, calcite occurs as euhedral crystals in the center of the cavity and very fine grained towards the outside (Figure 4.7B). Most vug fillings are homogeneously calcite-rich, but two vugs exhibit quartz-rich outer bands, whereas another calcite-rich

vug has quartz restricted to its core. In total, ten vugs partly or entirely composed of pure calcite were qualified for carbon and oxygen stable isotope analysis. It is worth mentioning that the largest vug sample is a 30 cm-wide bluish celestine vug (e.g., sample SA08-91) that was found at the base of an impact melt breccia outcrop (Figure 4.7F). However, the strontium sulfate ($SrSO_4$) composition and the absence of calcite signify that no stable isotope analysis could be performed on this hydrothermal vug sample.

4.3.3.2 Intra-Melt Breccia Hydrothermal Vugs at Haughton River Locality

Distinct calcite laminations associated with marcasite are observed at this locality, the largest of the intra-breccia vug occurrences (Figure 4.8) (Osinski et al., 2001). As discussed in the previous paragraph, sulfides are absent from isolated intra-breccia vug fillings. However, this specific locality exhibits significant dissemination but most impressively radiating marcasite coating. Also, additional hydrothermal phases previously observed by Osinski et al. (2005a) using XRD and electron dispersive spectrometry (EDS) analysis include, in decreasing abundances, fibroferrite ($Fe(SO_4)(OH).5H_2O$), celestine ($SrSO_4$), barite ($BaSO_4$), fluorite (CaF_2) and quartz (SiO_2). For this study, the vast majority of samples analysed by XRD are composed of calcite (i.e., samples HMP99-130 and HMP99-135). Two unique samples, SA08-89 and SA008-90, consist of marcasite-calcite laminated mineralisation (Figure 4.8). The pronounced occurrence of juxtaposed marcasite and calcite laminae (e.g., sample SA08-89) would indicate rapid changes in fluid chemistry (i.e., Murrowchick and Barnes, 1986; Osinski et al, 2005a). Sample SA08-90 reveals possible evidence of hydraulic fracturing, where interstices in the fractured early calcite deposit are progressively filled by superposed hydrothermal calcite layers (Figure 4.8C) (Phillips, 1972). This sample also shows slight changes

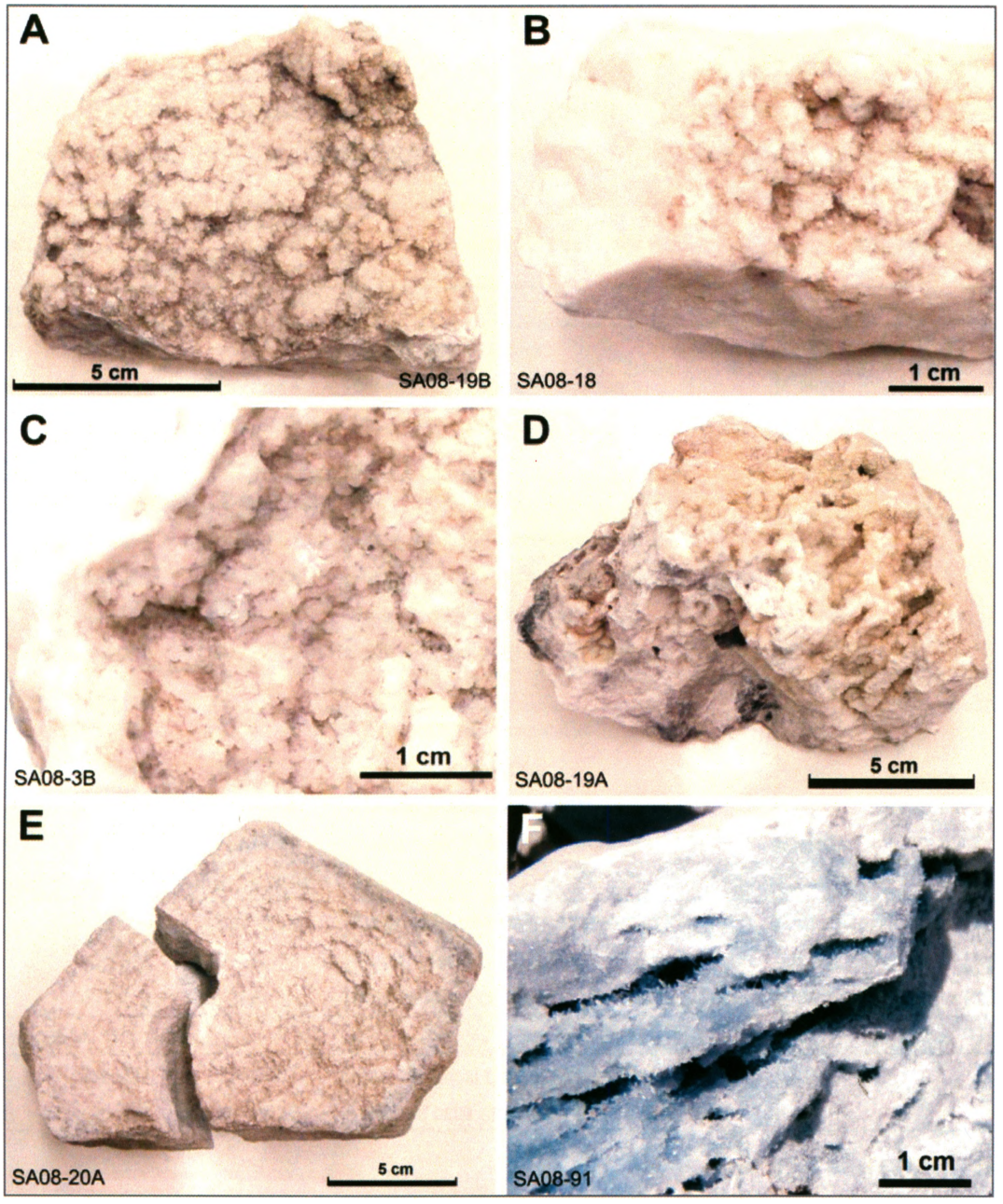

Figure 4.7. Representative occurrences of hydrothermal vug fillings within impact melt breccias at the Haughton impact structure. A, B, C and D: The calcite occurs mainly as clear to milky mm-size crystals usually overlying a massive or finer-grained precursor calcite mineralisation (well-developed in B and C); inter-connected crystal lining occurs locally (D). The stable isotopic data for these samples are presented in Chapter 5.
E: Example of quartz vug filling with concentric bands of mineralisation. F: Celestine, a strontium sulfate, is also found as vug filling but less frequently than calcite. In this case, a large 30cm-wide vug shows bands of very fine-grained sulfates deposited parallel to the outer surface of the vug, and crystalline sulfates partially fill the voids between bands. The absence of carbonate in E and F means that no stable isotope analysis was performed.

Table 4.3. Representative mineralogy of the four major hydrothermal settings at Haughton based on X-Ray Diffraction (XRD) analyses. The semi-quantitative nature of XRD data interpretation in this study only allows for relative mineral abundances to be given, which is sufficient for identifying candidate samples for stable isotopes analysis.

Sample ID	Coordinates - UTM NAD 83		Sample Description	XRD Mineralogy
	Easting	Northing		
Hydrothermal Intra-Breccia Vugs				
SA08-18-A	428379	8371586	Calcite vug; massive	Calcite
SA08-18-B	428379	8371586	Calcite vug; euhedral crystals	Calcite
SA08-92	428379	8369268	Large blue clestine vug	Celestine
SA08-20B	427549	8370683	Qz vug	Quartz (+ Calcite trace)
Hydrothermal Intra-Breccia Vugs at Haughton River Locality				
SA08-89-1	428034	8364700	Clear calcite on botrioidal marcassite	Calcite
SA08-90-1	428073	8364673	Very fined grained laminated calcite	Calcite
99-135-2	428000	8364425	Hydrothermal vug precipitate; coating	Calcite
SA08-93	428073	8364673	Laminated hydrothermal calcite	Calcite
Hydrothermal Veins				
SA08-10	426968	8371742	Calcite and pyrite veins in dolomite	Calcite
02-050	426540	8362015	Quartz vein; massive	Quartz
SA08-24	429400	8370737	Calcite and sulfide veinlet	Calcite >> Dolomite
SA08-59D	429309	8366947	Calcite veins in dolomite/shale	Calcite
Hydrothermal Brecciated Central Uplift				
SA08-4	425826	8371884	Eleanor River Fm Brecciated block	Dolomite = Quartz > Calcite
SA08-21	425023	8369279	Blue mineral coating; Eleanor Bay Fm	Quartz > Calcite >> Dolomite
SA08-33	427896	8366446	Blue mineral coating on Eleanor Bay Fm	Calcite > Quartz >> Dolomite
Hydrothermal Pipe Structures				
06-097	430536	8366607	Hydrothermal pipe structure; Calcite vug	Calcite
SA08-47B	430539	8366606	Layered pipe structure, euhedral crystals	Calcite

in marcasite composition from one layer to another (Figure 4.8D). For these reasons, XRD analysis was done on discrete calcite layers in order to determine if the mineralogy is similar throughout, and to study their distinct isotopic composition later.

As stated earlier, a longitudinal transect was completed at this cliff-section. Overall, systematic sampling across the collapsed zone revealed minor mineralogical variations. From the twenty sampling sites spaced every five metres, 16 have been analysed by XRD: 11 are pure calcite, and five samples show different amounts of calcite and dolomite. No other hydrothermal mineral or alteration phase was identified. Two of the dolomites (e.g., samples SA08-75 and SA08-76) were recognised as clasts from target rocks within the impact melt breccias, as evidenced by the presence of shatter cones.

4.3.3.3 Hydrothermal Veins

The hydrothermal vein deposits are calcite fracture fillings that cross-cut target rocks found exclusively within the impact structure, particularly the Thumb Mountain, Allen Bay and Bay Fiord formations. Veins are normally millimetre to centimetre in size and planar, irregular or sometimes suggestive of millimetre-scale displacement. In general, calcite veins are in sharp contact with the surrounding host rock. Most of the vein samples collected seem to have originated from a single mineralising event, i.e. show a single calcite filling. Nevertheless, multiple fillings can be observed especially in the larger centimetre-wide veins, as seen in Figure 4.9B. For this study, the multi-generation veins were not investigated by stable isotope analysis since the different calcite fillings could not be accurately separated. XRD analysis shows that samples collected at various locations in the impact structure equally consist of calcite (Table 4.3). In total, 31 calcite

vein samples were collected and a dozen were selected for XRD analysis. Veins with apparent multiple generations of infill were not analysed. Many of the rock samples were too friable or veins were too small to be able to accurately isolate the hydrothermal calcite from the host-rock. The XRD data indicated at first that a few samples were not pure calcite: they contained variable amounts of contaminant dolomite from the host rock, which made them unsuitable for stable isotopes analysis. Fortunately, powder samples that originally contained trace amounts of wall-rock dolomite were re-sampled with a more precise hand-drill: this resulted in the wall-rock dolomite fraction to be completely eliminated, as shown by the now dolomite-free XRD patterns.

4.3.3.4 Hydrothermal Pipe Structures

The pipe structures essentially developed in the crater periphery during the main stage of hydrothermal activity (Osinski et al., 2001). Hydrothermal minerals deposits are limited to calcite, quartz, marcasite, pyrite and late-stage sulfates and goethite. Several pipe structures were visited during the 2008 fieldwork but most of them were highly weathered and no significant calcite mineralisation was sampled. Generally, calcite could not be separated from the brecciated host-rock in which it precipitated, which resulted in most of pipe structure samples not being submitted for XRD or stable isotopes analysis. Importantly, two different samples (e.g., HMP06-097 and SA08-47B) from a pipe structure located on the eastern rim of the impact structure exhibit well-crystallised calcite filling of different crystal shapes and colours (Figure 4.9C). The XRD patterns confirm that they are composed of pure calcite. The altered carbonate host-rock displaying unusual banded textures, as seen in Figure 4.9D, was not analysed by XRD but is believed to be caused by intense iron oxy-hydroxide alteration.

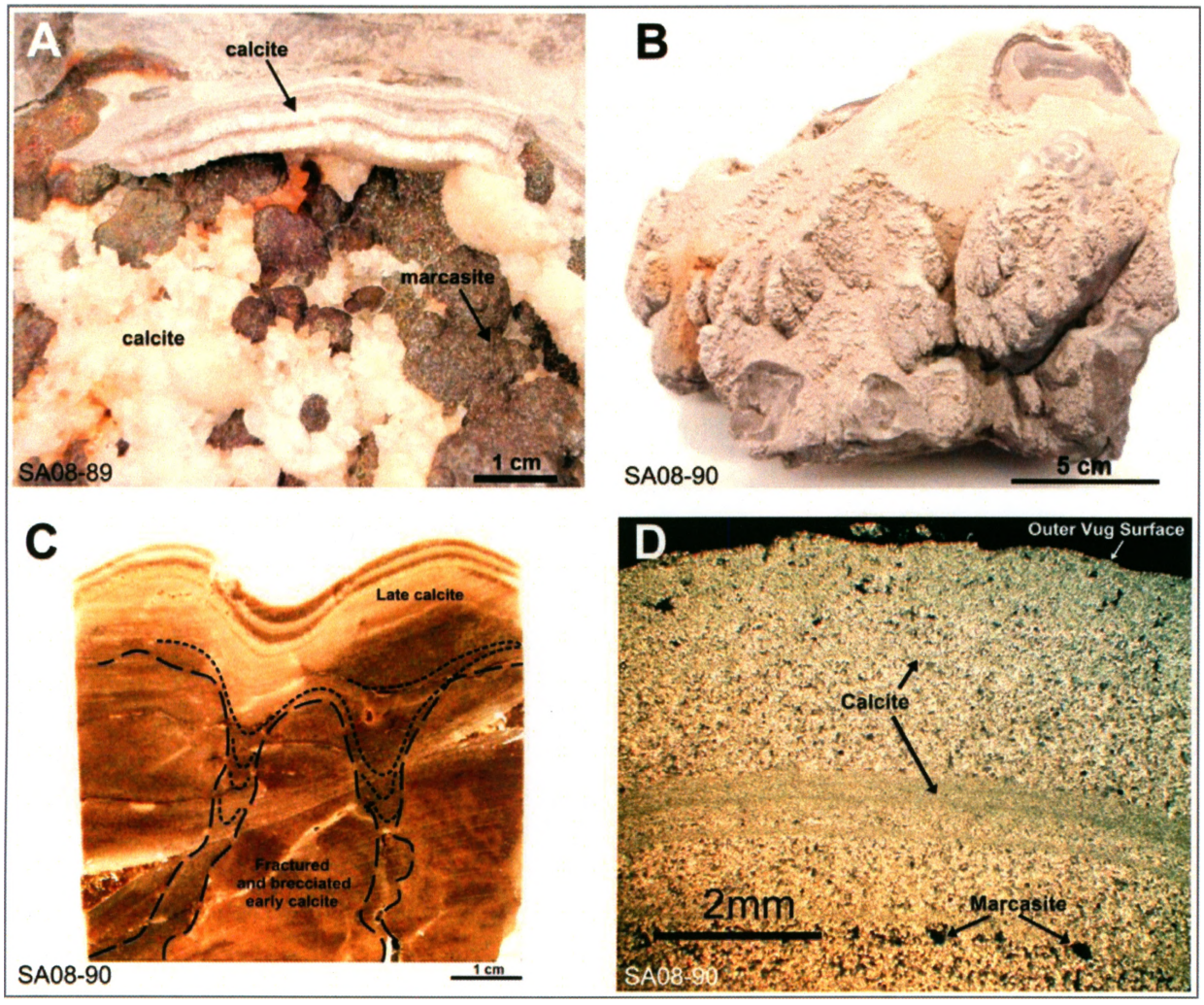

Figure 4.8. Representative occurrences of laminated calcite-marcasite mineralisation within impact melt breccias at the Haughton River valley locality. A: Multi-stage cavity-lining composed of coarse-grained calcite and radiated marcasite, overlain by medium- to fine-grained calcite laminea. B: Late-stage calcite laminea directly overlying impact melt breccias. C: Polished thin-section of multi-generation calcite laminae (same as B), where brecciated channels covered by new calcite precipitates are interpreted as evidence or forceful disruption by fluid, or hydraulic fracturing (Phillips, 1972;). D: Photo-micrograph of calcite laminea (same as B and C) showing the various abundances in marcasite disseminations within each distinct layer. Data from stable isotope analysis presented in Chapter 5.

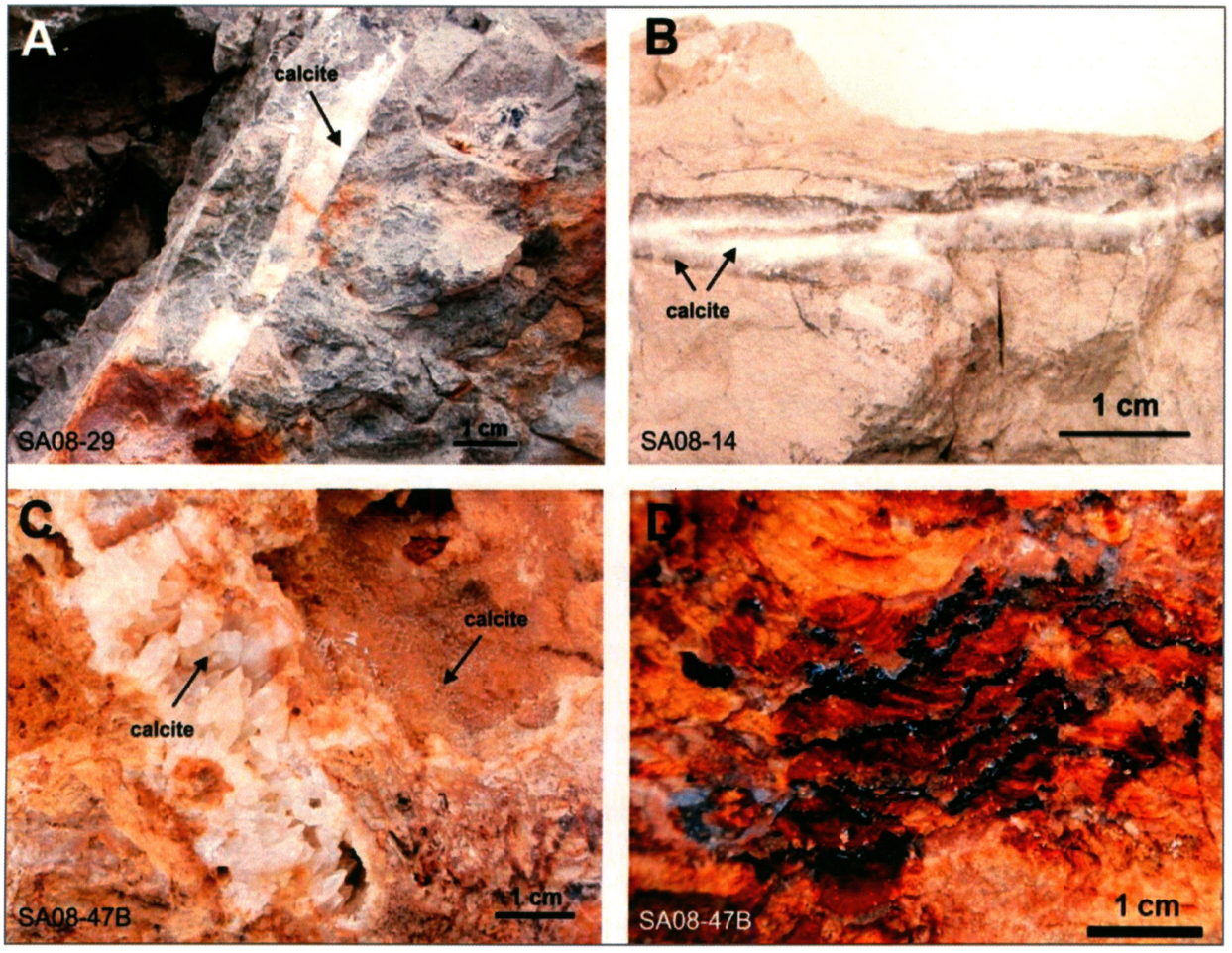

Figure 4.9. Prominent occurrences of hydrothermal calcite fillings within veins and pipe structures cross-cutting target rocks at the Haughton impact structure. These calcite veins only occur in the shocked sequence of target rocks, and are absent from identical lithologies outside the crater region. A: Field image of sub-vertical centimetre-wide calcite vein in a dolomite/shale outcrop located in the interior of the crater (north-east region). B: Multi-generation calcite vein showing local displacement, with brownish calcite on the walls and white calcite in center of vein, and cross-cutting units of the Thumb Mountain Formation. C and D: Field image of mineralised hydrothermal pipe structure cross-cutting dolomite bedrock on the eastern edge of the Haughton crater. The structure hosts crystalline calcite wall- and cavity-lining. The strongly banded alteration of the host-rock shown in D is suspected to be iron oxy-hydroxides. Sulfates are present in other pipe structures around the crater rim, but seem to be absent in this particular one. Stable isotope analysis was done on vein and pipe structure calcites (see Chapter 5).

Chapter 5. Carbon and Oxygen Stable Isotope Geochemistry

5.1 Introduction

As mentioned throughout this work, carbonate minerals commonly precipitate from aqueous solutions carrying carbonate ions (H_2CO_3, HCO_3^-, CO_3^{2-}) normally in equilibrium with atmospheric CO_2 gas (Hoefs, 1973). The resulting solid mineral phase (e.g., calcite) is enriched in ^{13}C relative to carbonate ions in the solution and the atmosphere, since heavier isotopes tend to bond more readily in the solid phase than in the liquid or vapor phases. Carbonate rocks formed by precipitation of carbonate ions dissolved in seawater have $\delta^{13}C$-values close to 0‰ on the V-PDB scale, since the V-PDB standard is itself a marine shell in equilibrium with seawater (Faure et al., 2005).

The fractionation of oxygen isotopes between water and calcium carbonate is temperature sensitive, as first demonstrated by Urey (1947), and provides one of the most commonly used geothermometre for low-, moderate- and high-temperature systems. The oxygen isotopic composition of carbonates depends on both the ^{18}O-isotope content of the water and the carbonate precipitation temperature. Thus, the variations in $\delta^{18}O$-values of calcite can be explained by both fluid composition and precipitation temperature (De Ronde et al., 1988).

The majority of low-temperature ($0< T \leq 30°C$) freshwater and marine carbonates have a $\delta^{13}C$-value near 0‰, in the -5 to +5‰ range, and most are between -2 and +2‰ (Hoefs, 2004). For example, the sequence of marine sedimentary carbonates at Haughton has an average $\delta^{13}C$-value of -0.5‰ (V-PDB) (Martinez et al., 1994). For oxygen

isotopes, $\delta^{18}O$-values of typical low-temperature carbonates are much more variable and typically fall between +10 and +35‰.

For the moderate temperatures of the hydrothermal calcite samples studied here, different equations describing the fractionation of ^{18}O isotopes between water and calcium carbonate are available. The equation used in this study is described by both O'Neil et al. (1967) and Zheng (1999),

Eq. 5.1

$$10^3 \ln \alpha_{calcite\text{-}water} = A\,(10^6)/T^2 + B\,(10^3)/T + C\,,$$

where $\alpha_{calcite\text{-}water}$ is the calcite-water fractionation factor $(\delta^{18}O_{calcite} + 10^3) / (\delta^{18}O_{water} + 10^3)$, at a temperature T in Kelvin, and A, B and C are constants. The constants from O'Neil et al. (1967) for this equation are A = 2.78 K^2, B = 0 K^2, and C = -2.89 for generation temperatures ranging from 0° to 500°C, whereas constants from Zheng (1999) are A = 4.01 K^2, B = 4.66 K^2 and C = 1.71 for temperatures between 0° and 1200°C. For simplification purposes, hydrothermal water is equivalent to hydrothermal fluid.

Essentially, carbon and oxygen isotopic compositions of carbonates formed in higher-temperature environments are both more depleted in the heavy isotope (^{13}C and ^{18}O) than low-temperature carbonates. At higher temperatures, the carbonate-water fractionation of light and heavy oxygen isotopes is less important since the stronger atomic bonds of heavy oxygen isotopes are more readily broken due to higher energy levels (Hoefs, 2004). Thus, the carbonate $\delta^{18}O$-value is lower than a comparable carbonate formed at a lower temperature. The $\delta^{18}O$-values keep decreasing gradually towards the oxygen composition of water (commonly $\leq$ 0‰) as temperature increases,

because of a weaker fractionation between ^{16}O- and ^{18}O-isotopes of water and carbonate at higher temperature. Usually, high-temperature carbonates display $\delta^{18}O$-values between ~5-20‰, while low-temperature ones are not as depleted and cluster near ~20-30‰.

The post-impact hydrothermal activity at Haughton resulted in various types of mineralisation in the lower levels of the impact melt breccias layer, and in the shattered target rocks of the central uplift and crater rim region (Osinski et al., 2001). As fluids percolated through the host-rocks, secondary carbonate deposits gradually filled interstices such as vugs and fractures left open in the host-rocks. The predominant hydrothermal carbonate present at Haughton is calcite, and, as previous studies have documented (Osinski et al., 2001, 2005a), no dolomite of hydrothermal origin has been observed. In brief, dolomite does sometimes precipitate from hydrothermal fluids, for instance in tectonically faulted carbonate plateforms (i.e., Katz et al., 2006), but it is uncommon. Hydrothermal dolomite has only been reported at a few impact structures: examples include the Kärdla and Neugrund craters (versh et al., 2006). At these sites, the rhomboedral to saddle-shaped dolomite crystals occur as fracture fillings (Versh et al., 2005). It was noted that these dolomites are noticeably richer in manganese and iron compared to sedimentary or diagenetic dolomite (Goldsmidt et al., 1961; Reeder, 1983).

5.1.1 Rationale for Stable Isotopes Geochemistry

The purpose of conducting a survey on the stable isotope geochemistry of target lithologies at Haughton was twofold: firstly, it helped verify that our analytical results compared well with those already in the literature; and secondly, isotopic composition of host-rocks might be linked to that of hydrothermal calcite, as later discussed in this study.

Ultimately, the characterisation of hard-rock target and impact-generated lithogies (e.g., impact breccias) is improved by identifying their stable isotope geochemical signatures.

For samples of hydrothermal nature, the use of stable isotope geochemistry is meant to further the available knowledge on the formation mechanisms and conditions of carbonate precipitation, as well as the source of elements in solution and their isotopic ratios, which in turn provides evidence on the source of fluids responsible for such mineralisation. Since the hydrothermal system within an impact crater is constantly evolving, analysing the composition of a series of carbonate deposits gives insight on fractionation processes and the evolution of the system. The potential to gain this type of data, in addition to the conventional XRD analysis, contributes to a better interpretation of the system and the origin of the samples. Approximately a dozen impact structures have already been scrutinised by stable isotope geochemistry techniques of their post-impact hydrothermal minerals (Table 5.1), which is a small number considering the amount of data these types of analytical means provide.

As hydrothermal processes play a major role in the formation of most ore bodies, gaining knowledge on such processes helps to understand ore deposits more accurately. In recent decades, stable isotopes have become an undeniable tool for geological studies, including ore deposit studies (Taylor, 1974; Ohmoto, 1986). The application of stable isotopes geochemistry principles on hydrothermal mineral deposits could certainly achieve important milestones in the comprehension of their genesis. This is also the case for less traditional geological settings in which ore deposits can be found, particularly

Table 5.1. Table of terrestrial impact structures for which studies on stable isotope geochemistry of carbonates have been reported. The upper part of the table shows a compilation of craters studied for their impact-generated hydrothermal carbonates, whereas the lower portion relates to studies on carbonates of a different origin (i.e., impact breccias, shocked target rocks, etc.). The current work on hydrothermal carbonates from the Haughton impact structure is not included here; a previous study on non-hydrothermal carbonates (Martinez et al., 1994) is however cited. The current study on hydrothermal carbonates at Haughton adds to the previous inventory of only 10 craters for which isotopic compositions of hydrothermal carbonates had been studied.

Impact Structure	Location	Age (Ma)	Diameter (km)	*Target rocks	Post-impact carbonate minerals	Stable isotopes data		References
						$\delta^{13}C$ [‰, VPDB]	$\delta^{18}O$ [‰, VSMOW]	
Post-impact hydrothermal carbonate minerals					*Hydrothermal origin*			
Chicxulub	Mexico	64.98 ± 0.05	180	S(t + c)	Calcite	[-7 to +2]	[+22 to +30]	Zürcher et al. (2005)
Kara	Russia	70.3 ± 2.2	65	S(t) + V	Calcite	[-10 to -3]	[+16 to +22]	Versh et al. (2006)
Kärdla	Estonia	~ 455	4	C + S(t)	Calcite, dolomite	[-23 to -2]	[+12 to +30]	Versh et al. (2005)
Lappajärvi	Finland	73.3 ± 5.3	23	C	Calcite	[+3 to +5]	[+25 to +26]	Versh et al. (2006)
Lockne	Sweden	455	7.5	C + S(t)	Calcite	[-14 to -2.2]	[+10.1 to +14.1]	Sturkell et al. (1998)
Neugrund	Estonia	~ 470	9	S	Calcite, dolomite	[-25 to -13]	[+23 to +25]	Versh et al. (2006)
Popigai	Russia	35.7 ± 0.2	100	C + S(t + c)	Calcite	[-14 to +7]	[+7 to +17]	Versh et al. (2006)
Puzhezh-Katunki	Russia	167 ± 3	80	C + S(t + c)	Calcite	[-27 to -2]	[+18 to +25]	Masaitis and Naumov (1993); Naumov (1999)
Siljan	Sweden	376.8 ± 1.7	55	C + S(t + c)	Calcite	[-21 to +8]	[+7.3 to +22.3]	Valley et al. (1988); Juhlin et al. (1991)
Sudbury	Canada	1850 ± 3	~ 250	C	Calcite (from SEDEX)	n/a	[+9 to +10.2]	Davies et al. (1990)
Non-hydrothermal carbonate minerals only (e.g. secondary, shocked clasts)					*Non-Hydrothermal origin*			
Haughton	Canada	39	24	S(t + c)	Calcite/dolomite in impact-melt breccias	[-4 to +9]	[+15 to +20]	Martinez et al. (1994)
Ries	Germany	15.1 ± 0.1	24	Cg + S(t + c)	Calcite in breccias, suevites	[-13 to +2]	[+8 to +28]	Skála and Žák (2001)
Chicxulub	Mexico	64.98 ± 0.05	180	S(t + c)	Carbonates in impact-melt breccias	[-5 to -1]	[+11 to +20]	Kettrup et al. (2000)
Sudbury	Canada	1850 ± 3	~ 250	C	Dolomite, calcite, kutnorite, manganosiderite (from host-rock matrix)	n/a	[+10.43 to +21.96]	Davies et al. (1990)

Locations, ages, diameters and target rocks from Earth Impact Database Website and Naumov (2005)

*Target rocks: C=Crystalline rocks; S=Sedimentary rocks: t=terrigenous, c=carbonate rocks, t + c=terrigenous and carbonate rocks; V: Volcanogenic rocks

impact craters (Greive et al, 1994).There is an increasing number of terrestrial impact craters that have been discovered. In comparison with the 118 impact structures reported in the 1980's (Gurov et al., 1988), more than 176 impact craters are now recognised (Earth Impact Database, 2010). Since a strong incentive for studying the stable isotopic ratios of minerals is to give information on the physical processes regulating ore deposition in a region, it could also be utilised to clarify whether an impact structure has the potential for hosting an economically profitable ore deposit (Reimolds et al., 2005). In a larger sense, this study of stable isotopes at the Haughton impact crater therefore achieves the goal of providing new or complementary information about the origin of the hydrothermal fluid, the temperatures of mineralisation and the physico-chemical conditions for mineral deposition, all of which are essential in understanding the genesis of ore deposits. As a result, the data presented in this manuscript could be utilised to understand the potential formation and the extent of significant ore bodies within the Haughton impact structure, and within craters of similar size in carbonate-dominated target rocks.

5.1.2 X-Ray Diffraction Geochemistry Link to Stable Isotopes

The X-Ray Diffraction data described in Chapter 4 were used to verify which samples were composed solely of calcite in order to proceed with the stable isotope analysis. As first, we had hoped to analyse carbonate mixtures with different extraction techniques (see Chapter 3). However, it was decided to perform stable isotope analysis only on samples composed of pure carbonate composition (e.g., all calcite or all dolomite) at first, and then proceed with samples composed of carbonate mixtures. Samples with a pure calcite composition were prioritised and analysed first on the MultiPrep; carbonate

mixtures would have been more complex to analyse. The analytical technique used for this study, the MultiPrep, allowed for a large number of calcite analyses to be made relatively quickly and reliably compared with the analysis of dolomite or carbonate mixtures. The reaction time of dolomite with phosphoric acid for CO_2-extraction and isotopic analysis is much longer than for calcite (see Chapter 3). In addition, since there were representative sets of samples of pure calcite composition from nearly all geological settings, and hydrothermal calcite had been recognised in different styles of mineralisation, a meaningful stable isotope study could be attempted using calcite as the main isotopic tracer. The pure dolomite-bearing and multiple-carbonate samples could be analysed later in a complementary study. As such, it will be explained in the following sections that the analysis of stable carbon and oxygen isotopes of calcite proves to be adequate for the Haughton impact structure as it provides additional means to distinguish the various types of hydrothermal calcite deposits.

5.2 Results from Stable Isotope Analysis

From a general point of view, samples analysed throughout this study show a range of $\delta^{13}C_{calcite}$ of approximately -14 to -2‰, and a range of $\delta^{18}O_{calcite}$ being approximately +8 to +26‰. The non-hydrothermal carbonates have a range in $\delta^{13}C_{calcite}$ from approximately -2 to 0‰, and the range of $\delta^{18}O_{calcite}$ is +20 to +26‰. The ranges for strictly hydrothermal calcites are as follows: the $\delta^{13}C_{calcite}$ ranges from -14 to -2‰ and the $\delta^{18}O_{calcite}$ ranges from +8 to +18‰. The detailed results for the different categories of non-hydrothermal and hydrothermal calcites will be presented later.

5.2.1 Non-Hydrothermal Carbonates Results

5.2.1.1 Unshocked Lithologies

For the current study, the two unshocked reference limestone samples originate from outside the crater, and are known to be unaffected by impact-shock metamorphism. These limestones have $\delta^{18}O$-values of +23.9‰ and +25.5‰ for the Lower Member of the Allen Bay Formation and the Irene Bay Formation, respectively. These values are within the range of carbonate rocks formed from normal precipitation from seawater that display $\delta^{18}O$-values ranging from around +18 to +30‰ (Hoefs, 2004) (Figure 5.1). More specifically, they match the range for marine limestone of the Ordovician-Silurian, which typically have $\delta^{18}O$-values of +21.5 to +25.5‰ (Keith and Webber, 1964). To create a more substantial dataset along with unshocked reference material, some of the shocked samples were selected for stable isotopes analysis. Overall, the stable isotopic compositions of limestone target rocks selected for this study vary from a low $\delta^{18}O$-value of +20.3‰ to a high value of +25.5‰, and a high $\delta^{13}C$-value of -0.2‰ to a low of -1.7‰ (Figure 5.2).

Since freshwater is normally depleted in the ^{18}O-isotope as compared to ocean water, and also more variable in the $^{13}C/^{12}C$ ratio caused by possibly higher contribution of organically derived CO_2, it seems possible to differentiate between marine and freshwater limestones. An equation by Keith et al. (1964) is used to establish if a limestone is from marine or freshwater origin,

Eq. 5.2

$$Z = a*(\delta^{13}C + 50) + b*(\delta^{18}O + 50),$$

where a and b are 2.048 and 0.498, respectively, and Z is the discriminating factor. A sample with a Z-value below 120 would be considered a freshwater limestone, whereas a sample with a Z-value above 120 would be considered as marine.

Although the calculated Z-values for all five limestone samples from Haughton are above 120 (Z= 133.95 to 139.8), the samples are much older (>400 Ma) than the age constraint given for the equation. It is important to note that freshwater could, in specific cases, be isotopically similar to seawater, thus the exact nature of the limestone can be difficult to evaluate. In any case, stable isotope compositions of sedimentary rocks do not provide unequivocal evidence for the origin of water involved during deposition and diagenesis, but should be added to the paleontologic, petrographic and lithostratigraphic observations (Hoefs et al., 1973). By analogy, crater-fill lake sediments from the Haughton Formation have a similar composition to marine carbonates since they reflect the contribution of detrital carbonates from the surrounding country rocks, as opposed to normal lacustrine sediments from limestone-free environments (Martinez et al., 1994).

5.2.1.2 Shocked Lithologies

Some samples were considered as potential reference material, although they had certainly been shocked as they were found lying on the rim or in the interior of the Haughton impact structure. These samples are part of the Lower Member of the Allen Bay, the Thumb Mountain and the Eleanor River formations. The Allen Bay Formation sample was found on the western crater rim region, where shock levels were relatively weak. The $\delta^{18}O$-value of +24.8‰ is within range of known typical values of +24 to +25‰ for this formation, as discussed previously. A similar oxygen-isotope value seems

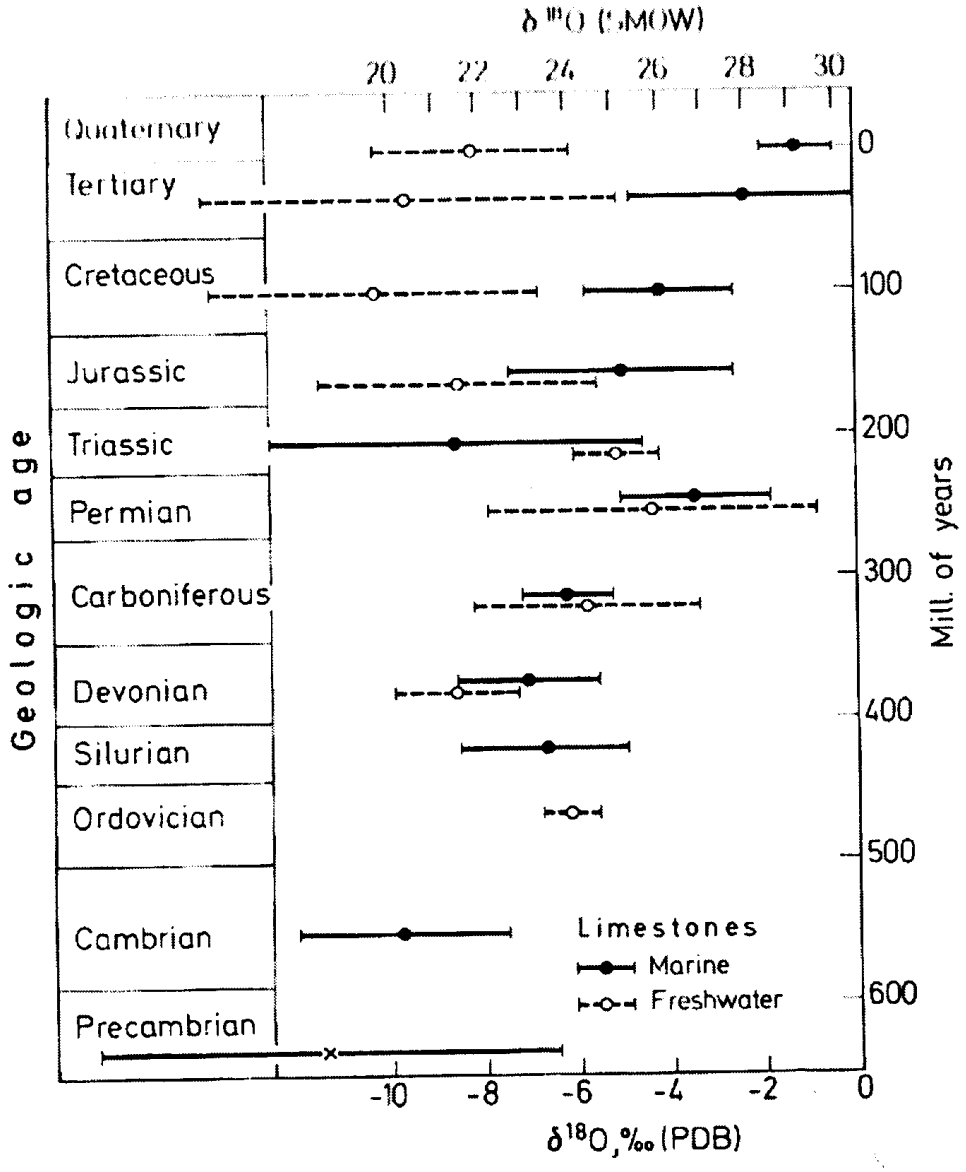

Figure 5.1. Variations of $\delta^{18}O$-ratios for marine (full line) and freshwater (dashed line) limestones through geological times. The sedimentary target sequence at Haughton is marine in origin and Ordo-Silurian in age. Carbonates from the Allen Bay Formation, for instance, were deposited between the Upper Ordovician and Lower Silurian. The vertical scale shows both geological ages (left) and number of million years (right). The horizontal axis shows $\delta^{18}O$-values in ‰ relative to PDB (lower) and to SMOW (upper). The V-SMOW reference system is preferred throughout this study and has the same scale as SMOW. (After Keith and Weber, 1964).

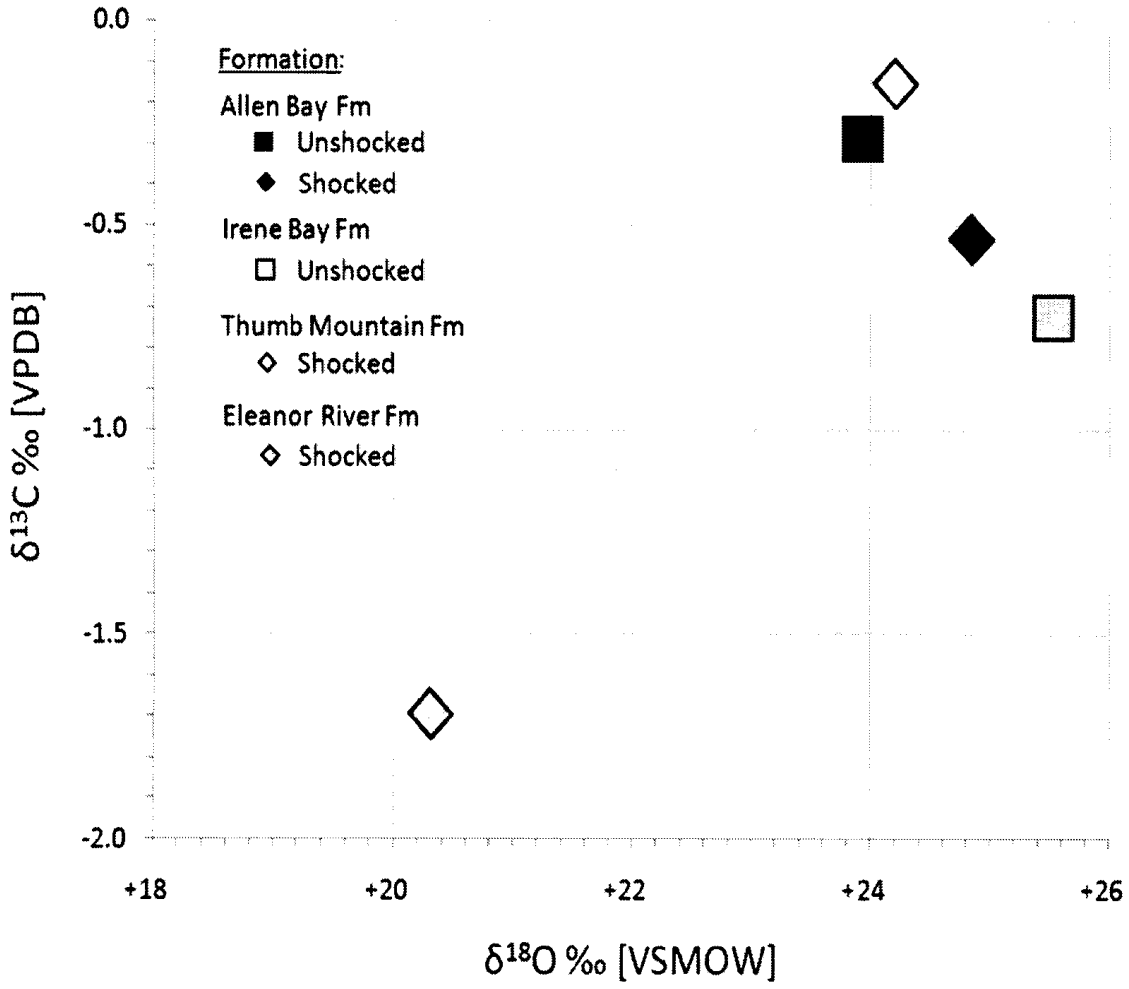

Figure 5.2. Carbon and oxygen stable isotope compositions of calcite-rich samples from reference target rock formations at the Haughton impact structure. The most widespread carbonate lithologies at the site of impact belong to the Allen Bay Formation, thus isotopic data are given for unshocked ($\delta^{18}O$= + 23.9‰, $\delta^{13}C$= -0.3‰; black box) and shocked ($\delta^{18}O$= +24.8‰, $\delta^{13}C$= -0.55‰; black diamond) carbonate rock units. The Irene Bay (grey box) and Thumb Mountain (white diamond) formations also show similar isotopic compositions. The shocked sample from the Eleanor River Formation (grey diamond) shows ^{13}C and ^{18}O isotopes depletion compared to other formations.

to characterise the Thumb Mountain Formation, with a $\delta^{18}O$-value of +24.2‰, although no sample from outside the crater has been analysed for comparison. The lowest of all oxygen-isotope values recognised belongs to a rock from the crater interior, which implies that possible shock processes may have altered its initial isotopic composition. The sample was collected on the outer margin of uplifted blocks of the Eleanor Formation that occupy the center of the crater. As a result, its $\delta^{18}O$-value of +20.3‰ might not be representative of the original isotopic composition prior to the impact. Unfortunately, as for the Thumb Mountain Formation, no pure calcite sample from the Eleanor River Formation was collected outside the crater to serve as unequivocal reference material for stable isotopic analysis, and no additional data regarding this formation could be found in the literature.

5.2.1.3 Impact Melt Breccias

The mineralogical study on impact melt breccias described in the previous chapter concluded whole rock samples were composed of carbonate mixtures and none was pure calcite, therefore, isotopic analysis was not performed (see Section 5.1). However, since the proportion of clasts in the impact melt breccias is not negligible, a selection of seven representative clasts from the impact melt breccia layer were analysed for isotopic composition (Appendix 2). Isotopic analyses were performed on these samples since their carbonate composition is pure calcite, and also because they represent allochtonous fragments from target lithologies of various provenances. Their $\delta^{13}C$-values vary from -6.0 to +1.1‰ (average: -1.5‰), and their $\delta^{18}O$-values from +11.3 to +24.3‰ (average: +23.9‰). Shocked sandstone clasts are, in contrast, more variable in composition with $\delta^{13}C$-values ranging from -6.2‰ to +1.1‰, and $\delta^{18}O$-values between +11.3 and +13.9‰.

5.2.2 Hydrothermal Carbonates Results

The unique morphologies and styles of mineralisation (i.e., void and fracture fillings, laminea) displayed by post-impact hydrothermal calcites demonstrated in this study allow for an evaluation of the hydrothermal context that has prevailed at Haughton. These carbonates are distinct from pre-impact reference carbonates as they have been formed exclusively from impact-induced hydrothermal fluids, as opposed to being present in the host-rocks prior to impact. The hydrothermal carbonates are not observed outside of the impact structure and restricted to fractures and cavities within pre-and syn-impact rocks. The geochemical signatures of non-hydrothermal carbonates are, however, typical of marine carbonates and are found in lithologies both inside and outside of the impact structure. Hence, hydrothermal carbonates provide a direct means of evaluating the post-impact environmental conditions within the Haughton impact crater.

At Haughton, the hydrothermal calcite is found in these three distinct spatial settings: 1) as fracture fillings within target rocks across the displaced zone and crater rim region; 2) as two types of vug fillings within the impact melt breccias, and 3) as interstial fillings in hydrothermal pipe structures in the faulted crater periphery. A distinction is made between vug fillings within the impact melt breccias: firstly, a family of discrete vugs (up to 30 cm in diameter) distributed sparsely in the impact breccias; secondly, another type of vug filling (up to 10 meter in diameter), which is marcasite-rich and found exclusively in two locations at the base of the impact breccias. Consequently, this means there are four different types of calcite mineralisation under investigation. The geological processes that led to the precipitation of impact-induced hydrothermal calcite at Haughton are not fully understood, thus, the study of carbon and oxygen stable isotopes should help

to shed light on their paragenesis. To date, the only stable isotope data ever published on the Haughton impact structure is known from the study of Martinez et al. (1994). As explained in the previous section, the authors have characterised shocked lithic clasts from the impact breccias and unshocked reference material from outside the crater. However, their study does not report any stable isotope data on hydrothermal deposits. Thus, the lack of stable isotope data from hydrothermal carbonates at the Haughton impact structure was an additionally important incentive for conducting a new stable isotope study.

Here, we present the detailed findings from stable carbon and oxygen isotope analysis of hydrothermal calcites for each of the four different hydrothermal settings. The full set of hydrothermal calcite samples analysed in this study display carbon isotopic compositions between -2.8 and -14.3‰ (VPDB), and oxygen isotopic compositions ranging from +8.8 to +17.2‰ (VSMOW) (Figure 5.5). For a complete listing of results, refer to Appendix 2. Subsequently, we will discuss the results by looking at the properties of the calcite precipitates and of the hydrothermal fluids.

5.2.2.1 Vug Fillings within Impact Melt Breccias

The infiltration of hydrothermal fluids into the impact intra-melt breccias left behind calcite deposits or encrustation that are isolated and confined to voids and surfaces of lithic clasts. The vugs do not exhibit any other hydrothermal carbonate mineral than calcite. The eight distinct samples analysed show $\delta^{13}C$-values ranging from –7.8 to -5.7‰ and $\delta^{18}O$-values from +10.4 to +13.1‰ (Figure 5.3). No firm correlation between carbon and oxygen isotopic compositions could be observed. Interestingly, sample SA08-58B-A

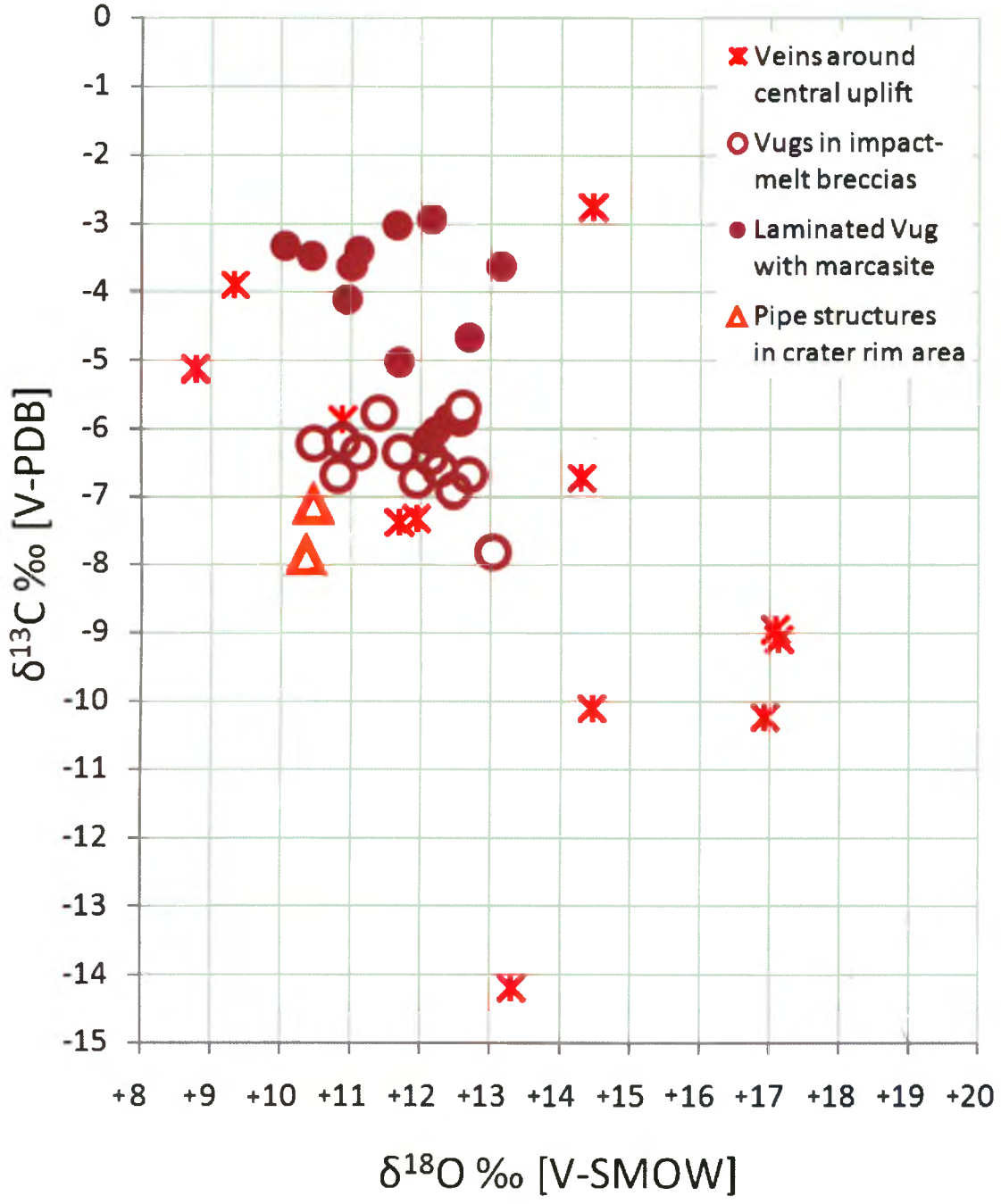

Figure 5.3. Carbon and oxygen isotopic compositions of the various hydrothermal calcite precipitates at the Haughton impact structure. The post-impact hydrothermal system generated calcites with $\delta^{18}O$-values ranging from >+8‰ to <+18‰, and $\delta^{13}C$-values between >-15‰ and <-2‰. The majority of calcite vugs (filled and empty circles) have $\delta^{13}C$-values between -8‰ and -3‰, and $\delta^{18}O$-values between +10‰ and +14‰. On average, calcite-marcasite vug fillings (filled circle) show higher $\delta^{13}C$-values, by nearly +2‰, than monomineralic vugs (empty circle). Veins (cross) have wide isotopic ranges, both in $\delta^{18}O$ and $\delta^{13}C$. Pipe structures (triangle) are characterised by low $\delta^{18}O$- and $\delta^{13}C$-values. Since different types of mineralisation are distinguishable by different isotopic signatures, it allows for interpretation of the particular conditions of mineralisation.

shows both the lowest $\delta^{13}C$-value and the highest $\delta^{18}O$-value of all samples. However, no visible feature or difference compared to other samples can explain its unique isotopic compositions. For homogeneous monomineralic vugs, only one isotopic analysis was performed. However, since many of the discrete vugs host two recognisably different types of calcite infill, normally in the form of a finer grained border with a coarser crystalline core, two stable isotope analyses were necessary to evaluate their respective compositions. As a result, there are 14 data points in total. The outer and inner portions of sample SA08-19B, for instance, were analysed separately and revealed an ^{18}O-enriched core by about 1.7‰ as opposed to the outer layer (Table 5.2). This apparent enrichment is observed for many of the calcite vug samples, on average by +0.7‰, and greater than the analytical precision of ±0.2‰.

5.2.2.2 Marcasite-Rich Vug Fillings within Impact Melt Breccias

This type of mineralisation associated with marcasite is similar to the abovementioned monomineralic calcite vug deposits, but is found at a large basal impact-melt breccia outcrop in the southeast of the impact structure. Twenty-three samples from the Haughton River valley locality were submitted for stable isotopes analysis. In terms of isotopic compositions, this type of calcite mineralisation is somewhat distinguishable from monomineralic calcite vug deposits. Indeed, calcites have $\delta^{13}C$-values within the -6.2 to -2.9‰ range, and $\delta^{18}O$-values between +10.1 and +13.2‰. In comparison to monomineralic calcite vugs, these calcites are on average similar in terms of oxygen isotopic composition but are enriched in ^{13}C by nearly 2‰. As shown in Table 5.2, two samples identified as SA08-89 and SA08-90 are important to consider because of laminated calcite textures, an important indicator of continuous or at least repeated events

Table 5.2. Representative carbon and oxygen stable isotope compositions of hydrothermal calcite samples from Haughton, with data sorted by setting. The entire dataset of $\delta^{13}C$- and $\delta^{18}O$-values, along with XRD and XRF data, is found in Appendix 2.

Sample ID	Coordinates - UTM NAD 83		Sample Description	$\delta^{13}C$	$\delta^{18}O$
	Easting	Northing		‰ (VPDB)	‰ (VSMOW)
Hydrothermal Intra-Breccia Vugs					
SA08-18-A	428379	8371586	Calcite vug; massive outer section	-6.20	+10.46
SA08-18-B	428379	8371586	Calcite vug; inner euhedral crystals	-6.34	+11.10
SA08-19B-A	428455	8371450	Calcite vug; massive outer section	-6.68	+10.81
SA08-19B-B	428455	8371450	Cc vug, inner octahedral crystals	-6.90	+12.46
Hydrothermal Intra-Breccia Vugs at Haughton River Locality					
SA08-89-1	428034	8364700	Clear calcite on botrioidal marcassite	-6.03	+12.22
SA08-90-1	428073	8364673	Very fined grained laminated calcite	-4.66	+12.67
SA08-90-2	428073	8364673	Fine grained calcite, underlying SA08-90-1	-4.11	+10.94
Hydrothermal Veins					
SA08-29	429271	8369432	Cm-wide calcite veins with local sulfides	-6.71	+14.31
SA08-36	420419	8371023	Calcite vein perpendicular to bedding	-3.89	+9.33
SA08-56	428811	8371895	Vertical vein cross-cut horizontal dolomite	-5.87	+10.87
Hydrothermal Pipe Structures					
HMP06-097	430536	8366607	Hydrothermal pipe structure; Calcite vug	-7.13	+10.46
SA08-47B	430539	83666606	Layered pipe structure, euhedral crystals	-7.87	+10.36

of mineralisation. Two of the calcite layers visible in sample SA08-90 were analysed for isotopic compositions: the outer-most layer, and a second layer ~2 centimetres underneath. The results indicate ^{18}O-enrichment of the outer-most laminae ($\delta^{18}O$ = 12.7‰) compared to the underlying one ($\delta^{18}O$ = 10.9‰), and slight depletion in ^{13}C from these same layers ($\delta^{13}C$ of -4.7 and -4.1‰), which is arguable as it lies close to the detection limit (± 0.2‰). The same strategy was applied to some of the laminae found in sample SA08-89, which has a 1-cm thick marcasite coating. However, the $\delta^{13}C$-values ranging from -6.0 to -5.8‰ (average: -5.9‰) and $\delta^{18}O$-values of +12.2 to +12.5‰ (average: 12.4‰) are identical for each layer within the analytical precision limit. Lastly, massive hydrothermal calcite samples have their $\delta^{13}C$-values ranging between -4.1 to -2.9‰ and cluster around -3.5‰, whereas late-stage calcite coatings have lower $\delta^{13}C$-values between -6.2 to -4‰.

Regarding the longitudinal transect across the collapsed vug, the overall small variability in isotopic compositions is similar to the uniform mineralogical compositions discussed in Chapter 4 (Figure 5.4). Two samples differ greatly with unusually high isotopic compositions: sample SA08-75 has a $\delta^{13}C$-value of -1.3‰ and $\delta^{18}O$-value of +21.6‰, and sample SA08-76A has a $\delta^{13}C$-value of -1.3‰ and $\delta^{18}O$-value of +21.0‰ (see Appendix 2). These values are similar to limestone and could either be derived from a clast or from the uppermost portion of underlying bedrock (e.g., Bay Fiord Formation), as evidenced by the presence of shatter cones in both samples. As such, these results show that for these specific samples, it is difficult to determine whether these samples only contain pure hydrothermal carbonates. Finally, the two vertical cross-sections have not been analysed for stable isotopes ratios since prerequisite XRD analysis was not done.

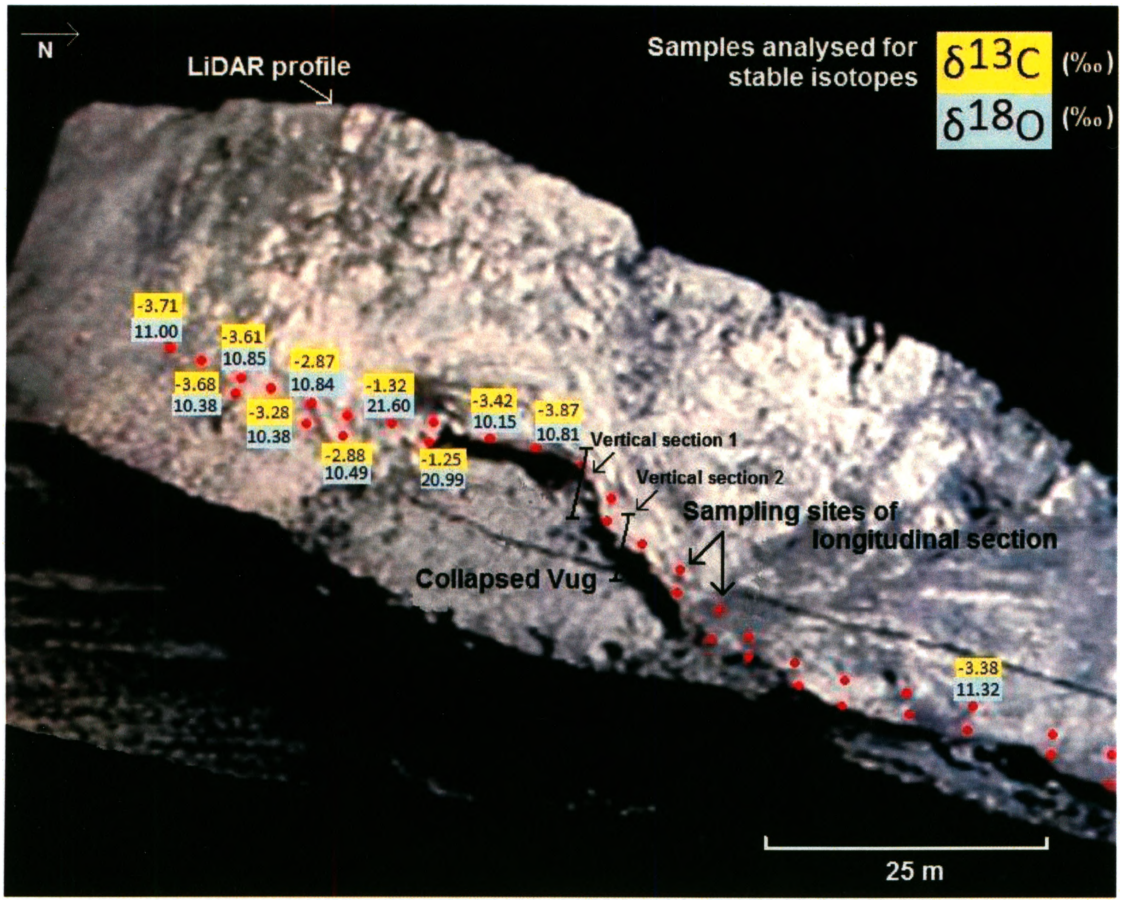

Figure 5.4. Carbon (yellow) and oxygen (blue) stable isotope data from samples collected on a longitudinal transect at the Haughton River valley locality. The data are superimposed on a low-resolution LiDAR image of the mineralised outcrop. Additional modeling of this outcrop has been made by Osinski et al. (2010). Impact melt breccias represent a large proportion of the outcrop (pale grey) in the center and left-side, and dolomitic blocks of the target Bay Fiord Formation medium grey) are seen on the far right-side. Samples without isotopic value have not been analysed either for time constraints, or due to samples containing a proportion of dolomite with the calcite. The locations of the two additional sampling transects (vertical) are also indicated.

5.2.2.3 Vein Fillings within Shocked Target Rocks

Hydrothermal veins that are composed of pure calcite only were selected for stable isotopes analysis, considering that wall-rock contamination was avoided by sampling with the hand-held drill equipped with a mm-size carbide bit (see Section 5.1). Furthermore, veins that exhibit clear evidence of multiple generations of calcite infill (i.e., samples SA08-13 and SA08-14) were not analysed. This means that only a dozen vein calcite samples were appropriate for analysis. It is worth mentioning that, although rare calcite veins have been found cross-cutting clasts and groundmass in impact melt breccias samples (Osinski et al., 2005a), this particular type of mineralisation is not studied here.

The distribution of isotopic compositions from calcite veins in this study is shown on a map of the Haughton impact structure (Figure 5.5). Results from stable isotope analysis indicate vein samples are more variable in terms of isotopic composition compared to the other styles of hydrothermal calcite deposits at Haughton. Both carbon and oxygen isotopic variations are much larger than for calcite vug fillings. As seen in Figure 5.5, $\delta^{13}C$-values of vein calcite range from -14.2 to -2.8‰, and $\delta^{18}O$-values vary from +8.8 to +17.2‰. The majority of samples have a similar or higher $\delta^{18}O$-value than intra-breccia calcite vug fillings. The lightest oxygen-isotope calcite veins (e.g., samples SA08-59E and SA08-36) have $\delta^{18}O$-values of +8.8 and +9.3‰; their $\delta^{13}C$-values are also among the highest. The most ^{13}C-depleted calcite vein (e.g., sample HMP02-053) and most ^{13}C-enriched vein (e.g., sample SA08-10) occur in the southern and northern periphery of the central uplift, respectively, and at a similar radial distance of ~5 kilometres to the centre of the crater. Also, samples that have the highest $\delta^{18}O$-values

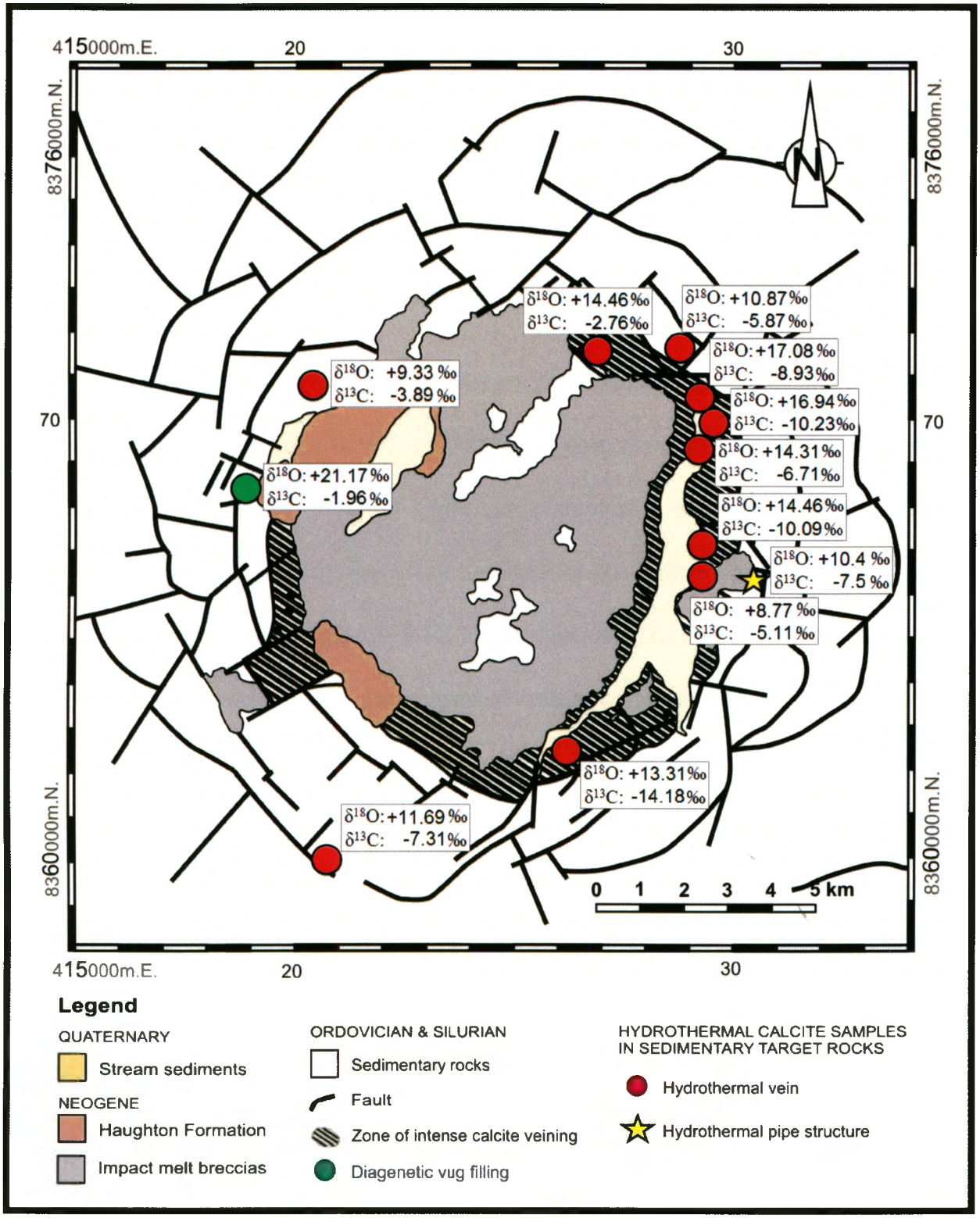

Figure 5.5. Distribution of carbon and oxygen stable isotopic compositions of hydrothermal calcite veins (red circle) and pipe structure (yellow star) at the Haughton impact structure. For reference, the isotopic composition of a diagenetic vug precipitate (green circle) located in the Middle Member of the Allen Bay Formation is also shown. A zone of intense veining occupies the inner crater annulus and crops out in the eastern portion. (After Osinski et al., 2001).

(e.g., HMP99-104 and SA08-27) were found at two closely-spaced localities of Bay Fiord Formation outcrops on the periphery of the central uplift. Also, an isolated calcite vug found in rocks from the Allen Bay Formation in the western part of the crater has a $\delta^{13}C$-value of -2.0‰ and a $\delta^{18}O$-value of +21.2‰ (Figure 5.5).

5.2.2.4 Cavity Fillings within Hydrothermal Pipe Structures

Localised calcite mineralisation along with sulfides (e.g., marcasite, pyrite, chalcopyrite, goethite) occur within hydrothermal pipe structures situated strictly in the faulted crater annulus and not in the impact melt breccias (Osinski et al., 2001). The hydrothermal vent analysed in this study outcrops in the eastern crater rim region, east of the Haughton River Valley (Figure 5.5). These deposits differ from calcite fracture fillings as they are vertical cylinder-shaped alteration patterns, similar to gossans, and mainly located around faults (Osinski et al., 2001). The strong pervasive alteration of the brecciated wall-rocks enhances weathering, therefore, sampling pristine calcite is almost impossible. Stable isotope analysis of two samples from this location has been performed: sample HMP06-097 has $\delta^{13}C$-value of -7.1‰ and $\delta^{18}O$-value of +10.5‰; sample SA08-47B has $\delta^{13}C$-value of -7.9‰ and $\delta^{18}O$-value of +10.4‰ (Table 5.2). This data are similar to that of the most ^{13}C- and ^{18}O-depleted intra-breccia vugs, as well as some of the veins.

5.2.3 Predicted Hydrothermal Fluid Composition

First of all, the analysis of stable isotope ratios of both hydrothermal minerals and fluid inclusions have been applied broadly in studies of hydrothermal ore deposits in order to define the temperatures, fluids, and physical and chemical processes involved in

ore deposition (Taylor, 1974). Shepherd et al. (1985) made a complete review on the use of fluid inclusions in geology.

Since no direct isotopic measurement of trapped fluids was performed in this study, it was decided to use fluid inclusion geothermometry data for some of the calcite samples to help identify a temperature range for the hydrothermal fluid at the time of calcite deposition. For this, temperatures of homogenisation of the vapour and liquid phases were used. The $\delta^{18}O$-value attributed to the hydrothermal fluid was, therefore, evaluated using fluid inclusion data reported by Osinski et al. (2005a). Many studies, such as the one by Molnar et al. (1999) on Cu-Ni-PGE veins in the Sudbury impact structure, examined mineral fluid inclusions to learn about the characteristics of hydrothermal solutions. For our study, the key samples are three pure calcite specimens (e.g., HMP00-136, HMP99-135 and HMP99-104) for which reliable fluid inclusion data were already available. Also, these samples had to be physically available for re-sampling so that a powder subsample could be extracted to perform stable isotopes analysis. The samples represent two calcite vein fillings in shocked target rocks and a calcite vug filling in impact melt breccias from the Haughton River valley.

The present results are based on primary aqueous-salt fluid inclusions uniquely, and not on secondary or hydrocarbon-rich inclusions. For primary fluid inclusions, the salinity is overall very low, generally < 2% NaCl equivalent (Osinski et al., 2005a). The three calcite samples used for calculating the $\delta^{18}O_{fluid}$-value are shown in Table 5.3. Unexpectedly, the reliability of temperatures of homogenisation derived from sample HMP99-104 is somewhat lower than for samples HM00-106 and HMP99-135. The large majority of primary fluid inclusions in this sample are one-phase (liquid-filled) therefore,

no heating experiments could be performed. The presence of liquid-filled fluid inclusions indicates calcite precipitated from vapour-free fluids (Osinski et al., 2005a).

5.3 Discussion

5.3.1 Overview of Available Data and Rationale

In general, silica minerals – including quartz – precipitate in oxygen isotopic equilibrium with coexisting water and are not typically affected by isotopic exchange at temperatures < 250 °C (e.g., Clayton et al, 1968; O'Neil, 1987). Clay minerals are also quite resistant to oxygen isotopic exchange but less so than silicates, and at lower temperatures (O'Neil, 1987). In comparison to silicates and clays, calcite exchanges oxygen isotopes relatively rapidly at temperatures down to about 100°C (Clayton et al, 1968; O'Neil, 1987). Results from previous studies also show that carbonate minerals tend to equilibrate readily with fluids down to ~100°C in zones of sufficient permeability, so that isotopic values observed are indicative of fluid geochemistry (Clayton et al., 1968; Blattner, 1975; Sturchio et al., 1990). In any case, the isotopic composition of calcite is used as an indicator of the precipitation conditions for environments such as hydrothermal systems (see Figure 5.4). The study of isotopic compositions of several co-existing minerals within a system is ideal since data from different minerals are used together and compared to have more precise information on a particular hydrothermal system (e.g., Sturchio et al., 1990). Hydrothermal calcite is the basis of this study since it is widespread throughout the impact structure, and was precipitated through most of the lifetime of the impact-hydrothermal system.

Several observations support the fact that the original isotopic compositions of calcite at Haughton have been largely preserved, and could be used to ascertain information on the nature of the host fluid. Firstly, $\delta^{13}C$- and $\delta^{18}O$-values are variable, suggesting calcite has not undergone chemical exchange after deposition since this would tend to show a trend of homogenised isotopic values. Secondly, distinct clusters of carbon and oxygen isotopic signatures are present that are related to mode of occurrence. Therefore, each type of calcite deposit can be more or less identified based on its own carbon and oxygen isotopic signature. Thirdly, available data from calcite fluid inclusions indicate a high-temperature environment of deposition, which strongly suggests that the initial isotopic composition of crystals has not been reset either. Fourthly, isotopic values have most likely been preserved because hydrothermal activity in an impact crater is only transient and retrograde in nature, which means that a second episode of hydrothermal activity did not occur. There is debate on the fact that calcite might be more vulnerable than other minerals, for instance quartz, to isotopic exchange after deposition in active intra-continental geothermal systems (i.e., Stipp, 1998). Again, these data suggest that there is a clear variability in isotopic composition between different deposits, and also that temperatures of calcite precipitation given from fluid inclusions are viable. An important fact to highlight is that co-existing calcite layers within a single intra-melt breccia vug often show significant shifts in isotopic compositions, thereby indicating that the original isotopic signatures of layers have been preserved. Finally, the very dry and cold environment seen on Devon Island could have also contributed to minimise isotopic interaction between calcite and meteoric water, although weathering has been occuring.

5.3.1.1 Significance of Results and Distinction from Previous Studies

The geochemistry work by Martinez et al. (1994) on carbonates from Haughton might, at first, be recognised as a precursor study of the current one presented in the manuscript. However, the impact-hydrothermal carbonates were first reported by Osinski et al. (2001), many years after the study by Martinez et al. (1994), and had not been analysed by stable isotope techniques prior to our study. The main science goal of Martinez et al. (1994) was oriented on syn-impact processes such as trying to understand carbonate target decomposition upon impact, through carbonate-silicate reactions and the formation of secondary carbonates from back-reactions between impact-released CO_2 and residual Ca oxides. The mineralogical and isotopic evidence they discuss suggest that impact-related processes would retain more volatiles within rocks produced during impact events than previously thought. In order to achieve this, Martinez et al. (1994) used SEM and stable isotope geochemistry to study pre-impact target lithologies around Haughton, plus the mineralogy and textures of the impact breccias, as well as the shocked fragments incorporated in the breccias. Although the present study does not have the same objectives, a similar approach to the one by Martinez et al (1994) was to characterise target lithologies, both in a mineralogical and stable isotopes perspective. The possible link or correlation that was expected between the general isotopic compositions of target rocks versus that of hydrothermal carbonates also necessitated to first investigate reference target rocks. Fortunately, the isotopic compositions of the reference material analysed in this study are similar to the ones reported by Martinez et al. (1994). Another difference is that the study presented here has only looked into mono-mineralic samples containing calcite, whereas Martinez et al. (1994) analysed mixed carbonate samples by

measuring the calcite and dolomite fractions from a single sample separately. However, for the purpose of our study, each sample analysed has a record of its specific location (geographic coordinates), as well as a description of the type of lithology and most importantly the rock formation to which it belongs. In the case of Martinez et al. (1994), there is no reference to the name of the rock formation for reference material, and only denoted as dolomite, sandstone or lake sediment sample. By recording the host formation of a sample, the present study ensured that isotopic compositions of the different sedimentary target rock samples can be linked to their respective stratigraphic unit, which can then be joined to field and mineralogical observations from previous study. For samples of hydrothermal material, an identical methodology to that of reference material samples has been followed. This way, information on the spatial and geological features relative to a sample can be given, which might have an influence on its isotopic compositions. As stated above, secondary carbonates have been analysed by Martinez et al. (1994) and are dominated by calcite. Far from being hydrothermal, this calcite rather comes from back-reactions between silica and carbonate phases (or from actual impact melt carbonates). The CO_2 released from shocked target rocks upon impact is believed to have interacted with the residual oxides that settled throughout the impact melt breccias to produce secondary calcite. In contrast, the calcite discussed in the present study has not been produced from impact processes, but later, since it occupies vugs within the solidified breccias and was precipitated from solution. An important fact is that hydrothermal calcite is restricted to the lower reaches of the impact melt breccias layer, and in target rocks across the impact structure (Osinski et al., 2005a). In addition, the isotopic compositions of the matrix-forming calcite in impact breccias described by Martinez et al. (1994) have unique signatures: $\delta^{13}C$-values range from -3.5 to +9‰ and

$\delta^{18}O$-values from +15 to +22‰. Interestingly, the isotopic compositions of hydrothermal calcite do not overlap with those of impact-generated calcite: hydrothermal calcites analysed in the present study show lower values, both for $\delta^{13}C$ and $\delta^{18}O$.

Again, the recognition of a significantly larger melt component within the impact breccias at Haughton came with Osinski et al. (2001) – who proposed the term impact melt breccias – much after the study by Martinez et al. (1994). This implies that the theories brought forward by Martinez et al. (1994) with respect to carbonate decomposition, and the formation of syn-residual oxides and carbonates, might have to be revisited. Certainly, the syn- and post-impact processes in a carbonate-rich target like the one at Haughton are far from being understood.

5.3.2 Interpretation of Results for Non-Hydrothermal Carbonates

Reference material from outside the Haughton impact structure had previously been analysed for isotopic compositions (Martinez et al., 1994). A majority of reference material reported by the authors are dolomite-rich carbonate rocks with $\delta^{18}O$-values of +24.1 to +28.9‰, and sandstones containing smaller carbonate fractions with $\delta^{18}O$-values ranging between +22.7 and +25.4‰. The one unshocked reference limestone sample analysed by Martinez et al. (1994) is characterised by a $\delta^{18}O$-value of +24.3‰, which is very similar to our average value of +24.7‰.

Whole-rock $\delta^{18}O$-values from the Allen Bay Formation are, however, slightly lower than those observed by Land et al. (1975) in the northwest part of Devon Island. Land et al. observed $\delta^{18}O$-values throughout the Allen Bay Formation carbonate beds ranging from +26.2 to +31.3‰. Similarly, about half of the dolomite samples from

Martinez et al. (1994) have $\delta^{18}O$-values ranging between +27 to +29‰, whereas the remaining samples have $\delta^{18}O$-values in the +24 to +25 ‰ range.

The variability in these $\delta^{18}O$-values is probably attributable to the various rock formations that were sampled. However, no precise information is given by Martinez et al. (1994) on the provenance of the various samples: all their reference samples are labelled RS and the types of rocks are listed (i.e., dolomite, sandstone, etc.), but no formation name is indicated. A large proportion of the rocks outcropping within the Haughton crater and its vicinity, mostly in the western section, belong to the Middle Member of the Allen Bay Formation mainly composed of dolomite. As a result, these rocks were not analysed for stable isotopic compositions in this study. It is, therefore, possible that dolomites from the Middle Member of the Allen Bay Formation have a different isotopic composition than the Lower Member (+24 to +25‰), judging from the higher $\delta^{18}O$-values of +28 to +29‰ observed by Martinez et al. (1994).

Lastly, it is worth noting that dolomite usually shows higher $\delta^{18}O$- and $\delta^{13}C$-values than co-occurring carbonates (Bausch et al., 1972). Although the isotopic fractionation of carbon and oxygen in the dolomite-water system is not really well understood, experimental studies of mineral equilibration at high temperatures allow for extrapolation of the fractionation factors. The results show that the oxygen isotopic composition of dolomite is 3 to 5‰ heavier than syngenetic calcite. A more attenuated carbon isotope fractionation occurs as dolomite is 1 to 2.5‰ heavier than calcite. These values are, however, very rarely observed in nature and the isotopic fractionation is often not as predictable (Bausch et al., 1972). Natural dolomite-rich rocks are, therefore, susceptible to having slightly higher $\delta^{18}O$- and $\delta^{13}C$-values than limestones.

Sample HMP06-093 from the Eleanor River Formation has also been analysed by XRD, and its composition is mostly calcite. As for the other samples of this formation, they come from the central uplift, a region where only quartz is present as a secondary hydrothermal phase, precipitated in late-stage of hydrothermal activity. The mineralogy of sample HMP06-093 does not indicate hydrothermal quartz as a constituent of the rock, as opposed to other samples from this formation that were consequently not analysed for the stable isotopic compositions. The sample seems homogeneous in composition and texture; however, more in depth petrography has to be done. Thus, it is considered likely that the sample does not show hydrothermal carbonate alteration and that the calcite composition revealed by XRD represents the original limestone mineralogy. In this case, the carbon and oxygen stable isotope data are probably meaningful. However, the fact that this sample was collected near the centre of the crater means that it was affected by shock-metamorphism. In fact, the sample displays shatter cones. Therefore, the observations made on its isotopic compositions should take into consideration the shocked nature of this material, and are strictly regarded as a rough reference for the composition of the Eleanor River Formation. This is similar to other reference material, since not all formations have solely unshocked limestone samples coming from outside the crater. The lower isotopic compositions, both in terms of $\delta^{13}C$- and ^{18}O-values, compared to other unshocked and shocked rock formations could indeed illustrate the effect of shock metamorphism (Figure 5.1).

The fact that only limestone was analysed in this study as opposed to the studies by Land et al. (1975) and Martinez et al. (1994), which considered calcite- and dolomite-bearing rocks, is not believed to be a major factor for the observed stable isotopic

variation. In fact, in the Martinez et al. (1994) study some calcite-rich rock samples show very similar compositions ($\delta^{18}O$ = +24‰) to dolomite-rich rocks. Also, some of their dolomite-rich samples are depleted in ^{18}O ($\delta^{18}O$ = +24‰) while others are enriched ($\delta^{18}O$ = +28‰), which would not be observed if the type of carbonate mineral composing the rock were to affect directly the isotopic composition. Thus, the oxygen isotopic values for the limestone samples are thought to be representative of their respective formations.

As stated in the results section, the impact melt breccias contain shocked sandstone clasts that are variable in composition. Interestingly, a calcite-rich sandstone clast (e.g., sample HMP99-069C) has a different isotopic composition and shows a composition of -1.1‰ for $\delta^{13}C$ and +11.3‰ for $\delta^{18}O$. Possibly, this apparent depletion in ^{18}O could be linked to carbonate decomposition during an impact event, a very complex process which we will not address in detail here, but that was put forward for the Haughton and Ries Impact craters, for instance (Martinez et al., 1994; Skála and Žák, 2001). Moreover, the study performed by Martinez et al. (1994) was done on thirty highly shocked clasts from the polymict breccias in the center of the crater: $\delta^{13}C$-values range from -3.5 to +7.5‰ and $\delta^{18}O$-values from +15 to +22‰. In addition, they have analysed nine clasts that were sampled in different parts of the impact breccias: the $\delta^{13}C$-values range from -4 to +2‰ and $\delta^{18}O$-values from +17 to +21‰. In comparison to our study, these values are very similar to the isotopic compositions we have found.

5.3.3 Interpretation of Results for Hydrothermal Carbonates

Importantly, the present study contributes to the knowledge of hydrothermal systems within impact craters on Earth. The $\delta^{18}O$-values of hydrothermal calcites from

Haughton are usually lower than +26‰ and the $\delta^{13}C$-values are less than 0‰: this is consistent with carbonates formed at higher temperatures. This is the case for the majority of hydrothermal carbonates from other terrestrial impact craters as well. Figure 5.6 displays stable isotope data from Haughton relative to other impact craters. One of the exceptions is the Chicxulub impact structure, whose impact-induced carbonate deposits show $\delta^{13}C$-values slightly above 0‰, typical of marine carbonates, a fact that is corroborated by the average $\delta^{18}O$-value of 25‰ indicative of a marine environment. More difficult to interpret is the Popigai structure, whose calcites show lower $\delta^{18}O$-values suggestive of a meteoric water source, but with $\delta^{13}C$-values >0‰ indicative of a marine source.

The Haughton impact structure is one of the few meteorite impact craters, and one of the youngest, to have been studied for the stable isotopic composition of impact-induced hydrothermal carbonates (Table 5.1 and Figure 5.6). Most of these impact structures are either located in Europe or Russia, and are found in either crystalline, sedimentary or a combination of these target rocks (Earth Impact Database, 2010; Naumov, 2005). In general, calcite is the main hydrothermal phase but dolomite has been reported for the Neugrund and Kärdla impact structures (Versh et al., 2006). By mistake, dolomite had previously been reported as a hydrothermal phase at Haughton (Versh et al., 2005). In terms of $\delta^{18}O$-values, all craters display lower values compared to normal fresh- or seawater carbonates (±26 ‰) (Figure 5.6). A first cluster, with $\delta^{18}O$-values near normal to moderately ^{18}O-depleted carbonates, is represented by the Chicxulub, Kärdla, Kara, Puchezh-Katunki, Neugrund and Lappajärvi impact structures (Zürcher et al., 2005;

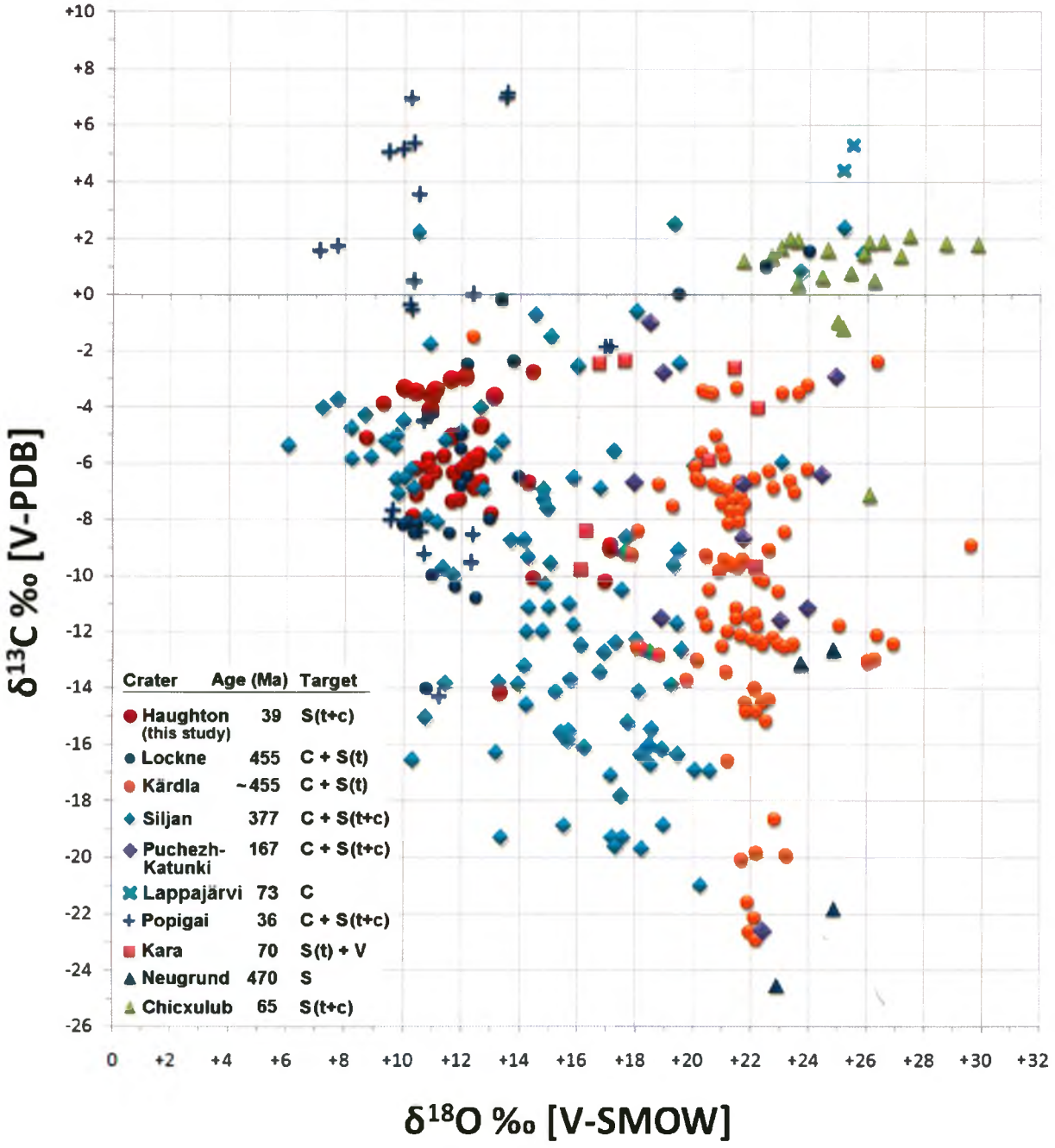

Figure 5.6. Carbon and oxygen isotopic compositions of hydrothermal carbonates deposited within impact structures on Earth (as seen in Table 5.2; references therein). This compilation includes data from the current study at the Haughton impact structure (red circles). Of all craters, carbonate deposits from Haughton have oxygen isotopic compositions among the lowest. However, carbon isotopic compositions are closer to average. Lower values are seen at the Siljan and Kara impact structures, and higher values are noted at the Popigai and Chicxulub impact craters for instance. Ages of impact structures and target lithologies are also shown. Abbreviations: C= Crystalline rocks; S= Sedimentary rocks: t: terrigenous, c: carbonate; V= Volcanogenic rocks. (Modified from Versh et al., 2006).

Masatis and Naumov, 1993; Versh et al., 2006). A second group has strongly lower oxygen isotopic compositions, with $\delta^{18}O$-values ranging from +6 to +14 ‰. This group represents calcites from the Lockne and Popigai impact structures (Sturkell et al, 1998; Versh et al., 2006), as well as from Haughton. In terms of carbon isotopes, most samples are moderately depleted in ^{13}C ($\delta^{13}C$-values from -14 to -2‰) in comparison to calcite deposited in fresh or seawater at Earth's surface temperature, and this relative depletion is typically seen in hydrothermal carbonates (Versh et al., 2006). The most strongly ^{13}C-depleted calcites are from the Neugrund, Siljan and Kärdla craters, whereas the most ^{13}C-enriched calcites originate from the Chicxulub, Lappajärvi and Popigai impact structures. Despite the unique nature of the calcite dataset from Haughton, stable isotopic compositions are similar in many respects to part of the data from the Lockne, Siljan and Popigai impact structures. These calcites are distinguished by a strong depletion in ^{18}O (>10‰) and a normal depletion in ^{13}C (>5‰) relative to normal seawater carbonates.

Commonly, carbonates found in geothermal environments on Earth have similar $\delta^{13}C$- and $\delta^{18}O$-values to those of impact-induced hydrothermal carbonates. Figure 5.7 delineates the isotopic region of hydrothermal calcite at Haughton shown earlier, which will later be discussed in detail. Carbonates formed in geothermal fields have $\delta^{13}C$-values that generally range from -5 to +5‰. The apparently greater ^{13}C depletion for many impact-hydrothermal carbonate deposits as opposed to geothermal ones is not well-explained, but may indicate different generation processes or a stronger involvement of light biogenic carbon (Versh et al., 2006).

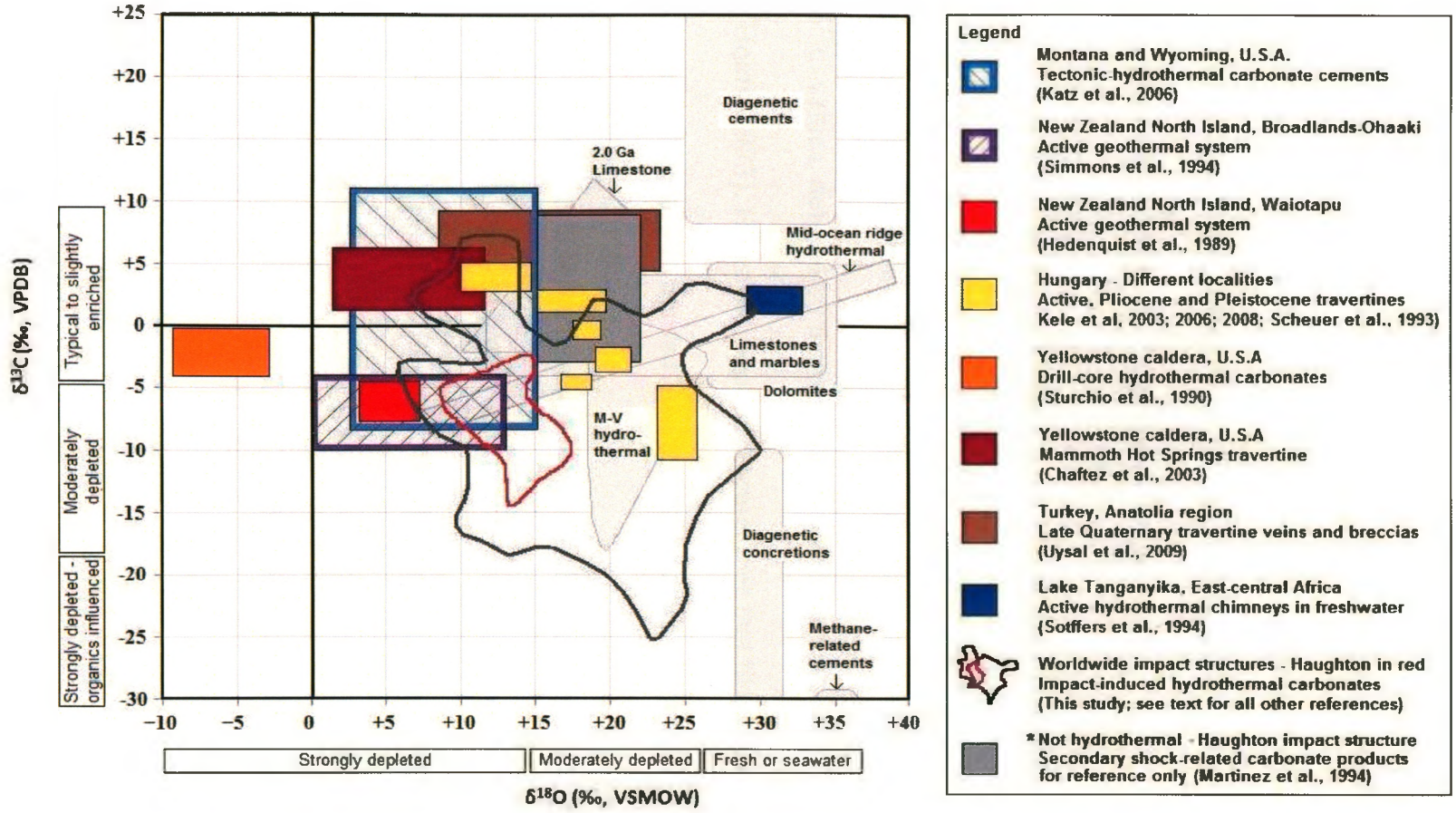

Figure 5.7. Diagram showing carbon and oxygen isotopic compositions of terrestrial carbonates formed in a variety of freshwater, marine and hydrothermal environments. The pale grey boxes in the background were compiled by Rollinson (1995), and highlight the composition ranges of main carbonate materials. The general ranges of higher versus lower isotopic compositions for carbonates are shown along the horizontal (bottom) and vertical (left-hand side) rules. Coloured boxes show various hydrothermal environments (details shown in legend). The summed stable isotope data for impact-hydrothermal carbonates are outlined in dark grey, with data from Haughton outlined in red. As a reference, data from Haughton (Martinez et al., 1994) for non-hydrothermal impact-induced carbonates are also shown (medium grey box in centre of diagram).

For oxygen isotopic compositions, Figure 5.7 shows that impact-generated hydrothermal carbonates are sharing similar compositional ranges to those of many other geothermal environments, both active and extinct (i.e., Kele et al., 2003; Chaftez et al., 2003). Thus, it is important to expand on the context of impact-hydrothermal systems by showing some examples of known geothermal deposits and their respective carbonate stable isotopic compositions. From this, a more global comprehension of the composition of carbonate deposits at Haughton will arise.

As a reference, carbonates precipitated by hydrothermal fluids at the mid-ocean ridges have well-documented isotopic compositions (Stakes and O'Neil, 1982). They exhibit a wide distribution of $\delta^{18}O$-values, from +10 to +40‰, and a narrow range of $\delta^{13}C$-values, defined by the mixing of mantle and seawater carbon sources (Figure 5.7) (Hoefs, 1973). However, one must remember that hydrothermal systems found in impact craters are generally not fed by a mantle-derived water source.

First, carbonates found in active hydrothermal chimneys of Lake Tanganyika, in Eastern-central Africa, have very similar stable isotopic compositions to low- or ambient-temperature carbonates (Figure 5.4). The findings from Stoffers et al. (1994) show that hydrothermal fluids ($\delta^{18}O$ = +1.4 to +2.7‰) discharged on the lake floor have a temperature range of 50° - 104 °C at different sites. However, the $\delta^{18}O$-values of calcite range from +29 to +33‰, indicating lower generation temperatures, which means calcite precipitated at low temperatures (17° - 37°C) due to mixing of hydrothermal fluids with freshwater from the lake.

Different surface carbonate deposits from currently active and extinct geothermal fields in Hungary have been studied with regards to stable isotope chemistry, and compiled by Kele et al. (2008). The wide distribution in isotopic compositions of these hydrothermal carbonate deposits, composed primarily of calcite and minor aragonite, indicates different fluid temperatures as well as variable isotopic sources (Kele et al., 2003, 2006, 2008; Scheuer et al., 1993). The moderately to strongly ^{18}O-depleted calcites have $\delta^{18}O$-values from +10.5 to +26‰, while typical $\delta^{13}C$-values range from -11 to +4.3‰ (Figure 5.7). An inverse correlation between the $\delta^{13}C$- and the $\delta^{18}O$- values from the various study sites seems perceptible. The study of Kele et al. (2008) on a specific actively forming travertine mound at Egerszalók indicates specific $\delta^{18}O$-values ranging from +10.5 to +14.7‰, and $\delta^{13}C$-values from +2.7 to +4.3‰. The measured $\delta^{18}O$-value of the fluid fluctuates between -11.1 and -10.2‰; the temperature of the fluid varies as well, ranging from 70° down to 40°C.

The recent geothermal deposits from the Yellowstone National Park have been studied by numerous authors. Briefly, magmatic activity in the Yellowstone area has been attributed to the presence of a mantle plume acting as a significant heat source (Humphreys et al., 2000). The hot spring waters are derived from meteoric water collected by mountains to the north (Chaftez et al., 2003). Groundwater is heated to temperatures as high as 300 °C, then returns to the surface charged with dissolved ions. In reality, isotopic analyses indicate < 5% of this water is magmatic in origin (Craig, 1961). One example of a stable isotope study of carbonate deposits at Yellowstone is the Mammoth Hot Springs Travertine examined by Chafetz et al. (2003). At this locality, the strongly ^{18}O-depleted sub-surface hydrothermal calcite range from +2 to +12‰; slightly

^{13}C-enriched calcites range between +2 and +7‰ (Figure 5.4). Although no isotopic composition of the fluid has been reported, the *in situ* fluid temperature averages 73 °C (Chaftez et al., 2003). In another case, a higher level of ^{18}O-depletion in carbonates was noted by Sturchio et al. (1990) in drill holes from Yellowstone: the observed $\delta^{18}O$-values range as low as -9 to -3‰ (Figure 5.7). Interestingly, this site seems not to be unusual in terms of fluid source compared to other sites in the Yellowstone geothermal field, and the carbon isotopic composition ($\delta^{13}C$ = -4 to -1‰) is within the normal range for this type of carbonate (Sturchio et al., 1990). The hydrothermal waters encountered by Sturchio et al. (1990) have *in situ* $\delta^{18}O$-values ranging from -17.8 to -16.6‰, with temperatures between ~80° and 200 °C.

The active geothermal systems of the Taupo Volcanic Zone, situated on New Zealand's North Island, have been analysed by many authors especially to characterise known ore deposits, and to explore for new deposits. A study by Simmons et al. (1994) on several deposits found in this zone indicates hydrothermal calcites have strongly lower $\delta^{18}O$-values ranging from ~0 to +13‰, and moderately lower $\delta^{13}C$-values from -10 to -4‰ (Figure 5.7). The composition of the fluid is variable and predominantly meteoric in origin, with a $\delta^{18}O$-value between -7 and -4‰. Fluid temperatures encountered are in the 160° to 310 °C range (Simmons et al., 1994). More specifically for the Waitopu geothermal field, Hedenquist et al. (1989) reported isotopic compositions of hydrothermal calcites within that range: $\delta^{18}O$-values are from +4 and +7‰, while $\delta^{13}C$-values range from -7.5 to -4‰. In this case, the fluid is also meteoric in origin with a $\delta^{18}O$-value between 0 and -7‰, at similar temperatures from < 160° up to 350°C, where it boils

adiabatically – from a drop in pressure but without heat transfer to the wall-rock – between 230° to 300°C.

The study by Uysal et al. (2009) provides stable isotope data for late Quaternary travertine deposits in the Anatolia region, in Eastern-Central Turkey. The calcites analysed show a wide range in $\delta^{18}O$-values, ranging from +8 to +23‰. A more limited variation in $\delta^{13}C$-values, from +4.5 to +9‰, shows a pronounced enrichment in ^{13}C (Figure 5.7). Evidence of previously deposited travertines being brecciated by sudden degassing of the fluids is evidenced at this site: an examination of the processes responsible for the deposition of these carbonates will be made later in this text.

As an additional note, isotopic compositions of hydrothermal carbonate cements (calcite and dolomite) from tectonic origin in Wyoming and Montana (USA) have been reported by Katz et al. (2006). The late-stage calcite shows a wide range in $\delta^{18}O$-values, from +3 to +15‰, and $\delta^{13}C$-values from -8 to +11‰, which is probably related to the large-scale environment of deposition (Figure 5.7). Katz et al. (2006) specify that the tectonic-hydrothermal fractures and breccias did not form under a single event and a single fluid temperature. Moreover, these calcites and dolomites were formed in a relatively different geological setting than most of the carbonates in geothermal systems discussed here.

5.3.3.1 Calcite Vug Fillings within Impact Melt Breccias

Before evaluating the analytical results, the three main possible scenarios anticipated were that stable isotopic compositions of hydrothermal calcites could be: 1) similar for all types of mineralisation throughout the impact structure, 2) variable but

without any correlation to the type of mineralisation, or 3) variable and show a correlation with the type of mineralisation and/or location in the crater. Additionally, the variations in carbon and oxygen isotopic compositions of calcite would have to be studied separately at first and, ultimately, co-variation trends could be observed. That is why, at first, as many hydrothermal calcite samples as possible were collected on a crater-wide scale: the goal was to better characterise each mineralisation setting and consequently maximise the chances of finding such trends in isotopic signatures. However, due to laboratory and time constraints, analysing all samples for stable isotopic compositions was not realistically feasible. Nonetheless, carbon and oxygen stable isotope analyses were performed on most of the pure hydrothermal calcite samples that had been identified by XRD and XRF analyses. Then, once the isotopic composition of hydrothermal calcite is analysed, it is useful to extrapolate on the isotopic composition and temperature of hydrothermal fluids. Also, the comparison with other isotopic signatures observed at other impact sites gives appreciable clues on the conditions prevalent at Haughton. From the analytical results presented above and displayed in Figure 5.4, the third case scenario seems to be observed: calcites deposited in different settings at Haughton appear to hold different pieces of information about the conditions of mineralisation and the hydrothermal fluids, which will be discussed below.

5.3.3.1.1 Evidence from Oxygen-Isotope Data

Although vertical variations in stable isotopic compositions of vuggy calcite within the impact melt sheet are not observed, a key characteristic is the *in situ* variation in isotopic compositions within vugs themselves. As previously mentioned, the mineralogical textures of many intra-melt breccia vug occurrences indicate at least a dual

stage of vug filling, where rhombohedral calcite occupies the inner-most portion of the void surrounded by a more fine-grained to massive border. In this sense, monomineralic vug zoning might be equivalent to laminations observed in marcasite-calcite deposits from the Haughton River valley vugs, as they locally demonstrate an increasing trend in $\delta^{18}O$-values for calcite deposited later in the sequence. Overall, these two deposits display very similar oxygen isotopic compositions when only the late-stage crystalline calcite is considered: $\delta^{18}O$-values of calcite from monomineralic vugs range from +10.5 to +13.0‰, and similarly $\delta^{18}O$-values of marcasite-rich calcite vugs range from +10.9 to +12.7‰. The successive calcite layers analysed either display $\delta^{18}O$-values that are very similar with variations below the analytical precision limit, or increasingly larger as late-stage calcite is reached. As mentioned earlier, discrete superposed layers deposited centimetres apart show a $\delta^{18}O$ increase from +10.9 to +12.7‰: the amplitude of this increase in ^{18}O is almost identical to some of the monomineralic vug filling. For instance, sample SA08-19B has a $\delta^{18}O$ of +10.8‰ for calcite in the outer margin and a $\delta^{18}O$ of +12.5‰ for crystalline calcite in the core. Although some samples clearly show hydrothermal calcite across the entire vug, some have diffuse outer borders that were once attached to impact melt breccia carbonates, so that a slight contamination of the hydrothermal calcite sample could have occurred. Nevertheless, it is safe to state that the isotopic data from crystalline cores of monomineralic vugs is reliable, as for the various types of calcite laminea found in marcasite-rich vugs. In the later type of deposit, the last hydrothermal calcite laminae strongly suggest higher $\delta^{18}O$ compositions than the younger calcite laminae. Most importantly, it seems that similar hydrothermal fluids were responsible for the deposition of the different types of calcite vug fillings. The distinct calcite zoning observed reveals variations in oxygen-isotope ratios in single vugs, which

could be used as a proxy for characterising the evolution of the hydrothermal fluids. The increased $\delta^{18}O$-value in the core of many vugs could be interpreted as a direct consequence of the physico-chemical evolution of the hydrothermal fluids. From stable isotope analysis, enrichment in ^{18}O is often observed from the outer band towards the core of zoned vugs. This is interpreted to represent a temperature decrease as the system evolved.

On a different note, Bargar et al. (1988) point out that extensive glacial ice cover during the last ice age periods over the Yellowstone area probably resulted in a temperature increase of the hydrothermal system. The greater pore-fluid pressures in the underlying rock column increased as a function of the thickness of the ice cover. As such, fluid-inclusion homogenisation temperatures from hydrothermal minerals recorded higher temperatures than that of the maximum theoretical water temperature attainable for that period (Bargar et al., 1988). Again, this example highlights the fact that peripheral processes, such as those caused by an overlying ice sheet, might cause important changes in an apparently well-constrained hydrothermal system. With respect to hydrothermal activity at Haughton, the same concern must be kept in mind. In reality, it is not impossible that, following the impact event, glacial ice surrounded or covered the region, even with a positive thermal anomaly at the site of impact, and modified the initial oxygen isotopic composition of the groundwater recharge in a way that calcite composition was changed.

5.3.3.1.2 Evidence from Carbon-Isotope Data

Carbon is the fourth most abundant element in the solar system (Faure et al., 2005). The distribution of carbon takes many forms including organic matter, carbonate and carbide minerals, graphite, diamonds, CO_2 and hydrocarbon gases such as CH_4. On Earth, the two main carbon reservoirs are: 1) the biosphere, and 2) the carbonates (Hoefs, 1973). Although not totally mutually exclusive, these reservoirs isotopically differ from each other because of two reaction mechanisms: 1) a kinetic effect during photosynthesis that leads to the depletion of ^{13}C in CO_2, and concentrates the ^{12}C in the synthesised organic material, and 2) a chemical exchange effect between atmospheric CO_2, dissolved HCO_3^- and $CaCO_3$, where enrichment of ^{13}C is taking place within the bicarbonate ($CaCO_3$). As an outcome, carbonates precipitated from aqueous solution in the oceans and freshwater bodies can acquire their carbon content from two different reservoirs, both of which are linked and can exchange with CO_2 from the atmosphere: 1) reduced carbon from biological matter, and 2) oxidised carbon of dissolved carbonate ions (Hoefs, 2004). The origin of the carbon incorporated into carbonate minerals upon their formation might be evaluated from the ratio of ^{13}C to ^{12}C, and by comparing it to known carbon reservoirs (Hoeffs, 2004). Organic matter, fossil fuels and hydrocarbon gases are depleted in ^{13}C because of fractionation processes occurring during their formation. The subsequent formation of biogenic compounds also tends to induce noticeable depletion in ^{13}C. Different sources or processes involving depletion in ^{13}C applicable for hydrothermal carbonates can be summarised as: 1) meteoric or groundwater depleted HCO_3^-, 2) atmospheric or soil derived light CO_2, 3) thermal degradation of pre-existing organic material, and 4) fractionation by microbial organisms that possibly inhabited the system

(Versh et al., 2006). In addition, a mantle or metamorphic source of CO_2 is not addressed since the hydrothermal calcites in this study are not linked to regional-scale geological processes. Also, mantle and extraterrestrial carbon sources are not considered. Finally, it should be noted that the carbon isotopic composition of hydrothermal water is less commonly studied than for oxygen (e.g., Craig, 1953; Simmons et al., 1994). For instance, Stoffers et al. (1994) have reported a $\delta^{13}C$-value of -8.6‰ for hydrothermal CO_2 gas. Since gas emissions from geothermal fumaroles sometimes contain small amounts of CH_4 in addition to CO_2, the separate analysis of carbon isotopic composition of CO_2 and CH_4 can be used for geothermometry.

The depletion in ^{13}C relative to ^{12}C observed in impact-hydrothermal and geothermal carbonates (refer to Figure 5.7) could be caused by different factors. Firstly, the source of carbon could initially be depleted in ^{13}C. For instance, the meteoric or groundwater from which carbonates are precipitated could contain depleted HCO_3^- species, but also light atmospheric or soil-derived CO_2 could be involved. Secondly, the thermal degradation of pre-existing organic material could affect the ^{13}C-isotope concentration in a system. As well, biological activity within a hydrothermal system results in fractionation of carbon isotopes from the original source, which would result in ^{13}C-depleted carbonate precipitates (Versh et al., 2006). As for the reasons explaining the greater ^{13}C-depletion for impact-induced hydrothermal carbonates in comparison to geothermal carbonates, no tangible explanation seems available in the literature, although a difference in carbon source might be one cause.

According to Versh et al. (2005), impact-hydrothermal calcites displaying the strongest ^{13}C depletion, with $\delta^{13}C$-values ranging from -20 to -26‰ (Figure 5.6), suggest

the presence of light biologically reduced carbon in the system. They propose the possible involvement of a multi-metabolic system of microbial activity, which is probably of methanogenic or sulfate-reducing metabolism (Versh et al., 2005). However, in our study of Haughton hydrothermal calcite, none of the samples analysed display δ^{13}C-values below -15‰; moreover, the bulk of δ^{13}C-values cluster between -8 and -2‰ (Figure 5.3). The carbon isotopic fractionation induced by different processes is seen as a likely cause of the isotopic signatures encountered here, and less likely an isotopic signal of organic compounds from biogenic activity.

On a similar note, data from Yellowstone hot springs demonstrate that δ^{13}C-value of organic matter (thermophilic algae inhabiting the system) is more dependent on the concentration of dissolved inorganic carbon than on the temperature of the water (Estep, 1984). This shows the clear complexity in assessing stable isotopic compositions of carbonates, because not only the temperature plays a role, but several factors such as the amount of dissolved compounds and sometimes incalculable biogenic isotopic fractionation.

Calcite vug fillings from Haughton display carbon isotopic compositions typical of hydrothermal carbonates found in other terrestrial geological settings. The δ^{13}C-values are lower than those normally attributed to marine carbonates and, at the same time, are too strongly enriched for a possible involvement of light carbon from organic matter (Versh et al., 2006). This way, a hydrothermal source of carbon is most probable. There is no correlation observed between carbon and oxygen isotopic compositions. Moreover, the overall variations in δ^{13}C-values are limited to ~2‰ for monomineralic vugs and ~3‰ for marcasite-rich vugs. An interesting fact regarding marcasite-rich calcite vug fillings is

that the more massive early calcites have their $\delta^{13}C$ clustered around -3.5‰, whereas the very late-stage calcite coatings have $\delta^{13}C$-values ranging from -4 to -6.2‰. The later range is very similar to monomineralic calcite vug fillings values (Figure 5.3). The possibility of discriminating the two different types of calcite vug mineralisation based on carbon isotopic compositions seems more pronounced than in the case of oxygen isotopic compositions.

5.3.3.2 Vein and Pipe Structure Calcite Fillings

An assessement of the spatial distribution and variability in isotopic compositions of calcite veining within target rocks could be made, as opposed to calcite vug fillings in impact melt breccias. The isotopic compositions observed are relatively dissimilar from one another (Figure 5.3), and a rather large number of samples are dispersed around the impact structure (Figure 5.5). A limiting factor in interpreting the spatial distribution is that the western half of the crater is underrepresented in terms of samples from the outer margin of the central uplift. There is an apparent lack of carbonate mineralisation in the shocked lithologies in the interior of the central uplift, which is only affected by late-stage quartz alteration. Nonetheless, hydrothermal calcite deposits are found as veins in the faulted outer margin of the central uplift and crater periphery (Osinski et al., 2001, 2005a), both of which have been sampled and analysed. Interestingly, some samples from the periphery of the central uplift show clear evidence of multi-generations of calcite fracture fillings (i.e., samples SA08-13 and SA08-14). This tends to corroborate the rather long-lived nature of vein calcite precipitation (Osinski et al., 2005a).

5.3.3.2.1 Evidence from Oxygen-Isotope Data

The impact melt breccias probably confined the hydrothermal system in underlying fractured rocks. This is a view supported by the presence of unaltered impact melt and diaplectic glass clasts within the impact melt breccias (Osinski et al., 2005c). The fluids being restricted in the vertical axis were forced to flow outwards at the interface with the base of the impact melt sheet, away from the central uplift. From volcanic settings, it well known that hydrothermal fluids in gaseous and liquid phases can migrate independently, and that fluids could travel for kilometres in a lateral direction away from the heat source (Nicholson, 1993). This would have been favourable to calcite infilling of fractures in the displaced zone as fluids were transported away from the central uplift, and eventually concentrated deposits on the crater periphery. Clearly, veins at Haughton are presumed to be derived from post-impact hydrothermal activity since none are found outside the crater in corresponding lithologies.

The initial hypothesis was that veins closer to the rim might show different $\delta^{18}O$-values than in other parts of the crater, and the type of host lithology might play a role in the distribution of ^{18}O-enriched versus ^{18}O-depleted calcite veins. Indeed, the lowest $\delta^{18}O$-values are <12‰ and come from calcite veins perpendicular to host-rock bedding as well as from a hydrothermal vent. Also, some of these veins are located on the inner crater rim region, thus are the farthest from the central uplift. As such, these observations seem to indicate more ^{18}O-depleted calcites within the faulted crater periphery, and moderately ^{18}O-depleted to more enriched calcites closer to the outer margin of the central uplift (Figure 5.5). Correlations with the type of host lithology are not fully conclusive since many samples from the same rock formation show various stable

isotopic compositions. The two samples from the Allen Bay Formation show very low $\delta^{18}O$-values, but similar values are also found in other formations as well. In addition, many of the samples from the crater's north-eastern quadrant show moderately enriched $\delta^{18}O$-values ranging from +14 to +17‰, regardless of the host-rock formation.

From the point of view of oxygen isotopic composition of vein calcite from the outer margin of the central uplift, the positive ^{18}O-shift could be attributed to: 1) a cooler fluid temperature, which is in agreement with retrograde impact-induced hydrothermal fluids, or, 2) an input of ^{18}O by wall-rock interaction, since the water-rock ratio is assumed to be low and the country rocks have $\delta^{18}O$-values averaging +24‰. Moreover, the deposition of ^{18}O-enriched calcite could be due to a strong influence of boiling by Rayleigh fractionation processes and the escape of light oxygen isotopes from the system. The nature of the various calcite fracture cementation in the periphery of the central uplift is indicated by wide temperature ranges of fluid inclusions (Osinski et al., 2005a). The wide variation in δ-values, for both carbon and oxygen isotopes, is seen as another piece of evidence pointing towards an evolving hydrothermal fluid with time.

The lower isotopic composition of the hydrothermal vent is probably linked with an early high temperature vapour phase enriched in light oxygen isotopes. In addition, fossil conduits are generally structures of high fluid flow that create strong alteration of the wall-rock and alter the $\delta^{18}O$-values (Hoefs, 2004). The accepted fluid-rock interaction model thus suggests that rocks are depleted in ^{18}O at the site of a pipe structure relative to surrounding rocks. This is useful for identifying fossil vents in rock types that have no visible alteration mineral assemblages. The pipe structures at Haughton, however, generally show strong diagnostic weathering patterns of iron sulfides into hydroxides

(Osinski et al., 2005a). Nevertheless, oxygen isotopic values are useful proxies for exploring hydrothermal ore deposits; for instance, anomalously ^{18}O-depleted carbonate rocks have been correlated to ore mineralisation (e.g., Vazquez et al., 1998).

5.3.3.2.2 Evidence from Carbon-Isotope Data

For calcite veins, some of the $\delta^{13}C$-values are much lower than calcite vug fillings. However, veins with the lowest $\delta^{13}C$-values (-14‰) are not depleted enough to suggest light biologically reduced carbon. For instance, some calcites from the Neugrund impact structure with $\delta^{13}C$-values of -26‰ are indicative of potential involvement of light carbon generated by thermophilic micro-organisms (see Figure 5.6) (Versh et al., 2006). Nonetheless, the most ^{13}C-depleted occurrences at Haughton might reflect an organic carbon source. Liquid hydrocarbons are known to be present at Haughton in some calcite crystals within veins, as they were most likely entrained by impact-induced hydrothermal fluids from deep host- rocks (Parnell et al., 2003). Heavy-carbon isotopic depletion in some of the vein samples might be attributed to: 1) meteoric water that is depleted in HCO_3^- complexes and CO_2 (source of lighter carbon), 2) thermal break-down of pre-existing organic matter, or 3) biogenic fractionation of carbon.

Also, when considering many of the vein calcite data points, a weak inverse correlation may be characterised by a ^{13}C depletion concomitant with an enrichment in ^{18}O (Figure 5.3). This trend is relatively weak but might reflect actual change in the calcite being deposited, as the fluid becomes isotopically depleted in ^{13}C throughout thermal breakdown of isotopically ^{13}C-enriched carbon complexes, and enriched in ^{18}O through wall-rock interactions. Thus, the more ^{18}O-enriched and ^{13}C-depleted veins are

possibly those that have been deposited the latest. The carbon isotopic composition of calcite found within hydrothermal pipe structures is similar to other types of deposits, and does not seem to indicate biogenic precipitation as it is not significantly depleted in ^{13}C.

On a different note, the isolated calcite vug sample from the western crater rim region is believed to be diagenetic and, therefore, represents pre-impact calcite not of hydrothermal origin (Figure 5.5). This is supported by the confined nature of the vug and its distinct $\delta^{18}O$-value of +21.2‰ and $\delta^{13}C$-value >-2‰, which is not observed in any other calcite sample from this study. The veins show significantly lower $\delta^{13}C$-values than the country rocks: -7.5‰ on average, and down to -14‰. As a result, this case exemplifies the distinction that can be made between non-hydrothermal and hydrothermal calcite based on field observations, textures and stable isotopic compositions. Thus, the calcites studied here are believed to be hydrothermal and not re-precipitated carbonates derived from carbonate-rich target lithologies such as limestone. This argument has been proposed for part of the calcites found at the Siljan impact structure (Valley et al., 1998) to account for the isotopic compositions approaching those of carbonate target rocks. The authors claim that calcites would not be hydrothermal in origin but contemporaneous low-temperature precipitates. This does not seem to apply for veins found at Haughton based on the evidence shown above, notably the fluid inclusion data. However, a detailed mineralogical study is probably required for some of the veins that do not have fluid inclusion data and do not seem to cross-cut target rock bedding perpendicular, or with the highest $\delta^{13}C$-values.

Lastly, the carbon and oxygen stable isotopic compositions from the Lockne Impact crater are very similar to those found at Haughton. Nevertheless, the origin of the

fluid at the Lockne impact structure is not well-constrained and ranges from a meteoric to a seawater source (Sturkell et al., 1998). The $\delta^{18}O$-values are homogeneous, varying from +10 to +14 ‰. However, the $\delta^{13}C$-values for calcite are between -14 and -2 ‰, which indicates mixing with carbon from a marine and an organic source. The Haughton impact event occurred inland and fluid inclusion salinities reflect meteoric water (Osinski et al, 2005a). Nevertheless, carbon from marine carbonates in sedimentary target rocks entrained in the hydrothermal fluids would produce $\delta^{13}C$-values similar to calcites from the Lockne Impact crater. Finally, the $\delta^{13}C$-values of calcites from Popigai are very similar to those found at Haughton (see Figure 5.6). In fact, some samples are slightly more enriched ($\delta^{13}C > 0$‰), which means once again that a possibly different carbon source than at Haughton is responsible for the positive isotopic shift (Versh et al., 2005).

In the end, there is no clear global positive or negative correlation between the carbon and the oxygen isotopic ratios within hydrothermal calcites at Haughton. Although the sensitivity of carbon isotopic fractionation to the effect of temperature is usually taken to be negligible (Berger et al., 1986), co-genetic calcites from hydrothermal environments do show positive or inverse covariation in $\delta^{18}O$- and $\delta^{13}C$-values (Zheng et al., 1993). This correlation between δ-values in calcite is often caused by a change in isotopic composition of the fluid induced by a change in temperature. Indeed, the isotopic covariation in carbonates of some hydrothermal deposits is clearly linked to a change in the fluid's temperature (Davis et al., 1990; Sturkell et al., 1998). For example, Kele et al. (2008) have shown that at the Egerszalók Travertine mound, Turkey, continuous CO_2 degassing and a temperature drop of thermal waters between the spring orifice and the

distal part of the system resulted in an increase of the $\delta^{18}O$- and $\delta^{13}C$-values of precipitating travertines. Further analysis might reveal additional covariation trends.

5.3.4 Characterisation of Fluid

Essentially, an important limitation comes from the fact that the isotopic composition of past hydrothermal fluids can no longer be measured *in situ* at any given time of its existence (Blattner, 1985). As such, given that no active hydrothermal system within an impact structure has been studied *in situ* – all known terrestrial occurrences are extinct today – it is essential to refer to other types of active hydrothermal systems on Earth as a comparative tool to understand the context in which impact-induced hydrothermal activity developed at Haughton. This study on stable isotopic compositions of calcite helps to circumscribe the nature and properties of the hydrothermal fluid, as well as provide more insights on the deposition of hydrothermal calcite. The aim is to deduce the formation conditions (e.g., to define carbon and oxygen isotope sources and precipitation temperatures) of calcite associated with paleo-hydrothermal activity at the Haughton impact structure. This is similar to evaluating the conditions in an extinct geothermal field where mineralisation was deposited, or *in situ* observation of a currently active system.

The context of formation of hydrothermal systems either in an impact crater or in a geothermal field share both similarities and differences. The driving heat for geothermal systems is usually induced by sub-surface intrusive magmas (e.g., sills, plutons) and an elevated geothermal gradient in zones of tectonic uplift and intense metamorphism, subduction or creation of new crust (i.e., mid-ocean ridges; Blattner, 1985; Staudigel et

al., 2006). These hydrothermal systems are initiated when the deep heat source rises in overlying country rocks and entrains water that already occupies the rock column (Ellis et al., 1977). For impact-hydrothermal systems, however, a body of hot molten impactites is emplaced onto rocks of the final crater and acts as the main heat source. The lowered water table slowly reintegrates the crater region both laterally and from below. The quasi-instantaneous nature of impact-induced hydrothermal systems always results in a retrograde alteration mineral assemblage which, in a sense, appears more likely to preserve geochemical information on the original fluids than for typical geothermal systems (Naumov, 2005). As for the similarities between impact-hydrothermal and geothermal systems, the convection of groundwater commonly occurs as circulation cells in the vicinity of the heat source, and may extend kilometres away from that source. Also, water discharged either in intra-continental geothermal or impact-induced hydrothermal systems is known to be composed primarily of groundwater that originated as meteoric water on the surface of the Earth, whose isotopic composition was altered to some extent by hydrothermal processes (Naumov, 2005). In any case, intra-continental geothermal systems tend to have a finite volume of rocks where the highest temperatures occur: this represents the reaction zone that all interacting fluids have to flow through (Blattner, 1985). Toward the ground surface, the reaction zone is usually limited by a cap of rock of reduced permeability (Ellis and Mahon, 1977). Moreover, it is limited laterally by a temperature drop sometimes associated with inflow of a cooler water recharge, and at depth by the geothermal gradient with rising temperatures towards the central heat source, in many ways similar to a meteorite impact-generated hydrothermal system (Naumov, 2005).

Another limitation arises from the difficulty to characterise the heat source responsible for the development of a hydrothermal system within an impact structure (French, 1998). With a structural uplift of the target lithologies averaging 2 km at Haughton, the geothermal gradient within the crater would have been raised to a maximum temperature of ~70 °C. This is not sufficient to explain the higher temperature of formation of a wide range of post-impact mineralisation, especially in the early and main stage of hydrothermal activity (Osinski et al., 2001). The passage of the shock wave through the crater floor and rim region is likely to add a certain heat component during the excavation and modification stages, at a level which has yet to be determined. What is more certain is that the impact melt breccia layer produced a sufficient amount of heat for a significant period of time in order to sustain hydrothermal activity. This is corroborated by stronger hydrothermal alteration within the impact melt breccias as opposed to significantly weaker alteration in the central uplift and at lower temperature. Indeed, the central uplift region would have been covered by a thinner impact melt sheet than the annular trough, and heat would have dissipated more rapidly, explaining the weaker alteration pattern. Also, alteration conduits described as pipe structures in the crater rim region formed in close proximity to the outer edges of the melt sheet, which is usually thicker than in the central part of the crater, so this may indicate it was the likely main heat source.

5.3.4.1 Oxygen Isotopic Composition of Hydrothermal Fluid

The wide distribution of oxygen isotopes provides an effective means of studying the origin and history of fluids in hydrothermal systems and mineral deposits in the Earth's crust (Clayton et al., 1968; Taylor, 1974). Two primary parameters involved in

the $\delta^{18}O$-values of hydrothermal minerals are: 1) the $\delta^{18}O$-value of water, and 2) the temperature of water (De Ronde, 1988). In turn, the $\delta^{18}O$-value of a hydrothermal water or fluid is strongly dependent on the level at which the initial water source has been modified by stable isotope exchange (most commonly by passing through previously unaltered rocks), by evaporation, dilution, or a combination of those phenomenon. Several geothermal systems on Earth, for instance the Yellowstone National Park in the U.S., or the Taupo Volcanic Zone in New Zealand, have already been examined from this point of view (De Ronde et al., 1988).

As briefly discussed previously, Valley et al. (1988) studied calcite vein fillings at the Siljan impact structure, in Sweden. The calcite veins show $\delta^{18}O$-values ranging from +7.3 to +22.3‰. In this case, vein fillings were most likely derived from circulation of freshwater in fractures formed within granites, and fluid temperatures played a direct role in the distribution of isotopic compositions. Since the fluids were at higher temperatures several kilometres deep, it resulted in the precipitation of ^{18}O-depleted (+7.3‰) calcites at depth, compared to more enriched (+22.3‰) calcites at shallow depth. This illustrates how the isotopic composition of carbonates could be indicative of temperature gradients and spatial variations within hydrothermal fluids. The study of hydrothermal fluids at Haughton is essential in understanding post-impact alteration processes in this ubiquitous geological environment in the solar system.

In sub-aerial regions, including continental impact craters, the isotopic composition of hydrothermal fluids is mostly dominated by that of the initial meteoric water (Sturchio et al., 1990). This initial composition might vary significantly according to a number of geographic parameters (Craig, 1961), meteorological effects (Dansgaard,

1964), incorporation of water from hydrous minerals in the target (Naumov, 2005), and subsequent processes that include mixing, boiling and steam separation, as well as water-rock isotopic exchange (Truesdell and Hulston, 1980). Also, numerous studies of oxygen and hydrogen isotopic compositions in minerals and rocks from volcanic-plutonic complexes around the world have evidenced that heated meteoric water can extend several kilometres deep, as reviewed by Criss and Taylor (1986). The oxygen and hydrogen stable isotopic compositions of hydrothermal waters from active geothermal springs were summarised by Truesdell and Hulston (1980) and Criss and Taylor (1986). A perfect example showing that it is possible to track the water source is the Yellowstone caldera, which hosts one of the largest hydrothermal systems on Earth with several active geysers and hot springs (Fournier, 1989). Early isotopes studies (i.e., Craig, 1953) and later work (i.e., Truesdell and Fournier, 1976) demonstrated that sub-surface fluids of the Yellowstone hydrothermal system are practically pure meteoric water that has undergone hydrothermal processes.

Contrary to this, Versh et al. (2005) assumed that the majority of hydrothermal systems they have analysed were fed by intruding seawater, in order to simplify their calculations of ^{18}O isotope fluid composition and temperature range. They explain, however, that perhaps the involvement of a lighter (^{18}O depleted) water source, such as meteoric water, could give similar results. This would possibly be the case for the Popigai and Lockne impact craters, they note. Indeed, the type of target (arid, on land, shallow basin, etc.) is important to consider since different water saturation levels, as well as the different ^{18}O content at the impact site will govern the resulting isotopic composition of the initial and final hydrothermal fluids. In the case of the Haughton impact structure,

very low salinities of fluid inclusions of hydrothermal minerals reveal that freshwater was the predominant source of hydrothermal fluids (Osinski et al., 2005a). The observations made throughout this study indicate that the fluid composition at Haughton probably evolved as the system slowly cooled and became less active.

The fractionation of oxygen isotopes between a fluid and a mineral is dependent upon temperature (Hoefs, 2004). Since the $\Delta^{18}O$-value ($\delta^{18}O_{calcite}$- $\delta^{18}O_{fluid}$) is unknown in the case of Haughton, generation temperatures of calcite could not be determined directly so fluid inclusion temperature data were used instead. The oxygen isotopic compositions of three calcite samples were used in combination with their temperatures of homogenisation from fluid inclusions to obtain a calculated $\delta^{18}O$-value for the hydrothermal fluid (Table 5.3). Water-calcite fractionation equations for oxygen isotopes that could be applied in our case are those of O'Neil et al. (1969) and Zheng et al. (1999), which are relevant for temperatures ranges of 0° - 500°C and 0° - 1200°C, respectively. Based on the different calculated values reported in Table 5.3, a practical average $\delta^{18}O_{fluid}$ -value of -4‰ has been selected. This composition is not arbitrary as it takes into consideration the majority of the values calculated with both the O'Neil et al. (1969) and Zheng (1999) equations. In fact, the lowest $\delta^{18}O_{fluid}$-value calculated is -7.1‰, and most of the higher values approach -2‰ (Figure 5.8). In Figure 5.9, it could be seen that the fluid composition delimited by the $\delta^{18}O$-values and homogenisation temperatures of the three calcite samples range from -4 to 0‰. Thus, a $\delta^{18}O$-value of -4‰ for the hydrothermal fluid composition seems reasonable considering the range of calculated compositions. This particular $\delta^{18}O$-value for the fluid is not what was first expected.

Table 5.3. Predicted range of oxygen isotopic compositions of the hydrothermal fluid responsible for calcite precipitation at the Haughton impact structure, calculated using equations by O'Neil et al. (1969) and Zheng et al. (1999).

Sample	$\delta^{18}O$ calcite [‰, VSMOW]	*Fluid inclusion Th [°C]	$\delta^{18}O$ fluid [‰, VSMOW]	
			(O'Neil et al., 1969)	(Zheng, 1999)
00-136 Vein in periphy of central uplift	+11.69	Min = 93.2	-6.2	-7.1
		Max = 133.5	-2.2	-2.8
		Average = 113.5	**-4.0**	**-4.8**
99-135 Vug in impact-melt breccias	+12.08	Min = 117.7	-3.3	-4.0
		Max = 156.1	-0.1	-0.1
		Average = 132.0	**-2.0**	**-2.6**
99-104 Vein in periphy of central uplift	+16.94	Min = 81.5	-2.3	-3.5
		Max = 140.5	+3.6	+3.1
		Average = **99.6	**-0.2**	**-1.1**

O'Neil et al., 1969 (0-500°C): 1000 ln α = A (10^6)/T^2 + B (10^3)/T + C (A=2.78, B=0, C=-2.89)

Zheng, 1999: 0-1200°C: 1000 ln α = A (10^6)/T^2 + B (10^3)/T + C (A=4.01, B=-4.66, C=1.71)

*Fluid inclusion temperatures of homogenisation are based on primary aqueous-salt inclusions

**For sample 99-104, the large majority of aqueous-salt inclusions are one-phase (liquid-filled) so no heating experiments could be performed on those.

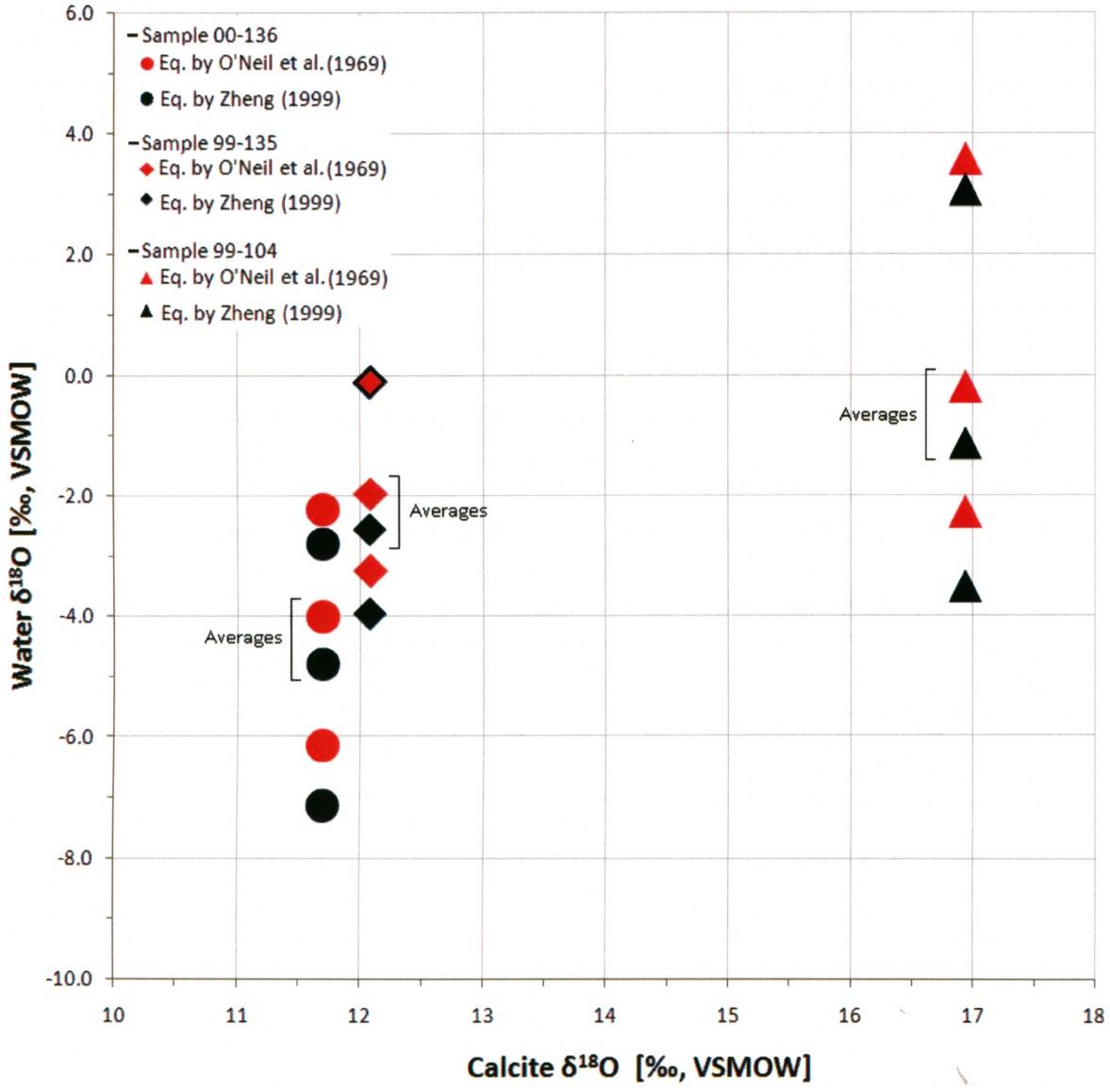

Figure 5.8. Calculated oxygen isotopic compositions of the hydrothermal fluid (Water $\delta^{18}O$) based on $\delta^{18}O$-values of three different calcite samples (e.g., HMP00-136 as circles, 99-135 as diamonds and 99-104 as triangles) and their respective temperature of homogenisation of fluid inclusions, as shown in Table 5.3. The equations by O'Neil et al. (1969) (red symbols) and Zheng et al. (1999) (black symbols) were used for all three calcite samples. From these, minimum, average and maximum Water $\delta^{18}O$-values were calculated. Note that calcites are presumed to have been in equilibrium with the hydrothermal fluid at the time of deposition.

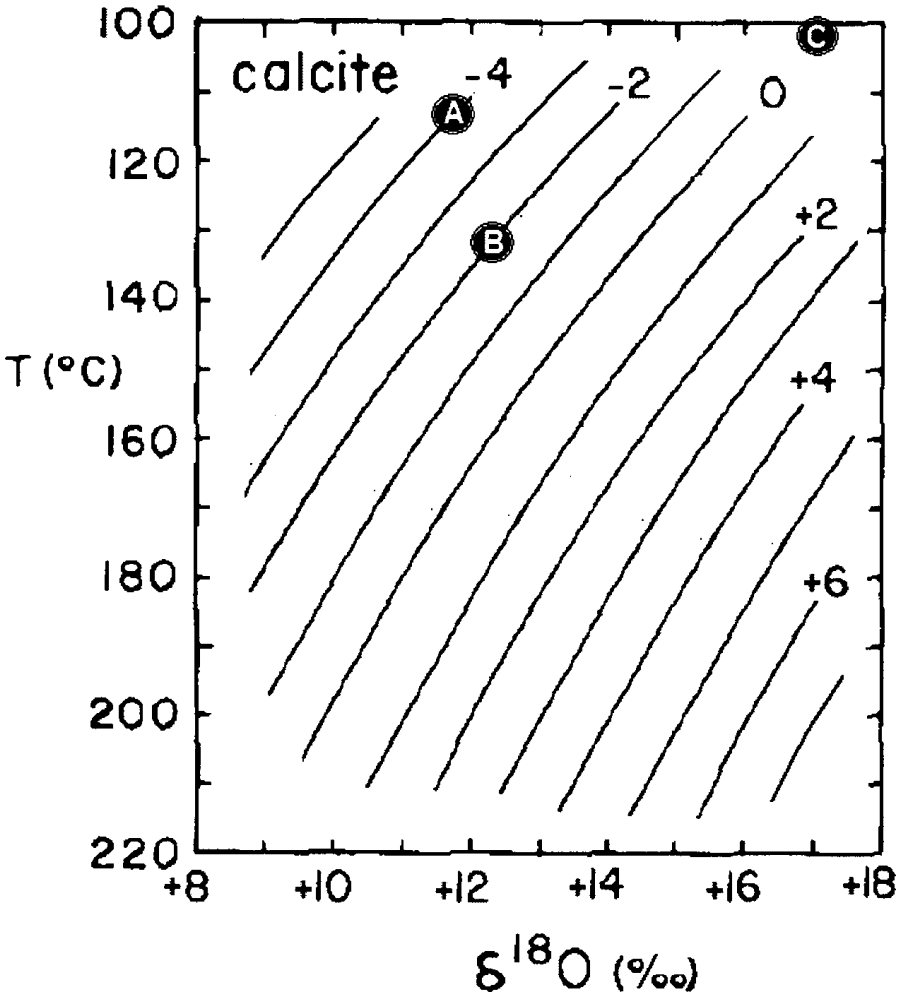

Figure 5.9. Diagram showing average $\delta^{18}O$-values of the three hydrothermal calcite samples chosen in this study (filled circles A, B and C) and their average fluid-inclusion temperatures of homogenisation (T °C). Temperatures increase from the top to bottom of the horizontal rule. Solid diagonal lines define calculated $\delta^{18}O$-values for calcite in equilibrium with water having a constant $\delta^{18}O$-value as indicated, according to the calcite-water fractionation factors of O'Neil et al. (1969); the lines for the fractionation factors of Zheng et al. (1999) are not shown here. Thus, filled circle A represents sample HMP00-136 with a hydrothermal water oxygen isotopic value of -4‰, circle B is sample HMP99-135 with a water of -2‰, and circle C is sample HMP99-104 with water ~0‰ (see Table 5.3). (Modified from Sturchio et al., 1990).

In reality, the latitude at which Devon Island has been located for the past 45 Ma has not changed significantly (Jahren et al., 2002), and the present-day $\delta^{18}O$-value for meteoric water at ~75° N latitude where Devon Island lies today is approximately -22‰ (Yurtsever, 1975) (Figure 5.10). However, Jahren et al. (2002; 2008; 2009) found a $\delta^{18}O$-value of -15.1‰ for meteoric water in the Eocene (circa 45 Ma) based on oxygen isotopic analysis of fossil wood from Axel Heiberg Island. This island is currently at 80° N latitude, but its paleolatitude was 78° N at the time the forest covered the area. The $\delta^{18}O$-value of -15.1‰ could be used as a proxy for paleo-meteoric water isotopic composition at the Haughton impact structure, because the impact event occurred approximately 39 Ma ago and at a similar latitude to Axel Heiberg Island. This isotopic composition is more depleted in ^{18}O with respect to the calculated values from fluid inclusion temperatures presented above. However, the data brought forward by these authors seem reasonable. One important factor to consider, then, might be the exact geomorphology of Devon Island at the time of the Haughton Impact event, which is uncertain. Also, the clearly unique setting of an impact structure might well play a role in the values observed. If we accept a $\delta^{18}O$-value of -15‰ for meteoric water at the time of impact, and we consider that meteoric water was the main source for the impact-induced hydrothermal system, then some other mechanism(s) should have enriched this water in ^{18}O-isotopes to be in agreement with the isotopic composition of -4‰.

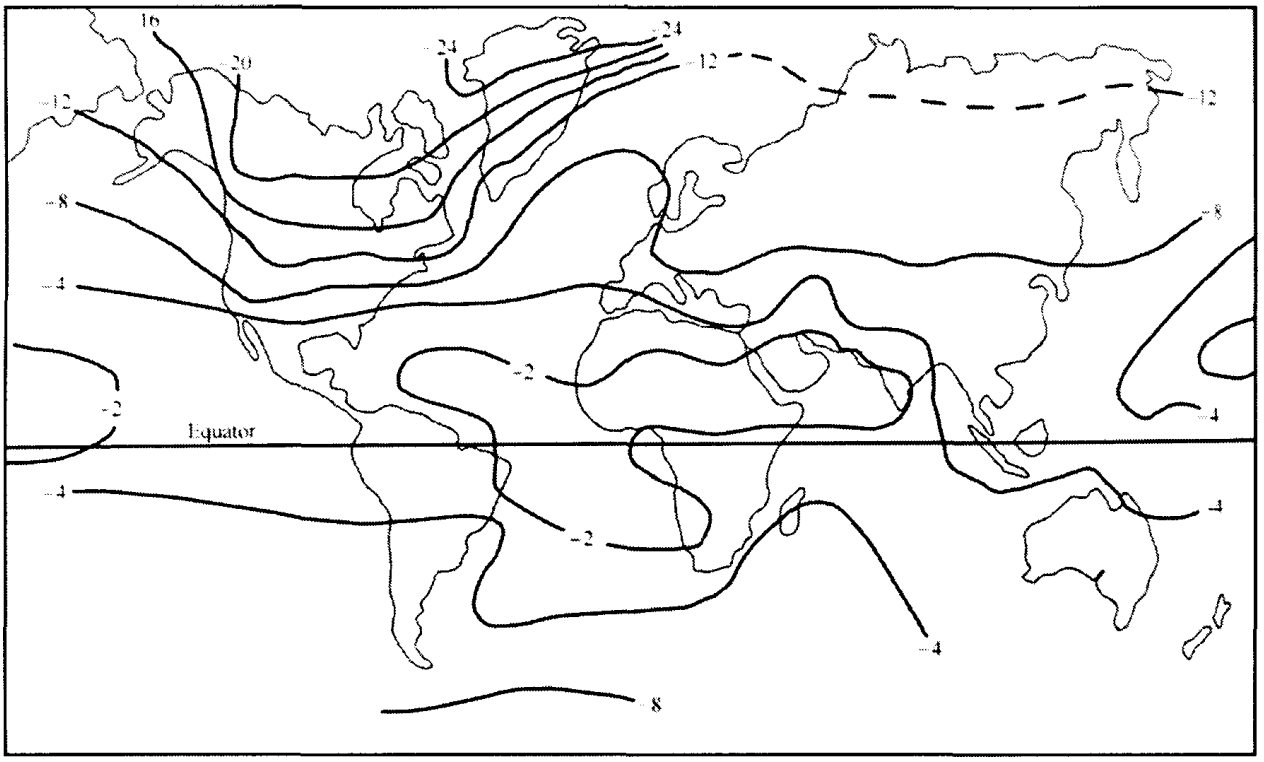

Figure 5.10. Contour map of average annual $\delta^{18}O$-values of meteoric precipitation at stations in the global network of the International Atomic Energy Agency (IAEA). A 35-year long survey of the isotopic composition of monthly precipitation worldwide was conducted by the IAEA. The global distribution of ^{18}O isotopes in rain has been monitored through a station network since 1961 (Yurtsever, 1975). The Canadian Arctic Archipelago, including Devon Island and Axel Heiberg Island, are not shown on this map but would be located directly north of North America and west of Greenland. This region has average annual $\delta^{18}O$-values of meteoric precipitations between -24 to -20‰. Adapted from Gat (1981) and based on a compilation of Yurtsever (1975).

For instance, samples of epigenetic calcite from southern Victoria Land in Antarctica were analysed by Faure et al. (1984). The average $\delta^{18}O$-value of these calcite samples was +11.34‰. This implies that the $\delta^{18}O$-value of the groundwater that precipitated the calcite was approximately -19.7%, based on the calcite-water equation of Kim and O'Neil (1997) and assuming a water temperature of 10°C. This considerably low negative $\delta^{18}O$-value for the water suggest that south Victoria Land, whose present latitude is 75° S, was already located at high latitude when the calcite precipitated. In comparison, the Haughton impact structure is also located in a polar environment, and calcites exhibit similar $\delta^{18}O$-values. However, fluid inclusion data restricts the temperatures at which calcite could have precipitated, therefore, the low (10°C) temperature assumption made by Faure et al. (1984) is not applicable in our case. As a result, a different $\delta^{18}O$-value for the hydrothermal waters other than purely meteoric must be considered for Haughton.

5.3.4.2 Mechanisms of ^{18}O-enrichment

From what has just been mentioned, some possible explanations regarding the presence of a ^{18}O-enriched hydrothermal fluid at Haughton are: 1) the meteoric water recharge could have been relatively enriched in ^{18}O because of temporal variations in climate, or 2) the meteoric recharge water was not relatively ^{18}O-enriched, but the fluid was rather enriched in ^{18}O through hydrothermal processes (i.e., Sturchio et al., 1990). The first explanation seems possible since the exact oxygen isotopic composition of meteoric water at the time and site of impact 39 Ma is somewhat equivocal. However, the findings from Jahren et al. (2008) must be taken as a reliable source of information regarding the isotopic composition of meteoric water (~15‰) at this latitude circa 45 Ma.

It is possible that the meteoric water isotopic value at Haughton may have been lower or higher than that presented by Jahren et al. (2008), although very large temporal isotopic variations of meteoric water due to climate, as the one inferred here, is not likely (Faure et al., 2005). Thus, the data at hand from Jahren et al. (2008) must be considered a good approximation since it is proximal both in time and space to the Haughton impact event. Therefore, it appears likely that the second explanation stated above explains, at least partially, the higher fluid isotopic composition calculated in our study. In that case, we infer that hydrothermal processes probably account for a gradual ^{18}O-enrichment of the hydrothermal fluid at Haughton. In the following paragraphs, the main mechanisms likely to explain this isotopic enrichment will be evaluated.

5.3.4.2.1 Water-Rock Interaction

As hydrothermal fluids flow along open fractures, geochemical interaction takes place between the relatively high-temperature fluids and the colder host-rocks (Zheng et al., 1992). This interaction generally involves variable degrees of cation exchanges, redox reactions, or both. Thus, the precipitation of fracture-filling minerals can be influenced by this interaction (Holland et al., 1979). The loss of H+ from the rocks (for instance from the sulfates – H_2SO_4 –of the Bay Fiord Formation) brings hydrothermal fluids toward saturation relative to carbonates, and the input of cations, such as Ca^{2+}, Mg^{2+} and Fe^{2+}, reinforces this movement. If calcite is deposited from a fluid due to fluid-rock interaction, the isotopic compositions of carbon and oxygen in the calcite are greatly determined by the differences of isotopic ratios between the fluid and the wall-rock Zheng et al. (1992).

From the simplification that target rocks at Haughton have an average $\delta^{18}O$-value of +30‰, and that the hydrothermal fluid's $\delta^{18}O$-value was approximately -4‰ at the time of calcite precipitation, the expected composition of calcite would then be somewhere between these two extremes. This is the case, as calcite samples analysed have $\delta^{18}O$-values ranging from +9 to +17‰. However, determining the exact contribution from each process responsible for the specific values observed for Haughton calcites is more complex than averaging wall-rock and fluid compositions. In general, the fluid and wall-rock are not in isotopic equilibrium prior to interacting with each other. In consequence, at a given interaction temperature, fluid and rock (representing two isotopic composition end-members) tend to exchange their isotopes in order to approach isotopic equilibrium. At low temperatures ($\leq$ 60°- 80°C), the oxygen isotopic composition of groundwater does not tend to change considerably since the oxygen isotope exchange rates between water and rock are low (Gat, 1981). However, when the temperature of a fluid is more than 80 °C, the higher rates of isotopic exchange will cause a significant change in the oxygen isotopic composition of the fluid. The magnitude of isotopic exchange first relies on the oxygen isotope ratios for the fluid and the host-rock. Then, it depends on the initial isotopic compositions of fluid and rock, on the fluid-rock isotopic fractionation factors (temperature dependent), and also on the duration and surface of contact. In the case of an open system with a constant meteoric water recharge, the incoming water commonly experiences a slow positive isotopic shift. Furthermore, if water-rock interaction exhausts the host-rock in the heavy oxygen isotope, water returns to more depleted values, characteristic of the initial meteoric water input (Blattner, 1985).

It is very difficult to quantify the water-rock interaction and associated water/rock ratios involved in the hydrothermal system at Haughton as our study focused on hydrothermal minerals, and not on the altered wall-rock. Although it is possible to approximate the oxygen isotopic composition of the initial and final fluids, as well as that of the initial wall-rock, the final (or post-alteration) wall-rock composition has not really been assessed. The large-scale stable isotope evaluation of reference material made in Chapter 3 was meant for comparative grounds between isotopic signatures of unaltered target rocks and those of secondary hydrothermal carbonates. As a result, a separate study made on zones of high fluid flow, such as on hydrothermal pipe structures, could provide data on the level of oxygen isotopic exchanges between the fluids and the country rocks. In addition to ^{18}O enrichment of the fluid from Rayleigh fractionation processes, there is probably a significant contribution of wall-rock oxygen isotopes in order for the positive ^{18}O-isotope shift of the fluid to be important. The extent at which the host rocks have been depleted in ^{18}O isotopes is unclear, and we know that hydrothermal deposits are limited in volume. Moreover, repetitive fluid passages within the circulation cells may have contributed to cause a greater alteration of the wall-rock at Haughton.

In general, when groundwater and rocks are in isotopic equilibrium, the water-rock fractionation factor α is directly related to the $\delta^{18}O$-values (in permil, ‰) of the water (or fluid) and the wall-rock (or minerals) by the equation (Faure et al., 2005),

Eq. 5.3

$$\alpha_{rock\text{-}water} = (\delta^{18}O_{rock} + 10^3) / (\delta^{18}O_{water} + 10^3).$$

The isotopic composition of the final fluid after fluid-rock interaction can be calculated by the mass balance equation (e.g., Taylor 1977),

Eq. 5.4

$$W\,\delta^{18}O^{i}_{fluid} + \delta^{18}O^{i}_{rock} = W\,\delta^{18}O^{f}_{fluid} + R\,\delta^{18}O^{f}_{rock},$$

where superscripts i and f denote the 'initial' and 'final' $\delta^{18}O$-value of either fluid or rock; W represents the mole percentage of oxygen in the fluid (consisting mainly of water, thus W), and R the mole percent of oxygen in the rock.

By dividing equation 5.6 by R and solving for the water-rock W / R ratio, we get

Eq. 5.5

$$W / R = (\delta^{18}O^{f}_{rock} - \delta^{18}O^{i}_{rock}) / (\delta^{18}O^{i}_{fluid} - \delta^{18}O^{f}_{fluid}).$$

Setting $\delta^{f}_{rock} - \delta^{f}_{fluid} = \Delta$ yields

Eq. 5.6

$$W / R = (\delta^{18}O^{f}_{rock} - \delta^{18}O^{i}_{rock}) / (\delta^{18}O^{i}_{fluid} - \delta^{18}O^{f}_{fluid} + \Delta).$$

However, Δ relates to the isotope equilibration temperature, and approximates to:

Eq. 5.7

$$\Delta = \delta^{18}O^{f}_{rock} - \delta^{18}O^{f}_{fluid} = 10^{3} \ln \alpha_{rock\text{-}fluid} = A\,(10^{6})/T^{2} + B\,(10^{3})/T + C$$

Using this equation, the term $10^{3} \ln \alpha_{rock\text{-}fluid}$ can be calculated for a dolomite-fluid fractionation at a given temperature T; higher temperatures lead to smaller $10^{3} \ln \alpha_{dolomite\text{-}fluid}$ values. The constants for dolomite-fluid fractionation are slightly different than those

for calcite seen earlier, but the bulk of rock at Haughton is simply considered dolomite. According to Zheng et al. (1999), for temperatures between 0° and 1200°C, A = 4.06, B = -4.65 and C = 1.71. Since the value of $10^3 \ln \alpha_{\text{dolomite-fluid}}$ is equivalent to $\Delta (\delta^{18}O^{f}_{\text{rock}} - \delta^{18}O^{f}_{\text{fluid}})$, and the value of $\delta^{f}_{\text{fluid}}$ is known, thus the final isotopic composition of the rock δ^{f}_{r} can be resolved using equation 5.8 for any given water-rock ratio (W / R). In addition, the fraction of oxygen in H_2O is ~89%, whereas it is approximately 50% in dolomite ($CaMg(CO_3)_2$), therefore, the value of W/R as the ratio of mole percent calculated above can be converted to the ratio of atom percent oxygen (Taylor, 1977),

Eq. 5.8

$$(W / R)_{\text{weight}} = 0.5\ (W / R)_{\text{oxygen}}\ .$$

The curves of $\delta^{18}O^{f}_{\text{rock}}$ as a function of the W / R (oxygen) ratio at temperatures of 50°, 150° and 250°C are displayed in Figure 5.11. As the W/ R ratio increases, indicating that more interaction occurs between the water and the country rocks, the value of $\delta^{18}O^{f}_{\text{rock}}$ tends to decrease. This shows the effect of isotopic exchange between ^{18}O-depleted water and ^{18}O-enriched rocks, which tend to shift their respective compositions in opposite directions. For a given W / R ratio, oxygen isotope exchange will happen more readily at a higher temperature. Although more isotopic fractionation occurs at a temperature of 50°C comparatively to 150° or 250°C, it is the water-rock interaction that dominates isotopic equilibration at higher temperatures, so that the composition of the fluid will approach that of the rocks more readily, and vice-versa (Faure et al., 2005).

At Haughton, an initial $\delta^{18}O^{i}_{\text{rock}}$ of +30‰ for the average oxygen isotopic composition of dolomite-rich country rocks at Haughton is based on data by Land et al.

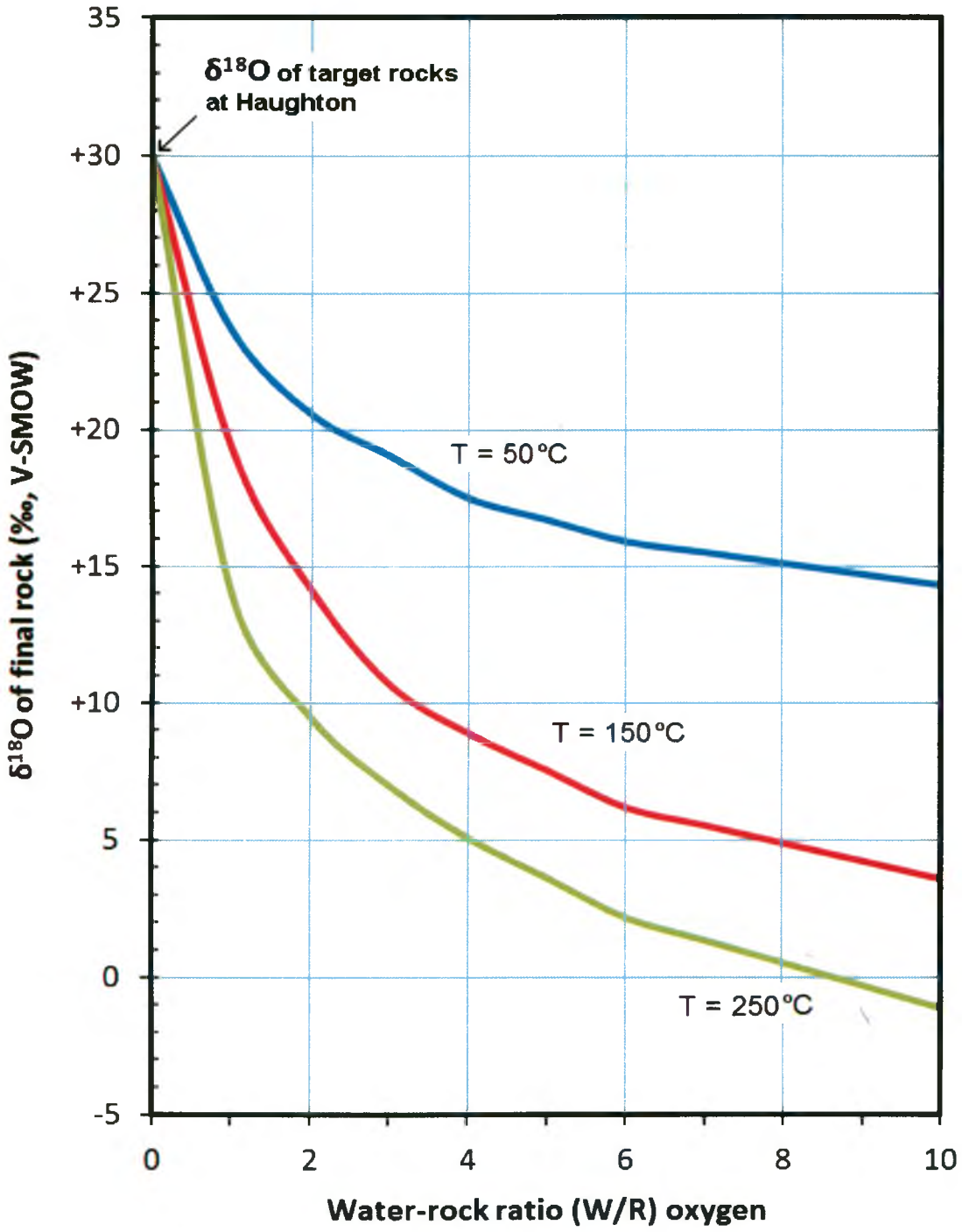

Figure 5.11. Diagram showing the inferred equilibration of initial carbonate country rocks ($\delta^{18}O^{i}_{r} \approx +30‰$) with initial water ($\delta^{18}O^{i}_{w} \approx -15‰$) at Haughton during hydrothermal alteration, as a function of increasing water-rock ratio (W / R) (expressed here as the ratio of atom percent of oxygen) in a closed system. The various models (coloured curves) are calculations made for temperatures of 50, 150, and 250°C. The pre-impact country rocks at Haughton are dominated by dolomite-rich lithologies with an approximate $\delta^{18}O$-value of +30‰, based on data from Land et al. (1975) and Martinez et al. (1994); limestones have slightly lower $\delta^{18}O$-values but are less important in terms of volume within the target sequence. The initial $\delta^{18}O$-value of -15‰ for the fluid is taken from paleo-meteoric water data by Jahren et al. (2002).

(1975), Martinez et al. (1994) and limestone data from this study. The initial $\delta^{18}O^{i}_{fluid}$ of -15.1‰ would represent a probable fluid composition at the onset of hydrothermal activity, long before mineral deposition (Jahren et al., 2002). First, we could assume that fluids and rocks were not in isotopic equilibrium with each others in the early hydrothermal stage. Although it is not known if complete equilibrium was reached during hydrothermal exchange, the intensity of disequilibrium was likely less pronounced after a period of isotopic exchange in the system and at the time calcite precipitated. Thus, a final $\delta^{18}O^{f}_{fluid}$ of -4‰ can be used in equation 5.8. However, this value does not account for the proportion of potential enrichment by liquid-vapour fractionation during phase separation and liquid-vapour fractionation effects discussed earlier. Above all, the final isotopic composition of country rocks is unknown at this point, which compromises a precise evaluation of water-rock interaction magnitude. Furthermore, the water-rock (W / R) ratio is based on the assumption of a closed-system; this may not have been the case at Haughton since residual water likely became enriched as it left the system, and a water recharge has most likely been replenishing the system. Nevertheless, this preliminary assessment shows the possible range in oxygen isotopic composition of the wall-rock at various water-rock ratios, and for the temperatures observed at Haughton (Figure 5.11).

5.3.4.2.2 Vaporisation of Fluid

It is known that degassing effects will lead to isotopic disequilibrium between the gaseous – or aqueous – and the solid molecules involved in a chemical exchange reaction (Gonfiantini et al., 1968). The decompression of subsurface water or fluids to shallower levels can induce boiling and a phase separation, which results in the fractionation of

oxygen isotopes, and subsequent ^{18}O enrichment of the residual liquid phase relative to the vapour phase (Uysal et al., 2009). As observed in geothermal environments such as the Yellowstone area, a gas-pressure release mechanism involving boiling explains geyser eruptions (White, 1967). Similarly, a gas-pressure release mechanism has been suggested to account for hydrothermal eruption breccias in New Zealand (Hedenquist et al., 1985). Following such types of pressure release, under some conditions, heat stored in the rock may be sufficient to vaporise the water occupying pore spaces in the rocks. Moreover, relatively low levels of boiling are sufficient to cause precipitation of calcite by CO_2-removal from a calcite-saturated solution (Sturchio et al., 1990).

The difference in isotopic mass of water molecules results in a range of vapour pressures causing a preferential evaporation of the light $H_2{}^{16}O$ molecule relative to the heavier $H_2{}^{18}O$ (Gat, 1981). Therefore, water vapour is depleted in the ^{18}O relative to liquid water, and this fractionation is a direct result of the effect of the masses of isotopic molecules on their respective velocities. The degree of fractionation is inversely related to the temperature at which the phase change is happening, such that smaller fractionation of oxygen isotopes between liquid and vapour phases occurs at higher temperatures (Horita et al., 1994). This explains in part why fractionation between fresh- or seawater and evaporated water on the surface of the Earth is more pronounced in colder regions at higher latitude, resulting in more ^{18}O-depleted meteoric water (Gat, 1984). The fact that the evaporation of seawater, with a $\delta^{18}O$-value ~0‰, is the main source of precipitation also explains why meteoric water is generally depleted in ^{18}O, with $\delta^{18}O$-values < 0‰ (Gat, 1991).

Horita et al. (1994) have joined their high-temperature experimental with lower (≤100 °C) temperature data from the literature on oxygen isotopic fractionation between liquid water and water vapour. Their results thus encompass most of the existing data on this subject, in the 0° to ~375°C range, which were regressed to a single equation

Eq. 5.9

$$10^3 \ln \alpha_{\text{liquid-vapour}} (^{18}O) = -7.685 + 6.7123\,(10^3/T) - 1.6664\,(10^6/T^2) + 0.35041\,(10^9/T^3),$$

where $10^3 \ln \alpha_{\text{liquid-vapour}} (^{18}O) \approx \delta^{18}O_{\text{liquid}} - \delta^{18}O_{\text{vapour}}$, α is the fractionation factor between oxygen isotopes in the liquid and water $(^{18}O/^{16}O)_{\text{liquid}}/(^{18}O/^{16}O)_{\text{vapour}}$, and T is in Kelvin (Horita et al., 1994).

For a given constant temperature of calcite precipitation, this equation provides the appropriate fractionation factor, $\alpha_{\text{liquid-vapour}}$, which is used to calculate the $\delta^{18}O_{\text{fluid (liquid)}}$ of the remaining body of water in the system. The change in $\delta^{18}O_{\text{fluid (liquid)}}$ as a function of boiling can be considered an isothermal Rayleigh distillation process, according to the equation from Sturchio et al. (1990), expressed as

Eq. 5.10

$$\delta^{18}O_{\text{fluid (liquid)}} = (\delta^{18}O_0 + 1000)\,(1 - f)^{[(1/\alpha) - 1]} - 1000,$$

where $\delta^{18}O_0$ is the composition of the fluid at f = 0, f relating to the fraction of water vaporised, and α is the liquid-vapour fractionation factor as seen in Equation 5.3.

From Figure 5.12, it is evident that a considerable fraction of water vapour has to leave the system in order to induce a significant change in the oxygen isotopic

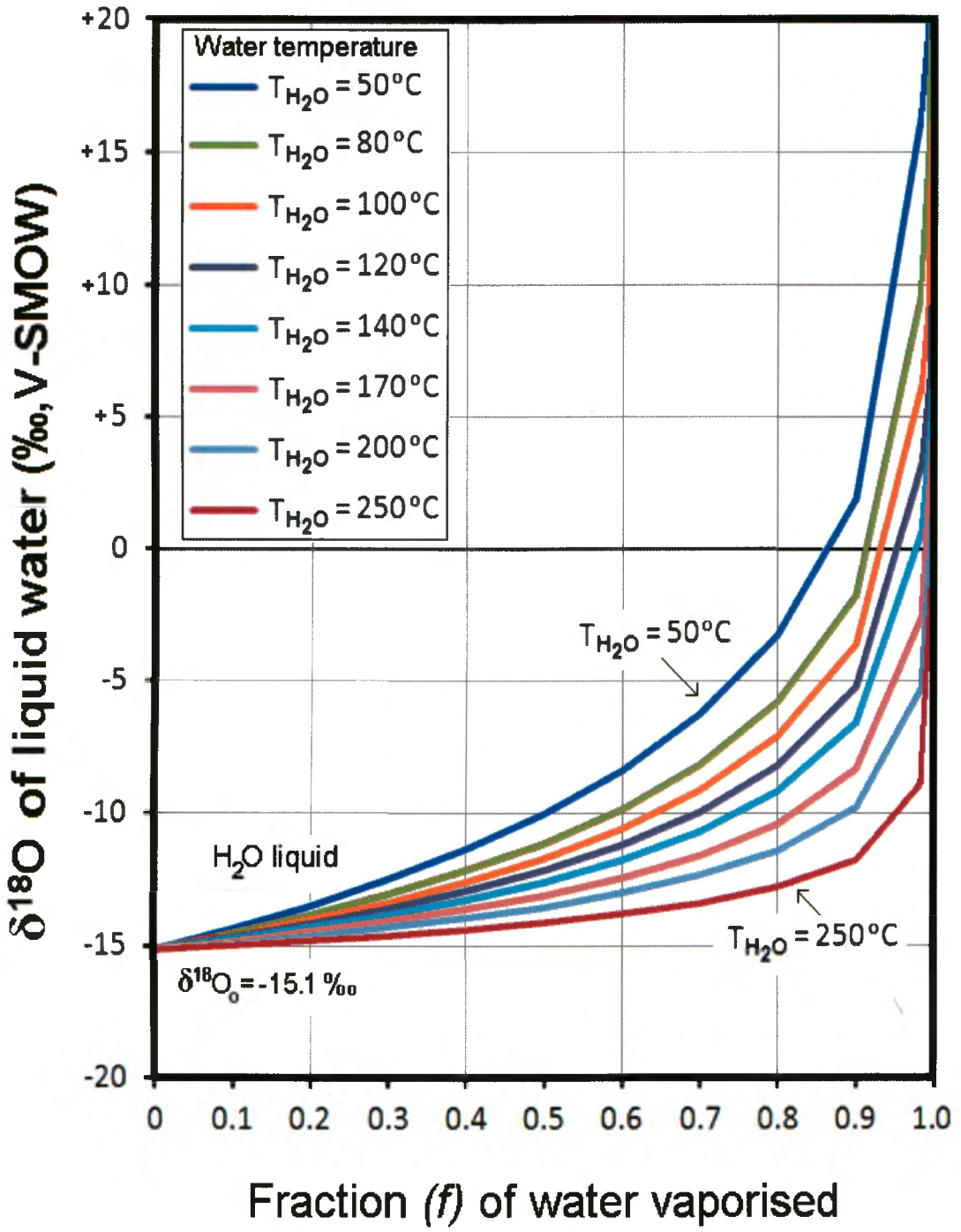

Figure 5.12. Diagram of $\delta^{18}O$-values of residual liquid water versus the fraction of H_2O vaporised in an isothermal Rayleigh fractionation model, according to the equation in text (Sturchio et al., 1990). The calculations imply an initial $\delta^{18}O$-value of -15.1‰ for meteoric water at Haughton, according to Jahren et al. (2002). The $\delta^{18}O$-value of residual liquid water increases as the fraction of water vaporised increases, but is inversely related to temperature. The models (coloured curves) were calculated with variable fractionation factors between the liquid and vapour phases for different temperatures (Horita et al., 1994). The following fractionation factors (α) were used various temperatures: 1.0075 at T= 50°C, 1.0059 at T= 80°C, 1.00506 at T= 100°C, 1.00436 at T= 120°C, 1.00375 at T= 140°C, 1.00299 at T= 170°C, 1.00235 at T= 200°C, and lastly 1.0015 at T= 250°C.

composition of the residual hydrothermal fluids, as stated by (Sturchio et al., 1990). The magnitude at which the initial amount of hydrothermal water is vaporised will dictate the $\delta^{18}O$-value of the residual body of water remaining in the crater. The temperature at which the water is maintained will also influence the intensity of oxygen isotopic fractionation (Sturchio et al., 1990). At lower temperature, isotopic fractionation will occur more readily and the residual liquid phase will be more enriched in ^{18}O compared to the vapour phase.

In the case of Haughton, the initial fluid composition of $\delta^{18}O_o$ (same as $\delta^{18}O^i_{fluid}$) is considered to be approximately -15‰, based on fossilised organic material of similar age than the Haughton impact event (Jahren et al., 2002). However, the composition of the final fluid is calculated from our range of $\delta^{18}O$ -values for hydrothermal calcites, as reported in Table 5.3. The models in Figure 5.12 demonstrate clearly that a large fraction of hydrothermal water ($f \geq 0.5$) must turn into vapour in order to create a ^{18}O enrichment of ~8 to 15‰, which is based on the difference between the initial and final fluid composition of -15‰ and -7 to ~0‰, respectively. By strictly considering an isotopic enrichment of the fluid at Haughton as an effect of liquid-vapour fractionation only – and not from other processes such as fluid-rock interaction – approximately 70% to ≥ 95% of the initial water would have to be vaporised (at temperatures between 80° and 250°C indicated by calcite precipitation) (Figure 5.12). Consequently, the residual liquid remaining in the system would undergo the necessary positive oxygen-isotope shift, as exemplified by calcite isotopic compositions (see Table 5.3). A positive shift in the ^{18}O composition of post-impact hydrothermal fluids has been described for the Chicxulub impact structure (Zürcher et al., 2004). Stable isotopic data from hydrothermal silicate

and carbonate minerals suggest that ^{18}O-enrichment of the fluids probably occurred if meteoric water was involved in the system. As for the Haughton crater, Zürcher et al. (2004) base these findings from the current meteoric water line observed at the impact site, which is believed to have remained constant for the last 150Ma (Taylor, 1974). At Haughton, a water recharge of meteoric origin is thought to have existed to supply the long-lived hydrothermal system (Osinski et al., 2001). According to the processes regulating oxygen isotope fluxes in evaporative systems, a gradual step-process could be responsible for extreme enrichment of a body of water (Gat and Bowser, 1991). Normally, the vapour phase is depleted in the $H_2{}^{18}O$ species, thus the residual water becomes enriched in this molecule. As the fluids evaporate and a continuous replenishment of water occurs, it seems possible to generate fluids with unusually high $\delta^{18}O$-values, even higher than the normal plateau reached in closed systems (Gat and Bowser, 1991). It is hypothesised that this concept might apply to the hydrothermal cells of an impact crater as fluids that remain in the crater are subject to a vapour output and a meteoric water inflow.

The textures seen in hydrothermal pipe structures indicate brecciation of wall rocks, which is analogous to hydrothermal eruption breccias that are characteristic of shallow parts of geothermal systems (Figure 5.13) (Hedenquist et al., 1985; Browne et al., 2001). In brief, the hydrothermal mineral veins and breccias observed in these shallow environments represent hydrofractures formed as extensional cracks developed from internal overpressure of CO_2-rich fluids (Gudmundsson et al., 2002). This overpressure that results from positive or vertical buoyancy of fluids is the driving force for hydrofractures to propagate to the surface. Hydraulic fracturing is a good indicator that

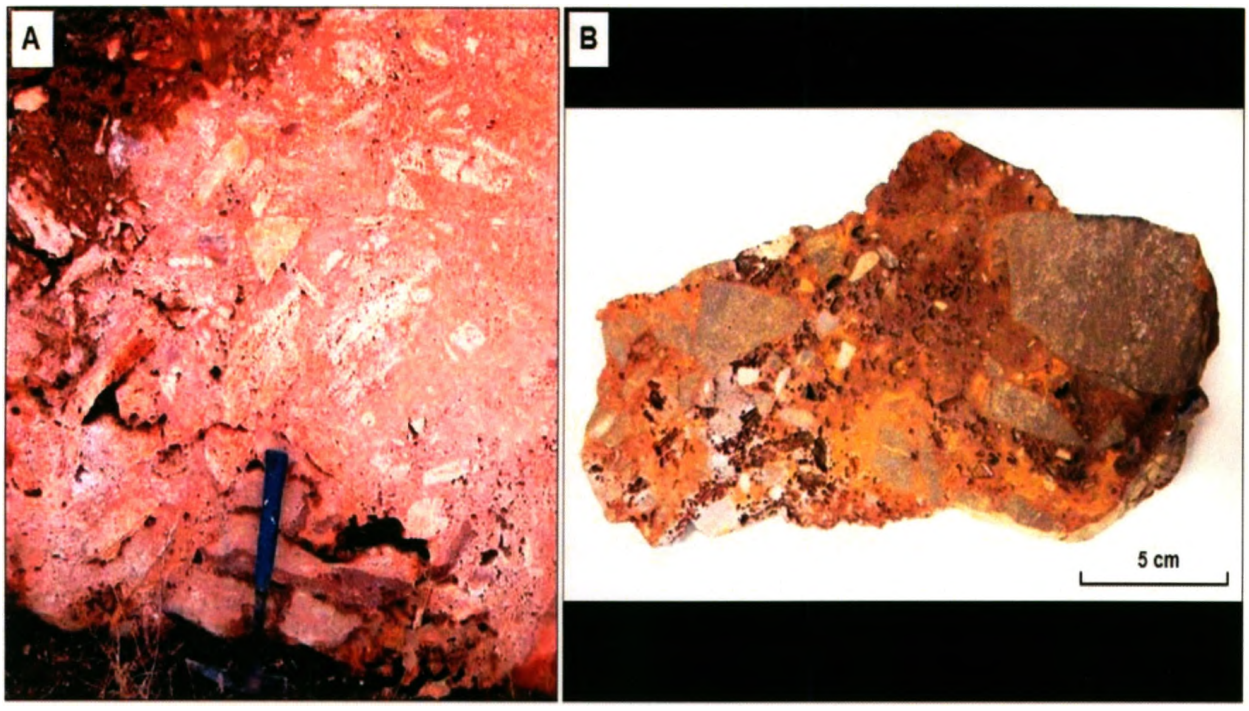

Figure 5.13. Comparative textural observations between: A) *in-situ* hydrothermally-generated breccias in late Quaternary travertine deposits in Turkey, with rock hammer for scale (Uysal, 2009); and B) breccia block (not *in situ*), containing wall-rock dolomite clasts, found near a hydrothermal pipe structure on the south-eastern rim of the Haughton impact structure (this study). The origin of the breccias observed in the block seen in (B) is hypothesised to have been formed by similar near-surface forceful hydrothermal processes than that shown in (A) and described by Uysal et al (2009). In general, mineral textures in extinct hydrothermal vents at Haughton are poorly preserved, but brecciation of the wall rock is clearly visible, suggesting active discharge of hydrothermal fluids to the surface. Since the sample contains a mixture of calcite and dolomite, stable isotopic analysis was not performed. For the Turkish travertine deposits, pre- and syn-breccia hydrothermal carbonates make up the majority of the outcrop, with zones of Fe-oxide-rich material.

hydrostatic pressures locally exceed lithostatic pressure, perhaps due to hydrothermal minerals being precipitated sealing the fluid pathways, or an increase in gas levels in the fluid (De Ronde et al.,1988). A perfect example of this is the travertine veins associated with poorly sorted breccia deposits in carbonate host-rocks seen in the Anatolia region, in central and western Turkey (Uysal et al., 2009).

Similar to Haughton pipe structures, the deposits explored by Uysal et al. (2009) are interpreted to be hydrothermal eruption products (i.e, Nelson and Giles, 1985; Browne and Lawless, 2001) since they occur only along fracture zones – no late clastic sedimentary system that can produce such high energy surface breccia deposits are described. However, at Haughton the nearby presence of a large body of impact melt breccia deposits implies that the rocks shown in Figure 5.13B might be the product of shock-related processes. Nevertheless, hydrothermal pipe structures on the rim of the Haughton crater do show these types of brecciated and secondary hydrothermal fracture-filling, although poorly preserved *in situ* (Osinski et al., 2001, 2005a). As stated above, the travertine deposits described by Uysal et al. (2009) are explained by a pressure drop, which resulted in a decrease in the solubility of CO_2 in the hydrothermal fluid. Consequently, the deposition of travertines in fracture zones occurred relatively quickly, and the newly-precipitated carbonates cemented previously deposited eruption deposits. This water reached the surface and deposited horizontal travertine beds juxtaposed to breccias. The eruption vents are now represented by vertical travertine veins and breccia zones. Comparatively, the Haughton hydrothermal vent deposits are much older and were subject to erosion, which implies that the surface deposits, if ever they occurred, were likely not preserved. Although not negligible, the degree of erosion observed at Haughton

is believed to be on the order of at least 200 meters (Grieve, 1988), thus subsurface hydrothermal deposits exposed today were formed at shallow depth. This is similar to epithermal deposits formed in the first kilometre of the crust, at depths ≤500 m (e.g., Hedenquist et al., 1989). It might be interesting to characterise the petrography of the highly-brecciated rock sample shown in Figure 5.13B, and perform stable isotope analysis on the carbonate fraction of the matrix to reveal their exact nature.

Furthermore, Uysal et al. (2009) noted a positive correlation exists between $\delta^{13}C$- and $\delta^{18}O$-values for calcite from the Kirsehir geothermal field, but not for the Pamukkale geothermal field. They believe that a positive isotopic correlation for travertine veins from Kirsehir could indicate that a more pronounced CO_2–water phase separation occurred at Kirsehir, resulting in a change of chemical composition of the fluid through CO_2-degassing. They base this hypothesis on the fact that considerable oxygen isotope fractionation generally occurs between CO_2 and water (Bottinga, 1968). In a CO_2–water mixed fluid, CO_2 becomes enriched in the ^{18}O-isotope relative to water, as shown in hydrothermal systems (Higgins and Kerrich, 1982). Therefore, a CO_2-dominated fluid separated from the original geothermal fluid may display higher $\delta^{13}C$- and $\delta^{18}O$-values. In contrast, as the CO_2-water ratio increases, water–rock interaction is attenuated, which means that the CO_2-rich fluid reacts less with the wall-rock (Uysal et al., 2009). Normally, more chemical exchange with the wall-rock amplifies the concentrations of rare-earth elements (REE) in the fluid. Uysal et al. (2009) indeed noted that travertine veins are remarkably depleted in rare earth elements, and proposed that the rapid ascent of CO_2-bearing fluids without significant interaction with host-rocks has generated the brecciated deposits observed in Turkish geothermal fields. This may be a possible

explanation, although likely only partial, for the isotopic composition of early hydrothermal pipe structure calcite at Haughton, which are more depleted in ^{18}O than most other calcite deposits at this site. As advanced by Uysal et al. (2009), low water-rock interaction and strong phase separation of CO_2-rich fluids would cause hydrothermal deposits that are depleted in ^{18}O compared to later deposits, such as intra-breccia calcite vug-fillings deposited at Haughton after the fluid had cooled down. Although no correlation between $\delta^{13}C$- and $\delta^{18}O$-values for calcite at Haughton is clearly observable as of today, a larger sample set might contribute to point out any isotopic trend between carbon and oxygen isotope ratios as for those from the Kirsehir geothermal field.

On a different note, it is worth mentioning that in contrast to Haughton pipe structures formed by the circulation of hot water (liquid and vapour), the degassing pipe structures found at the Ries impact structure seem to have remained dry during post-impact alteration, with water supplied probably only from rainfall (Newsom et al., 1986). These degassing pipes were likely formed by concentration of gas flow into discrete channels in the suevite deposits – a type of impact breccia (Newsom et al., 1986). The origin of the gas pressure might be from the release of volatiles from shocked and melted clasts, or from air trapped, within the suevites. Finally, this shows that distinct processes can result in the formation of flow structures in impact breccias.

5.3.5 Model of Hydrothermal Activity at Haughton

Information about the evolution of the fluids over time could be tracked to some extent by looking at the isotopic compositions of calcite vug and vein fillings throughout the impact crater, and also by evaluating their temperatures of formation. Over time, the

retrograde conditions of the hydrothermal system seem to have permitted sporadic episodes of mineral deposition, with calcite being deposited in most of the main and late stages of hydrothermal activity and over a wide range of temperatures (Table 5.4). Moreover, calcite could have been deposited at two separate episodes within a particular setting. The presence of discrete marcasite coating occurrences within calcite laminations is one piece of evidence to support that changes occurred in the physico-chemical properties of the hydrothermal solutions (Osinski et al., 2005a). Lastly, the fluids have probably been recycled more or less continuously by circulating in the hydrothermal cells within the subsurface of the crater depression, as seen by the positive ^{18}O shift from initial calcite to late-stage calcite deposits, which is concordant with a progressive incorporation of ^{18}O from the wall-rock into the fluids. For these reasons, the present stable isotopes study could not reveal the entire geochemical chronology of the hydrothermal system. Nevertheless, it provides unique and complementary information on the system.

As described previously, an approximate $\delta^{18}O_{fluid}$-value of -4‰ was found from calculations based on fluid inclusion temperatures of homogenisation from Osinski et al. (2005a). Once the oxygen isotopic composition of the hydrothermal fluids was known, it was possible to find the relative temperature of formation for each hydrothermal calcite sample. These findings are compiled in Appendix 2. Also, the average temperature of formation has been derived for each type of calcite deposit to highlight potentially significant variations (see Appendix 2). The averaged calculated temperatures for the various styles of calcite mineralisation seem to be in agreement with previous observations by Osinski et al. (2001, 2005a). Certainly, the fluid inclusion temperatures came from the same authors; however, the trends in isotopic compositions should be

similar for any given $\delta^{18}O_{fluid}$-value. Thus, the observations made here should reflect the temperatures of formation of calcite.

As the temperature of the system decreases, isotopic fractionation increases and Δ^{18} ($\delta^{18}O_{calcite}$ - $\delta^{18}O_{fluid}$) values become larger (Hoefs, 2004). This implies that hydrothermal calcite deposits become progressively enriched in ^{18}O. From Table 5.5, this is what is observed from the averaged data (for *n* number of samples) for each different type of hydrothermal calcite deposit, in decreasing order of temperature of formation: (1) cavity fillings in pipe structures have an averaged $\delta^{18}O$-value of +10.4‰ at 128°C (n=2) ; (2) marcasite-rich intra-breccia vug fillings have a $\delta^{18}O$-value of +11.3‰ at 118°C (n=24); (3) monomineralic intra-breccia vug fillings have a $\delta^{18}O$ of +11.9‰ at 112°C(n=14), and (4) vein fillings in target rocks have a $\delta^{18}O$ of +13.4‰ at 100°C (n=10). Most importantly, these observations are concordant with those of Osinski et al. (2001, 2005a). Moreover, the $\delta^{18}O_{fluid}$-value of -4‰ used to calculate the calcite generation temperature is conservative: if a higher $\delta^{18}O$-value such as those reported in Table 5.3 was used, temperatures would have been on average 15° to 20°C higher. Similarly, the lowest $\delta^{18}O_{fluid}$-value (-7‰) would result in lower generation temperatures.

The main source of heat in the impact melt breccias was the melt sheet itself; therefore, its relatively uniform thickness throughout the crater would mean a relatively uniform temperature at any given location and time within the sheet. This could have been a controlling factor in keeping isotopic compositions relatively similar throughout the impact breccias. However, it is suggested that temperatures could have been higher towards the base of the impact melt sheet (Naumov, 2005), thus ^{18}O-enriched calcites at lower levels are possible. In this sense, it was known that monomineralic calcite vugs

similar for any given $\delta^{18}O_{fluid}$-value. Thus, the observations made here should reflect the temperatures of formation of calcite.

As the temperature of the system decreases, isotopic fractionation increases and Δ^{18} ($\delta^{18}O_{calcite}$ - $\delta^{18}O_{fluid}$) values become larger (Hoefs, 2004). This implies that hydrothermal calcite deposits become progressively enriched in ^{18}O. From Table 5.5, this is what is observed from the averaged data (for *n* number of samples) for each different type of hydrothermal calcite deposit, in decreasing order of temperature of formation: (1) cavity fillings in pipe structures have an averaged $\delta^{18}O$-value of +10.4‰ at 128°C (n=2) ; (2) marcasite-rich intra-breccia vug fillings have a $\delta^{18}O$-value of +11.3‰ at 118°C (n=24); (3) monomineralic intra-breccia vug fillings have a $\delta^{18}O$ of +11.9‰ at 112°C(n=14), and (4) vein fillings in target rocks have a $\delta^{18}O$ of +13.4‰ at 100°C (n=10). Most importantly, these observations are concordant with those of Osinski et al. (2001, 2005a). Moreover, the $\delta^{18}O_{fluid}$-value of -4‰ used to calculate the calcite generation temperature is conservative: if a higher $\delta^{18}O$-value such as those reported in Table 5.3 was used, temperatures would have been on average 15° to 20°C higher. Similarly, the lowest $\delta^{18}O_{fluid}$-value (-7‰) would result in lower generation temperatures.

The main source of heat in the impact melt breccias was the melt sheet itself; therefore, its relatively uniform thickness throughout the crater would mean a relatively uniform temperature at any given location and time within the sheet. This could have been a controlling factor in keeping isotopic compositions relatively similar throughout the impact breccias. However, it is suggested that temperatures could have been higher towards the base of the impact melt sheet (Naumov, 2005), thus ^{18}O-enriched calcites at lower levels are possible. In this sense, it was known that monomineralic calcite vugs

Table 5.4. Summary table listing the main characteristics of all the different styles of hydrothermal mineralisation at the Haughton impact structure. Carbonate alteration has been found in the different settings exposed, except in the interior of the central uplift where only quartz is present. The temperature ranges of mineral precipitation, as well as specific stage of hydrothermal activity, are indicated. (From Osinski et al., 2001).

Setting	Style of alteration	Distribution[b]	Hydrothermal minerals (decreasing order of abundance)	Temperature range (°C)	Stage		
					Early	Main	Late
Interior of central uplift	Cementation of breccias	<3 km	Quartz (SiO_2)	<60; 90–250	A	R	A
Outer margin of central uplift	Veins	~5.0–6.5 km	Calcite ($CaCO_3$)	~150 to ~60	X	A	A
Within impact melt breccias	Vugs and veins	up to ~7 km[c]	Calcite	210 to <60	R	A	A
			Selenite ($CaSO_4.2H_2O$)	<80	X	R	A
			Marcasite (FeS_2)	~200 to 80	X	A	X
			Fibroferrite ($Fe(SO_4)(OH).5H_2O$)	<80	X	X	R
			Quartz	>200; <80	R	X	R
			Celestite ($SrSO_4$)	~200 to 80	X	R	X
			Barite ($BaSO_4$)	~200 to 80	X	R	X
			Fluorite (CaF_2)	~200 to 80	X	R	X
Faulted crater periphery	Hydrothermal pipe structures; veins	>7 km	Calcite	>200 to <60	?	A	A
			Quartz		?	A	A
			Marcasite		?	A	R
			Pyrite (FeS_2)		?	A	R

[a]Compiled with data from Osinski et al. (2001), Osinski (2004a), and Osinski et al. (2005b). Abbreviations: A = abundant; R = rare; X = absent.
[b]Given as the radial distance from crater center.
[c]Mineralization within the crater-fill impact melt breccias is concentrated in the lower levels of the impact melt breccia layer.

Table 5.5. Carbon and oxygen stable isotope compositions for the main types of hydrothermal calcite deposits analysed in this study. For each type of calcite, the corresponding average temperature of the hydrothermal fluid is provided. The $\delta^{13}C$- and $\delta^{18}O$-values and the calculated fluid temperatures, represent average values based on the entire dataset for each type of mineralisation (see Appendix 1).

Type of calcite mineralisation	Averaged $\delta^{13}C_{calcite}$ (‰, VPDB)	Averaged $\delta^{18}O_{calcite}$ (‰, VSMOW)	$\delta^{18}O_{fluid}$ (‰, VSMOW)	Calculated fluid temperature (K)	Calculated fluid temperature (°C)
1) Cavity filling in pipe structure	-7.5	+10.41	- 4‰	400	128
2) Marcasite-rich Intra-breccia vug filling	-4	+11.32	- 4‰	391	118
3) Monomineralic Intra-breccia vug filling	-6.44	+11.85	- 4‰	385	112
4) Vein filling in target rocks	-7.63	+13.36	- 4‰	373	100

within the impact melt-breccias were formed at lower temperatures than marcasite-calcite mineralisation found directly at the base of the melt sheet (Table 5.4) (Osinski et al., 2005a). However, the relationship between this carbonate mineralisation and the sulfide-carbonate mineralisation is unclear. Although the exact relationship between monomineralic calcite vugs and marcasite-rich calcite mineralisation is uncertain, calcite and calcite-marcasite veins have been found cross-cutting impact melt breccias in close proximity, which seems to suggest a close genetic and temporal relationship (Osinski et al., 2005a). For monomineralic calcite vug fillings, temperatures of homogenisation of primary fluid inclusions range from ~70° to 95°C. The presence of many liquid-filled fluid inclusions indicates calcite formed <60°C within the impact melt breccias (Osinski et al., 2005b). In contrast, fluid inclusion temperatures of homogenisation from marcasite-bearing samples from the Haughton River valley vugs are consistently >100°C. This is reflected in the calculated temperatures of formation of all intra-breccia vug samples displayed above (Table 5.5). More precisely, the averaged temperature is higher for marcasite-rich vuggy calcite than monomineralic vug fillings, and also shows the highest single temperature data point (>130°C). Similarly, calcite originating from a hydrothermal pipe structure shows a calculated temperature of 128°C which is one of the highest, although it is based on only two data points. Unfortunately, no fluid inclusion measurement exists for hydrothermal vent calcite. For calcite veins, large variations in homogenisation temperature (>100°C) of primary fluid inclusions suggest that precipitation of calcite around the outer margin of the central uplift was continuous over a long time period. There are two different types of calcites composing the veins found in the periphery of the central uplift and the inner crater rim region. In general, fluid-inclusions found in hydrocarbon-bearing calcites yield temperatures of homogenisation in

the 90° to 175°C range (i.e., sample HMP99-104) (Osinski et al., 2005a). However, slightly lower temperatures ranging between 62° to 101°C are also observed (i.e., sample HMP02-048). Hydrocarbon-free calcites, on the other hand, show temperatures that range from 65° to 145°C, with a temperature of 90°C being typical (i.e., samples HMP99-104, HMP02-048). In rare cases, much higher temperatures are noted but this is probably due to the stretching of the inclusion, therefore, are not considered (Osinski et al., 2005a). In brief, calcite veining shows fluid inclusion homogenisation temperatures <100°C, but in reality, hydrocarbon-free calcite continued to crystallise down to <60°C (Table 5.4). As such, temperature calculations are based on a broad range of isotopic compositions. Notwithstanding the fact that temperatures of formation of vein calcite could exceed 140°C locally, the averaged calculated temperature of formation is consistent with previous observations (Osinski et al., 2005a): the value is lower than for the other types of calcite deposits, and many single temperature measurements are <70°C. However, averaged temperatures from calcite veining are an estimate as the range in isotopic compositions is large.

By taking into account the information presented in Tables 5.4 and 5.5, the findings hereby discussed are consistent with calcite being deposited during the main stage of hydrothermal activity, first in impact melt breccias and pipe structures on the crater rim, then as veining around the periphery of the central uplift. Rare calcite veins lying in the crater rim region present isotopic compositions similar to the hydrothermal pipe structure; this is interpreted as calcite that was deposited early in fractures at similar temperatures as in hydrothermal vents. The possibility that a recent regional overprint of meteoric fluids would have altered the isotopic composition of calcite is unlikely. As a

matter of fact, fluid inclusions within calcite show no sign of geochemical resetting (Osinski et al., 2005a). Moreover, the significant variations observed in both carbon and oxygen isotopic compositions within the various types of calcite mineralisation (this study) eliminate the possibility of a uniform late-stage meteoric overprint.

Between the main and late stage of calcite deposition at Haughton, the chemistry of the fluid is believed to have changed. First, the once vapour-dominated fluid progressively became liquid-rich. As boiling occurred, CO_2 degassing and cooling induced the precipitation of calcite (Osinski et al., 2005a). Thus, it is possible that pre- and post-marcasite calcite deposits are marked by a shift in isotopic composition. A change in the fluid's chemistry is evidenced by a drop in pH < 5 believed to be responsible for marcasite deposition (Osinski et al., 2001). A concurrent change in the stable isotope ratios of the fluid is, therefore, possible. As such, earlier and late calcite deposits would have precipitated from fluids with different $\delta^{18}O$-values. The resumption in calcite precipitation in the late-stage of hydrothermalism is presumed to have occurred as the conditions became slightly alkaline (Osinski et al., 2005a). Thus, it is possible that not only temperature fluctuations could explain the variation in calcite composition, but an oxygen isotope excursion of the fluid as well. The models from Figure 5.13 show the extent at which the host-rocks are affected by interacting with the fluid. However, the final $\delta^{18}O$-value of the fluid after ^{18}O-isotope leaching of the wall-rock could not be obtained from Figure 5.11: it only provides a final $\delta^{18}O$-value for the wall-rock after fluid-rock interaction. By extrapolating these values, however, one could postulate that the $\delta^{18}O$-value of the fluid increases as the $\delta^{18}O$-value of the wall-rock decreases, and that the fluid is increasingly enriched in ^{18}O with time.

In summary, as the hydrothermal system was generated, a probable oxygen isotopic composition for the fresh fluid would have been around -15‰, based on evidence of oxygen isotopic composition of meteoric water from the fossil forest on Axel Heiberg Island, Canada, revealed by Jahren et al. (2009). Soon thereafter, while the hydrothermal fluids were still very hot and calcite was not being deposited yet, the light oxygen isotopes were incorporated in the vapour phase and escaped the system laterally, notably through hydrothermal pipe structures. The heavy isotopes were accumulated in the residual fluids and were entrained in the hydrothermal cells. This cycle within the crater floor continued until it shifted to a liquid dominated regime. At this point, large oxygen isotope fractionation between fluids and calcite due to lower temperatures resulted in higher $\delta^{18}O$-values for calcite. The increase in $\delta^{18}O$-values of calcite probably also occurred because of the small water-rock ratio suspected to have been present in this restricted basin. As water influx was probably limited to the system, the isotopic composition of the hydrothermal fluids was controlled by that of the host-rocks, as well as temperature. By circulating through the target lithologies, wall-rock interactions occurred and the isotopic signature of the host-rocks slowly affected the composition of the fluids. Thus, the fluids became progressively enriched with $\delta^{18}O$-values likely starting around -15‰ and reaching a -7 to 0‰ range, as indicated by the most reliable measurements made from fluid inclusion temperatures. As a result, the variations observed in the composition of the hydrothermal fluids seem to have been reflected in the oxygen isotopic composition of various calcite deposits found in the Haughton impact structure, which we reported in this study (see Figure 5.14).

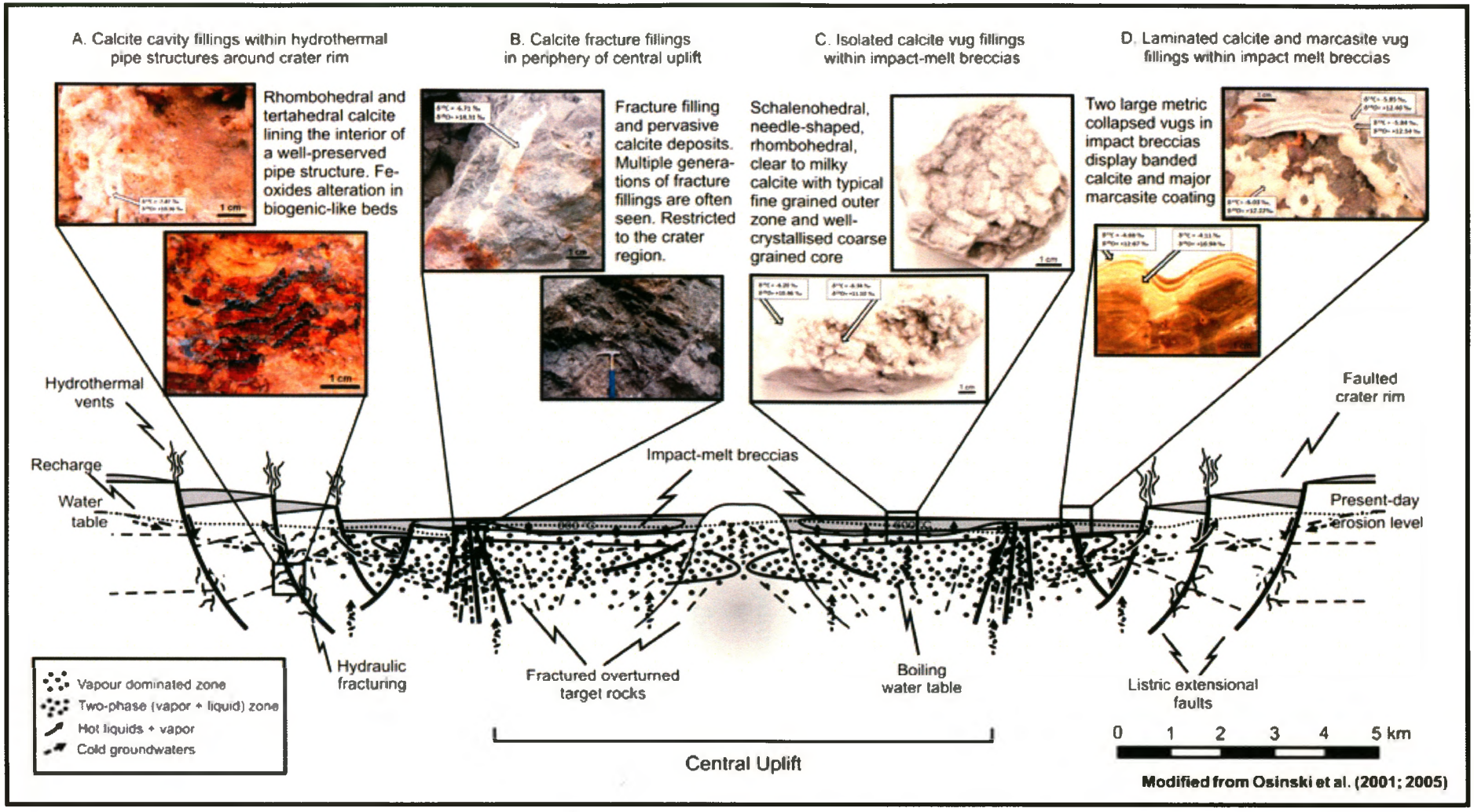

Figure 5.14. Cross-section of the Haughton impact structure showing the main types of hydrothermal calcite occurrences and isotopic compositions. A: Void and fracture filling in pipe structures developed in the faulted crater periphery; B: Fracture filling in target rocks from the outer margin of the central uplift and inner crater rim; C: Vug filling in the lower levels of the impact melt breccias layer; D: Laminated calcite-marcasite vug filling within impact melt breccias. (Modified from Osinski et al., 2005a).

It is believed though that in the mid- to late-stage liquid dominated hydrothermal regime, little or no vapour was lost and fluids would have remained in the sub-surface beneath the crater floor and the impact melt breccias. As a consequence, the water recharge would have been less important than in the vapour-dominated stage. A progressive enrichment in ^{18}O would characterise the recycled fluids because of the low water-rock ratio in effect within the system. The isotopic signature of the fluids would likely be overprinted by the highly enriched host-rocks ($\delta^{18}O$ >25‰), which would cause this positive shift in isotopic composition of the hydrothermal fluids. In the end, as discussed by Horita and Wesolowski (1994), the fractionation of oxygen isotopes of water at high temperatures is not well documented, therefore, the entire mechanism by which isotopes are fractionated in impact-induced hydrothermal fluids is far from being fully understood. More studies on impact-induced hydrothermal carbonates, and certainly other types of mineralisation, are required to address the full nature of hydrothermal fluids within impact structures. A prudent claim would be that at Haughton, different factors causing the fractionation of oxygen isotopes in hydrothermal solutions were probably responsible for the $\delta^{18}O_{fluid}$-values hereby discussed.

Chapter 6. Conclusions and Recommendations

The incentive for conducting this geological study at the Haughton impact structure was twofold: 1) to investigate the nature of reference carbonate material in the vicinity of the crater and, 2) to distinctively characterise impact-induced hydrothermal carbonates within the impact structure, by keeping in mind the implications of such study for planetary exploration and astrobiology.

6.1 Pre-, Syn- and Post-Impact Lithologies

In the first part of this study, X-Ray Diffraction mineralogy (XRD)analysis was used for identifying samples containing pure calcite to be analysed on the MultiPrep for carbon and oxygen stable isotopic composition. In the meantime, a stable isotope analysis technique and intra-laboratory dolomite standards were tested, possibly to be used for naturally occurring dolomite and mixed carbonate samples from the Haughton impact structure. A methodology utilising the MultiPrep in parallel with the GasBench was proposed, but further experimentation is required.

Overall, data from XRD, X-Ray Fluorescence (XRF) and stable isotopes of reference carbonate material are consistent with earlier studies (Thorsteinsson et al., 1987; Martinez et al., 1994; Land et al., 1969). Moreover, the present report provides, for the first time, data for all the main rock formations known to have been affected by the Haughton impact event. The lithologies under study, mainly limestone (and dolomite characterised by XRD) for the most part sampled outside the crater area, have $\delta^{13}C$ ranging from -1.7 to -0.1‰ and $\delta^{18}O$ values between +20.2 and 25.5‰. Few of the rocks that were analysed originate from the interior of the crater, but no definitive carbon or

oxygen-isotope shift in shocked samples, relative to those that are unshocked, could be determined. However, from a mineralogical point of view, higher amounts of quartz in shocked samples from the central uplift are noted, and are suspected to have been induced by late-stage cementation by silica-rich fluids.

6.2 Impact-Induced Hydrothermal Deposits

The XRD study served as a discriminating tool for selecting pure hydrothermal calcite samples. According to stable isotope analysis, variations are observed in carbon and oxygen isotopic compositions for the various styles of calcite mineralisation at Haughton. The data indicate moderate and strong depletion in heavy carbon and oxygen isotopes, respectively, in comparison with fresh or marine carbonates: these values are, therefore, typical of hydrothermal carbonates. In addition, the $\delta^{18}O$ values observed at Haughton are among the lowest reported for impact-induced hydrothermal carbonates. However, in general, the $\delta^{13}C$- and $\delta^{18}O$-values are similar to the majority of samples from two other localities, the Lockne and Popigai impact structures (Sturkell et al., 1998; Versh et al., 2006), and compare well with the lowest $\delta^{18}O$-values seen at the Siljan impact structure (Juhlin et al., 1991).

Spatial variations in isotopic contents of calcite vug fillings are not obvious since many samples were composed of a mixture of carbonate minerals, and hydrothermal calcite is sometimes contaminated by a wall-rock fraction. Nonetheless, many pure calcite samples were analysed and the two different styles of calcite vug filling are generally distinct in terms of isotopic composition: monomineralic calcite vugs show an average $\delta^{13}C$-value of $-6.5 \pm 1.5‰$ and $\delta^{18}O$-value of $+11.5 \pm 1.5‰$, whereas marcasite-bearing

vug deposits have an average $\delta^{13}C$-value of -4.5 ± 1.5‰ and $\delta^{18}O$-value of +11.5 ± 1.5‰. The similar range in oxygen isotopic compositions probably reflects the close genetic and temporal nature of these two types of deposits. Interestingly, an increase in $\delta^{18}O$-values seems to characterise the inner portion of most of the monomineralic vug fillings, and similarly the very late calcite laminae in marcasite-rich vug deposits. In contrast, hydrothermal calcite veins within target rocks have an approximate $\delta^{13}C$-value of -8‰ and $\delta^{18}O$-value of +13‰. However, these calcite samples display a very broad range of isotopic compositions, with $\delta^{13}C$- values from -14 to -2.5‰ and $\delta^{18}O$-values from +9 and +17‰. Comparatively, calcite crystals from the hydrothermal pipe structure analysed for this study have an average $\delta^{13}C$-value of -7.5 ± 0.5‰ and $\delta^{18}O$-value of +10.4 ± 0.5‰.

In summary, variations in isotopic composition of hydrothermal calcite are found within different geological settings within the crater. This likely reflects the cooling of the hydrothermal fluid and its evolution in terms of ^{18}O- and ^{13}C contents, probably from the combined effects of kinetic fractionation as the fluid boils, and also from water-rock interaction under a low water/rock ratio. This would imply that host-rock geochemistry played a role in the observed isotopic composition of precipitated calcites. In addition, when a sequential deposition of mineral layers occurs in a single fracture or vug, the corresponding succession of $\delta^{18}O$-values may indicate the mechanism of precipitation (Stuchio et al., 1990). Local isotopic variations are observed for some samples (i.e., outer and inner portions of intra-melt breccia vugs). For the laminated intra-breccia calcite vug filling at Haughton, the relative difference in $\delta^{18}O$-values between the two adjacent layers could signify either a slight (17°C) temperature decrease or a slight (1.7‰) increase in fluid $\delta^{18}O$-value between each deposition stage.

Equally important are the wide variations in isotopic values of vein samples, which tend to support the relatively long-lasting nature of fracture fillings. In other words, these samples seem to record the developing conditions throughout the lifetime of the hydrothermal system. This is consistent with observations of multi-generation and cross-cutting relationships, as well as a relatively strong pervasive calcite alteration in some cases (Osinski et al., 2005a), and possible spatial heterogeneity in the fluid conditions in different parts of the crater (closer to central uplift or to the faulted rim).

6.3 Hydrothermal Fluids

Cooling of the crater, and of the hydrothermal system itself, was accentuated by the circulation of fluids into fractured and porous lithologies. As the solubility of carbonates increase with decreasing temperature (Hoefs, 2004), it is evident that cooling of a hydrothermal fluid cannot be solely responsible for the precipitation of carbonate minerals in a closed system. The hydrothermal system must be open and processes such as CO_2 degassing, fluid-rock interaction or mixing of fluids will cause the precipitation of carbonate minerals (Hoefs, 2004). Overall, at Haughton the combined effects from Rayleigh liquid-vapour fractionation of the fluid, with the interaction of the same fluids with country rocks in the most active hydrothermal zones, likely resulted in a measureable ^{18}O enrichment of the residual hydrothermal fluid from which calcite was deposited. This may have been further enhanced by a process similar to that of the "stream-of-lakes" model (Gat and Bowser, 1991), where a depleted meteoric water recharge can account for a gradual ^{18}O-enrichment by multiple episodes of fractionating, and by confining this residual ^{18}O-enriched fluid.

The significant variations in $\delta^{18}O$-values suggest a complex geochemical evolution of the hydrothermal fluids prior to, and during the time of, carbonate deposition. The fluid source is meteoric water with a nominal $\delta^{18}O$-value possibly approximating -15‰ (Jahren et al., 2004). The fluid then evolved to higher $\delta^{18}O$-values between -7 and -2‰, as indicated by calculations from calcite fluid inclusion temperatures. As evidenced already by fluid inclusion salinities of ~1.7% NaCl eq. (Osinski et al., 2005a), the input of trapped pore water from Paleozoic marine sedimentary target rocks was not significant. A slight positive oxygen-isotope shift suggested by late-stage intra-melt breccia vug calcite would reflect a temperature decrease. The average temperature of deposition is higher for sulfide-calcite mineralisation, averaging 128°C, than for monomineralic calcite vug fillings at 118°C. Furthermore, an ^{18}O enrichment occurred from the loss of isotopically light vapour (e.g., by kinetic Rayleigh fractionation) and continuous fluid-rock interaction with the target rocks of higher $\delta^{18}O$-values. The veins are generally formed at lower temperatures of formation, averaging 100°C. However, the lower $\delta^{18}O$-values belong to some of the calcite veins and to the pipe structure in the crater rim region, which would support the early deposition and higher generation temperatures model, as suggested by Osinski et al. (2005a). The higher $\delta^{18}O$-values indicate temperatures of formation as low as 67°C. Finally, carbon isotopic signatures are not suggestive of a direct input from an organic source, but rather influenced by an inorganic source. In addition to stable isotope analysis, more in depth microscopic characterisation could be used to identify mineral precipitates from a biogenic origin.

Finally, since fluid inclusion data are not available for the whole set of calcite samples, the observations made in this study may not apply directly to every sample analysed. This particularly applies to vein samples, which are the most depleted samples in both ^{13}C and ^{18}O depleted. In the future, a thorough petrographic and geochemical inventory of all samples would be necessary.

6.4 Implications for Astrobiology and Planetary Exploration

This study is intimately linked to the search for life in extreme environments on Earth and on other planetary bodies. In fact, hydrothermal systems in impact craters are considered potentially favourable habitats for thermophilic and hyper-termophilic micro-organisms, and might have been a key environment for the emergence of life in the Solar System. As for the Siljan impact structure (Hode et al., 2009), the potential for finding biogenic-like features in the fossil hydrothermal system of the Haughton crater is relatively high. Although no actual impact-hydrothermal system is currently active to be studied directly, the characterisation of fossil hydrothermal systems might allow for the detection of fossilised microbial organisms. This would accentuate the work that is being done on known terrestrial impact craters.

6.5 Recommendations for Future Work

As a final comment, it would be useful to study the stable isotopic composition of wall-rock carbonates directly adjacent to hydrothermal calcite veins, in order to better assess the relationship between their respective isotopic compositions. Since most of the vein-bearing target rocks in this study were not composed of pure calcite, isotopic analysis using the MultiPrep technique was not undertaken. A different stable isotope

analysis technique allowing for the study of carbonate mixtures, similar to those presented in Chapter 3, would help in achieving this objective. In addition, multi-generation vein samples should be scrutinised in more detail as each episode of calcite infill might hold distinct geochemical information about the developing hydrothermal system. In this study, multi-generation veins were not studied microscopically, therefore, accurate sampling of separate calcite families for stable isotope analysis was not achievable. Fortunately, it was possible to analyse some of the intra-melt breccia vugs showing more than one generation of calcite filling, which provided additional information on these deposits. The techniques for analysing carbonate mixtures will also benefit the study of calcite vug fillings, and will result in a better understanding of the spatial distribution of isotopic compositions across the entire impact melt breccia layer. Finally, it is believed that the oxygen and hydrogen isotopic composition of post-impact hydrothermal fluids at Haughton could be studied by sampling directly the liquids and gases trapped in mineral fluid inclusions. The analysis of heavier stable isotopes (i.e., sulfur or calcium) in carbonates and other hydrothermal minerals could give more insights on the evolution of the fossil hydrothermal system at Haughton.

7. References

Abramov, O., and Kring, D. A. (2005) Impact-induced hydrothermal activity on early Mars. Journal of Geophysical Research, 110, E12S09.

Agrinier, P., Deutsch, A., Schärer, U., and Martinez, I. (2001) Fast back-reactions of shocked-released CO_2 from carbonates: An experimental approach. Geochimica and Cosmochimica Acta, 65:15, 2615-2632.

Al-Aasm, I. S., Taylor, B. E., South, B. (1990) Stable isotope analysis of multiple carbonate samples using selective acid extraction. Chemical Geology (Isotope Geoscience Section), 80, 119– 125.

Alfonso, P., Prol-Ledesma, R. M., Canet, C., Melgarejo, J. C., and Fallick, A. E. (2005) Isotopic evidence for biogenic precipitation as a principal mineralisation process in coastal gasohydrothermal vents, Punta Mita, Mexico. Chemical Geology, 224, 113-121.

Allen, M., Lollar, B. S., Runnegar, B., Oehler, D. Z., Lyons, J. R., Manning, C. E., and Summers, M. E. (2006) Is Mars Alive? EOS, 87:41, 433-448.

Ames, D. E., Watkinson, D. H., and Parrish, R. R. (1998) Dating of a regional hydrothermal system induced by the 1850 Ma Sudbury impact event. Geology, 26:5, 447-450.

Ames D. E., Jonasson J. R., Gibson H. L., and Pope K. O. (2006) Impact-generated hydrothermal system: Constraints from the large Paleoproterozic Sudbury crater, Canada. In Biological processes associated with impact events, Eds. Cockell C. S., Gilmour I., and Koeberl C. Berlin: Springer-Verlag. 376 p.

Bada, J.F., and Lazcano, A. (2002) Some like it hot, but not the first biomolecules. Science, 296, 1982-1983.

Bain, J. G., and Kissin, S. A. (1988) A preliminary study of fluid inclusions in shock-metamorphosed sediments at the Haughton impact structure, Devon Island, Canada. Meteoritics, 23, 256.

Banner, J. L., and Hanson, G. N. (1990) Calculation of simultaneous isotopic and trace element variations during water-rock interaction with application to carbonate diagenesis. Geochimica and Cosmochimica Acta, 54, 3123-3137.

Baker, E. H. (1962) The Calcium Oxide – Carbon Dioxide System in the Pressure Range 1-300 Atmosphere. Huffield Research Group in Extraction Metallurgy, Imperial College of Science and Technology, London, S.W.7, 464-470.

Bargar, K.E., and Fournier, R.O. (1988) Effects of glacial ice on subsurface temperatures of hydrothermal systems in Yellowstone National Park, Wyoming: Fluid-inclusion evidence. Geology, 16, 1077-1080.

Barnes, H. L. (1979) Solubilities of hydrothermal ore minerals, in Barnes, H. L., ed., Geochistry of hydrothermal ore deposits. New York, Wiley Interesci., 404-460.

Barrat, J. A., Boulègue, J., Tiercelin, J. J., and Lesourd, M. (2000) Strontium isotopes and rare-earth element geochemistry of hydrothermal carbonate deposits from Lake Tanganyika, East Africa. Geochimica and Cosmochimica Acta, 64:2, 287-298.

Berger, W. H., Vincent, E. (1986) Deep-sea carbonates: Reading the carbon-isotope signal. Geologische Rundschau, 75:1, 249-269.

Bibring, J.-P., Langevin, Y., Mustard, J. F., Poulet, F., Arvidson, R., Gendrin, A., Gondet, B., Mangold, N., Pinet, P., Forget, F., and the OMEGA team (2006) Global Mineralogical and Aqueous Mars History Derived from OMEGA/Mars Express Data. Science, 312, 400-404.

Bischoff, L., and Ostertag, R. (1986) Der Haughton Dome. Eine multi-disziplinare Untersuchung eines Meteoritenkraters in Nord-kanada. Geowissenschaften in unserer Zeit, 4, 105-115.

Bischoff, L., and Osierski, W. (1988) The Surface Structure of the Haughton Impact Crater, Devon Island, Canada. Meteoritics, 23, 209-220.

Blattner, P. (1985) Isotope Shift Data and the Natural Evolution of Geothermal Systems. Chemical Geology, 49, 187-203.

Bogard, D. D., Clayton, R. N., Marti, K., Owen, T., and Turner, G. (2001) Martian volatiles: Isotopic composition, origin, and evolution. Chronology and Evolution of Mars, 96, 425-458.

Boynton, W. V., Ming, D. W., Kounaves, S. P., Young, S. M., Arvidson, R. E., Hecht, M. H., Hoffman, J., Niles, P. B., Hamara, D. K., Quinn, R. C., Smith, P. H., Sutter, B., Catling, D. C., and Morris, R. V. (2009) Evidence for Calcium Carbonates at the Mars Phoenix Landing Site. Science, 325, 61-64.

Brakenridge, G. R., Newsom, H. E., and Baker, V. R. (1985) Ancient hot springs on Mars: Origins and paleoenvironmental significance of small Martian valleys. Geology, 13, 859-862.

Bridges, J. C., Catling, D. C., Saxton, J. M., Swindle, T. D., Lyon, I. C., and Grady, M. M. (2001) Alteration assemblages in Martian meteorites: Implications for near-surface processes. Space Science Reviews, 96, 365-392.

Browne, P.R.L., and Lawless, J.V. (2001) Characteristics of hydrothermal eruptions, with examples from New Zealand and elsewhere. Earth-Science Reviews, 52 (4), 299-331.

Campbell, K. A., Farmer, J. D., and Des Marais, D. (2002) Ancient hydrocarbon seeps from the Mesozoic convergent margin of California: carbonate geochemistry, fluids and palaeoenvironments. 2, 63-94.

Carr, M.H. (1996) Water on Mars, Oxford University Press. New York.

Clayton, R. M., Muffler, L. J. P., and White, D. E. (1968) Oxygen isotope study of calcite and silicates of the River Rand No. 1 well. Salton Sea geothermal field, California, American Journal of Science, 266, 968-979.

Cloutis, E. A., and Osinski, G. R. (2009) Spectral Reflectance Properties of Carbonates from Diverse Environments and Related Phases: Implications for Mars. Abstract, AGU-GAC-MAC Joint Assembly, Toronto, Canada.

Cockell C. S., Osinski G. R. and Lee P. 2003. The impact crater as a habitat: Effects of impact alteration of target materials. Astrobiology, 3, 181–191.

Cockell, C. S. (2006) The Origin and Emergence of Life under Impact Bombardment. Philosophical Transactions of the Royal Society, 361, 1845-1856.

Coplen, T. B. (1996) New guidelines for the reporting of stable hydrogen, carbon, and oxygen isotope ratio data. Geochimica et Cosmochimica Acta, 60, 3359-3360.

Craig, H. (1953) The geochemistry of the stable carbon isotopes. Geochim. Cosmochim. Acta, 3, 53-92.

Craig, H. (1961) Standard for reporting concentrations of deuterium and oxygen- 18 in natural waters. Science, 133, 1833-1834.

Criss, R. E. (2008) Terrestrial Oxygen Isotope Variations and Their Implications for Planetary Lithospheres. Reviews in Mineralogy and Geochemistry, 58, 511-526.

Criss, R.E. and Taylor, H.P. (1986) Meteoric-hydrothermal systems. In: Valley, J., O'Neil, J.R. and Taylor, H.P (Eds), Stable Isotopes in High Temperature Geological Processes. Rev. Mineral., 16, 373-424.

Dansgaard, W. (1964) Stable isotopes in precipitation. Tellus, 16, 436-468.

Darby, D. A. (1998) Mysterious iron-nickel-zinc arctic spherules. Canadian Journal of Earth Sciences, 35, 23-29.

Davies, J. F., Leroux, M. V., Whitehead, R. F., and Goodfellow, W. D. (1990) Oxygen-isotope composition and temperature of fluids involved in deposition of Proterozoic

cedex deposits, Sudbury Basin, Ontario. Canadian Journal of Earth Sciences, 27, 1299-1303.

De Groot, P. A. (2004) Handbook of Stable Isotope Analytical Techniques, vol. 1, Elsevier B.V.

De Ronde, C. E. J., and Blattner, P. (1988) Hydrothermal Alteration, Stable Isotopes, and Fluid Inclusions of the Golden Cross Epithermal Gold-Silver Deposit, Waihi, New Zealand. Economic Geology, 83, 895-917.

Dressler, B. O., and Reimold, W. U. (2001) Terrestrial impact melt rocks and glasses. Earth-Science Reviews, 56, 205-284.

Earth Impact Database, 2010. http://www.unb.ca/passc/ImpactDatabase/index.html.

Ehrenfreund, P., Charnley, S.B. (2000) Organic Molecules in the Interstellar Medium, Comets, and Meteorites: A Voyage from Dark Clouds to the Early Earth. Annual Review of Astronomy and Astrophysics, 38, 427-483.

Eiler, J. M., Valley, J. W., Graham, C. M., and Fournelle, J. (2002) Two populations of carbonate in ALH84001: Geochemical evidence for discrimination and genesis. Geochimica and Cosmochimica Acta, 66:7, 1285-1303.

Ellis, A. J,, and Mahon, W. A. (1977) Chemistry and geothermal systems. New York, Academic Press, 392p.

Epstein, S., Graf, D. L., Degens, E. T., 1964. Oxygen isotope studies on the origin of dolomites. In: Craig, H., Miller, S. L., Wasserburg, G. J. (Eds.), Isotopic and Cosmic Chemistry. North-Holland, Amsterdam, pp. 169–180.

Farmer, J. (1998) Thermophiles, early biosphere evolution, and the origin of life on Earth: Implications for the exobiological exploration of Mars. Journal of Geophysical Research, 103:E12, 28 457-28 461.

Farr, T. G. et al. (2002) Terrestrial Analogs to Mars. The Future of Solar System Exploration, 2003-2013, ASP Conference Series, 272, 35-76.

Faure, G. and Botoman, G. (1984) Origin of epigenetic calcite in coal from Antarctica and Ohio based on isotope compositions of oxygen, carbon and strontium. Chemical Geology (Isotope Geosience Section), 2, 313-324.

Faure, G., and Mensing, T. M. (2005) Isotopes: Principles and Applications. John Willey and Sons (Third Edition), New Jersey, USA, 897 p.

Feldman, V. I. (1994) The conditions of shock metamorphism. Geological Society of America, Special paper 293, 121-132.

Forsythe, R. D. (1990) Lakes on Mars Impact craters – A case for martian salars and saline lakes during the Noachian. Lunar and Planetary Science Conf. 21st, 379–380.

Fournier, R.O. (1989) Geochemistry and dynamics of the Yellowstone National Park hydrothermal system. Annu. Rev. Earth Planet. Sci., 17, 13-53.

Fox, S. W. (1965) The Origins of Prebiological Systems, and of Their Molecular Matrices. In Proceedings of the NASA Conference at the Institute for Space Biosciences, Academic Press, New York.

French, B. M., and Short, N. M. (1968) Shock Metamorphism of Natural Materials. Mono Book Corp., Baltimore, 644 p.

French B. M. (1998) Traces of Catastrophe: A Handbook of Shock-Metamorphic Effects in Terrestrial Meteorite Impact Structures. LPI Contribution No. 954, Lunar and Planetary Institute, Houston. 120 p.

Friedman, I., and O'Neil, J.R. (1977) Compilation of stable isotope fractionation factors of geochemical interest. In: M. Fleischer (Ed.), Data of Geochemistry. U.S. Geological Survey, Prof. Pap, 440-KK, 12 p.

Frisch T. and Thorsteinsson R. (1978) Haughton Astrobleme: A Mid-Cenozoic impact crater, Devon Island, Canadian Arctic Archipelago. Arctic, 31, 108.

Fruh-Green, G. L., Kelley, D. S., Bernasconi, S. M., Karson, J. A., Ludwing, K. A., Butterfield, D. A., Boschi, C., and Proskurowski, G. (2003) 30,000 Years of Hydrothermal Activity at the Lost City Vent Field. Science, 301, 495-498.

Furnes, H., Banerjee, N. R., Staudigel, H., and Muehlenbachs, K. (2007) Pillow lavas as habitat for microbial life. Geology Today, 23:4, 143-146.

Furnes, H., Banerjee, N., Staudigel, H., Muehlenbachs, K., McLoughlin, N., De Wit, M., and van Kranendonk, M. (2007) Comparing petrographic signatures of bioalteration in recent to MesoArchean pillow lavas: Tracing subsurface life in oceanic igneous crust. Precambrian Research, 158: 156-176.

Garlik, G. D. (1969) Geochemistry of oxygen. In Wedepohl, K. A. (Editor), Handbook of Geochemistry, vol. 2, 1, Springer-Verlag.

Gat, J. R. (1981) Groundwater. In: Gat, J.R., Gonfiantini, R. (Eds). Stable isotope hydrology - Deuterium and oxygen-18 in the water cycle. IAEC, Vienna, Technical Report Series, 210, 223 240.

Gat, J. R., and Bowser, C. (1991) The Heavy Isotope Enrichment of Water in Coupled Evaporative Systems, Stable Isotope Geochemistry: A Tribute to Samuel Epstein, Taylor, H. P., O'Neil, J. R., and Kaplan, I. R. (Eds), The Geochemical Society, Special Publication No. 3, 159-168.

Gault, D. E., Quaide, W. L., and Oberbeck ,V. R. (1968) Impact cratering mechanics and structures. In Shock Metamorphism of Natural Materials (B. M. French and N. M. Short, eds.), Mono Book Corp., Baltimore, pp. 87–99.

Gersonde, R., Deutsch, A., Ivanov, B. A., and Kyte, F. T. (2002) Oceanic impacts – a growing field of fundamental geosciences. Deep-Sea Research II, 49: 951-957.

Global Network of Isotopes in Precipitation (2001) International Atomic Energy Agency and the World Meteorological Association.

Glover, E.D., 1961. Method of solution of calcareous materials using the complexing agent EDTA. J. Sediment. Petrol. 31, 622– 626.

Gomes, R., Levison, H. F., Tsiganis, K., and Morbidelli, A. (2005) Origin of the cataclysmic Late Heavy Bombardment period of the terrestrial planets. Nature, 435, 466-469.

Griener, H. R., Fortier Y. O., Blackadar R. G., Glenister B. F., Greiner H. R., McLaren D. J., McMillan N. J., Norris A. W., Roots E. F., Souther J. G. and Thorsteinsson R. (1963) Haughton Dome and area southwest of Thomas Lee Inlet. In Geology of the north-central part of the Arctic Archipelago, Northwest Territories (Operation Franklin). Geological Survey of Canada Memoir 320, pp. 208. Geological Survey of Canada, Ottawa.

Grieve, R. A. F. (1988) The Haughton Impact Strucure: Summary and Synthesis of the Results of the HISS Project. Meteoritics, 23, 249-254.

Grieve, R. A. F. (1991) Terrestrial impact: The record in the rocks, Meteoritics, 26, 175-194.

Grieve R. A. F. and Pesonen L. J. (1996) Terrestrial impact craters: Their spatial and temporal distribution and impacting bodies. Earth, Moon, Planets, 72, 357–376.

Grieve, R. A. F., and Masaitis, V. L. (1994) The economic potential of terrestrial impact craters, International Geological Review, 36, 105–151.

Gucsik, A., Koeberl, C., Brandstätter, F., Libowitzky, E., Reimold, W. U. (2003) Scanning electron microscopy, cathodoluminescence, and Raman spectroscopy of experimentally shock-metamorphosed quartzite. Meteoritics and Planetary Science, 38:8, 1187-1197.

Gudmundsson, A., Fjeldskaar, I., and Brenner, S.L. (2002) Propagation pathways and fluid transport of hydrofractures in jointed and layered rocks in geothermal fields. Journal of Volcanology and Geothermal Research, 116 (3-4), 257-278.

Gurov, E. P., and Gromov, E. I. (1988) Structural Features of Impact Structures in a Two-Layered Target. Geologicheskii Zhurnal, Kiev, USSR, 6, 115-122.

Hagerty, J. J., and Newsom, H. E. (2003) Hydrothermal alteration at the Lonar Lake impact structure, India: Implications for impact cratering on Mars. Meteoritics and Planetary Science, 38:3, 365-381.

Hayes, J. M. (2001) Fractionation of carbon and hydrogen isotopes in biosynthetic processes. In: Valley, J. W., Cole, D. R. (Eds), Stable Isotope Geochemistry, Rev. Min. Geochem., 43, 225-277.

Hecht, L., Wittman, A., Schmitt, R.-T., and Stöffler, D. (2004) Composition of impact melt particles and the effects of post-impact alteration in suevitic rocks at the Yaxcopoil-1 drill core, Chicxulub crater Mexico. Meteoritics and Planetary Science, 39:7, 1169-1186.

Hedenquist, J. W., and Henley, R. W. (1985) Hydrothermal eruptions in the Waiotapu Geothermal System, New-Zealand — their origin, associated breccias, and relation to precious metal mineralization. Economic Geology, 80 (6), 1640-1668.

Hedenquist, J. W., and Browne, P. R. L. (1989) The evolution of the Waiotapu geo-thermal system, New Zealand, based on the chemical and isotopic composition of its fluids, minerals and rocks. Geoch. et Cosmochimica Acta, 53, 2235-2257.

Heyl, A. V., and Brock, M. R. (1962) Zinc occurrence in the Serpent Mound structure of Southern Ohio. US Geological Survey, 450D, article 148.

Hickey, L. J., Johnson, K. R., and Dawson, M. R. (1988) The stratigraphy, sedimentlogy, and fossils of the Haughton Formation: A post-impact crater-fill, Devon Island, N.W.T., Canada, Meteoritics, 23, 221-231.

Higgins, N. C., and Kerrich, R. (1982) Progressive ^{18}O-depletion during CO_2 separation from a carbon dioxide rich hydrothermal fluid — evidence from the Grey River Tungsten Deposit, Newfoundland. Canadian Journal of Earth Sci., 19, 2247–2257.

Hode, T., Von Dalwigk, I., and Broman, C. (2003) A Hydrothermal System Associated with the Siljan Impact Structure, Sweden - Implications for the Search for Fossil Life on Mars. Astrobiology, 3:2, 271-289.

Hode, T., Cady, S. L., Von Dalwigk, I., Kristiansson, P. (2009) Evidence of Ancient Life in an Impact Structure and its Implications for Astrobiology : A Case Study. In: From Fossils to Astrobiology, Seckbach, J., and Walsh, M. (Eds.), Springer Science + Business Media B.V., 249-273.

Hoefs, J. (1973) Stable Isotope Geochemistry – Subseries: Isotopes in Geology. Springer – Verlag, Berlin, p.22-51.

Hoefs, J. (2004) Stable Isotope Geochemistry. Springer – Verlag, Berlin, 244 p.

Hofmann, B. A., and Farmer, J. D. (1999) Filamentous fabrics in low-temperature mineral assemblages: are they fossil biomarkers? Implications for the search for a subsurface fossils on early Earth and Mars. Plan. and Space Sci., 48, 1077-1086.

Holland, H. D., Malinin, S. D. (1979) The solubility and occurrence of non-ore minerals. In: Barnes, H.L. (Ed). Geochemistry of hydrothermal ore deposits, 2nd ed. Wiley, New York, pp. 461-508.

Horita, J., and Wesolowski, D. J. (1994) Liquid-Vapor Fractionation of Oxygen and Hydrogen Isotopes of Water from the Freezing to the Critical Temperature, Geochimica and Cosmochimica Acta, 58:16, 3425-3437.

Horneck, G., and Baumstark-Khan, C. (2002) Astrobiology: The Quest for the Conditions of life. Springer-Verlag, Berlin, 411p.

House, C. H., Schopf, J. W., and Stetter, K. O. (2003) Carbon isotopic fractionation by Archeans and other thermophilic prokaryotes. Organic Geochemistry, 34, 345-356.

Humphrey, J. D., 1988. Late Pleistocene mixing zone dolomitization, southeastern Barbados, West Indies. Sedimentology 35, 327– 348.

Humphreys, E. D., Dueker, K. G., Schutt, D. L., and Smith, R. B. (2000) Beneath Yellowstone: evaluating plume and nonplume models using teleseismic images of the upper mantle. GSA Today, 10, 1–7.

Irwin, L.N. and Schulze-Makuch, D. (2001) Assessing the plausibility of Life on Other Worlds. Astrobiology, 1, 2.

Ivanov, B. A., and Deutsch, A. (2001) The phase diagram of CaCO3 in relation to shock compression and decomposition. Physics of the Earth and Planetary Interiors, 129, 131-143.

Jahren, A. H., and Sternberg, L. S. L. (2002) Eocene Meridional Weather Patterns Reflected in the Oxygen Isotopes of Arctic Fossil Wood. GSA Today, 2:1, 4-9.

Jahren, A. H., and Sternberg, L. S. L. (2008) Annual patterns within tree rings of the Arctic middle Eocene (ca. 45 Ma): Isotopic signatures of precipitation, relative humidity, and deciduousness. Geology, 36:2, 99-102.

Jahren, A. H., Byrne, M. C., Graham, H. V., Sternberg, L. S. L., and Summons R. E. (2009) The environmental water of the middle Eocene Arctic: Evidence from δD, $\delta^{18}O$ and $\delta^{13}C$ within specific compounds. Palaeogeography, Palaeoclimatology, Palaeoecology, 271: 1-2, 96-103.

Jamtveit, B, and Yardley, B. (1997) Fluid flow and transport in rocks: Mechanisms and effects. Chapman & Hall, The Alden Press, Oxford. 319p.

Javaux, E. J. (2006) Extreme Life on Earth: Past, Present and Possibly Beyond. Research in Microbiology, 157, 37-48.

Jõeleht, A., Kirsimäe, K., Plado, J., Versh, E., and Ivanov, B. (2005) Cooling of the Kärdla impact crater: II. Impact and geothermal modeling. Meteoritics and Planetary Science, 40, 21-33.

Johansen, A., Oishi, J. S., Mac Low, M.-M., Klahr, H., Henning, T., and Youdin, A. (2007) Rapid planetesimal formation in turbulent circumstellar disks. Nature, 448, 1022-1025.

Jones, E. M., and Kodis, J. W. (1982) Atmospheric effects of large body impacts: The first few minutes. Geological Society of America, Special paper 190, 175-186.

Juhlin, C. et al. (1991) Scientific Summary Report of the Deep Gas Drilling Project in the Siljan Ring Impact Structure. FUD Report UG 1991 (14), Vattenfall Research and Development, Swedish State Power Board, 278p.

Katz, D. A., Eberli, G. P., Swart, P. K., and Smith, L. B. (2006) Tectonic-hydrothermal brecciation associated with calcite precipitation and permeability destruction in Mississipian carbonate reservoirs, Montana and Wyoming. AAPG Bulletin, 90 (11), 1803-1841.

Keith, M. L, and Weber, J. N. (1964) Carbon and oxygen isotopic composition of selected limestones and fossils. Geochimica and Cosmochimica Acta, 28, 1787-1816.

Kele, S., Demeny, A., Silklosy, Z., Nemeth, T., Toth, M., and Kovacs, M. B. (2008) Chemical and stable isotope composition of recent hot-water travertines and associated thermal waters, from Egerszalok, Hungary: Depositional facies and non-equilibrium fractionation, Sedimentary Geology, 211, 53-72.

Kelley, D. S., Baross, J. A., and Delaney, J. R. (2002) Volcanoes, Fluids, and Life at Mid-Ocean Ridge Spreading Centers. Annual Review of Earth Planetary Sciences, 30, 385-491.

Kerr, J. W. (1967) New Nomenclature for Ordovician Rock Units of the Eastern and Southern Queen Elizabeth Islands. Bulletin of Canadian Petroleum Geology, 15:1, 91-113.

Kerr, J. W. (1968) Stratigraphy of Central and Eastern Ellesmere Island, Arctic Canada. Part II, Ordovician. Geological Survey of Canada, Paper 67-27.

Kettrup, B., Deutsch, A., Ostermann, M., and Agrinier, P. (2000) Chicxulub impactites: Geochemical clues to the precursor rocks. Meteoritics and Planetary Science, 35, 1229-1238.

Kieffer, S. W., and Simonds, C. H. (1980) The role of the volatiles and lithology in the impact cratering process. Reviews of Geophysics and Space Physics, 18, 143-181.

King, D. T., Jr., Neathery, T. L., Petruny, L. W., Koeberl, C., and Hames, W. E. (2002) Shallow-marine impact origin of the Wetumpka structure (Alabama, USA). Earth and Planetary Science Letters, 202, 541-549.

King, D. T., Jr., and Petruny, L. W. Applications of stratigraphic nomenclature to terrestrial impact-derived and impact-related materials. In: Impact markers in the stratigraphic record (eds Koeberl, C., and Martinez-Ruiz, F.), vol. 2, pp. 41-64. Springer-Verlag, Berlin.

King, P. L., Lescinsky, D. T., and Nesbitt, H.W. (2004) Composition and evolution of primordial solutions on Mars, with applications to other planetary bodies. Geochimica et Cosmochimica Acta, 68:23, 4993-5008.

Kirsimäe, K., Suuroja, S., Kris, J., Kärki, A., Polikarpus, M., Puura, V., and Suuroja, K. (2002) Hornblende alteration and fluid inclusions in Kardla impact crater, Estonia: Evidence for impact-induced hydrothermal activity. Meteoritics and Planetary Science, 37, 449-457.

Komor, S. C., and Valley, J. W. (1990) Deep drilling at the Siljan Ring impact structure, oxygen-isotope geochemistry of granite. Contributions to Mineralogy and Petrology, 105, 516-532.

Kounaves, S. (2007) Life on Mars may hide like Earth's extremophiles. Nature, 449, 281.

Kyte, F. T., Zhou, Z., and Wasson, J. T. (1981) High noble metal concentrations in a late Pliocene sediment. Nature, 292: 417-420.

Land, L. S., Salem, M. R. I., and Morrow, D.W. (1975) Paleohydrology of Ancient Dolomites: Geochemical Evidence. The American Association of Petroleum Geologists Bulletin, 59:9, 1602-1625.

Landis, G. P. (1983) Harding Iceland Spar: A New $\delta^{18}O - \delta^{13}C$ Carbonate Standard for Hydrothermal Minerals. Isotope Geoscience, 1, 91-94.

Li, H. (2008) Comparison in Techniques in Carbonate Carbon and Oxygen Isotope measurements in LSIS. Laboratory for Stable Isotope Science April 22 Meeting, University of Western Ontario, London, Canada.

Lineweaver, C. H., and Schwartzman, D. (2004) Cosmic Thermobiology: Thermal Constraints on the Origin and Evolution of Life in the Universe. Origins, 233-248.

Lindgren, W. (1933) Mineral Deposits, 4th edition, McGraw-Hill Book Company, Inc., New York, 930 p.

Longstaffe, F. J. (1996) Chapter 6. An introduction to Stable Oxygen and Hydrogen Isotopes and Their Use as Fluid Tracers in Sedimentary Systems. Isotopic methods in sedimentology. 385-397.

Longstaffe, F. J., Calvo, R., Ayalon, A., and Donaldson, S. (2003) Stable isotope evidence for multiple fluid regimes during carbonate cementation of the Upper Tertiary Formation, Dead Sea Graben, southern Israel. Journal of Geochemical Exploration, 80, 151-170.

Luders, V., and Rickers, K. (2004) Fluid inclusion evidence for impact-related hydrothermal fluid and hydrocarbon migration in Creataceous sediments of the ICDP-Chicxulub drill core Yaxcopoil-1. Meteoritics and Planetary Science, 39, 1187-1197.

Lunine, J. I., Chambers, J., Morbidelli, A., and Leshin, L. A. (2003) The origin of water on Mars. Icarus, 165, 1-8.

Martinez, I., Schärer, U., and Guyot, F. (1993) impact-induced phase transformation at 50-60GPa in continent crust: and EPMA and ATEM study. Earth and Planetary Science Letters, 119, 207-223.

Martinez, I., Agrinier, P., Schärer, U., and Jovoy, M. (1994) A SEM-ATEM and stable isotope study of carbonates from the Haughton impact crater, Canada. Earth and Planetary Science Letters, 21, 559-574.

Martinez, I., Deutsch, A., Schärer, U., Ildefonse, P., Guyot, F., and Agrinier, P. (1995) Shock recovery experiments on dolomite and thermodynamical calculations of impact induced decarbonation. Journal of Geophysical Research, 100:B8, 15 465-15 476.

Martinez, I., Zhang, J., and Reeder, R. J. (1996) In situ X-ray diffraction of aragonite and dolomite at high pressure and high temperature: Evidence for dolomite breakdown to aragonite and magnesite. American Mineralogist, 81, 611-624.

Masaitis, V. L., and Naumov, M. V. (1993) Principal model of hydrothermal circulation in impact craters (in Russian). Doklady (Transactions) of Russian Academy of Sciences, 333, 70-72.

Matas, J., Gillet, P., Ricard, Y., and Martinez, I. (2000) Thermodynamic properties of carbonates at high pressures from vibrational modelling. European Journal of Mineralogy, 12, 703-720.

McLaren, D. J., and Goodfellow, W. D. (1990) Geological and Biological Consequences of Giant Impacts. Annual Reviews in Earth Sciences, 18, 123-171.

McCrea, J. M. (1950) The isotopic chemistry of carbonates and a paleotemperature scale. Journal of Chemical Physics, 18, 849-857.

McKinney, C. R., McCrea, J. M., Epstein, S., Allen, H. A., and Urey, H. C. (1950) Improvements in mass-spectrometers for the measurement of small differences in isotope abundance ratios. The Review of Scientific Instruments, 21, 724-730.

Melosh, H. J. (1989) Impact Cratering: A Geological Process. Oxford University Press, New York, 245 p.

Metzler, A., Ostertag, R., Redeker, H.-J., and Stoffler, D. (1988) Composition of the Crystalline Basement and Shock Metamorphism of Crystalline and Sedimentary Target Rocks at the Haughton Impact Crater, Devon Island, Canada. Meteoritics, 23, 197-207.

Molnar, F., Watkinson, D. H., and Everest, J. O. (1999) Fluid-inclusion characteristics of hydrothermal Cu-Ni-PGE veins in granitic and metavolcanic rocks at the contact of the Little Stobie deposit, Sudbury, Canada. Chemical Geology, 154, 279-301.

Moore, J. N., Allis, R., Renner, J. L., Mildenhall, D., and McCulloch, J. (2002) Petrological evidence for boiling to dryness in the Karaha-Telaga Bodas geothermal system, Indonesia. Proceedings of the Twenty-Seventh Workshop on Geothermal Reservoir Engineering, Stanford University, California.

Moynier, F., Albarede, F., and Herzog, G. F. (2006) Isotopic composition of zinc, copper and iron in lunar samples, Geochimica et Cosmochimica Acta, 70, 6103-6117.

Murowchick, J. B., and Barnes, H. L. (1986) Marcasite precipitation from hydrothermal solutions. Geochimica et Cosmochimica Acta, 50, 2615-2629.

NASA Phoenix Mission Website, http://www.nasa.gov/phoenix.

Naumov, M. V. (1999) The hydrothermal-metasomatic mineral formation (in Russian). In: Deep Drilling in the Puchezh-Katunki Impact Structure (eds Masaitis, V. L., Pevzner, L. A.), pp. 276-286. VSEGEI Press, St Petersburg.

Naumov, M. V. (2002) Impact-generated hydrothermal systems: Data from Popigai, Kara, and Puchezh-Katunki impact structures. In Impacts in Precambrian shields, Eds. Plado J. and Pesonen L. J., Berlin: Springer-Verlag, pp. 117-171.

Naumov, M. V. (2005) Principal features of impact-generated hydrothermal circulation systems: mineralogical and geochemical evidence. Geofluids, 5, 165-184.

Nelson, C. E., and Giles, D. L. (1985) Hydrothermal eruption mechanisms and hot-spring gold deposits. Economic Geology, 80 (6), 1633-1639.

Newsom, H. E. (1980) Hydro-thermal alteration of impact melt sheets with implications for Mars. Icarus, 4, 207-216.

Newsom, H. E., Graup, G., Sewards, T., and Keil, K. (1986) Fluidization and Hydrothermal Alteration of the Suevite Deposit at the Ries Crater, West Germany, and Implications for Mars. Proceedings of the Seventeenth Lunar and Planetary Science Conference Part 1 - Journal of Geophysical Research, 91:B13, E239-E251.

Newsom, H. E., Hagerty, J. J., and Thorsos, I. E. (2001) Location and Sampling of Aqueous and Hydrothermal Deposits in Martian Impact Craters. Astrobiology, 1, 71-87.

Nicholson, K. (1993) Geothermal fluids: Chemistry and exploration techniques. Berlin: Springer-Verlag. 263 p.

Nier, A. O. (1950) A redetermination of the relative abundances of the isotopes of carbon, nitrogen, oxygen, argon, and potassium. Physical Reviw, 77, 789-793.

Okulitch, A. V. (1991) Geology of the Canadian Archipelago and north Greenland. In Geology of the Innuitian Orogen and Arctic Platform of Canada and Greenland. Geology of Canada, vol. 3, ed. Trettin H. P. Ottawa: Geological Survey of Canada, pp. 435-458.

O'Neil, J. R. (1987) Preservation of H, C, and O isotopic ratios in the low temperature environment. In: T.K. Kyser (Ed), Stable Isotope Geochemistry of Low Temperature Fluids. Mineral. Assoc.Can., Short Course, 13, 85-128.

Ormö, J., Lindström, M., Lepinette, A., Martinez-Frias, J., and Diaz-Martinez, E. (2006) Cratering and modification of wet-target craters: Projectile impact experiments and field observations of the Lockne marine-target crater (Sweden). Meteoritics and Planetary Science, 41:10, 1605-1612

Oró, J., Miller, Stanley L., Lazcano, A. (1990) The Origin and Early Evolution of Life on Earth. Annual Review of Earth and Planetary Sciences, 18, 317-357.

Osinski G. R. and Spray J. G. (2001) Impact-generated carbonate melts: evidence from the Haughton Structure, Canada. Earth and Planetary Science Letters, 194, 17–29.

Osinski, G. R., Spray, and Lee, P. (2001) Impact-induced hydrothermal activity within the Haughton impact structure, Arctic Canada: Generation of a transient, warm, wet oasis. Meteoritics & Planetary Science, 36, 731-745.

Osinski G. R. and Spray J. G. (2003) Evidence for the shock melting of sulfates from the Haughton impact structure, Arctic Canada. Earth and Planetary Science Letters, 215, 357–370.

Osinski, G. R. (2005) Hydrothermal activity associated with the Ries impact event, Germany. Geofluids, 5, 202-220.

Osinski, G. R., Lee, P., Parnell, J., Spray, J. G., and Baron, M. (2005a) A case-study of impact-induced hydrothermal activity: The Haughton impact structure, Devon Island, Canadian High Arctic. Meteoritics and Planetary Science, 40:12, 1859-1877.

Osinski G. R., Spray J. G., and Lee P. (2005b) Impactites of the Haughton impact structure, Devon Island, Canadian High Arctic. Meteoritics & Planetary Science 40, 1789–1812.

Osinski, G. R., Lee, P., Spray, J. G., Parnell, J., Lim, D. S. S., Bunch, T. E., Cockell, C. S, and Glass, B. (2005c) Geological overview and cratering model for the Haughton impact structure, Devon Island, Canadian High Arctic. Meteoritics & Planetary Science, 40:12, 1759-1776.

Osinski, G. R., and J., Spray, J. G. (2005d) Tectonics of the Haughton impact structure. Meteoritics & Planetary Science, 40:12, 1813-1834.

Osinski, G. R., and Lee, P. (2005e) Intra-crater sedimentary deposits at the Haughton impact structure, Devon Island, Canadian High Arctic. Meteoritics & Planetary Science, 40:12, 1887–1900.

Osinski, G. R., Léveillé, R., Berinstain, A., Lebeuf, M., and Bamsey, M. (2006) Terrestrial Analogues to Mars and the Moon: Canada's Role. Geoscience Canada, 33:4, 175-188.

Osinski, G. R. (2007) Impact metamorphism of $CaCO_3$-bearing sandstones, Meteoritics and Planetary Science, 42:11, 1945-1960.

Osinski, G. R. (2008) Meteoritic impact structures: the good and the bad. Geology Today, 24:1, 13-19.

Osinski, G. R., Spray, J. G., and Grieve, R. A. F. (2008) Impact melting in sedimentary target rocks: An assessment. The Geological Society of America, Special paper 437, 1-18.

Osinski, G. R., Barfoot, T. D., Ghafoor, N., Izawa, M., Banerjee, N., Jasiobedzki, P., Tripp, J., Richards, R., Auclair, S., Sapers, H., Thomson, L., and Flemming, R. (2010) Lidar and the Scene Modeler (mSM) as scientific tools for planetary exploration. Planetary and Space Science, 58, 691-700.

Parnell, J., Lee, P., Osinski, G. R., Lee, P., and Cockell, C. S. (2005) Application of organic geochemistry to detect signatures of organic matter in the Haughton impact structure. Meteoritics & Planetary Science, 40:12, 1879-1885.

Pevzner, L. A., Kirjakov, A. F., Vorontsov, A. K., Masaitis, V. L., Mashchak, M. S., and Ivanov, B. A. (1992) Vorotilovskaya drillhole: First deep drilling in the central uplift of a large terrestrial impact crater. Lunar and Planetary Science Conference, 22, 1063-1064.

Phillips, W. J. (1972) Hydraulic fracturing and mineralization. Journal of the Geological Society, London, 128. 337-359.

Pike, R. J. (1977) Apparent depth/apparent diameter relations for lunar craters. Proceedings of the 8th Lunar Science Conference, p. 3427-3436.

Pirajno, F. (2005) Hydrothermal processes associated with meteorite impact structures: evidence from three Australian examples and implications for economic resources. Australian Journal of Earth Sciences, 52, 587-605.

Pirajno, F., and Van Kranendonk, M. J. (2005) Review of hydrothermal processes and systems on Earth and implications for Martian analogues. Australian Journal of Earth Sciences, 52, 329-351.

Pohl, J., Eckstaller, A., and Robertson, P. B. (1988) Gravity and magnetic investigations in the Haughton impact structure, Devon Island, Canada. Meteoritics, 23, 235–238.

Powell, J. L. (1998) Night comes to the Cretaceous—Dinosaur Extinction and the Transformation of Modern Geology. W.H. Freeman and Company Press, New York

Prantzos, N. (2007) On the "Galactic Habitable Zone". In Proceedings of the ExoBio'07 Conference, Propriano, France. C27, 1-12.

Price, P. B. (2007) Microbial life in glacial ice and implications for a cold origin of life. Federation of European Microbiological Societies – Microbial Ecology, 59, 217-231.

Priscu, J. C. (2005) Exploring Subglacial Antarctic Lake Environments. EOS, 86:20, 193-200.

Rathbun, J. A., and Squyres, S. W. (2002) Hydrothermal Systems Associated with Martian Impact Craters. Icarus, 157, 362-372.

Ray, J. S., Ramesh, R. (1998) Stable carbon and oxygen isotope analysis of natural calcite and dolomite mixtures using selective acid extraction. J. Geol. Soc. India 52, 323–332.

Ray, J. S., and Ramesh, R. (2000) Rayleigh fractionation of stable isotopes from a multicomponent source. Geochimica et Cosmochimica Acta, 62:2, 299-306.

Reed, S. J. B. (2005) Electron Microprobe Analysis and Scanning Electron Microscopy in Geology. Second Ed. Cambridge University Press, UK. 190p.

Reimolds, W. U., Koeberl, C., Gibson, R. L, and Dressler, B. O. (2005) Economic Mineral Deposits in Impact Sructures: A Review. in Koeberl, C., and Henkel, H., Eds. (2005) Impact tectonics – Impact Studies, vol.6, Spinger, Heidelberg, 552 + XIX p.

Reysenbach, A.-L., Voytek, M., and Mancinelli, R. (2001) Thermophiles – Biodiversity, Ecology and Evolution. Kluwer Academic/Plenum Publisher, New York.

Rezak, R., and Lavoie, D. L. (1993) Carbonate Microfabrics. Springer-Verlag, New York. 313p.

Ritcher, F. M. (2004) Timescales determining the degree of kinetic isotope fractionation by evaporation and condensation. Geochimica and Cosmochimica Acta, 68:23, 4971-4992.

Robertson P. B. and Mason G. D. (1975) Shatter cones from Haughton Dome, Devon Island, Canada. Nature, 255, 393.

Robertson P. B. and Grieve R. A. F. (1978) The Haughton impact structure. Meteoritics, 13, 615.

Rodriguez, J. A. P., Tanaka, K. L., Kargel, J. S., Dohm, J. M., Kuzmin, R., Fairén, A. G., Sasaki, S., Komatsu, G., Schulze-Makuch, D., and Jianguo, Y. (2007) Formation and disruption of aquifers in southwestern Chryse Planitia, Mars. Icarus, 191, 545-567.

Rollinson, H. R. (1995) Using geochemical data: Evaluation, presentation, interpretation. Longman Group, London, UK. 352p.

Rosebaum, J. and Sheppard, S. M. F. (1986) An isotopic study of siderites, dolomites and ankerites at high temperatures. Geochimica & Cosmochimica Acta, 50, 1147-1150.

Rowe, A. J., Wilkinson, J. J., Coles, B. J., and Morgan, J. V. (2004) Chicxulub: Testing for post-impact hydrothermal input into the Tertiary ocean. Meteoritics and Planetary Science, 39:7, 1223-1231.

Russel, M. J., Hall, A. J., Boyce, A. J., and Fallick, A. E. (2005) On Hydrothermal Convection Sytems and the Emergence of Life. Bulletin of the Society of Economic Geologists, 100th Anniversary Special Edition, 100:3, 419-438.

Sagan, C. and Druyan, A. (1986) Comet, Pocket Book, Random House, New York, 398p.

Schärer, U., and Deutsch, A. (1990) Isotope systematic and shock-wave metamorphism: II. U-Pb and Rb-Sr in naturally shocked rocks; the Haughton Impact Structure, Canada. Geochimica etg Cosmochimica Acta, 54, 3435-3447.

Schulze-Makuch, D., and Irwin, L.N. (2004) Life in the Universe: Expectations and Constraints. Springer-Verlag, Berlin.

Schulze-Makuch, D., Dohm, J. M., Fan, C., Fairén, A. G., Rodriguez, J. A. P., Baker, V. R., and Fink, W. (2007) Exploration of hydrothermal targets on Mars. Icarus, 189, 308-324.

Scott, D., and Hajnal, Z. (1988) Seismic signature of the Haughton structure. Meteoritics, 23, 239-247.

Scott, K. M., Lu, X., Cavanaugh, C. M., and Liu, J. S. (2004) Optimal methods for estimating kinetic isotope effects from different forms of the Rayleigh distillation equation. Geochimica et Cosmochimica Acta, 68:3, 433-442.

Shepherd, T. J., Rankin, A. H., and Alderton D. H. (1985) A practical guide to fluid inclusions. Glasgow: Blackie, 239p.

Sherlock S., Kelley S., Parnell J., Green P., Lee P., Osinski G. R., and Cockell C. S. (2005) Re-evaluating the age of the Haughton impact event. Meteoritics & Planetary Science, 40, 1777–1788.

Simmons, S. F., and Christenson, B. W. (1994) Origins of Calcite in a Boiling Geothermal System. American Journal of Science, 294, 361-400.

Skála, N., and Jakeš, P. (1999) Shock-induced effects in natural calcite-rich targets as revealed by X-ray powder diffraction. Geological Society of America, Special paper 339, 205-214.

Skála, N., and Žák, K. (2001) Stable isotope study of carbonates from the Ries meteorite crater – Evidence for impact-induced carbonate decomposition. Thirty-Second Lunar and Planetary Science Conference Abstract.

Skála, N. (2002) Shock-induced phenomena in limestones in the quarry near Ronheim, the Ries Crater, Germany. Bulletin of the Czech Geological Survey, 77:4, 313-320.

Skála, N., Ederová, J., Matêjka, P., and Hõrz, F. (2002) Mineralogical investigations of experimentally shocked dolomite: Implications for the outgassing of carbonates. Geological Society of America, Special Paper 356, 571-585.

Smith, P. H., and the Phoenix Science Team (2009) H_2O at the Phoenix Landing Site. Science, 325, 58-61.

Sorrel, W. H. (1997) Interstellar Grains as Amino Acid Factories and the Origin of Life. Astrophysics and Space Science, 253, 27-41.

Squyres, S. W. (1989) Water on Mars. Icarus, 79, 229-288.

Squyres, S. W., et al. (2004) The Spirit Rover's Athena Science Investigation at Gusev Crater, Mars, Science, 305, 794-799.

Stakes, D. S., and O'Neil, J. R. (1982) Mineralogy and stable isotope geochemistry of hydrothermally altered oceanic rocks. Earth and Plan. Science Letters, 57, 285-304.

Staudigel, H., Furnes, H., Banerjee, N., Dilek, Y., and Muehlenbachs, K. (2006) Microbes and volcanoes: A tale from the oceans, ophiolites, and greenstone belts. GSA Today, 16:10, 4-10.

Stetter, K. O. (2005) Volcanoes, hydrothermal venting, and the origin of life. In: Volcanoes and the Environment (J. Marti and G.G.J. Ernst eds.), Cambridge University Press, pp. 175-206.

Stipp, S. L. S. (1998) Surface analytical techniques applied to calcite: evidence of solid-state diffusion and implications for isotope methods. Palaeogeography, Palaeoclimatology, Palaeoecology, 140, 441-457.

Stöffler, D. Chair of Study Group for Impactites. Classification and Nomenclature of Impact Metamorphic Rocks (Impactites). IUGS Subcommission on the systematic of metamorphic rocks.

Sturchio, N.C., Keith, T.E.C.,and Muehlenbachs, K. (1990) Oxygen and carbon isotope ratios of hydrothermal minerals from Yellowstone drill cores. J. Volcanol. Geotherm. Res., 40, 23-37.

Sturkell, E.F.F., Broman, C., Forsberg, P., and Torssander, P. (1998) Impact-related hydrothermal activity in the Lockne impact structure, Jämtland, Sweden. European Journal of Mineralogy. 10, 589-606.

Swart, P. K., Melim, L.A., 2000. The origin of dolomites in tertiary sediments from the margin of Great Bahama Bank. J. Sediment. Res. 70, 738–748.

Taylor, H. P. (1974) The application of oxygen and hydrogen isotope studies to problems of hydrothermal alteration and ore deposition, Economic geology and the bulletin of the Society of Economic Geologists, 69:6, 843-883.

Taylor, H. P. (1977) Water/rock interactions and the origin of H_2O in granitic batholiths. Journal of the Geological Society. London, 133,509-558.

Taylor, S. R. (1992) Solar System Evolution: A New Perspective. Cambridge University Press, New York, 307p.

Therriault, A. M., Fowler, A. D., and Grieve, R. A. F. (1999) The Sudbury Igneous Complex: Mineralogy and Petrology of a Differentiated Impact Melt Sheet. 30th Annual Lunar and Planetary Science Conference, Houston, TX, abstract no. 1801.

Thorsos, I. E., Newsom, H. E., and Davies, A. G. (2001) Availability of heat to drive hydrothermal systems in large martian impact craters. Thirty-Second Lunar and Planetary Science Conference Abstract.

Thorsteinsson, R. (1958) Cornwallis and Little Cornwallis Islands, District of Franklin, Northwest Territories. Geological Survey of Canada, Memoir 294, 134p. (published 1959).

Thorsteinsson, R., and Fortier, Y. O. (1954) Report of Progress of the Geology of Cornwallis Island, Arctic Archipelago, Northwest Territories. Geological Survey of Canada, Paper 53-24.

Thorsteinsson, R., and Mayr, U. (1987) The Sedimentary Rocks of Devon Island, Canadian Arctic Archipelago, Geological Survey of Canada, Memoir 411, 182p.

Tona, F., Alonso, D., and Svab, M. (1985) Geology and Mineralization in the Carswell Structure – A General Approach. Geological Association of Canada, Special paper 29.

Tornabene, L. L., Moersch, J. E., Osinski, G. R., Lee, P, and Wright, S P. (2005) Spaceborne visible and thermal infrared lithologic mapping of impact-exposed subsurface lithologies at the Haughton impact structure, Devon Island, Canadian High Arctic: Applications to Mars. Meteoritics and Planetary Science, 40:12, 1835-1858.

Treiman, A. H., Amundsen, H. E. F., Blake, D. F., and Bunch, T. (2002) Hydrothermal origin for carbonate globules in Martian meteorite ALH84001: terrestrial analogue from Spitsbergen (Norway). Earth and Planetary Science Letters, 6440, 1-10.

Truesdell, A. H. and Fournier, R. O. (1976) Conditions in the deeper parts of the hot spring systems of Yellowstone National Park, Wyoming. U.S. Geol. Surv., Open-File Rep. 76-428, 29 p.

Truesdell, A. H., and Hulston, J. R. (1980) Isotopic evidence on the environments of geothermal systems. In: Fritz P., and Fontes, J.C. (Eds), Handbook of Envir. Isot. Geochem., Vol. 1, The Terrestrial Environment, Elsevier, Amsterdam, pp. 179-226.

Urey, H. C. (1947) The thermodynamic properties of isotopic substances. Journal of Chemical Society, London, 562-581.

Uysal, T., Feng, Y., Zhao, J., Isik, V., Nuriel, P., and Golding, S.D. (2009) Hydrothermal CO_2 degassing in seismically active zones during the late Quaternary. Geochemical Geology, 265, 442-454.

Valley, J. W., Eiler, J. M., Graham, C. M., Gibson, E. K., Romanek, C.S., and Stolper, E.M. (1997) Low temperature carbonate concretions in the martian meteorite ALH 84001: evidence from stable isotopes and mineralogy. Science, 275, 1633-1637.

Valley, J. W., Komor, S. C., Baker, K. (1998) Calcite crack cement in granite from the Siljan Ring, Sweden: stable isotopic results. In: *Deep Drilling in Crystalline Bedrock* (eds Boden, A., Eriksson, K.) vol. 1, pp. 156-179. Springer-Verlag, Berlin.

Venneman, T. W., Morlok, A., Von Engelhardt, W., and Kyser, K. (2000) Stable isotope composition of impact glasses from the Nördlinger Ries impact crater, Germany. Geochimica et Cosmochimica Acta, 65:8, 1325-1336.

Versh, E., Kirsimae, K., Joeleht, A., and Plado, J. (2005) Cooling of the Kärdla impact crater: I. The mineral paragenetic sequence observation. Meteoritics & Planetary Science, 40:1, 3-19.

Versh, E., Kirsimäe, K., Buchardt, B., Naumov, M. V., Öhman, T., and Jõeleht, A. (2006) Mineralogical and stable isotope study of impact-induced hydrothermal carbonate minerals. First International Conference on Impact Cratering in the Solar System Abstract, ESTEC, Netherlands, European Space Agency.

Vincent, W. F., Mueller, D., Van Hove, P., Howard-Williams, C. (2004) Glacial Periods on Early Earth and Implications for the Evolution of Life, Origins, 481-501.

Wachtershäuser, G. and Huber, C. (2007) Answer article to Bada, J. L. et al. (2007) Debating Evidence for the Origin of Life, Science, 315, 937-939.

Walters Jr., L.J., Claypool, G.E., Choquette, P.W. (1972). Reaction rates and $\delta^{18}O$ variation for the carbonate– phosphoric acid preparation method. Geochim. Cosmochim. Acta 36, 129– 140.

Walter, M. R., and Des Marais, D. J. (1993) Preservation of biological information in thermal spring deposits: Developing a strategy for the search of a fossil record on Mars. Icarus, 101, 129–143.

White, D. E. (1967) Some principles of geyser activity, mainly from Steamboat Springs, Nevada. American Journal of Science, 265,641-684.

Whiteway, J. A., Komguem, L., Dickinson, C., Cook, C., Illnicki, M., Seabrook, J., Popovici, V., Duck, T. J., Davy, R., Taylor, P. A., Patnak, J., Fisher, D., Carswell, A. I., Daly, M., Hipkin, V., Zent, A. P., Hecht, M. H., Wood, S. E., Tamppari, L. K., Renno, N., Moores, J. E., Lemmon, M. T., Daerden, F., and Smith, P. H. (2009) Mars Water-Ice Clouds and Precipitation. Science, 325, 68-70.

Wiegel, J., and Adams, M.W.W. (1998) Thermophiles: The keys to molecular evolution and the origin of life? Taylor & Francis, London, UK. 346p.

Wilhelms, D. E., McCauley, J.F., and Trask, N.J. (1987) The geologic history of the Moon. U.S. Geological Survey Prof. Paper 1348, 302p.

Yurtsever, Y. (1975) Worldwide Survey of Stable Isotopes in Precipitation, Rept. Sect. Isotope Hydrol. International Atomic Energy Agency, Vienna.

Yui, T.-F., and Gong, S.-Y. (2003) Stochiometric effect on stable isotope analysis of dolomite. Chemical Geology, 201, 359-368.

Zheng, Y.-F., and Hoefs, J. (1993) Carbon and oxygen isotopic covariations in hydrothermal calcites: Theoretical modeling on mixing processes and application to Pb-Zn deposits in the Harz Mountains, Germany. Mineralium Deposita, 28, 79-89.

Zheng, Y.-F. and Zhou, G.-T. (1999) Oxygen isotope fractionation in carbonate and sulfate minerals. Geochemical Journal, 33, 109-126.

Zürcher, L., and Kring, D.A. (2004) Hydrothermal alteration in the core of the Yaxcopoil-1 borhole, Chicxulub impact structure, Mexico. Meteoritics and Planetary Science, 39, 1199-1221.

Sample	Coordinates UTM NAD 83 Easting	Northing	Sample Description / Location	*XRD Mineralogy* (Semi-quantitative analysis based on ratio of peak heights)	*XRD Carbonates*
Dolomite Standards					
DOLO368			Dolomite / International Laboratory Standard	Dol	Dol
#3331			Dolomite / Internal Laboratory Standard / Slovakia	Dol	Dol
#3617			Dolomite / Internal Laboratory Standard / North West Territories, Canada	Dol	Dol
Reference - Unshocked (Outside Crater)					
01-047	440830	8365845	Bay Fiord Fm; outside crater	Dol>>Qtz(few%)	Dol
01-050	440830	8365848	Thumb Mountain Fm; outside crater	Dol>Cal (1/2)	Dol>Cal (1/2)
01-051	440830	8365848	Thumb Mountain Fm; outside crater	Dol>Cal(1/2)	Dol>Cal(1/2)
02-046	426570	8385815	Thumb Mountain Fm; outside crater, Thomas Lee Inlet	Cal>>Dol(1/10) (+Qz tr)	Cal>>Dol(1/10)
05-010	582940	8374420	Middle Memb. Allen Bay Fm.	Dol	Dol
05-044	454652	8355458	Bay Fiord Fm. Memb. A; limestone	Dol	Dol
05-052	454778	8355447	Bay Fiord Fm. Memb. A; limestone	Dol>Cal	Dol>Cal
SA08-43	420006	8380073	Stromatolitic limestone, Middle Allen Bay, Orbiter Lake	Dol	Dol
SA08-62	439338	8364271	Lower Allen Bay Fm; dolomite w/ burrows; Section 32	Cal>Dol(1/4) (+Qtz tr)	Cal>Dol(1/4)
SA08-63	439320	8364224	Lower Allen Bay Fm; dolomite w/ burrows; Section 32	Cal>>Dol(few%)>>Qtz(few%)	Cal>>Dol(few%)
SA08-64	439294	8364228	Bottom portion Lower Allen Bay Fm; dolomite w/ burrows; Section 32	Cal (+Qtz tr)	Cal
SA08-65	439292	8364228	Irene Bay Fm, dolomite, fossiliferous; Section 32	Cal>>Qtz(few%)	Cal
SA08-66	439293	8364231	Irene Bay Fm; greenish shale w/ dolomite; Section 32	Cal>>Qtz(1/7)>>Dol(few%)	Cal>>Dol(few%)
SA08-67	439270	8364263	Irene Bay Fm, limestone w/ crinoids, belemnite, corals; Section 32	Cal>>Qtz(1/10)>>DoL(few%)	Cal>>Dol(few%)
SA08-68	439272	8364260	Bottom of Irene Bay Fm, dolomite w/ burrows; Section 32	Cal>>Qtz(<10%)	Cal
08-048	514486	8350122	Lowermost Cass Fiord Fm; outside crater; bioturb. Limestone	Dol	Dol
08-049	514462	8350112	Lowermost Cass Fiord Fm; outside crater; quartzite	Dol	Dol
08-050	514442	8350088	Lowermost Cass Fiord Fm; outside crater; weath carb	Dol>>Py?(1/10)>>Qtz(<10%)	Dol
08-051	496633	8387681	Blanley Bay Fm. outside crater; thinly bedded carbonates	Dol (+Qtz tr)	Dol
08-052	496633	8387681	Blanley Bay Fm. outside crater; thinly bedded carbonates	Dol>>Qtz(few%)	Dol
08-053	496698	8387650	Cape Clay Fm.??	Dol (+Qtz tr)	Dol
08-054	439851	8381412	Thumb mountain Fm; outside crater	Dol>>Qtz(few%)	Dol
08-055	439854	8381401	Thumb mountain Fm; outside crater	Dol>>Cal(few%)	Dol>>Cal(few%)
08-056	440096	8381003	Bay Fiord fm; outside crater	Dol (+Qtz few%)	Dol
08-057	440096	8381003	Bay Fiord fm; outside crater	Dol (+Qtz tr) (+tr kutnohorite?)	Dol

Sample	Coordinates UTM NAD 83 Easting	Northing	Sample Description / Location	XRD Mineralogy (Semi-quantitative analysis based on ratio of peak heights)	XRD Carbonates
Reference - Low Shock (Crater Rim)					
00-106	422830	8359125	Allen Bay Fm. (MM); calcite vugs,hydrothermal	Cal	Cal
00-146-1	421080	8359355	Allen Bay Fm. (MM); calcite vugs; fine grained	Dol>>Cal(few%)	Dol>>Cal(few%)
00-146-2	421080	8359355	Allen Bay Fm. (MM); calcite vugs; coarse grained	Cal	Cal
05-004	419815	8371815	Middle Memb. Allen Bay Fm.	Dol	Dol
05-005	419902	8371815	Middle Memb. Allen Bay Fm.	Dol	Dol
05-007	417277	8372712	Middle Memb. Allen Bay Fm.	Dol	Dol
05-008	416329	8373256	Middle Memb. Allen Bay Fm.	Dol	Dol
05-021	417857	8364774	Ballistic ejecta; Thumb Mountain Fm.	Cal	Cal
Central Uplift					
02-118	423040	8372585	Eleanor River Fm.	Dol	Dol
06-001	420422	8371019	Lower Memb. Allen Bay Fm.	Cal	Cal
06-093	427823	8365859	Eleanor River Fm.	Cal (+Qtz tr=moganite)	Cal
SA08-4	425826	8371884	Eleanor River Fm Brecciated Ejecta Block ?? Ejecta in CU??	Dol=Qtz>Cal(1/2)	Dol>Cal(1/2)
SA08-11	426968	8371742	Thumb Mt "reference" sample; dolomite w/ burrows	Cal>>Dol(1/10)=Qtz(1/10)	Cal>>Dol(1/10)
SA08-12	426968	8371742	Thumb Mt "reference" sample; rare veins near-by; dolomite w/ burrows	Cal>>Dol(1/7)>>Qtz(few%)	Cal>>Dol(1/7)
SA08-15	428050	8371964	Monomict carbonate breccia slightly veined and coated by calcite	Cal>=Dol>Qtz(4/5)	Cal>=Dol
SA08-16	428050	8371964	Thumb Mt. Reference; massive limestone cut by sulfate veinlets	Dol>Cal(4/5)>>Qtz(few%)	Dol>>Cal(4/5)
SA08-21	425023	8369279	Blue mineral coating; Eleanor Bay Fm outcrop	Qtz>Cal(4/5)>>Dol(few%)	Cal(4/5)>>Dol(few%)
SA08-33	427896	8366446	Blue mineral + orange coating on Eleanor Bay Fm monomict breccia outcrop	Cal>Qtz(4/5)>>Dol(1/7)	Cal>>Dol(1/7)
Haughton Formation Crater-Fill Sediments					
03-019	419914	8369139	Haughton Formation	Dol>Qtz>Cal	Dol>Cal
03-052	419293	8368555	Haughton Fm.; limestone layer	Dol>Cal	Dol>Cal
03-053	419293	8368555	Haughton Fm.; nodule	Dol>>Cal(few%)	Dol>>Cal(few%)
04-057	424464	8367937	Haughton Fm.	Dol>>Cal(few%)	Dol>>Cal(few%)
06-060	422759	8369113	Haughton Formation; float	Dol>>Qtz(1/6)>>Cal(1/10)	Dol>>Cal(1/10)
Impact-Melt Breccias					
99-108	433100	8365565	Breccia dike	Cal>>Dol(few%)	Cal>>Dol(few%)
00-023	420560	8370965	Impact melt breccia	Cal>=Dol>>Qtz(<10%)	Cal>=Dol
00-035	420440	8370955	Impact melt breccia	Cal>=Dol>Qtz(1/4)	Cal>=Dol
00-175	418620	8363695	Impact melt breccia	Cal>Dol(1/4)>>Qtz(few%)	Cal>Dol(1/4)

Sample	Coordinates UTM NAD 83 Easting	Northing	Sample Description / Location	XRD Mineralogy (Semi-quantitative analysis based on ratio of peak heights)	XRD Carbonates
Impact-Melt Breccias (continued)					
00-220	425340	8372445	Impact melt breccia	Cal>Dol(1/3)>>Qtz(few%)	Cal>Dol(1/3)
02-132	422160	8370495	Impact melt breccia	Cal>Dol(1/2) (+Gismondine: CaAl2Si2O8•4H2O)	Cal>Dol(1/2)
05-026	418011	8364086	Impact melt breccia	Cal>Dol(1/3)	Cal>Dol(1/3)
06-109	422477	8372364	Impact melt breccia	Cal=Dol>>Qtz(1/7)	Cal=Dol
Clasts from Impact Melt Breccias					
99-052	425500	8367625	Clast from melt breccias; oolitic limestone	Qz>Cal(1/5) (+tr crystalline Qtz, wollastonite)	Cal(1/5)
99-059b	421800	8373555	Clast from melt breccias; carbonate	Cal (alpha and beta Cal)	Cal
99-069c	4264610	8368115	Clast from melt breccias; sandstone	Cal>>Dol(1/5)>>Qtz(1/10)	Cc>>Dol(1/5)
99-071c	424,560	8,367,865	Clast from melt breccias; sandstone	Qz +glass (+minor Cal, tr Dol)	minor Cal, tr Dol
99-097a	429,440	8364905	Impact melt breccia: oolitic limestone	Cal>Dol(1/4)	Cal>Dol(1/4)
00-174b	418560	8363375	Clast from melt breccias; sandstone	Qtz>>Cal(few%)	Cal(few%)
04-001	418585	8364468	Sandstone clast from IMB	Qtz	-
04-003	418585	8364468	Sandstone clast from IMB	Qtz>Cal(1/2)	Cal(1/2)
05-024	418011	8364086	Carbonate clast from IMB	Cal>Dol(1/4)	Cal>Dol(1/4)
05-025	418011	8364086	Carbonate clast from IMB	Cal>>Dol(1/10) (+Qtz tr)	Cal>>Dol(1/10)
05-025 Iso dup	418011	8364086	Carbonate clast from IMB	Cal>>Dol(1/10) (+Qtz tr)	Cal>>Dol(1/10)
05-033	418614	8364225	Impact melt breccia; dense; dark grey	Cal>>Qtz(few%)	Cal
Hydrothermal Veins					
99-104	429460	8370350	Calcite vein, periphery of central uplift; Fluid inclusion	Cal	Cal
00-136	420570	8359925	Hydrothermal precipitate; Calcite vein, crater rim in Allen Bay Fm	Cal	Cal
02-048	426540	8362015	Clear Calcite vein (Fluid inclusion, Th=67.9-85.1 deg C)	Cal (from FI)	Cal
02-050	426540	8362015	Quartz vein (south); massive; (described as Cc by Oz)	Qtz	-
02-053	426140	8362335	Calcite vein	Cal	Cal
SA08-10	426968	8371742	Calcite + Py veins in dolomite, 1mm-1cm multigen.	Cal	Cal
SA08-23	429396	8370737	Cc vein (coating) on dolomite + vein // to bedding; other side of HR	Cal (minor Dol cover)	Cal (minor Dol cover)
SA08-24	429400	8370737	Cc veinlet + bothrioidal sulfides on bedded dolomite	Cal>>Dol(1/10)	Cal>>Dol(1/10)
SA08-25	429400	8370737	Thin // Cc veins w/ Cc vug infils in dolomite	Cal>Dol(1/2)	Cal>Dol(1/2)
SA08-27	429356	8370543	Cm-size Cc vein, multigen?, Fe-stain, fossils; Bay Fiord Member C	Cal	Cal
SA08-29	429271	8369432	Cm-wide coarse Cc veins Heavily veined outcrop, locally pervasive	Cal	Cal
SA08-36	420419	8371023	Cc veins, Perpendicular to bedding, lower Allen Bay, West Trinity Lake	Cal	Cal

Sample	Coordinates UTM NAD 83 Easting	Northing	Sample Description / Location	XRD Mineralogy (Semi-quantitative analysis based on ratio of peak heights)	XRD Carbonates
Hydrothermal Veins (continued)					
SA08-50	418547	8368460	Spartic Cc in vug possibly from fossil, in Allen Bay entrance Foxi Valley	Cal	Cal
SA08-59D	429309	8366947	Cc veins in beds and // to bedding, organic-rich dolomite/shale	Cal	Cal
SA08-59E	429309	8366947	Cc veins vertical and perpendicular to bedding, organic-rich dolomite/shale	Cal	Cal
SA08-59F	429309	8366947	Cc veins, vertical planar, some Fe-stain, gently dipping beds ESE	Cal	Cal
Hydrothermal Intra-Melt Breccia Isolated Vugs					
SA08-3B	425945	8371522	2 carbonate vugs, 10-cm wide, white euhedral crystals	Cal	Cal
SA08-18-A	428379	8371586	Calcite vug; euhedral coarse crystals; massive	Cal	Cal
SA08-18-B	428379	8371586	Calcite vug; euhedral coarse crystals; crystals	Cal	Cal
SA08-19A-A	428455	8371450	Large Cc vug w/ sinusoidal ridges coated by crystals; massive	Cal>Qtz(4/5)	Cal
SA08-19A-B	428455	8371450	Large Cc vug w/ sinusoidal ridges coated by crystals; crystals+massive	Cal (+Qtz tr)	Cal
SA08-19B-A	428455	8371450	Cc vug, mm-size double-tetrahedral crystals on massive Cc; massive	Cal	Cal
SA08-19B-B	428455	8371450	Cc vug, mm-size double-tetrahedral crystals on massive Cc; crystals	Cal	Cal
SA08-19C-A	428455	8371450	Cc coating on cemented "silicified" clast; massive	Cal	Cal
SA08-19C-B	428455	8371450	Cc coating on cemented "silicified" clast; crystals	Cal	Cal
SA08-19D-A	428450	8371445	Vug; massive	Cal (+Dol tr)	Cal (+Dol tr)
SA08-19D-B	428450	8371445	Vug; massive+crystals	Cal (+Dol tr)	Cal (+Dol tr)
SA08-20A	427549	8370683	Qz vug; pentagonal shape, concentric bending	Qtz (+Cal tr)	Cal tr
SA08-20B	427549	8370683	Qz vug	Qtz (+Cal tr)	Cal tr
SA08-30	427789	8368809	2 milky Qz vugs + Cc?, similar to 20B but more cherty	Qtz	Qtz
SA08-32	428798	8366291	Chert vug in large IMB outcrop	Qtz	Qtz
SA08-46	430096	8366859	Qz and chert vugs, possibly shocked Sst clast? Gypsum vugs, rare Cc	Cal (+Dol tr)	Cal (+Dol tr)
SA08-57-A	428428	8371566	Cc vug, semi-transparent, 15cm-wide, outer vug seems silicified; massive	Cal>Qtz(3/5) (+Dol tr)	Cal (+Dol tr)
SA08-57-B	428428	8371566	Cc vug, semi-transparent, 15cm-wide, outer vug seems silicified; crystals	Cal>>Qtz(few%)	Cal
SA08-58A	428506	8371526	Cc vugs, 15cm and 10cm-wide; inner portion with crytals	Cal>>Qtz(1/8)	Cal
SA08-58B-A	428506	8371526	Cc vugs, 15cm and 10cm-wide; massive	Cal	Cal
SA08-58B-B	428506	8371526	Cc vugs, 15cm and 10cm-wide; crystals	Cal>Qtz(1/2)	Cal
SA08-58C	428506	8371526	Cc vugs, 15cm and 10cm-wide; massive	Dol>Cal(1/2)>>Qtz(few%)	Dol>Cal(1/2)
Haughton River Vug (Hydrothermal Intra-Breccia Vug)					
SA08-89-1	428034	8364700	Coarse grained clear Calcite coating on botrioidal marcassite	Cal	Cal
SA08-89-2	428034	8364700	Fine to medium grained translucent Calcite layer underlying 89-1	Cal	Cal

Sample	Coordinates UTM NAD 83 Easting	Northing	Sample Description / Location	XRD Mineralogy (Semi-quantitative analysis based on ratio of peak heights)	XRD Carbonates
Haughton River Vug (Hydrothermal Intra-Breccia Vug) (continued)					
SA08-89-3	428034	8364700	Very fine grained medium grey Calcite layer underlying 89-2	Cal	Cal
SA08-90-1	428073	8364673	Laminated very fined grained calcite, white outermost layer	Cal	Cal
SA08-90-2	428073	8364673	Laminated very fined grained calcite, gradational layer, underlying SA08-90-1	Cal	Cal
SA08-90-3	428073	8364673	Laminated very fined grained calcite, massive lower layer, underlying SA0890-2	Cal (+Dol tr)	Cal (+Dol tr)
99-130-1	428000	8364425	Layered IMB; Haughton River Vug Hydrothermal precipitate); fine grained	Cal	Cal
99-130-2	428000	8364425	Layered IMB; Haughton River Vug Hydrothermal precipitate); coarse grained	Cal	Cal
99-135-2	428000	8364425	Haughton River Vug; Hydrothermal vug precipitate; coating	Cal	Cal
Haughton River Vug - Longitudinal Cross-Section (Hydrothermal Intra-Breccia Vug)					
SA08-69	428069	8364644	Haughton River Vug; Porous brecciated vug carbonate	Cal	Cal
SA08-70	428070	8364649	Haughton River Vug; Hydrothermal vug precipitate	Cal	Cal
SA08-71B	428070	8364654	Haughton River Vug; Hydrothermal vug precipitate	Cal	Cal
SA08-72	428071	8364659	Haughton River Vug; Hydrothermal vug precipitate	Cal	Cal
SA08-73B	428072	8364663	Haughton River Vug; Late-stage "travertine" hydrothermal vug precipitate	Cal	Cal
SA08-74A	428072	8364668	Haughton River Vug; Late-stage "travertine" hydrothermal vug precipitate	Cal	Cal
SA08-75	428073	8364673	Haughton River Vug; Hydrothermal vug precipitated with marcassite	Cal	Cal
SA08-76A	428073	8364678	Haughton River Vug; Massive dolomite; dark unit seen on LiDAR	Cal	Cal
SA08-77A	428073	8364684	Haughton River Vug; Hydrothermal vug pure Cc in horizontal layer	Cal	Cal
SA08-78A	428073	8364689	Haughton River Vug; Hydrothermal vug Cc + blue mineral + marcas.	Cal	Cal
SA08-79	428072	8364694	Haughton River Vug; Uniform monomict breccia Cc+/-Dol	Cal>>Dol	Cal>>Dol
SA08-81B	428072	8364705	Haughton River Vug; Above shear zone, greenish limestone, Cc veins	Cal=Dol	Cal=Dol
SA08-85B_MATRIX	428066	8364722	Haughton River Vug; Hydrothermal vug precipitate	Cal=Dol	Cal=Dol
SA08-87A	428063	8364731	Haughton River Vug; Hydrothermal vug precipitate, flat dolomite	Dol>Cal	Dol>Cal
SA08-88	428062	8364735	Haughton River Vug; End of outcrop; Brecciated carbonate bedrock	Dol>Cal	Dol>Cal
SA08-VUG1	428073	8364673	Haughton River Vug; Large Drapperie Hydrothermal Cc w/ marcassite	Cal	Cal
Hydrothermal Pipe Structures					
06-097	430536	8366607	Hydrothermal pipe structure; Calcite vug	Cal	Cal
SA08-47B	430539	8366606	Pipe near Sapphire Lake. Banding, euhedral carbonates, vug, Allen Bay Fm	Cal	Cal

Abbreviations: Cal = calcite; Dol = dolomite; Qtz = quartz

Sample	Description	Easting - NAD83 (metres)	Northing - NAD83 (metres)	XRD Mineralogy	$\delta^{13}C$ (‰, VPDB)	$\delta^{18}O$ (‰, VSMOW)	$\delta^{18}O$ of fluid source (‰, VSMOW)	Calculated fluid temperature (Kelvin)	Calculated fluid temperature (°Celsius)
Unshocked Reference Material outside crater									
SA08-64	Bottom portion Lower Allen Bay Formation; dolomite; burrows	439294	8364228	Cal (+Qtz tr)	-0.29	23.92	-2	310.61	37.61
SA08-65	Irene Bay Fm, dolomite, fossiliferous	439292	8364228	Cal>>Qtz(few%)	-0.72	25.53	-2	302.32	29.32
Shocked Material (crater rim or periphery of central uplift)									
05-021	Ballistic ejecta: Thumb Mountain Formation	417857	8364774	Cal	-0.15	24.20	-2	309.15	36.15
06-001	Lower Memb. Allen Bay Formation	420422	8371019	Cal	-0.54	24.84	-2	305.77	32.77
Shocked Material from Central Uplift									
06-093	Eleanor River Formation	427823	8365859	Cal	-1.69	20.31	-2	332.14	59.14
Clast from Impact Melt Breccias									
99-069c	Clast from melt breccias; sandstone; highly shocked	4264610	8368115	Cal>>Dol(1/6)>>Qtz(1/10)	1.09	11.31	n/a	n/a	n/a
04-003	Clast from melt breccias; sandstone	418585	8364468	Qtz>Cal(1/2)	-6.02	13.86	n/a	n/a	n/a
05-024	Clast from melt breccias; carbonate	418011	8364086	Cal>Dol(1/4)	-1.56	24.27	n/a	n/a	n/a
05-025	Clast from melt breccias; carbonate	418011	8364086	Cal>>Dol(1/10) (+Qtz tr)	-1.46	23.60	n/a	n/a	n/a
***05-025 Duplicate**	Clast from melt breccias; carbonate	418011	8364086	Cal>>Dol(1/10) (+Qtz tr)	-1.54	23.62	n/a	n/a	n/a
99-059b	Clast from melt breccias; carbonate; highly shocked	421800	8373555	Cal (+Qtz tr=moganite)	-5.28	16.44	n/a	n/a	n/a
SA08-75	Carbonate clasts with shatter cones; Haughton River Vug	428073	8364673	Cal	-1.32	21.60	n/a	n/a	n/a
SA08-76A	Carbonate clasts with shatter cones; Haughton River Vug	428073	8364678	Cal	-1.25	20.99	n/a	n/a	n/a
Impact Melt Breccias									
99-108	Breccia dike	433100	8365565	Cal>>Dol(few%)	-4.78	10.56	n/a	n/a	n/a
Hydrothermal Veins in Shocked Material									
99-104	Calcite vein, periphery of central uplift	429460	8370350	Cal	-10.23	16.94	-4	341.54	68.54
00-136	Hydrothermal precipitate; Calcite vein, crater rim in Allen Bay Fm	420570	8359925	Cal	-7.31	11.93	-4	384.33	111.33
***00-136 Duplicate**	Hydrothermal precipitate; Calcite vein, crater rim in Allen Bay Fm	420570	8359925	Cal	-7.37	11.69	-4	386.86	113.86
02-053	Calcite vein	426140	8362335	Cal	-14.18	13.31	-4	370.98	97.98
SA08-10	Calcite + Py veins in dolomite, 1mm-1cm multigen.	426968	8371742	Cal	-2.76	14.46	-4	360.82	87.82
SA08-27	Cm-size Cc vein, multigen?, Fe-stain, fossils; Bay Fiord	429356	8370543	Cal	-8.93	17.09	-4	340.47	67.47
***SA08-27 Duplicate**	Cm-size Cc vein, multigen?, Fe-stain, fossils; Bay Fiord	429356	8370543	Cal	-9.07	17.14	-4	340.13	67.13
SA08-29	Cm-wide coarse Cc veins, locally pervasive	429271	8369432	Cal	-6.71	14.31	-4	362.15	89.15
SA08-36	Cc veins, Perpendicular to bedding, lower Allen Bay Fm	420419	8371023	Cal	-3.89	9.33	-4	414.02	141.02
SA08-56	Mm-size Cc veins, vertical, cross-cut horizontal dolomite	426811	8371895	Cal	-5.87	10.87	-4	395.61	122.61
SA08-59D	Cc veins in beds and // to bedding, organic-rich dolomite/shale	429309	8366947	Cal	-10.09	14.46	-4	360.85	87.85
SA08-59E	Cc veins vertical and perp. to bedding, organic-rich dolomite/shale	429309	8366947	Cal	-5.11	8.77	-4	421.31	148.31
							Average:	*373.26*	*100.26*

Sample	Description	Easting - NAD83 (metres)	Northing - NAD83 (metres)	XRD Mineralogy	$\delta^{13}C$ (‰, VPDB)	$\delta^{18}O$ (‰, VSMOW)	$\delta^{18}O$ of fluid source (‰, VSMOW)	Calculated fluid temperature (Kelvin)	Calculated fluid temperature (°Celsius)
Hydrothermal Vugs within Impact melt breccias									
SA08-3B	2 carbonate vugs, 10-cm wide, white euhedral crystals	425945	8371522	Cal	-6.17	10.86	-4	395.71	122.71
SA08-18-A	Calcite vug; euhedral coarse crystals; massive	428379	8371586	Cal	-6.20	10.46	-4	400.24	127.24
SA08-18-B	Calcite vug; euhedral coarse crystals; crystals	428379	8371586	Cal	-6.34	11.10	-4	393.13	120.13
SA08-19A-A	Large Cc vug w/ sinusoidal ridges coated by crystals; massive	428455	8371450	Cal>Qtz(4/5)	-6.34	11.71	-4	386.65	113.65
SA08-19A-B	Large Cc vug w/ sinusoidal ridges coated by crystals; crystals	428455	8371450	Cal (+Qtz tr)	-6.41	12.11	-4	382.52	109.52
SA08-19B-A	Cc vug, mm-size double-tetrahedrons on massive Cc; massive	428455	8371450	Cal	-6.68	10.81	-4	396.26	123.26
SA08-19B-B	Cc vug, mm-size double-tetrahedrons on massive Cc; crystals	428455	8371450	Cal	-6.90	12.46	-4	379.07	106.07
SA08-19C-A	Cc coating on cemented "silicified" clast; massive	428455	8371450	Cal	-5.77	11.38	-4	390.04	117.04
SA08-19C-B	Cc coating on cemented "silicified" clast; crystals	428455	8371450	Cal	-6.67	12.68	-4	376.93	103.93
SA08-57-B	Cc vug, semi-transparent, 15cm-wide, massive+crystals	428428	8371566	Cal>>Qtz(few%)	-6.59	12.25	-4	381.10	108.10
SA08-58A	Cc vugs, 15cm and 10cm-wide; massive	428506	8371526	Cal>>Qtz(1/8)	-6.76	11.94	-4	384.24	111.24
SA08-58B-A	Cc vugs, 15cm and 10cm-wide; massive	428506	8371526	Cal	-7.81	13.02	-4	373.67	100.67
SA08-58B-B	Cc vugs, 15cm and 10cm-wide; crystals	428506	8371526	Cal>Qtz(1/2)	-5.84	12.55	-4	378.15	105.15
***SA08-58B-B Duplicate**	Cc vugs, 15cm and 10cm-wide; crystals	428506	8371526	Cal>Qtz(1/2)	-5.69	12.58	-4	377.82	104.82
							Average:	*385.40*	*112.40*
Hydrothermal Vug within Impact melt breccias - Haughton River Valley Locality									
SA08-89-1	Coarse grained clear Calcite coating on botrioidal marcasite	428034	8364700	Cal	-6.03	12.22	-4	381.43	108.43
SA08-89-2	Fine to medium grained translucent Calcite layer underlying 89-1	428034	8364700	Cal	-5.84	12.54	-4	378.28	105.28
SA08-89-3	Very fine grained medium grey Calcite layer underlying 89-2	428034	8364700	Cal	-5.85	12.40	-4	379.65	106.65
SA08-90-1	Laminated very fined grained calcite, white outermost layer	428073	8364673	Cal	-4.66	12.67	-4	376.98	103.98
SA08-90-2	Laminated very fined grained calcite, underlying SA08-90-1	428073	8364673	Cal	-4.11	10.94	-4	394.90	121.90
99-130-1	Layered IMB; Haughton River Vug Hydrothermal; fine grained	428000	8364425	Cal	-3.33	10.06	-4	404.98	131.98
99-130-2	Layered IMB; Haughton River Vug Hydrothermal; coarse grained	428000	8364425	Cal	-3.47	10.44	-4	400.52	127.52
99-133	Haughton River Vug; Hydrothermal vug precipitate	428000	8364425	Cal	-3.62	11.01	-4	394.11	121.11
99-134	Haughton River Vug; Hydrothermal vug precipitate	428000	8364425	Cal	-3.03	11.65	-4	387.20	114.20
99-135-2	Haughton River Vug; Hydrothermal vug precipitate; coating	428000	8364425	Cal	-6.17	12.08	-4	382.81	109.81
99-136	Haughton River Vug; Hydrothermal vug precipitate	428000	8364425	Cal	-3.39	11.10	-4	393.05	120.05
99-137-1	Haughton River Vug; Hydrothermal vug precipitate; center	428000	8364425	Cal	-3.61	13.13	-4	372.63	99.63
99-137-2	Haughton River Vug; Hydrothermal vug precipitate; outside	428000	8364425	Cal	-5.02	11.68	-4	386.92	113.92
99-139	Haughton River Vug; Hydrothermal vug precipitate	428000	8364425	Cal	-2.93	12.14	-4	382.22	109.22

Sample	Description	Easting - NAD83 (metres)	Northing - NAD83 (metres)	XRD Mineralogy	$\delta^{13}C$ (‰, VPDB)	$\delta^{18}O$ (‰, VSMOW)	$\delta^{18}O$ of fluid source (‰, VSMOW)	Calculated fluid temperature (Kelvin)	Calculated fluid temperature (°Celsius)
Hydrothermal Vug within impact melt breccias - Haughton River Valley Locality (continued)									
SA08-69	Haughton River Vug; Porous brecciated vug carbonate	428069	8364644	Cal	-3.71	11.00	-4	394.20	121.20
SA08-70	Haughton River Vug; Hydrothermal vug precipitate	428070	8364649	Cal	-3.68	10.38	-4	401.22	128.22
SA08-71B	Haughton River Vug; Hydrothermal vug precipitate	428070	8364654	Cal	-3.61	10.85	-4	395.83	122.83
SA08-72	Haughton River Vug; Hydrothermal vug precipitate	428071	8364659	Cal	-3.28	10.38	-4	401.23	128.23
SA08-73B	Haughton River Vug; Late-stage hydrothermal laminae	428072	8364663	Cal	-2.87	10.84	-4	395.97	122.97
SA08-74A	Haughton River Vug; Late-stage hydrothermal laminea	428072	8364668	Cal	-2.88	10.49	-4	399.90	126.90
SA08-77A	Haughton River Vug; Hydrothermal vug Cc in horizontal layer	428073	8364684	Cal	-3.42	10.15	-4	403.92	130.92
SA08-78A	Haughton River Vug; Hydrothermal vug Cc + marcas.	428073	8364689	Cal	-3.87	10.81	-4	396.35	123.35
SA08-85B_XALS	Haughton River Vug; Hydrothermal vug precipitate	428066	8364722	Cal	-3.38	11.32	-4	390.68	117.68
SA08-VUG1	Haughton River Vug; Large laminated Cc with marcassite	428073	8364673	Cal	-4.19	11.34	-4	390.51	117.51
							Average:	*391.06*	*118.06*
Hydrothermal Pipe Structures									
06-097	Hydrothermal pipe structure; Calcite vug	430536	8366607	Cal	-7.13	10.46	-4	400.24	127.24
SA08-47B	Pipe near Sapphire Lake. Fine banding, euhedral carbonate filling	430539	8366606	Cal	-7.87	10.36	-4	401.45	128.45
99-152	Haughton River Vug; Hydrothermal vug precipitate, Allen Bay Fm.	428000	8364425	Carbonate mixture	-2.99	18.32	-	-	-
							Average:	*393.95*	*127.85*
Vugs within Shocked Material									
SA08-50	Spartic Calcite from fossil, in Allen Bay Formation	418547	8368460	Cal	-1.96	21.17	-2	326.61	53.61
***SA08-50 Duplicate**	Spartic Calcite from fossil, in Allen Bay Formation	418547	8368460	Cal	-2.02	21.08	-2	327.17	54.17
							Average:	*326.89*	*53.89*

Abbreviations: Cal = calcite; Dol = dolomite; Qtz = quartz

Precision level: $\delta^{13}C \pm 0.5$ ‰ ; $\delta^{18}O \pm 0.2$ ‰